CONFORMAL ANTENNAS, RESEARCH PROGRAM REVIEW AND WORKSHOP, HELD AT CRYSTAL CITY, ARLINGTON, VIRGINIA, ON 15-16 APRIL 1975

Naval Air Systems Command
Washington, D. C.

April 1975

RESEARCH PROGRAM REVIEW and WORKSHOP

CONFORMAL ANTENNAS

15-16 APRIL 1975

NAVAL AIR SYSTEMS COMMAND
RESEARCH and TECHNOLOGY GROUP

INTRODUCTION

This report is a compilation of the papers given at a Workshop on Conformal Antenna Arrays held at "Crystal City" Arlington, Virginia, on 15-16 April 1975. The objectives of the Workshop were twofold:

(1) To present to the antenna community the significant results that had been achieved on the conformal antenna research program, sponsored by the Research Administrator's Office of the Naval Air Systems Command, and to highlight other research uniquely related to the application of such arrays.

(2) To seek the viewpoint of recognized leaders in the field of antennas as to the problem areas which have not yet been solved and thus where future research should be concentrated.

To all of those who presented a paper at this Workshop, your efforts are greatly appreciated.

TABLE OF CONTENTS

CONFORMAL ARRAYS IN TACTICAL MISSILES, RPVs, AND AIRCRAFT

by

F. C. Alpers
Consultant for Advanced Concepts
Electronic Warfare Department
Naval Weapons Center
China Lake, California

This presentation discusses, in general terms, a number of potential applications for conformal antenna arrays in surface- and air-launched tactical missiles, remotely piloted vehicles (RPVs), and Navy and Marine Corps aircraft. It will not enter into any array design technology nor suggest just how the various conformal arrays that are mentioned might be achieved. Note that the applications to be shown are described as "potential"; the writer knows of no specific plans to procure antennas for the particular applications described, and this discussion should in no way be interpreted as a call for "unsolicited" proposals in the areas discussed. Rather, the intention is to point to typical application needs and challenges toward which array design specialists might aim a portion of their research and exploratory development efforts. Also note that the presentation is unclassified. This means that certain details and relationships to specific Navy weapons or aircraft may not be brought out, and a number of your questions may go unanswered. Persons having a need for classified data on specific antenna applications should establish security clearances and approach technical personnel in the appropriate systems command.

SURFACE-TO-AIR MISSILES

Two potential new surface-to-air missiles (SAMs) for the Navy are illustrated in a general way in Figures 1 and 2. These are a short range SAM which individual ships could use to defend themselves against enemy missiles or aircraft that penetrate other defenses, and a new medium-size SAM that might present certain advantages over present weapons in providing area air defenses for a Fleet Task Force, convoy, or the like.

As is indicated in Figure 1, the short range, point defense SAM might use an active microwave seeker to guide the terminal portion of its flight, and such a seeker could profit by use of a conformal array around the missile nose. As a rough indication of size, the nose might involve a 2:1 ogive with an 8-inch base. (While the 8 inches is drawn from certain system considerations, the 2:1 taper--like other "for instance" numbers that follow--should be interpreted as flexible. Moreover, at this point it does not appear consequential to go into further detail, such as whether the ogive should be tangential, Von Karmen, or other.) Missile size and accuracy considerations would point to selection of a high microwave frequency for the seeker. The fact that threats for point defense tend to be incoming radially limits the need for off-axis seeker operation to perhaps 25° (much of which accommodates the missile's own angle of attack). Size and cost considerations

POINT DEFENSE SAM

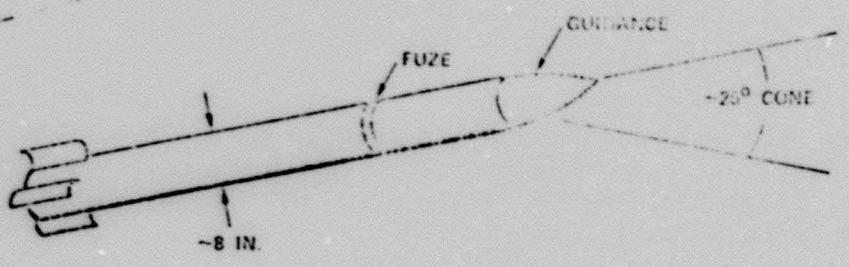

POSSIBLE VELOCITY

M 2.0 (<1/2 MINUTE)

POSSIBLE TERMINAL GUIDANCE

- ACTIVE
- HIGH MICROWAVE FREQUENCY
- VERY LOW POWER AND SHORT PULSE
- MONOPULSE

FIGURE 1

ADVANCED AREA DEFENSE SAM

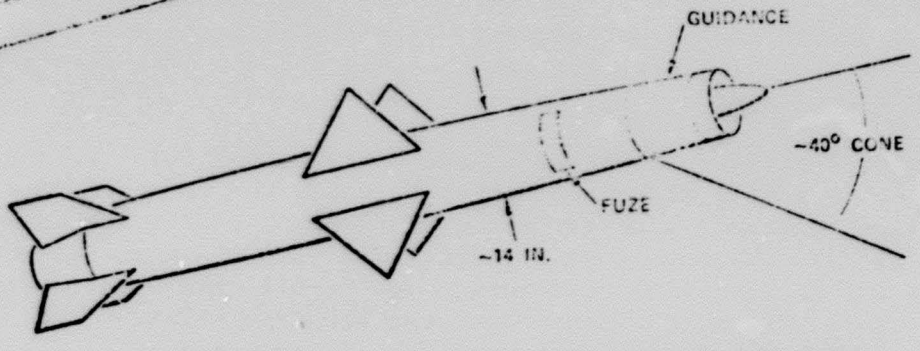

POSSIBLE VELOCITY

M 3TO4

POSSIBLE TERMINAL GUIDANCE

- DUAL MODE. . . ACTIVE/PASSIVE
- MODERATE MICROWAVE FREQUENCY
- MODERATE POWER WITH CHIRP
- MONOPULSE

FIGURE 2

(large numbers of this missile would be desired) would point to a low transmitter power level that should cause no significant problem in the array design. Also, the missile velocity and flight duration should present no material temperature problems. However, the desirability of two-dimensional monopulse reception for quick response may lead to various complications in the array design.

Another application of conformal arrays to a point defense SAM might come in the fuze target detection device (TDD). TDD antennas for nearly all missiles have been conformal, so this is not unusual. However, whether an optical or RF fuze would be used, and, if the latter, what operational requirements might be imposed, are questions that relate closely to warhead design and other classified areas and are therefore not amenable to discussion here. These comments on conformal antennas for fuzing similarly apply to other missiles that will be discussed herein.

The advanced area defense SAM, which is illustrated only in a general way by Figure 2, also might benefit by use of a conformal antenna in its terminal guidance mode. This weapon would naturally be expected to differ from the point defense missile in size and velocity (e.g., 14 in. diameter and Mach 3-4), but there are also other differences that may radically alter the array design problems. One is the strong possibility that this missile would be a ramjet type, which would take away much of the forward aperture and probably require an end-fire design to provide necessary dead-ahead antenna coverage. Also, it might be highly desirable to operate interchangeably between passively homing on an enemy emitter and actively homing on echo signals resulting from a missile-borne transmitter. This would require an antenna or set of antennas that might operate at a middle microwave for the active transmission and reception, and at other bands for passive reception. Yet other differences from the point defense SAM are in the angular coverage required of the antenna (circa 40° vs 25°) and a higher peak transmitter power that must be accommodated. Again, two dimensional monopulse reception would be highly desirable.

AIR-TO-AIR MISSILES

Some applications of conformal antennas to possible new air-to-air missiles (AAMs) are illustrated in Figures 3 through 5. The first missile, identified as a "dog fight" AAM, would be one intended for close-in aerial combat where friendly and enemy aircraft are intermixed and it may be necessary to close to visual recognition range before launching a weapon. The second missile illustrated is a medium range, general purpose AAM that could be regarded as a follow-on to the present SPARROW weapons. The third is an AAM which would offer longer range and higher velocity than weapons disclosed to date and which might be developed to give greater depth to present Fleet defenses.

The so-called "dog fight" AAM that is shown bears certain similarities to the point defense SAM previously discussed, but important differences might arise. To operate against highly maneuvering aircraft rather than radially incoming targets, a much greater maneuvering capability might be required of the AAM, and tracking targets at extreme angles (e.g., 120°) off the missile axis might be required. As opposed to an optical

approach, a microwave guidance design could provide the dog fight AAM with a capability to track enemy aircraft into clouds, and operation at a high microwave frequency would probably be attractive for the missile ranges of interest. To free the launch aircraft from any requirement to continuously position itself at certain angles from the target after the missile is launched, a guidance system that can operate independently from launch to impact would be desirable, and this might lead to an active system with higher transmitter power than would be required for terminal guidance only; however, the required power would probably not be high enough to cause serious problems in array design. Again, two-axis monopulse operation is strongly desirable.

For guidance of the advanced medium-range AAM (Figure 4), certain requirements for the guidance antenna could be relaxed from those of the dog fight AAM, but others could be more difficult. The tracking cone might be limited to 50°, but the missile velocity would probably be higher, resulting in higher nose temperatures. A somewhat sharper ogive (perhaps 3:1) would be desirable for aerodynamic reasons. A more consequential difference, however, might be a desirability of providing for as many as three modes of operation: semiactive and passive for midcourse guidance, and active and passive for terminal operation. The active and semiactive operations might be within the same frequency band but the passive operation would be at frequencies and polarizations dictated by specific enemy threats. Another difference might be the use of a continuous wave (cw) or other signal format rather than the more common pulse type.

Although the missile configurations and sizes might be significantly different, the terminal guidance for the long range AAM of Figure 5 and that for the previously discussed area defense SAM could be fairly similar. The chief difference might arise from the need to use a smaller radar to support midcourse guidance for the airborne weapon, and a consequent requirement for longer range terminal operation. This could lead to use of a larger antenna aperture and a higher frequency.

CRUISE MISSILES

Cruise missiles, which might be either air- or surface-launched, could also make use of various conformal antennas. These would be moderate or long range weapons that would typically be launched at a relatively safe standoff from enemy defenses. Two examples appear in Figures 6 and 7. The first of these might be configured to attack ships and the second to strike important land targets.

The cruise missile postulated in Figure 6 is one that uses a forward-directed, rapidly scanned, active seeker beam to acquire and track the target. Here the antenna is assumed to be conformal with a fixed ventral airfoil placed well forward on the missile. The suggested arrangement could give a wide aperture, and hence a narrow beamwidth, in the yaw plane. Operation would probably be at a very high microwave frequency.

Several much different types of conformal arrays are suggested by the missile configuration in Figure 7. The antennas shown in the nose and belly of the missile each feed signals to microwave radiometer

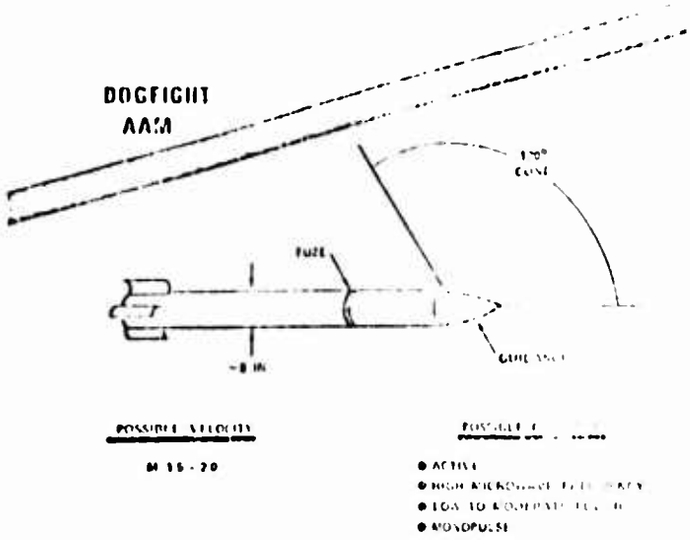

FIGURE 3

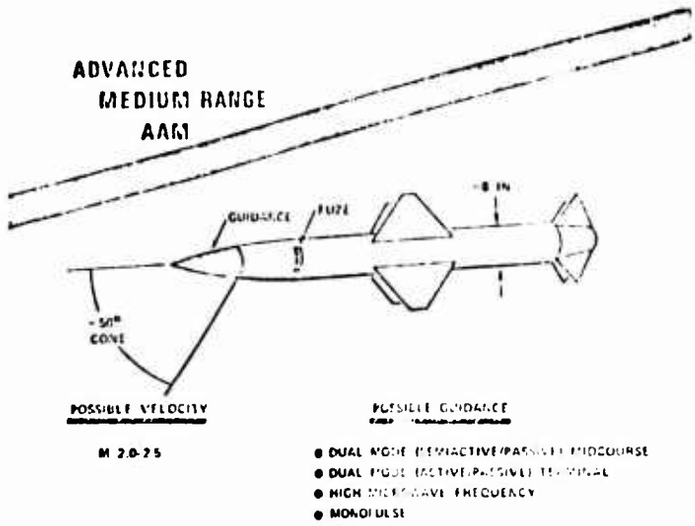

FIGURE 4

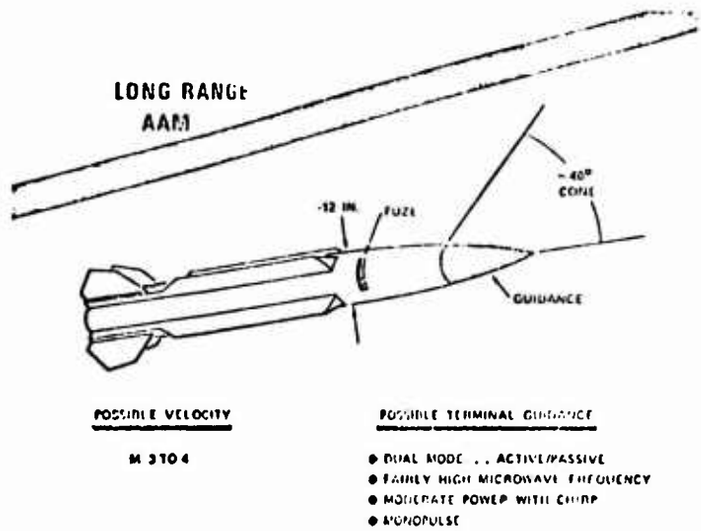

FIGURE 5

ACTIVE CRUISE MISSILE (ASM/SSM)

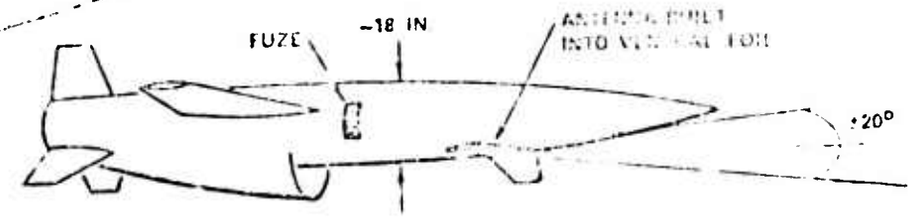

POSSIBLE VELOCITY

M 1.5

POSSIBLE GUIDANCE

- ACTIVE RADAR
- HIGH MICROWAVE FREQUENCY
- FORWARD LOOKING VERTICAL FAN BEAM RAPIDLY SCANNED IN AZIMUTH

FIGURE 6

PASSIVE CRUISE MISSILE (ASM/SSM)

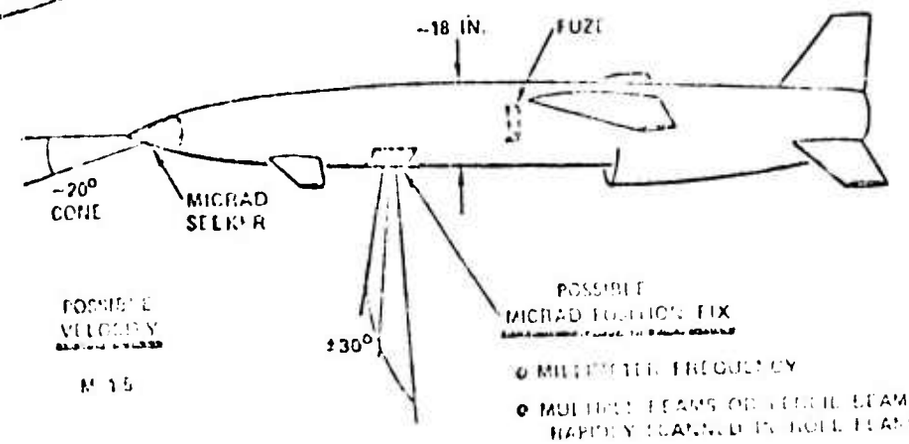

POSSIBLE VELOCITY

M 1.5

POSSIBLE MICRAD POSITION FIX

- MILLIMETER FREQUENCY
- MULTIPLE BEAMS OR RECTILINEAR BEAM RAPIDLY SCANNED IN ROLL PLANE

(MICRAD) receivers. These passive MICRAD signals are essentially white noise within a relatively broad reception band established by the respective receiver, and thus they offer no sustained phase coherency on which to base phase relationships over a wide aperture. That is, for an antenna with an aperture that is many wavelengths in width, the formation and control of a narrow receiving beam must depend on broad-band focussing techniques such as provided by lenses, rather than on techniques that depend on specific values of phase shift from element to element. For the cruise missile application that is shown, the MICRAD system in the belly develops data to aid the missile navigation by scanning the terrain below, while the system in the nose serves a homing function. Missile-borne MICRAD systems will typically operate at millimeter frequencies.

REMOTELY PILOTED VEHICLES

Although the Navy has not evidenced an interest in remotely piloted vehicles (RPVs) to the same extent as the Air Force and Army, these small, unmanned aircraft have the potential to expand the capabilities of the surface Navy in a number of missions. Primarily, they offer ships smaller than carriers an opportunity to operate airborne platforms and extend the horizon limits of sensors without certain limitations that would be imposed by helicopters. Two naval RPV applications are illustrated in Figures 8 and 9. The first of these shows an application for a sea control mission, and the second for operations against littoral areas.

In Figure 8 a medium size RPV carries a radar or pair of radars that scan a large swath of ocean surface on both sides of the vehicle as the latter moves forward along a prescribed path. Conformal arrays of the size noted (or perhaps larger) would provide fan beams that normally could look directly to port and starboard of the RPV, but might be angled as much as 30° ahead or behind under remote control in order to concentrate the scan on a particular area or target of interest. To provide detection of distant targets a high peak power would be used. A middle microwave band would appear to offer an advantageous frequency choice.

The similar RPV that is shown in Figure 9 has no radar but instead is equipped for all-weather reconnaissance of land areas by use of a MICRAD system. It is shown with a conformal array that would have the same design restraints related to a noise-like signal that were noted in the case of the cruise missile MICRAD application above. For the RPV use illustrated, a pencil beam would be required to rapidly scan the terrain below the missile as the latter moved forward at high speed (necessary for survival), and thereby would accumulate a MICRAD "photograph" of the region traversed.

PATROL AIRCRAFT AND HELICOPTERS

As compared to the Figure 8 system, a more complete ocean surveillance function, using other sensors as well as radar, could be performed by a manned patrol aircraft as illustrated in Figure 10. Moreover, patrol aircraft missions would include such activities as locating small objects amid sea clutter, and these would influence radar and antenna designs. Thus the antennas sketched in Figure 10 are to combine to provide 240° search coverage in the yaw plane, and, in comparison with

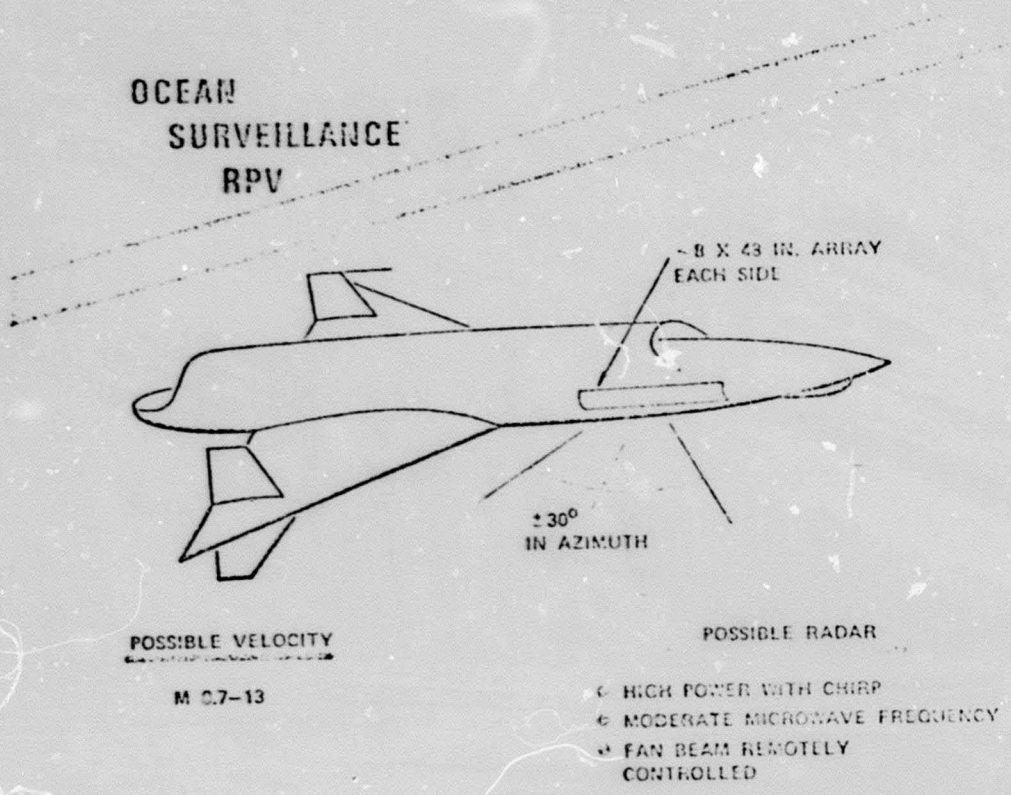

FIGURE 8

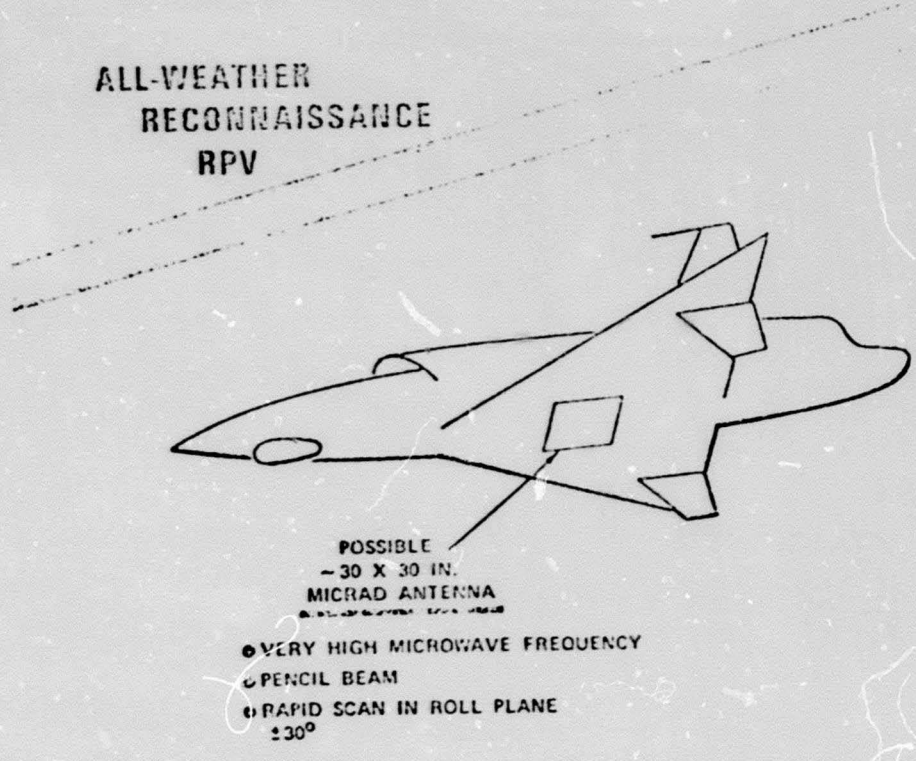

FIGURE 9

the RPV, a somewhat higher frequency might be selected to provide increased resolution. To adapt to a variety of missions, most of the remaining radar parameters might be variable.

A helicopter with a conformal radar is shown in Figure 11. This might perform surface search functions similar to those of the above patrol aircraft, but generally at much shorter range. For search and rescue missions it would be necessary to detect small objects (such as a downed pilot) in choppy seas, and such detection would typically require a narrow beam and very short pulse to obtain a satisfactory signal-to-clutter ratio. From an aerodynamic standpoint, the value of a conformal antenna is not nearly as great for a helicopter as it is for the missiles and high-speed RPVs previously discussed. However, conformal arrays could still be of high interest because of weight savings, better reliability and maintenance (no moving parts), and possibly reduced cost as well. (This statement with respect to aerodynamics might also apply to the above patrol aircraft, but to a lesser extent.)

FIGHTER AIRCRAFT

Potential advantages of conformal arrays to high performance fighter aircraft are readily apparent. Two such applications are brought forth in Figures 12 and 13. A vertical take-off and landing (VTOL) fighter as shown in Figure 12 could benefit by use of a conformal nose array for its basic airborne intercept (AI) radar, with a dual mode operation also providing passive direction finding (DF) on incoming signals from enemy radars. The active radar operation might be at a moderately high band, while the passive DF operation would, of course, be matched to enemy threat bands and appropriate polarizations. For ease in detecting targets flying at low altitudes over a cluttered sea, the AI operation might involve pulse doppler (PD) signal formats. In a VTOL aircraft it is of great importance to limit equipment weight, and this is a parameter in which a conformal design might markedly excel a more conventional approach.

While dual mode operation of the equipment in the VTOL nose might serve for detecting enemy radar signals arriving from the forward hemisphere and thereby warn the pilot of special threats, conformal radar warning (RW) antennas and related receivers elsewhere in the aircraft would be desirable for rear hemisphere coverage. Details of such requirements are classified, however.

For a catapult-launched (i.e., non-VTOL) high performance fighter, a possible application of conformal array technology might lie in making feasible a fairly long range warning radar without introducing an unacceptable aerodynamic penalty. As is indicated in Figure 13, such a fighter could fly as an escort to strike missions or serve a combat air patrol (CAP) role near Fleet units without receiving targeting support from the relatively slow, single purpose, airborne early warning aircraft. In other words, the suitably arrayed escort or CAP fighter could maintain surveillance of the air space through some 270° in much the same way that the above patrol aircraft provides an ocean surveillance function. High power transmission would be required, and operation might be at a middle microwave frequency.

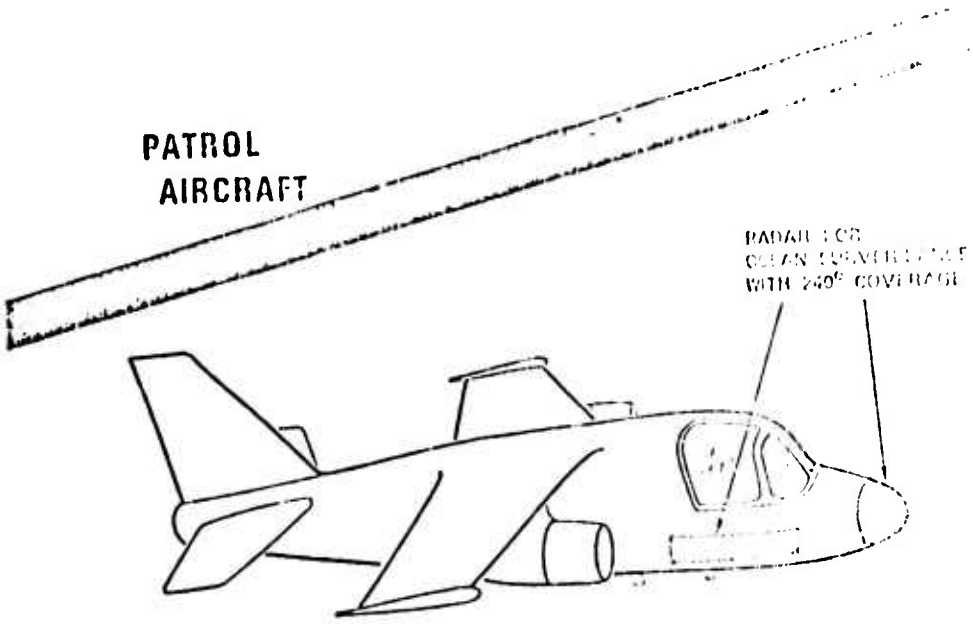

POSSIBLE PARAMETERS

- PULSED WITH HIGH PEAK POWER
- FAIRLY HIGH MICROWAVE FREQUENCY
- VARIABLE PW AND PRF
- VARIABLE COMPRESSION RATIO

FIGURE 10

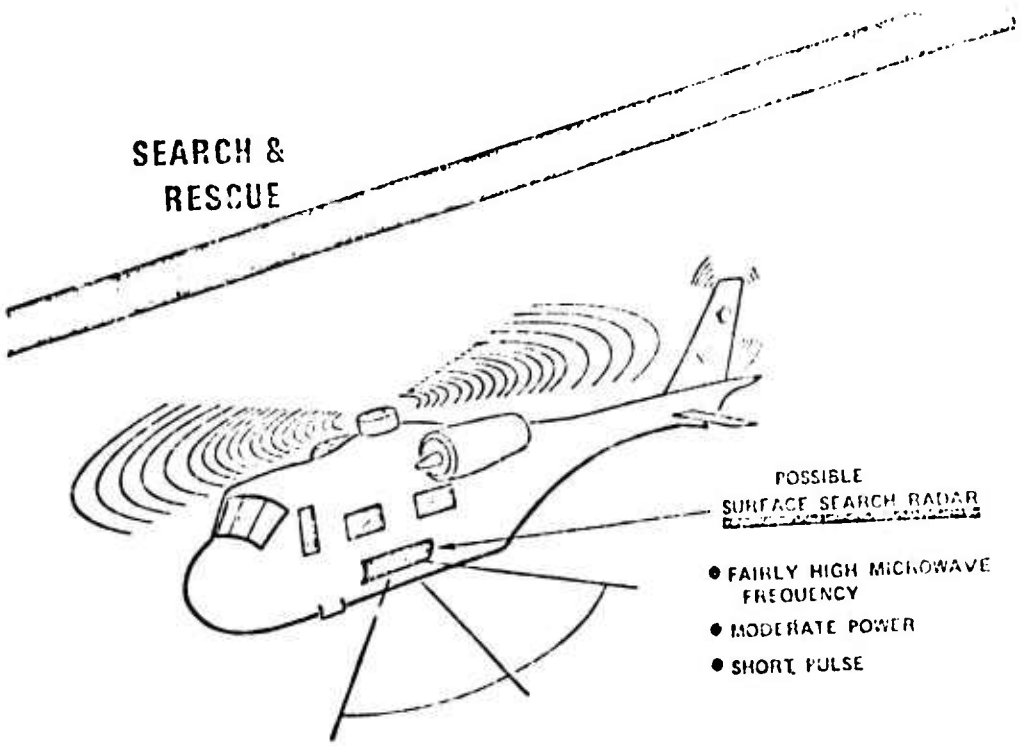

FIGURE 11

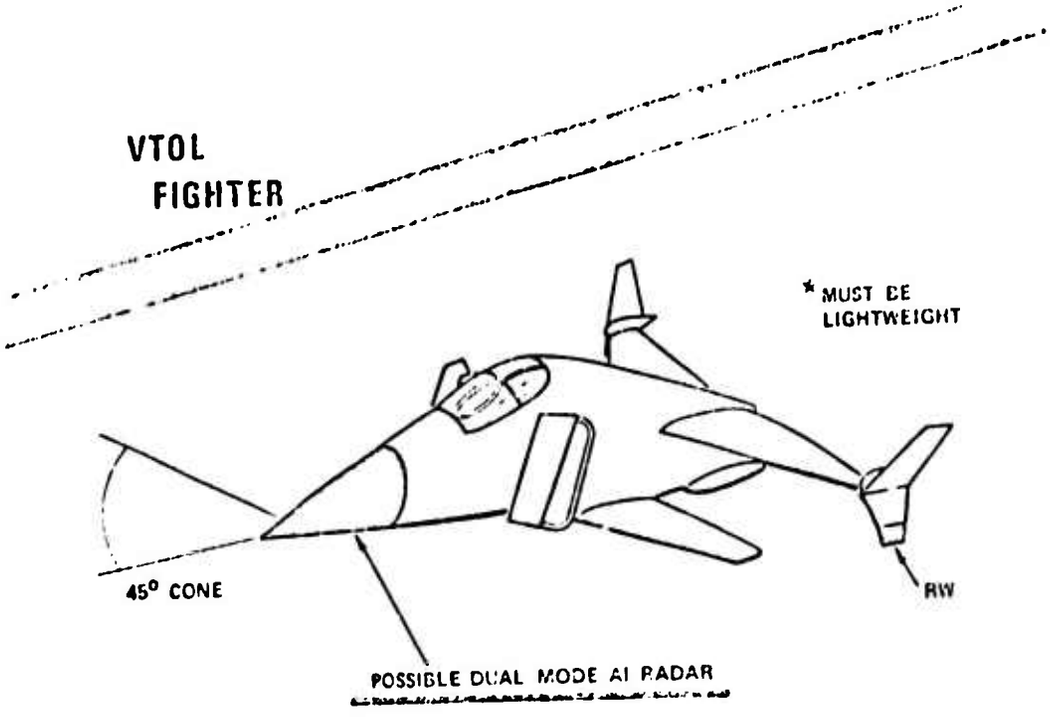

FIGURE 12

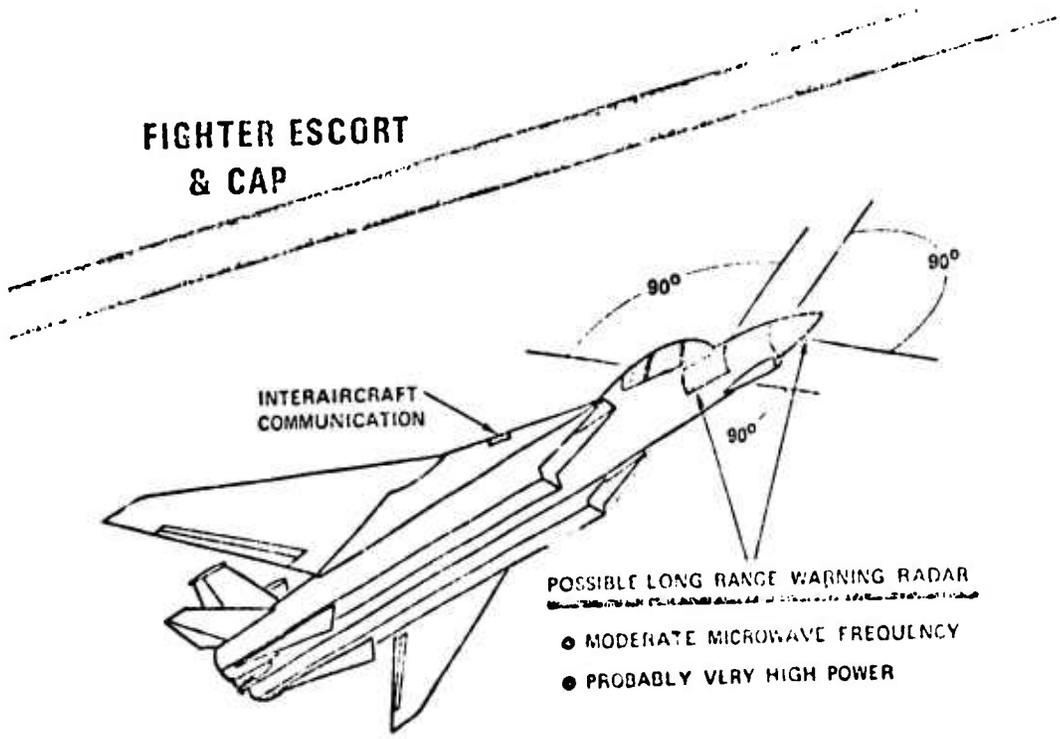

FIGURE 13

ATTACK AIRCRAFT

A remaining group of applications for conformal arrays relates to aircraft for attacking surface targets. These aircraft may be engaged in any of a variety of missions: (1) close air support (attacking enemy troops in immediate contact with own forces); (2) general air support (attacks on enemy ground forces in the overall battle area); (3) armed reconnaissance (locating and, if advisable, attacking enemy ground forces and logistic elements wherever they might be found); (4) interdiction (disrupting the flow of enemy supplies to the battle area); and (5) air strikes (attacks on factories, refineries, power houses, etc., that contribute to the enemy's war making capacity). A variety of Naval and Marine Corps fixed wing aircraft and Marine helicopters carry out such missions.

Close air support might be rendered by a "gunship" helicopter or by certain fixed wing aircraft. The gunship concept, together with a conformal radar for operation in foul weather, is illustrated in Figure 14. A wide antenna aperture, a high microwave frequency, and a very short pulse are combined to give the very high resolution at short range that is essential to this type of operation. A moderate power would suffice, but the conformal array must perform a rapid electronic scan through as much as ±30° in azimuth to "paint" a detailed radar picture from which the pilot or gunner can identify and attack the desired target.

A use of conformal arrays in general air support or armed reconnaissance is suggested in Figure 15. The configuration shown postulates a Navy adaptation of the Air Force A-10 which has limited space in the nose of the aircraft because of a large gun that is carried. In this case a ground search radar function might be implemented by a conformal antenna on one of the wheel housings as shown. The radar characteristics could be similar to those of the gunship radar discussed above, but with a smaller aperture the resolution would be lower. However, this might be acceptable where targets are generally larger and the immediate proximity of own troops is not a problem.

Aircraft used in all-weather strikes and interdiction operations might be aided by the conformal array designs suggested in Figure 16. Besides arrays for interaircraft communication and radar warning, a fairly large MICRAD antenna is shown on the underside of the aircraft. If it can withstand the environment, a thin conformal array might be located at the position shown (below the engine intake and just forward or aft of the nose wheel) where a conventional antenna, such as a feed system and parabolic reflector, would be out of the question. From this vantage location the MICRAD system could derive aircraft position fixes and provide all weather data in support of targeting without revealing the aircraft's position by active transmissions. A very narrow pencil beam is necessary to reveal desired terrain details from altitudes of interest, and a rapid scan is necessary to gain all the desired data before the aircraft moves on. Lightness in weight is again desirable.

Yet another application of conformal array technology that might aid attack aircraft would be in helping to implement a standoff reconnaissance capability as indicated by Figure 17. Here a synthetic array radar carried in a pod develops detailed radar data on a strip of terrain

MARINE GUNSHIP

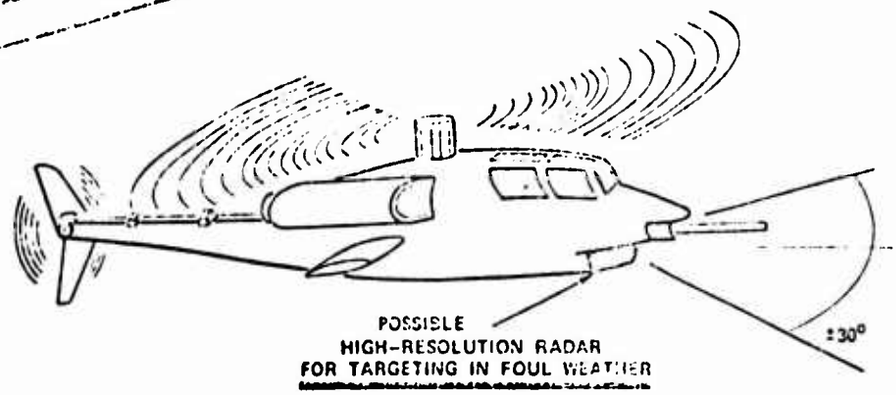

- HIGH MICROWAVE FREQUENCY
- MODERATE POWER
- VERY SHORT PULSE

FIGURE 14

ARMED RECONNAISSANCE

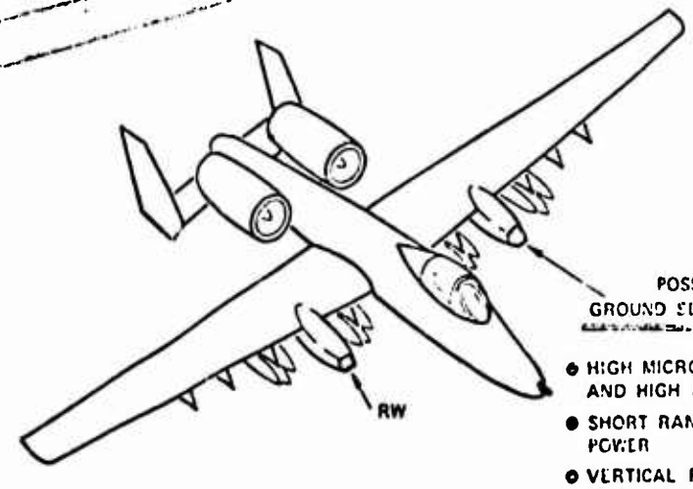

- HIGH MICROWAVE FREQUENCY AND HIGH RESOLUTION
- SHORT RANGE, MODERATE POWER
- VERTICAL FAN BEAM WITH RAPID AZIMUTH SCAN THROUGH ±20°

FIGURE 15

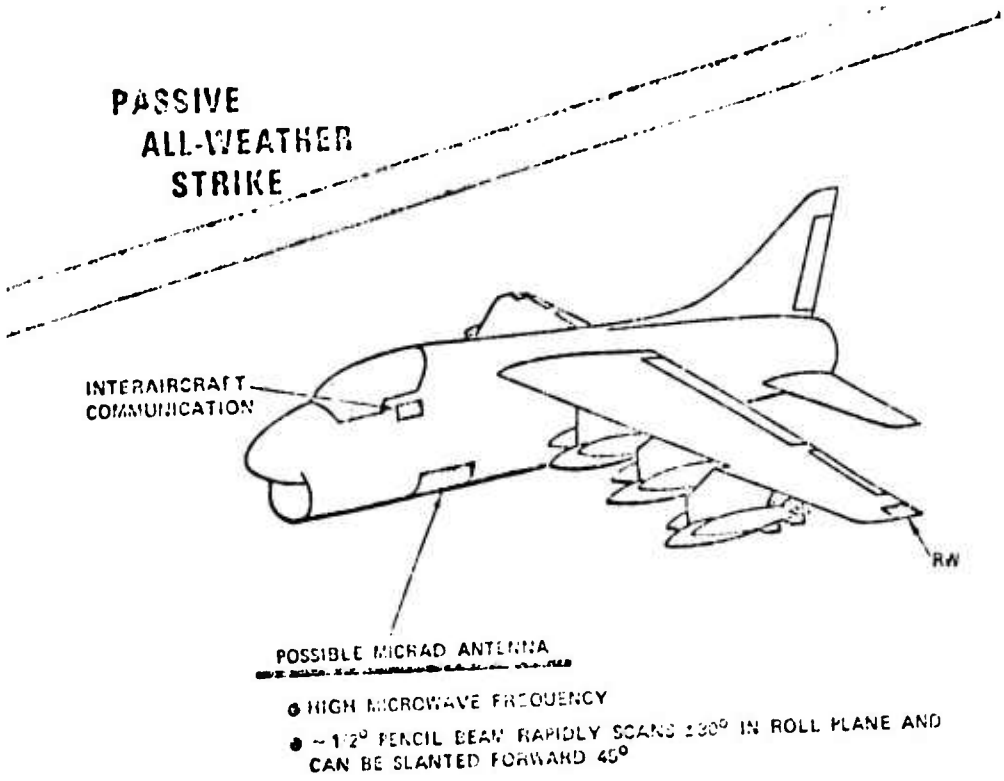

FIGURE 16

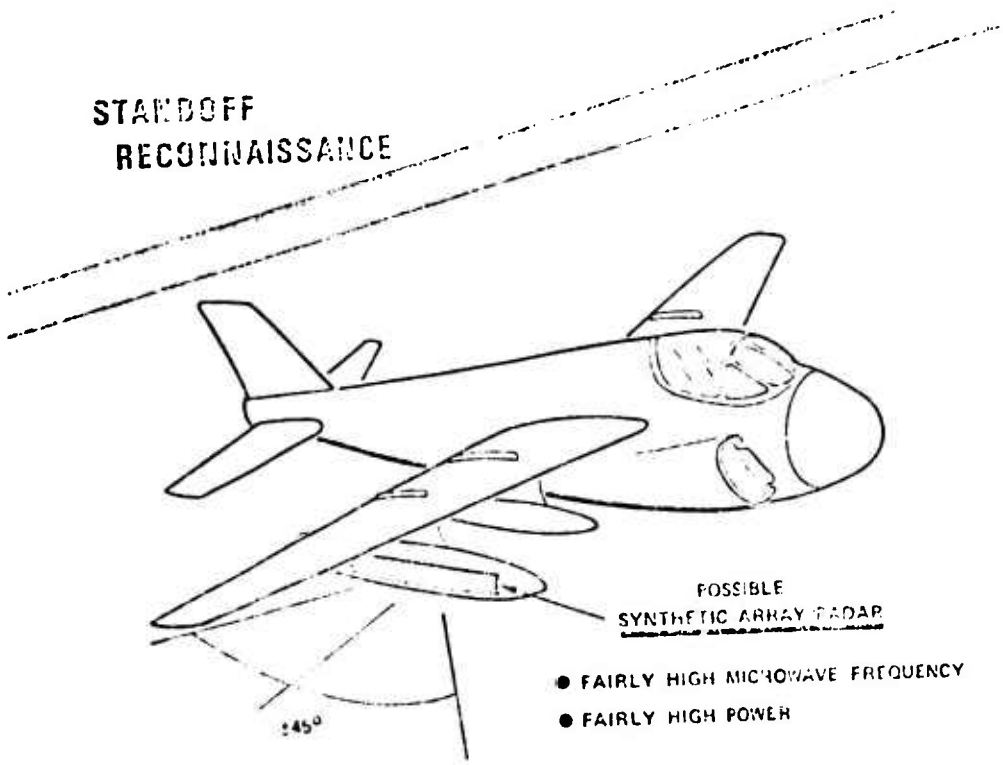

FIGURE 17

far off to starboard of the aircraft as the aircraft flies a prescribed flight path parallel to that strip. The conformal antenna approach would allow all necessary components, including a fairly powerful transmitter, to be carried within a reasonable size pod. (The antenna and other radar components might have been shown imbedded in the fuselage of the aircraft itself, except current Navy policy does not favor aircraft specially configured for reconnaissance duty.) An added requirement would probably be that the radar beam be slewable fore and aft perhaps 45° in order to allow a prolonged or repetitive look at a terrain area of particular interest.

CONCLUSIONS

A successful maturing of conformal array technology can contribute very significantly to future tactical missiles, RPVs, and manned aircraft systems for the Navy. Aside from the obvious advantages in form factor and aerodynamics that a conformal design can provide, advantages in reliability and maintenance (no moving parts) and in lightness in weight can be highly important. A variety of functions may be performed: missile guidance, missile fuzing, missile and aircraft position fixing, all-weather reconnaissance, airborne intercept, surface search, radar warning, and others. Frequencies of interest appear to stretch from the middle to the very high microwave bands, depending upon particular applications. Some needs call for narrow pencil beams and others for fan beams, and nearly all require a beam scanning or tracking capability, with the scanning generally being rapid--beyond speeds normally associated with mechanically scanned antennas. A particular challenge can be found in conformal antennas for MICRAD devices where the signal is noise-like and broadband, so that precision element-to-element phasing techniques may be unworkable.

POLARIZATION REQUIREMENTS FOR CONFORMAL ARRAYS

W. H. Kummer
Hughes Aircraft Co.
Culver City, CA 90230

Introduction

This paper is concerned with the polarization problems resulting from the use of radiating elements located on non-planar surfaces.

If a planar phased array is considered with all the radiating elements oriented to produce a given polarization, then the radiated polarization of a pencil beam will be that of the radiating element projected in the beam pointing direction. In other words, the element pattern can be factored from the summation in the equation for the radiated far field. If linearly polarized elements are used in an array for a radar system, then linear polarization will be transmitted and linear polarization will be received irrespective of the depolarization of the returns from the targets. For tracking, a monopulse system can be formed by dividing the array into four equal parts and using the output from each part appropriately to generate one sum channel and two difference channels. The depth of null, or tracking accuracy will depend on the antenna design: e.g., factors such as tolerances and fineness of phase control available on the phase shifting devices.

The conformal or non-planar arrays can be separated into several generic shapes such as the wedge, the cylinder, the cone and the sphere. The cylinder and cone will be discussed.

Cylindrical Arrays

For the pupose of this paper it will be assumed that the radiating elements will be equally spaced in azimuth and will be located in elevation on generatrices of the cylinder. As far as the limits of scan in azimuth, we may distinguish two cases: a scan of 360° in azimuth and a scan less than $\pm 90^{\circ}$ In the first case, the best design is to have physical symmetry for the layout of the radiating elements, (Fig. 1), so that all elements are oriented parallel to the generatrices. Since only part of the radiating elements contribute significant energy in the beam pointing direction, only that useful fraction of the elements is excited. This set of elements, the active sector, is commuted around the array as the beam is scanned in azimuth. Thus there is physical symmetry about the plane containing the beam pointing direction. In the second case the active array includes all the radiators, and phase scanning is used to obtain beam motion in azimuth. A combination of the two techniques is also possible.

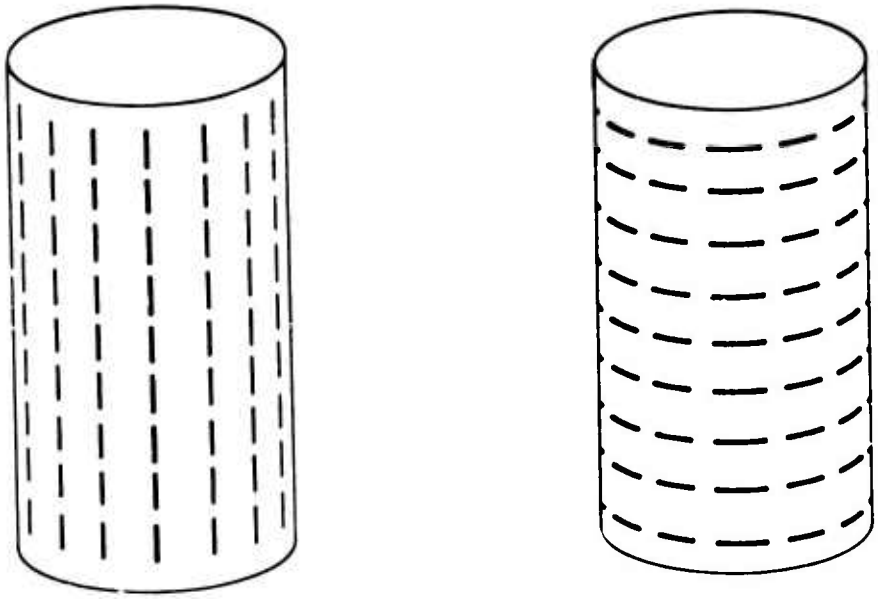

Fig. 1 Cylindrical Antenna Array
a) Axial Slots, b) Circumferential Slots

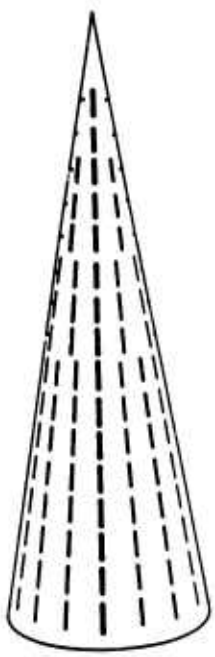

Fig. 2 Conical Array with Radial Slots

In the first technique, the physical symmetry assures that the sum pattern will be symmetric for symmetric excitation.

Linearly polarized elements such as axial or circumferential slots can be used as the radiating elements. These are linearly polarized elements. However, since these physically realizable elements are not isotropic, the amplitudes will be different in directions away from the beam pointing direction. The element pattern cannot be separated from the array factor as was the case for the planar array.

If we establish difference patterns in the azimuth and elevation planes there will be no cross polarization generated for a beam perpendicular to the generatrix (a broadside beam). If the beam is scanned in elevation, the polarization radiated by the elements located on the central generatrix will still be unchanged. The polarization from all other elements will be rotated with respect to the central generatrix. For the sum pattern the polarization will still be parallel to the central generatrix. For the difference patterns the antenna will respond to a cross polarized component.

If we examine the second case where the beam is scanned both in azimuth and elevation from the broadside direction, then there will be tracking errors for most beam positions. For a beam scanned in azimuth the amplitude from each quadrant will be the same if the elements are omnidirectional in that plane. Thus each quadrant will have equal excitation and there will be no tracking error. The scan cannot exceed one-half of the arc of the active sector; otherwise, some elements will be shadowed. If the elements are directional in that plane, then the amplitudes from the quadrants symmetrical about the generatrices will be unequal and no null will be obtained.

Conical Surfaces

If we now place the same array configuration on a conical surface, we encounter polarization problems even for a broadside beam. Broadside is the direction of a beam perpendicular to the generatrix centered in the active part of the array.

Circumferential slots will generate a polarization component parallel to the cone axis. This fact can be seen by examining Figure 2. However, a component perpendicular to the cone axis will also be generated for slots not on the central generatrix. For the sum pattern this cross-polarization component will vanish in the beam pointing direction. For the azimuth difference pattern, the cross-polarized component will peak. If there is a cross-polarized component in the incident field, there will be null filling and the possibility of a null shift. The same problem occurs for the elevation difference pattern with an additional complication. In order to obtain equal amplitude one must use unequal areas that generate the elevation difference patterns. Similar arguments hold for radial slots.

In the general case, the return signal, irrespective of its polarization, will give rise to two patterns in the difference port. Each pattern is weighted by the field strength of that particular polarization. There will be a pattern with a null in the beam pointing direction and a second pattern with a peak. Similarly, there will be two patterns in the sum port. For symmetrical excitation the one pattern will have a null and will not affect the boresight of the sum beam. In general, both sum and difference channels will respond to the cross polarized component.

Thus, the creation of sum and difference patterns in the conventional way using elements with fixed polarizations is not appropriate for conical arrays. Variable polarization for the radiating elements is one straightforward solution. Other methods have also been suggested.

Discussion of a Symmetrical Multibeam Feed Networks for Circular Arrays

Paul Shelton

Naval Research Laboratory

Introduction

This paper reviews a paper presented by the author at the first Conformal Array Antenna Conference held in January 1970.[1] Two errors in the original paper are pointed out, and the implications of these errors on the circular array symmetrical multifeed synthesis technique are discussed.

Review of Synthesis Technique

The reference paper sought a feed structure for generating multiple beams from a circular array which would have the same symmetry as the array. The proposed method takes transmission lines from the radiators and arrays these lines into cylindrical sets of parallel-coupled regions, an example of which is sketched in Figure 1. The synthesis procedure considers the aperture distribution in terms of the orthogonal eigenfunctions of the circular array. These functions are uniform amplitude distributions with progressive phase characteristics. It is possible to calculate the far-field phase of these eigenfunctions, and it is also possible to calculate the phase delay of the eigenfunctions through the coupling networks. Because of the circular symmetry of the

1. J.P. Shelton, "A Symmetrical Multibeam Feed Network for Circular Arrays", Conformal Array Antenna Conference, January 1970.

coupling networks these eigenfunctions apply to both the array and the networks. It was shown that the number of degrees of freedom required to focus the eigenfunction radiation patterns into a maximum-gain beam is N/2, corresponding to the number of coupled regions. A set of equations of the form,

$$\theta(i) - \theta(0) = -\sum_{k=1}^{N/2} 2c(k) \sin^2\left(\frac{ik\pi}{N}\right), \qquad (1)$$

was derived, where $\theta(0) = \sum_{k=1}^{N/2} 2c(k)$,

and $c(k)$ = coupling strength of kth region,

$\theta(i)$ = phase of ith eigenfunction,

N = number of elements in array.

It was stated that Equations (1) can be solved by matrix inversion, and a sample synthesis was performed. The resulting c(k) were positive and negative, and procedures were presented for obtaining c(k) of all one sign.

Errors in Original Paper

The synthesis technique described in the original paper and reviewed briefly above has (at least) two errors. First, the solutions of Equations (1) by matrix inversion, although normally the correct technique for solving a set of simultaneous equations, is an error in this case because the matrix elements are Fourier components. Thus, a straightforward Fourier analysis serves to solve for the c(k).

Second, solutions were sought for which all c(k) are of the same sign under the tacit assumption that only positive c(k) can be realized in practice. Actually, either plus or minus c(k) can be realized by the

technique shown in Figure 2. If a given c(k) is obtained for a set of parallel-coupled transmission lines, the coupling - c(k) can be obtained by introducting π phase shift into alternate lines on each side of the coupling region. Note that this technique applies only to coupling regions with even number of transmission lines. Thus, to be assured that the technique is always applicable, the number of elements in the circular array must be $N = 2^P$.

Discussion

The use of Fourier analysis to solve for the coupling coefficients does not alter the results of the original paper. It simplifies the computation of the coupling coefficients.

The ability to realize both positive and negative coupling coefficients materially alters the results of the original paper. It is found that the total coupling strength, i.e., the sum of the coupling coefficients, is approximately equal to the total coupling that would be used in a Butler-matrix fed multibeam circular array

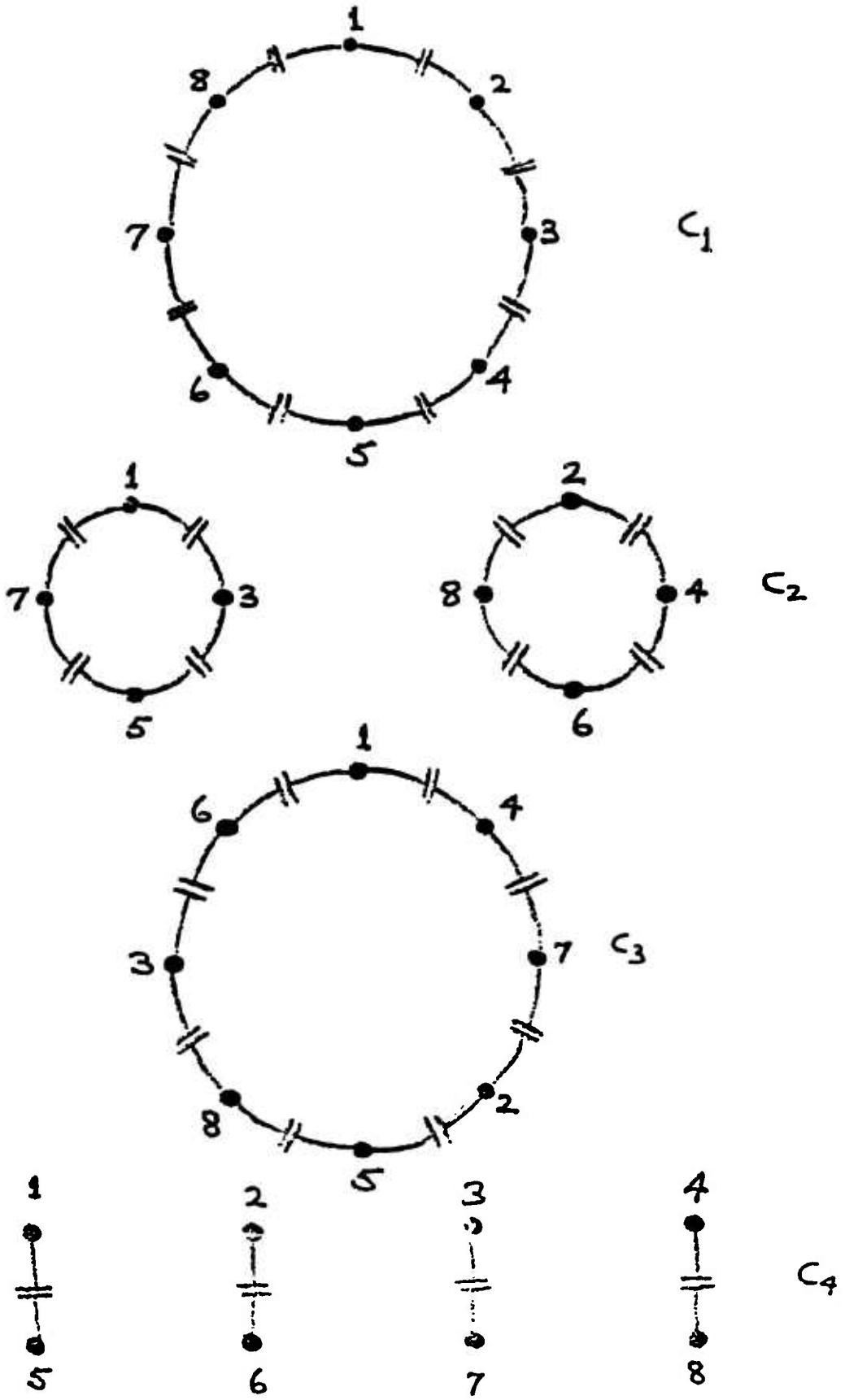

FIG. 1. MULTIPLE COUPLING REGIONS

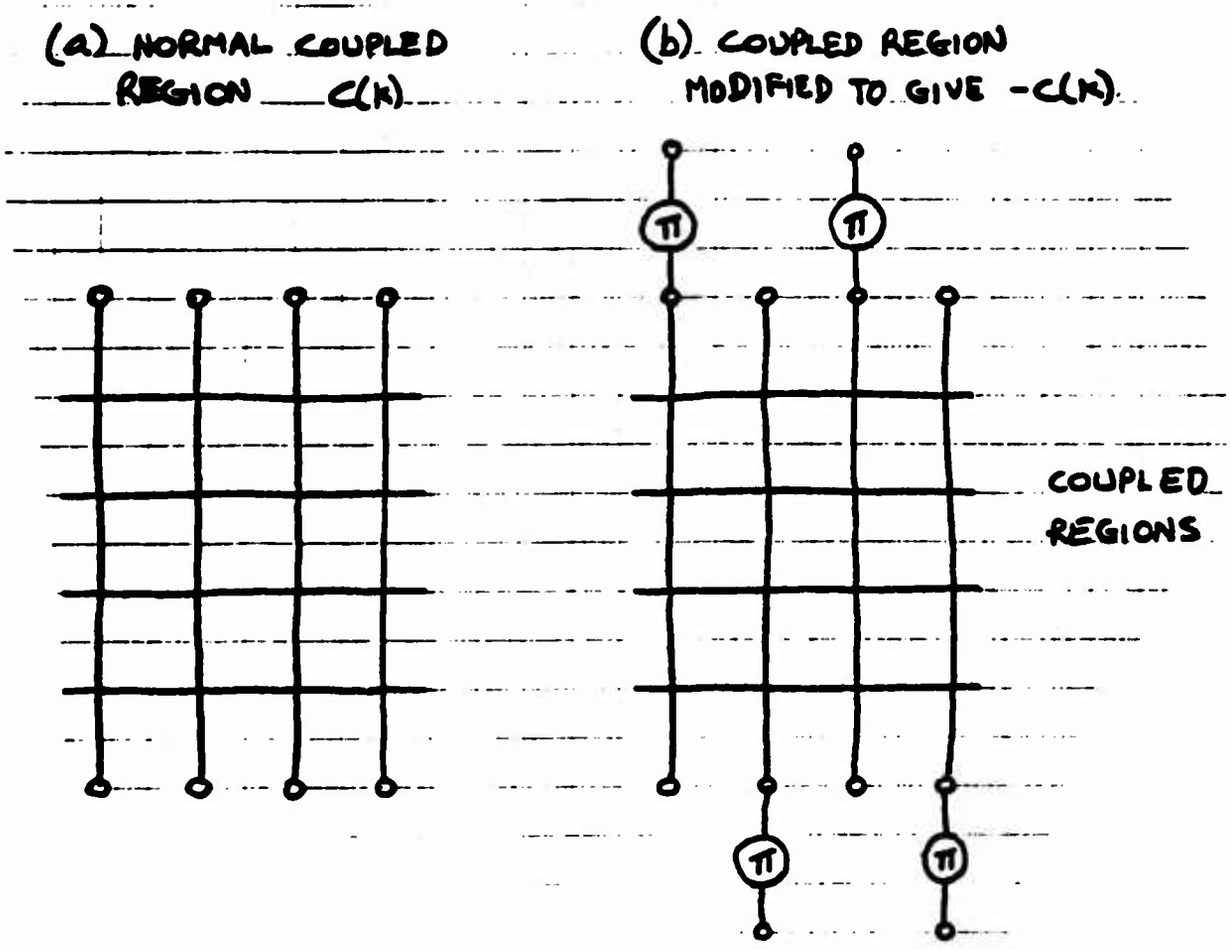

FIGURE 2. COUPLING REGIONS FOR PRODUCING BOTH POSITIVE AND NEGATIVE COUPLING COEFFICIENTS

CONICAL ARRAYS, STUDIES AND EXPERIMENT

A. T. Villeneuve
Hughes Aircraft Co.
Culver City, CA 90230

1. Introduction

The purpose of this paper is to present a summary of studies that have been conducted at Hughes Aircraft Co. on pattern analysis and synthesis for slots on conducting conical surfaces. The study reported here has consisted of several parts, which will be described herein. The parts may be classified as follows: Heuristic pattern synthesis techniques; equivalence principle pattern synthesis technique; modal series solution for the total radiation fields from circumferential and radial half-wave slots; asymptotic solution for the total radiation fields from circumferential slots.

2. Pattern Synthesis Techniques

Each antenna application has certain coverage requirements that dictate pattern characteristics to be approximated. For example, the beamwidth, sidelobe level and polarization of pencil beam patterns may be specified, and the antenna excitation must be determined to provide the desired pattern.

For arrays on planar surfaces, well known techniques are available to synthesize the required sources. Even for arrays on cylindrical and spheroidal surfaces, sources can be synthesized, at least in theory, by projecting the required cylindrical or spheroidal wave functions from the farfield back to the array surface. However, for most curved surfaces no synthesis techniques are available. Heuristic techniques can be used to form beams in specified directions by proper phasing of elements and by using a projected aperture concept to taper amplitudes in an attempt to control beamwidth and sidelobes, and for some surfaces with small curvature this technique may work well. However, accurate control of beamwidth, sidelobe levels and polarization is difficult for most curved surfaces.

A method of element excitation that leads to maximum gain for independently fed elements, is the adjustment of the amplitudes of the elements in proportion to the relative field strength of their patterns in the beam pointing direction. This weighting may be termed optimum weighting. It does not provide sidelobe control and, depending on the selection of active aperture shape, may not give equal E-plane and H-plane beamwidths. In order to achieve a desired polarization in the beam pointing direction when the beam is movable, a variable polarization element must be used. A small circular aperture or a crossed-slot element has this property. The latter has been used in calculating patterns. A number of patterns have been calculated for optimum weighting and various beam pointing directions. (Kummer, Seaton, Villeneuve 1973) They provide well defined beams and, depending on the number and arrangement

of elements their sidelobe levels may be kept low. Some examples of patterns from crossed slots located as shown in Figure 1 are shown in Figure 2 through 5. The patterns were calculated using simplified approximate element patterns that neglected tip diffraction. For the radial slots, they were essentially approximations to element patterns of slots on cylinders, while for the circumferential slots, the patterns of slots on planes were used. Figure 2 is an E-plane pattern of a beam along the cone axis. Figure 3 is essentially the corresponding H-plane pattern. It shows that the E-plane and H-plane beamwidths are not the same, even though the projected apertures in both planes are the same. The correct excitation to equalize these beamwidths is not evident from the heuristic approach. The effective grating lobes near the broadside direction are a consequence of the element spacing. They are eliminated by using more closely spaced elements. Figures 4 and 5 are, respectively, E-plane and H-plane patterns for a θ polarized beam normal to the cone generatrix. The notation used corresponds to the IRIG Standard (1966). Once again the so-called optimum excitation results in unequal E-plane and H-plane beamwidths. Cut and try methods can be used to adjust them for equality.

An alternative to the heuristic approach is one that may be termed the equivalence principle approach. (Kummer, Villeneuve, 1969) Using this approach it is possible to approximate prescribed patterns whose correct sources can be determined on some prescribed surface, for example, on a planar surface.

The problem is that of producing the pattern of a conventional antenna, as illustrated in figure 6 by sources on a curved surface. Let the conventional antenna be represented by a source distribution $\bar{J}_i$, $\bar{M}_i$ of electric and magnetic current distributions that produce the desired fields E,H as illustrated in Figure 7.

If the actual sources are surrounded by a closed mathematical surface S, the fields $\bar{E}$, $\bar{H}$ exterior to S will result if the actual sources are replaced by equivalent sources $\bar{J}_s$ and $\bar{M}_s$ on S where

$$\bar{J}_s = \bar{n} \times \bar{H}$$

$$\bar{M}_s = \bar{E} \times \bar{n}$$

and $\bar{n}$ is the exterior unit normal to S as illustrated in Figure 8 (Harrington, 1961). The equivalent sources produce no fields within S. Consequently, the mathematical surface S may be replaced by a perfectly conducting surface that lies just inside the equivalent source currents $\bar{J}_s$ and $\bar{M}_s$ without affecting the external fields $\bar{E}$, $\bar{H}$ as shown in Figure 9. It can be demonstrated that electric source currents on the surface of a perfect conductor do not radiate. The total field outside the surface may then be found from the magnetic currents $\bar{M}_s$ radiating in the presence of the conductor as shown in Figure 10. Consequently, if the proper equivalent magnetic source currents can be synthesized on the conducting surface, the original field will result at all points exterior to the surface. In the case of interest the original source may be a planar array and the metal surface is a

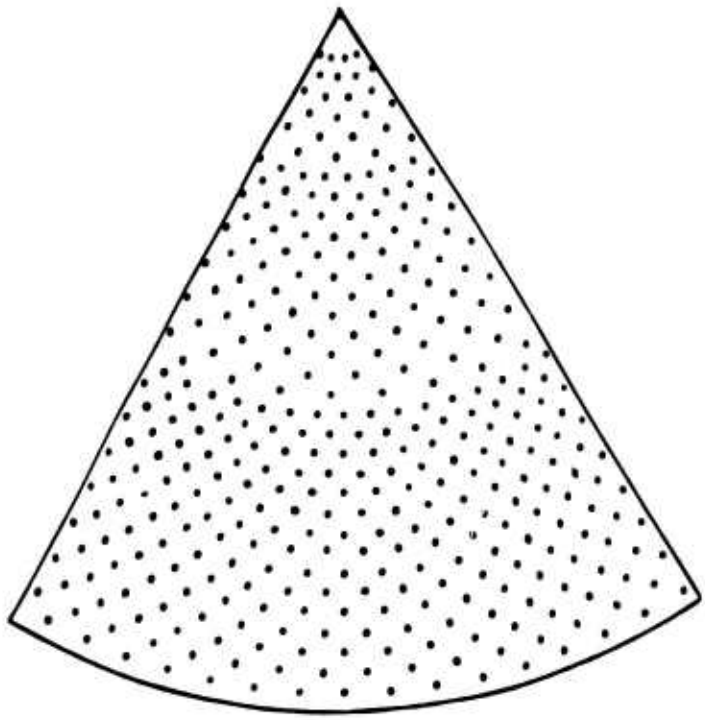

Fig. 1 Scale Drawing of Centers of Phase of the Elements on the Cone for the 360 Element Configuration

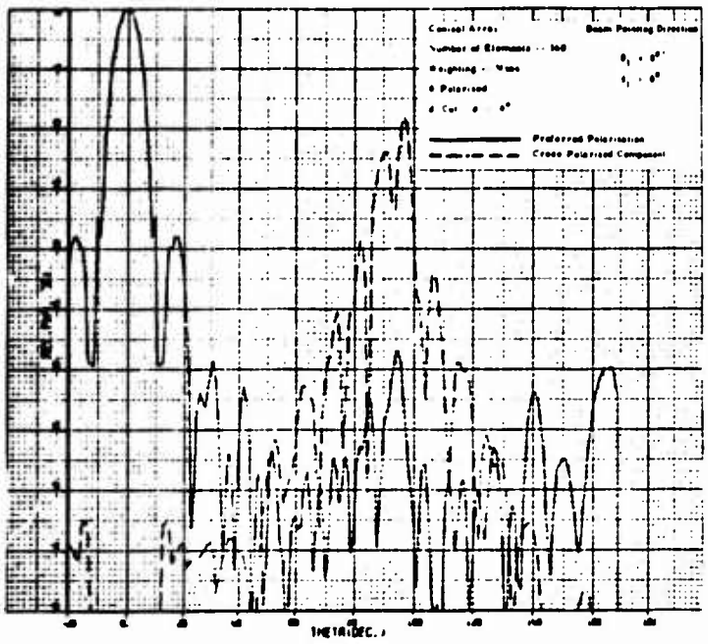

Fig. 2 θ-Polarized Pattern of a Nose-Fire Beam for a 360 Element Configuration

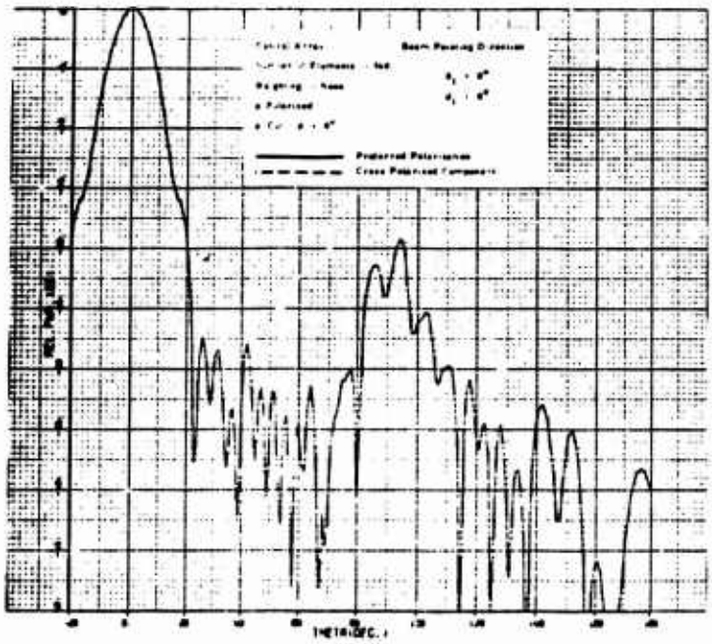

Fig. 3 ϕ-Polarized Pattern of a Nose-Fire Beam for a 360 Element Configuration

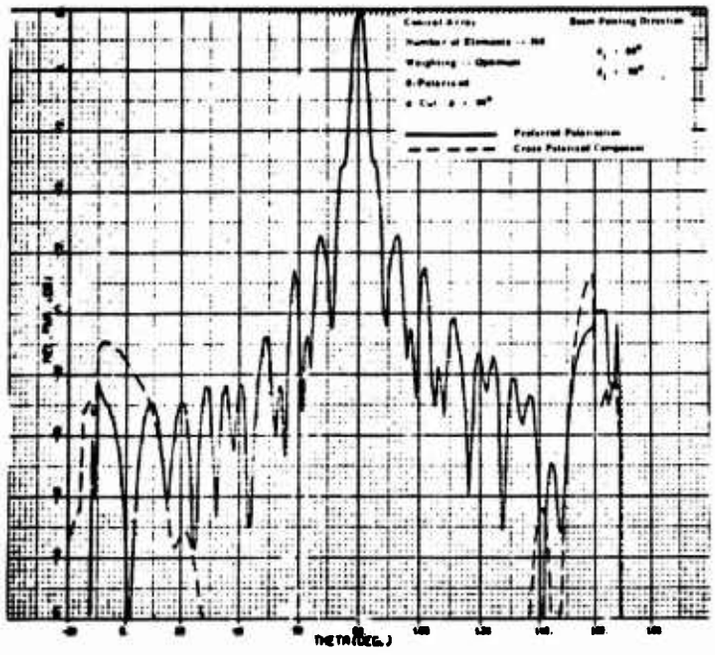

Fig. 4 θ-Polarized Pattern of Principal Plane Cut Through a Broadside Beam -- 360 Elements

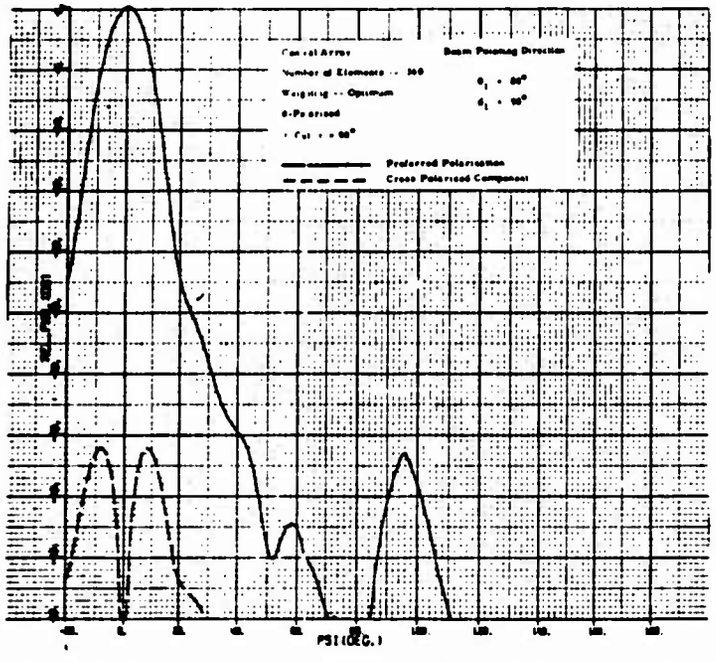

Fig. 5 θ-Polarized Pattern of a Principal Plane Cut ($\tau = 90^{\circ}$) Through a Broadside Beam -- 360 Elements

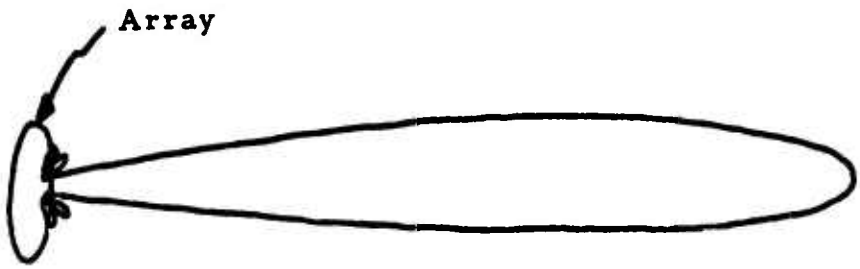

Figure 6. Array with Conventional Pattern

Figure 7. Sources and Resulting Fields

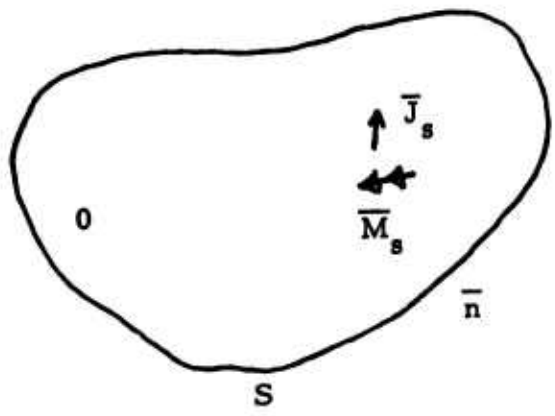

Figure 8. Equivalent Sources on Mathematical Surface

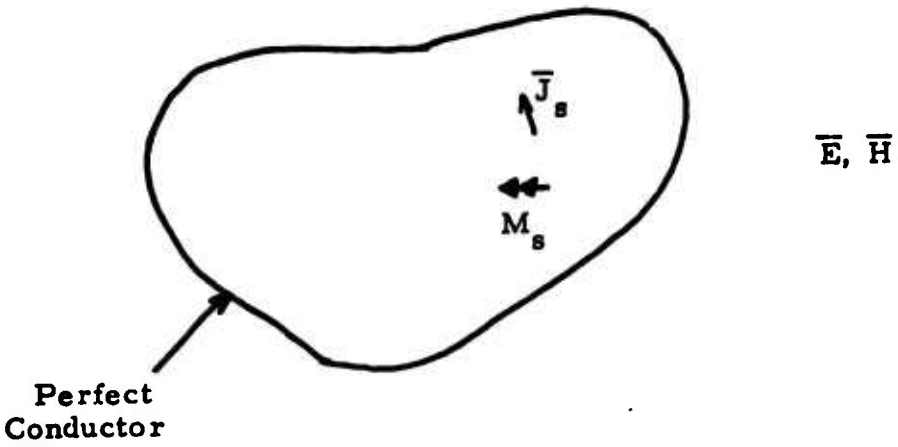

Figure 9. Equivalent Sources on Conducting Surface

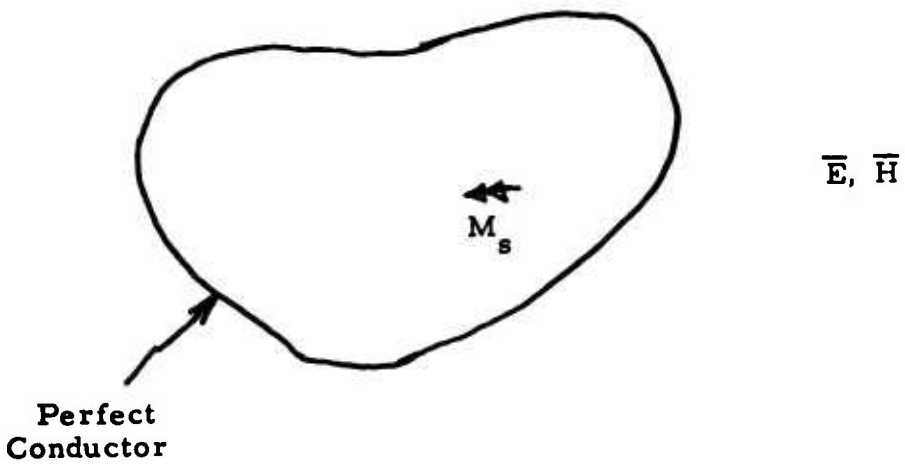

Figure 10. Equivalent Magnetic Sources on Conducting Surface

conical or ogival surface. The magnetic current sheets are surface distributions of magnetic dipoles. A magnetic dipole can be approximated by a slot on a conducting surface. Consequently, by properly orienting and exciting slots on the metallic surface the desired exterior field can be approximated. The required source distribution is known exactly since the initial fields are known.

The field equivalence principle has been used to synthesize beams from slots on a cone with a half-angle of 10 degrees. (Kummer, Seaton, Villeneuve, 1973) The desired pattern selected to illustrate the technique is that of a planar array consisting of 24 half-wavelength slots on a circular groundplane. The slots were spaced at 0.7 wavelength intervals on a square grid as illustrated in Fig. 11. The calculated E-plane and H-plane patterns of the planar array are shown in Fig. 12.

The cone on which the equivalent sources were placed has an angle, θ_o, of 170 degrees and a base diameter of 5.08 wavelengths. The sources on the cone were short crossed-slots arranged in rings about the cone. The adjacent rings were separated 0.7 wavelengths, with the first ring 0.7 wavelength from the tip. The azimuthal spacing of the crossed slots in the rings varied between 0.5 wavelength and 0.7 wavelength.

The pattern computation was performed in two steps. First, the equivalent sources on the cone were computed by determining the field of the planar array on the conical surface. Then the pattern of these equivalent sources was computed. In the pattern computations an approximate element pattern was used i.e., if the slot is visible from the field point, the element pattern is that of a short slot in a groundplane tangent to the cone; if the element is not visible, the element pattern is zero.

Patterns were calculated for two cases:

a. the beam directed along the cone axis
b. the same beam directed 70° from the cone axis with vertical polarization.

The E-plane and H-plane patterns for case (a) are shown in Figs. 13a and 13b. The coordinate system θ', ϕ', used to display the patterns, is oriented so that the beam pointing direction is $\theta' = 90^\circ$, $\phi' = 0^\circ$. The E-plane cut is taken through the beam with ϕ' held at 0°; the H-plane cut is taken through the beam with θ' held constant at 90°. It is apparent that the beamwidths agree well with those of the desired patterns, though in the region of the first sidelobe the synthesized pattern has a sidelobe only 16 dB down in the H-plane and 20 dB down in the E-plane, whereas the first sidelobe of the desired patterns is about 32 dB down in both planes. The remaining sidelobe levels are about the same for the synthesized patterns as for the desired patterns.

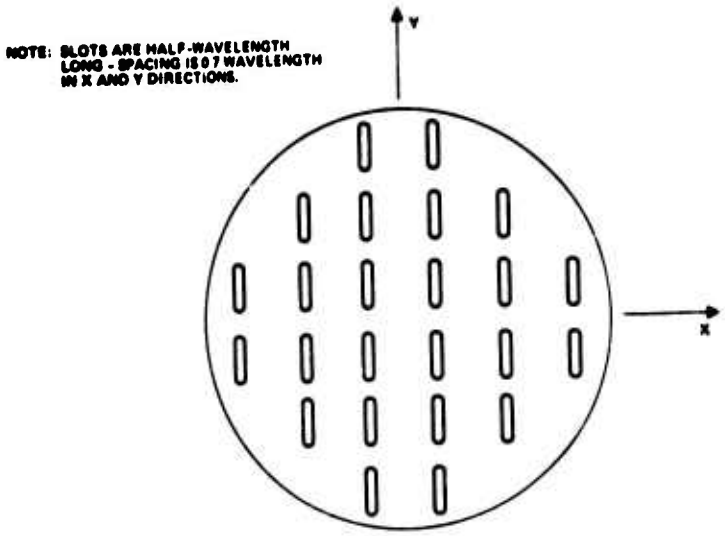

Figure 11. Reference Planar Array

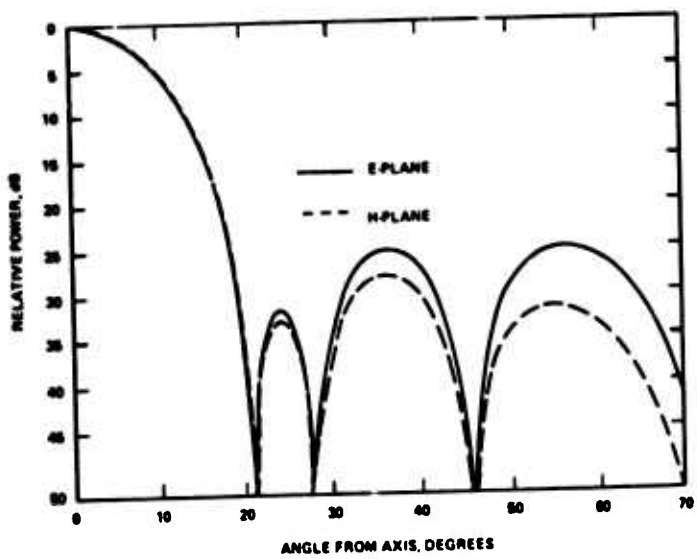

Figure 12. Patterns of Reference Planar Array

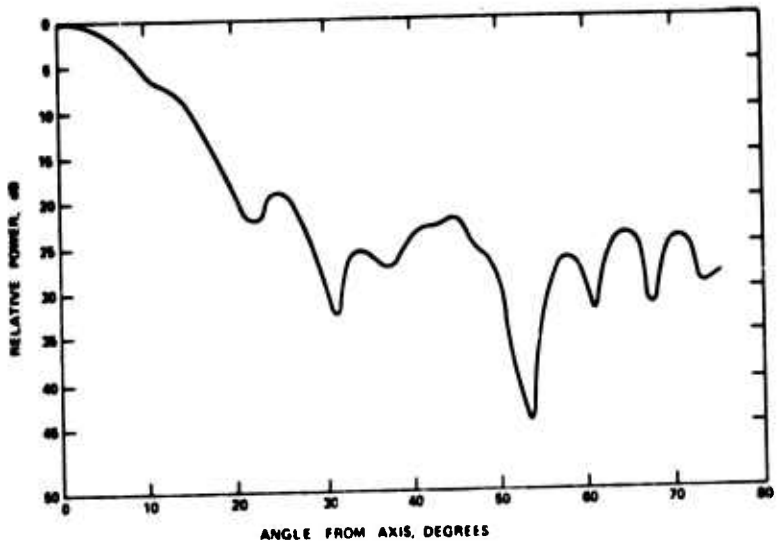

Figure 13a. E-Plane Pattern of Synthesized Beam Along Cone Axis

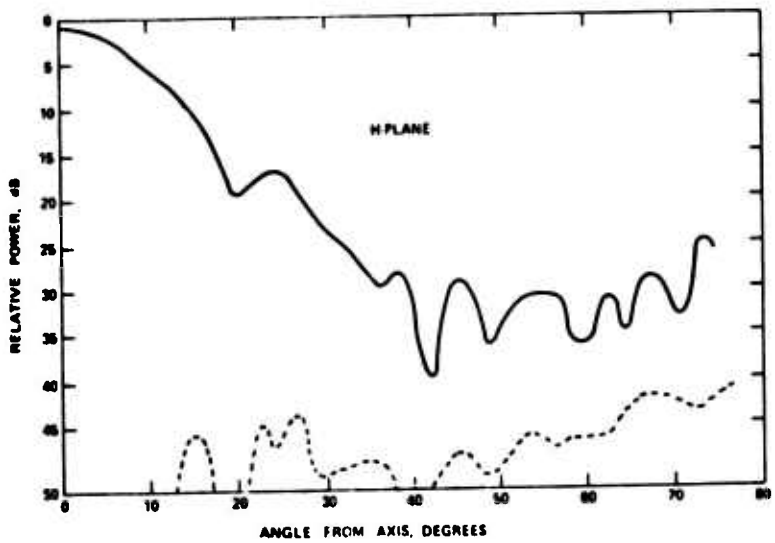

Figure 13b. H-Plane Pattern of Synthesized Beam Along Cone Axis

There are several reasons for the discrepancies between the desired patterns and the synthesized patterns. First, the sources of the synthesized patterns are discrete, whereas the required sources are continuous. Second, the element patterns used were only approximate patterns and do not account for the cone curvature or scattering by the cone tip. For the beam directed along the cone axis, the slots near the tip are strongly excited and tip scattering may be significant. The equivalence principle automatically includes these effects in determining the source distributions and, if they were accounted for in the element patterns, better agreement between synthesized patterns and desired patterns should result. Consequently, studies of improved element patterns were undertaken and are discussed in Sections 3 and 4. When the beam is steered away from the cone axis the tip region is not strongly illuminated and the effects of tip scattering should not be so significant. This effect is illustrated in Figs. 14a and 14b, which show the synthesized patterns for case (b). The agreement between the desired patterns and the synthesized patterns is excellent. The main beams agree very closely and the sidelobe structures are also in good agreement. This agreement is especially good in the H-plane, since the element patterns used for computation in that plane are closer to the correct element patterns. It is evident that the cross-polarized patterns are at very low levels. In the E-plane the symmetry of the slot arrangement on the cone cancels out any cross-polarization. In the H-plane the symmetry is not maintained at points away from the beam peak, but the excitations as determined from the equivalence principle, keep the cross-polarized patterns at a low level.

These calculations indicate that the equivalence principle can be a powerful tool when applied to the synthesis of antenna patterns from general conformal arrays. When combined with the more accurate element patterns discussed in Sections 3 and 4, a more precise assessment of its utility will be possible.

3. Modal Series Solution

The radiation fields from sources on conducting conical surfaces can be expressed as a series of modes that are characteristic of those surfaces. Bailin and Silver (1956, 1957) published an early analysis of such configurations and more recently Pridmore-Brown and Stewart (1972) presented results of analysis and computations for the θ-component of the radiation field of circumferential slots on conducting cones. The analysis and computations have been extended (Bargeliotes, Kummer and Villeneuve 1974, Bargeliotes 1974a, b) to include both the θ-component and the ϕ-component of fields from both circumferential and radial half-wavelength slots. Figure 15 illustrates the conical geometry and slot coordinates.

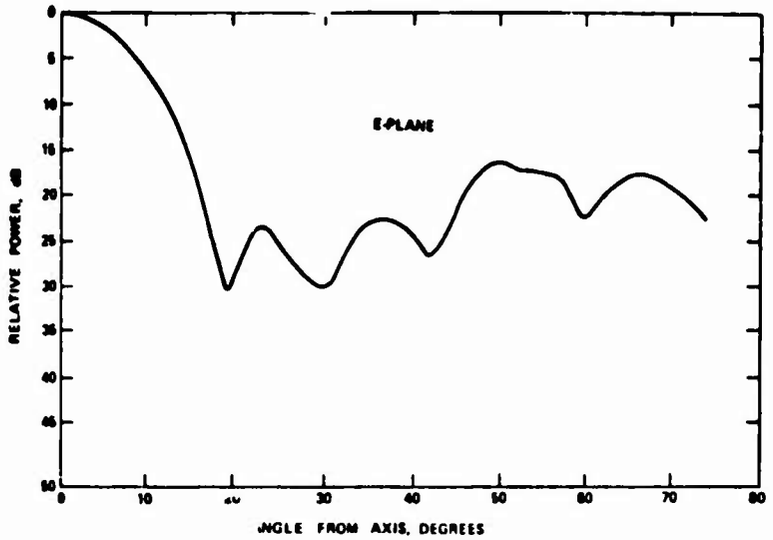

Figure 14a. E-Plane Pattern of Synthesized Beam 70° Off Cone Axis

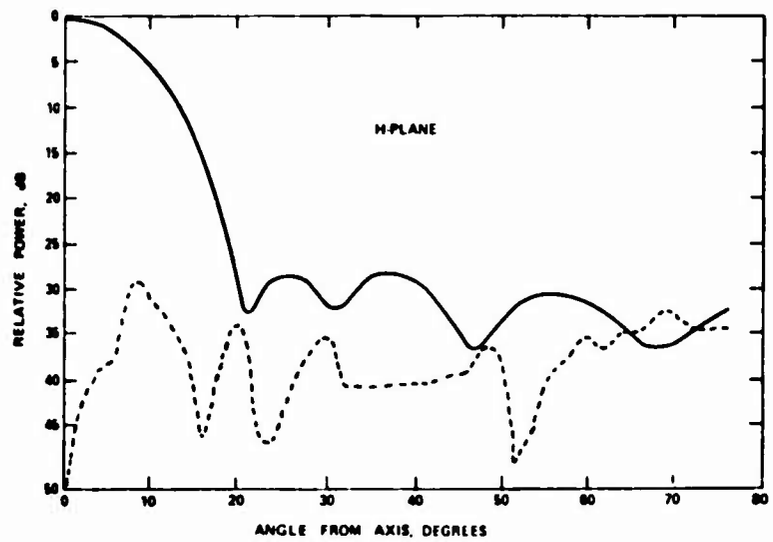

Figure 14b. H-Plane Pattern of Synthesized Beam 70° Off Cone Axis

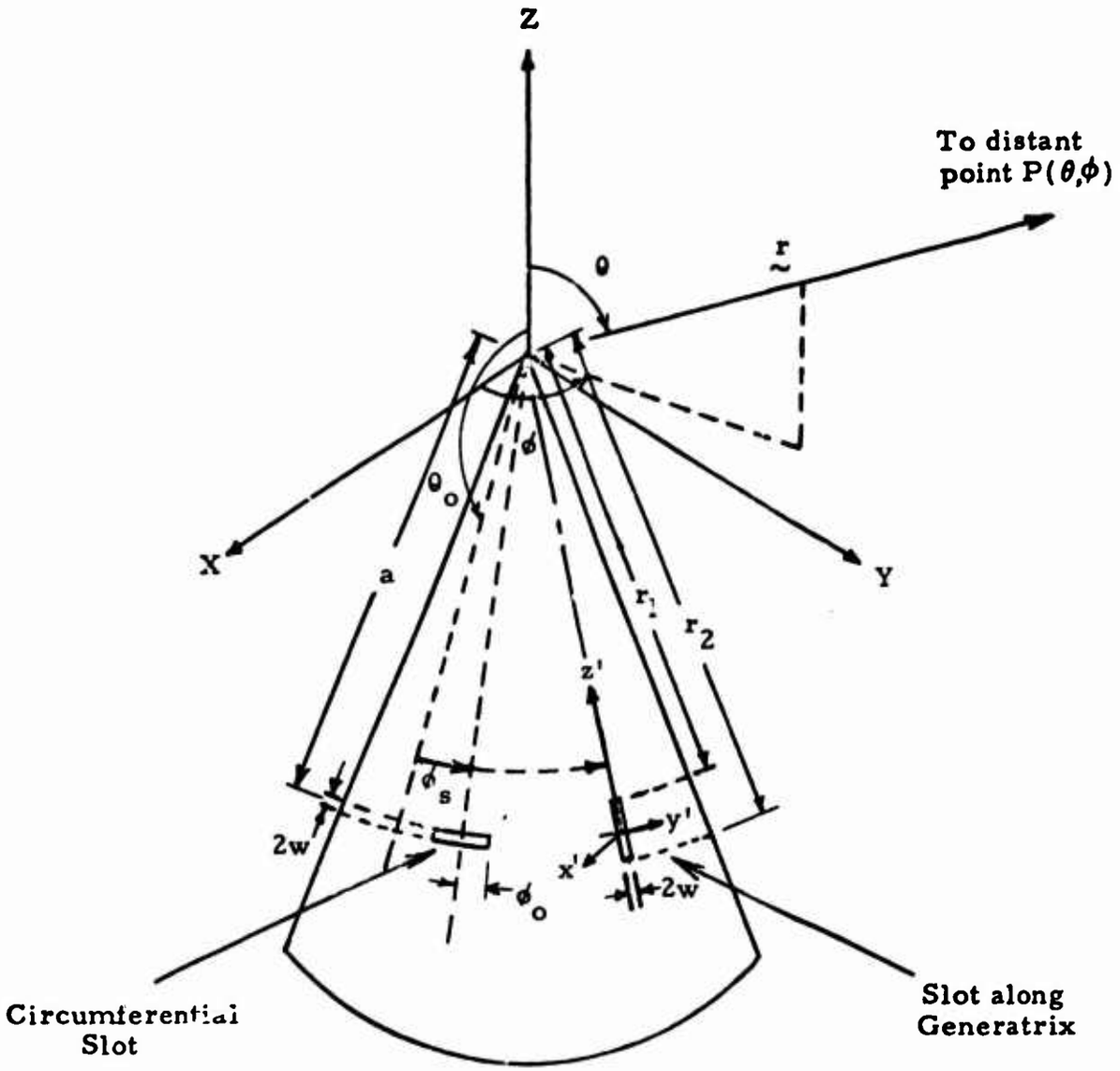

Figure 15. Conical Geometry and Slot Coordinates

The P_μ^q (cos θ) are the associated Legendre functions of degree μ and order q, the J_ν (x) are Bessel functions of the first kind and order ν, and k is the phase constant. The ν_i are the roots of the equation

$$P^{-m}_{\nu-\frac{1}{2}} (\cos \theta_o) = 0$$

and the ν_i' are roots of the equation

$$\frac{\partial P^{-m}_{\nu-\frac{1}{2}} (\cos \theta_o)}{\partial \theta} = 0$$

It is pointed out that the θ-dependence is represented by the Legendre function $P^{-m}_{\nu-\frac{1}{2}}$ (cos θ) instead of P^m_ν (cos θ). This choice simplifies the evaluation of the Legendre function on the digital computer and is preferred. Also, except for a constant factor of $1/\pi$, the expression for E_θ agrees with that reported by Pridmore-Brown and Stewart (1972) derived by the Kontorovitch-Lebedev transform method.

3.2 Radial Slot

A narrow slot of width 2 w<< circumference is assumed to be positioned along a generatrix of the cone and extends from r_1 to r_2 as shown in Figure 15. It is further assumed that the length of the slot, $(r_2 - r_1)$, is such as to allow definition of the ends of the slot by constant ϕ'. The slot is excited by a voltage V_o' resulting in an electric field in the ϕ-direction given by

$$E_\phi = V_o' \frac{g(r')\,\delta(\phi')}{r' \sin \theta_o}$$

The function g(r') describes the variation of the source excitation in the r' direction. The electric field components are as follows:

$$E_\theta = \frac{V_o' e^{-j(k r - \pi/4)}}{r \sin \theta_o} \sum_{m=1}^{\infty} j \sqrt{\frac{2}{\pi}} \; m \sin m\phi \; \frac{1}{\sin \theta} P_\theta$$

$$E_\phi = \frac{V_o' e^{-j(k r - \pi/4)}}{r \sin \theta_o} \sum_{m=0}^{\infty} j \sqrt{\frac{2}{\pi}} \; \frac{\cos m\phi}{(1 + \delta_{om})} P_\phi$$

where

$$P_\theta = \sum_{i=1}^{\infty} \nu_i' j^{\nu_i'} \frac{P_{\nu_i'}^{-m} - 1/2 (\cos \theta)}{\frac{\partial^2 P_{\nu - 1/2}^{-m}(\cos \theta)}{\partial \nu \partial \theta}} \Bigg|_{\substack{\theta = \theta_o \\ \nu = \nu_i'}} \cdot \int_{r_1}^{r_2} \frac{g(r')}{r'} \frac{J_{\nu_i'}(k r')}{\sqrt{k r'}} \, dr'$$

$$P_\phi = \sum_{i=1}^{\infty} \nu_i' j^{\nu_i'} \frac{\frac{\partial}{\partial \theta} P_{\nu_i'}^{-m} - 1/2 (\cos \theta)}{\frac{\partial^2 P_{\nu - 1/2}^{-m}(\cos \theta)}{\partial \nu \partial \theta}} \Bigg|_{\substack{\theta = \theta_o \\ \nu = \nu_i'}} \cdot \int_{r_1}^{r_2} \frac{g(r')}{r'} \frac{J_{\nu_i'}(k r')}{\sqrt{k r'}} \, dr'$$

3.3 Patterns

Numerous radiation patterns have been computed for half-wave slots with ka equal to 39. on a cone of half-angle 10^o, that is, slots 6.22 wavelengths from the cone tip with θ_o equal to 190 degrees. Patterns were measured for the same configurations and there was excellent agreement between measurements and calculations. Figure 16 through 19 are patterns for a circumferential slot. The departure of measured and calculated values for θ near 180^o results from the fact that the base of the experimental cone was imbedded in absorbing material that blocked the incident radiation, while the calculated patterns do not account for that effect.

Figures 20 through 24 are patterns for a radial slot. Once again the agreement is excellent and the effect of the absorber is evident for θ near 180^o. The asymmetry of the measured pattern in Figure 24 is attributed to improper polarization adjustment of the transmitting horn.

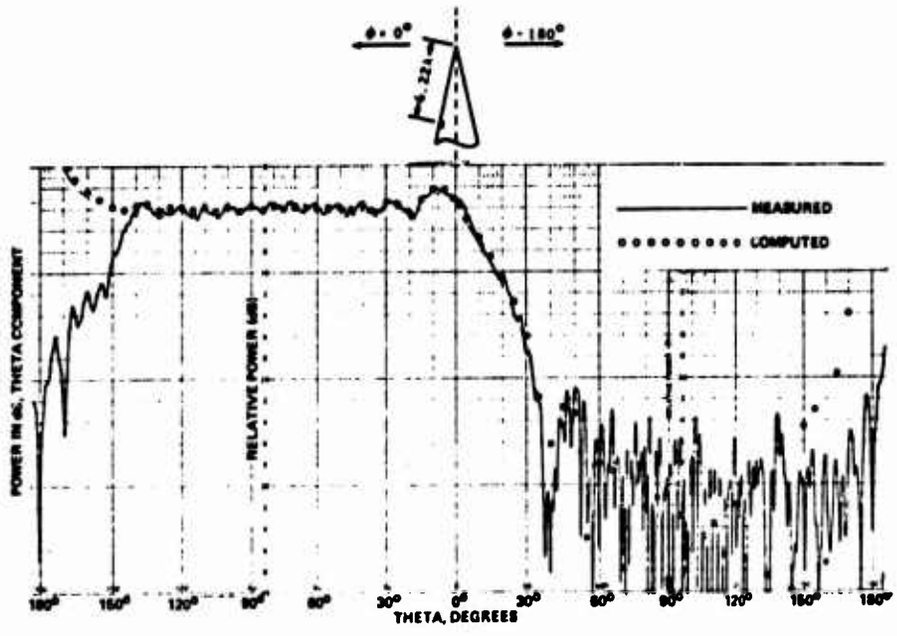

Figure 16. Measured and Computed θ-Polarized Patterns of λ/2 Circumferential Slot for $\phi = 0^{o}$, $\phi = 180^{o}$

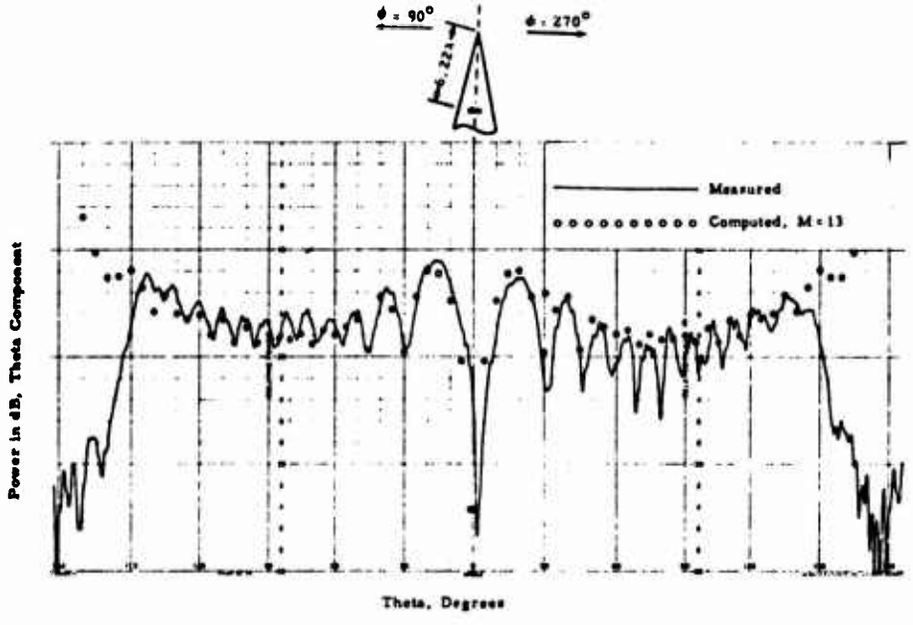

Figure 17. Measured and Computed θ-Polarized Patterns of λ/2 Circumferential Slot for $\phi = 90^{o}$, $\phi = 270^{o}$.

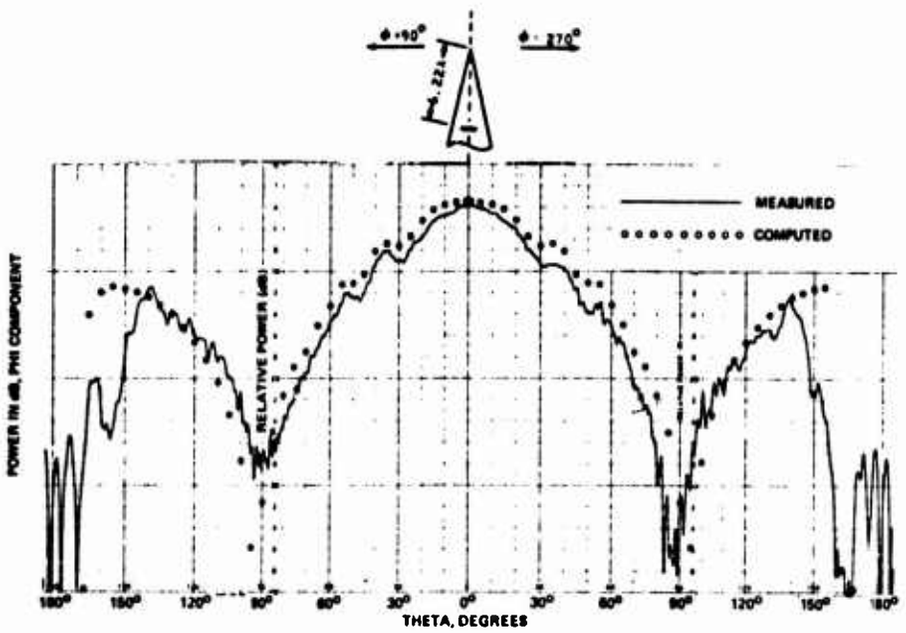

Figure 18. Measured and Computed ϕ-Polarized Patterns of $\lambda/2$ Circumferential Slot for $\phi = 90^{o}$, $\phi = 270^{o}$.

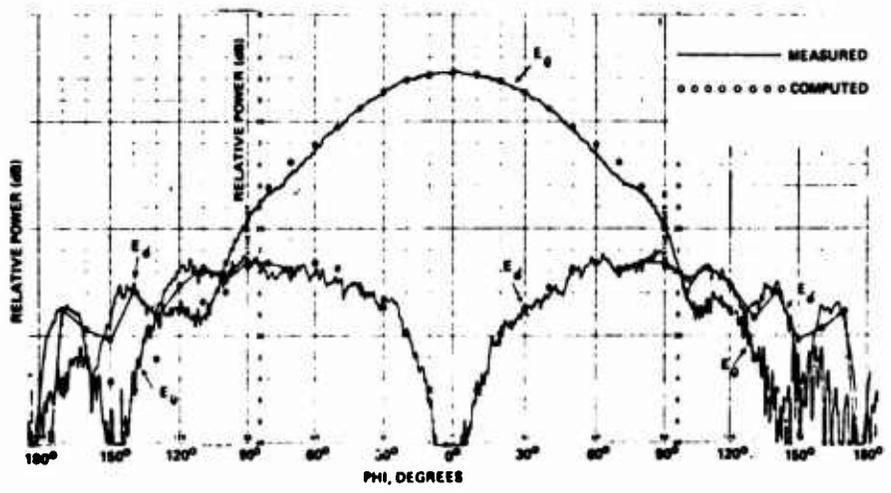

Figure 19. Measured and Computed Patterns of $\lambda/2$ Circumferential Slot for θ and ϕ Polarizations at $\theta = 80^{o}$.

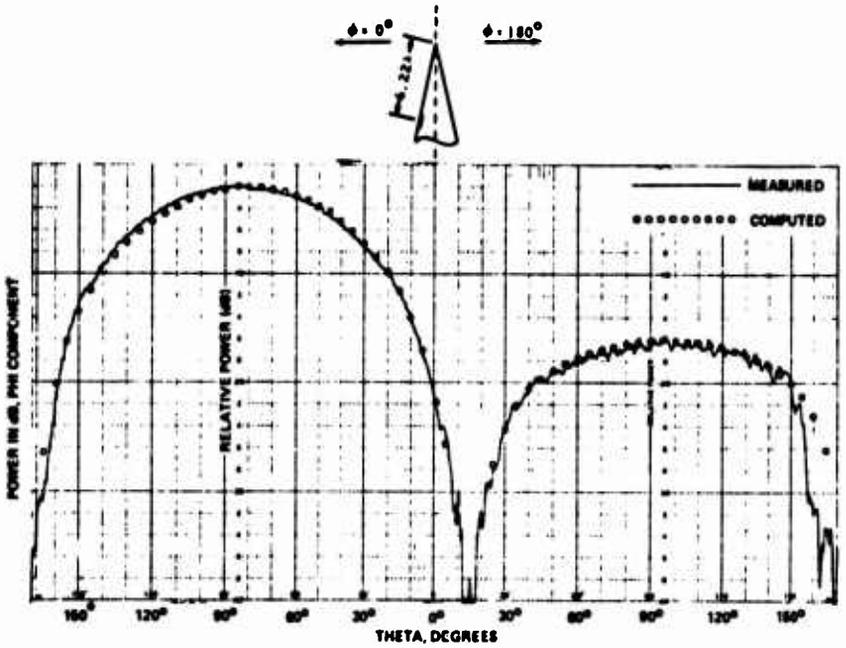

Figure 20. Measured and Computed ϕ-Polarized Patterns of $\lambda/2$ Radial Slot for $\phi = 0^{o}$, $\phi = 180^{o}$

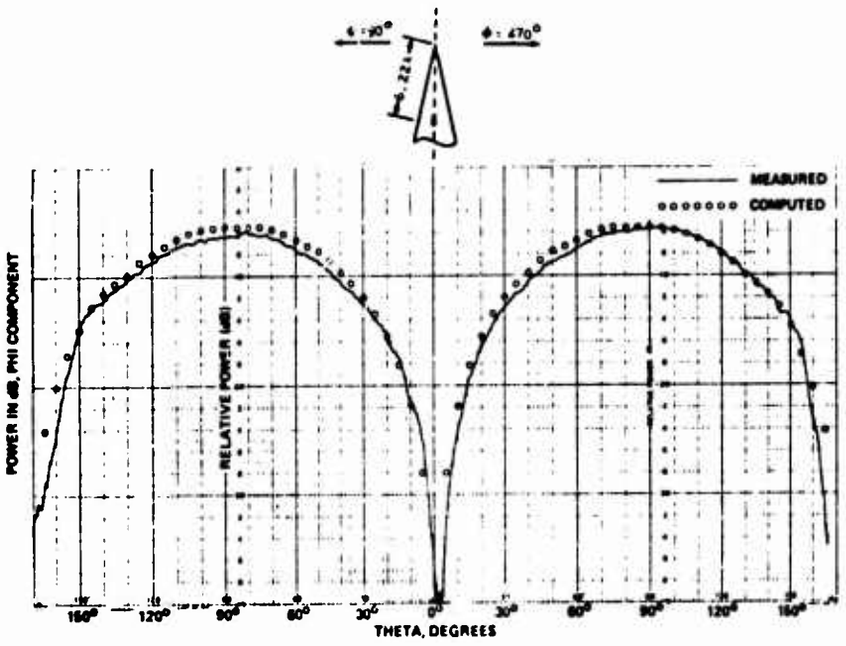

Figure 21. Measured and Computed ϕ-Polarized Patterns of $\lambda/2$ Radial Slot for $\phi = 90^{o}$, $\phi = 270^{o}$

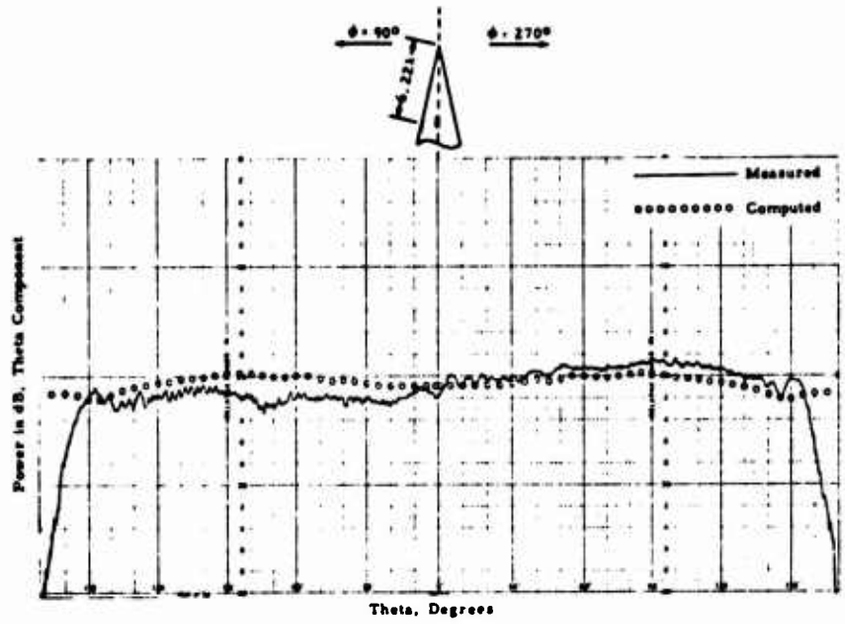

Figure 22. Measured and Computed θ-Polarized Patterns of λ/2 Radial Slot for $\phi = 90^{\circ}$, $\phi = 270^{\circ}$

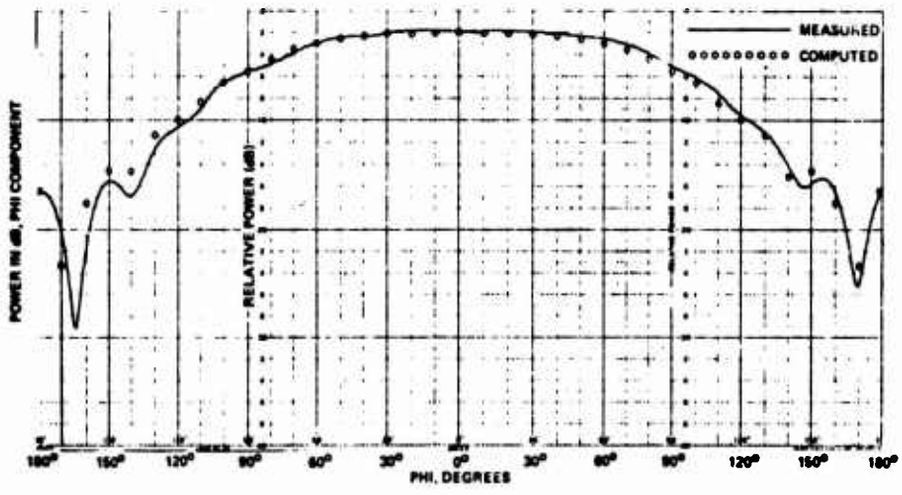

Figure 23. Measured and Computed φ-Polarized Patterns of λ/2 Radial Slot for $\theta = 80^{\circ}$

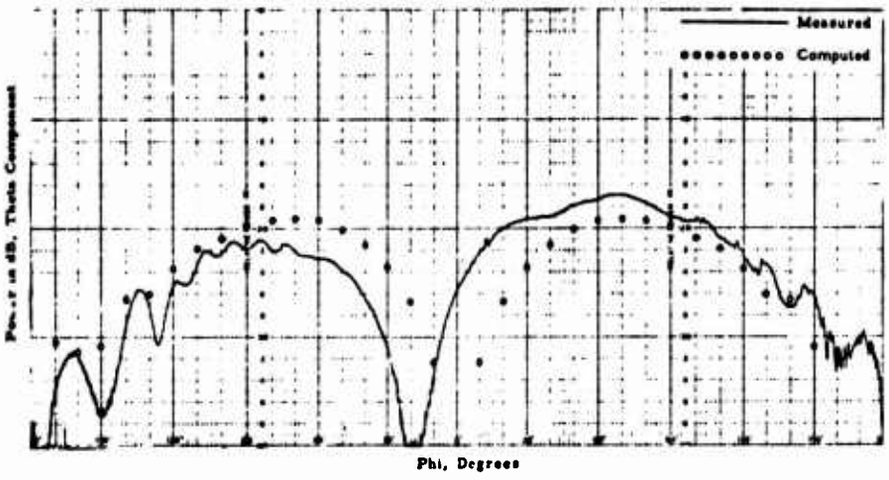

Figure 24. Measured and Computed θ-Polarized Patterns of λ/2 Radial Slot for $\theta = 80^{o}$

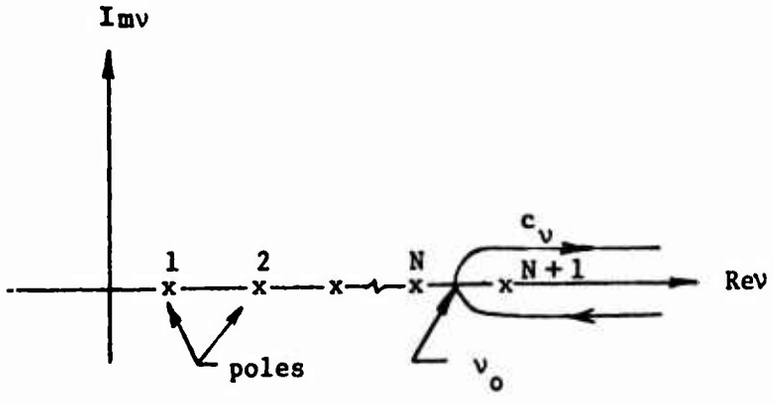

Figure 25. Displaced hairpin contour c_ν.

4. Asymptotic Solutions

The modal series solution gives correct results for slots at arbitrary distances from the cone tip. However, for slots many wavelengths from the tip the computation becomes lengthy, and numerical accuracy may become a problem as well. In that case the techniques of the geometric theory of diffraction have been applied to account for the effect of the surface curvature on the radiation patterns of sources on cones. (Shmoys & Hessel, 1974) However, as presently applied, the geometric theory of diffraction does not account for the diffraction of waves by the cone tip.

An approach has been devised by Pridmore-Brown (1972, 1973) to obtain an asymptotic solution for the θ-component of the fields of circumferential slots. Out of his formulation a term, which has been designated the tip-diffraction coefficient, has been identified. It describes the effect of the tip in terms of a function of θ and the cone angle and is independent of ka.

The geometry under consideration is a perfectly conducting conical surface coinciding with the coordinate surface $\theta = \theta_o$ of a spherical coordinate system r, θ, ϕ. A narrow azimuthal slot located at $r = a$ is excited by an alternating voltage.

$$V_o \cos m\phi$$

where the time variation $\exp(-i\omega t)$ has been suppressed. The external field generated by this excitation is give by

$$\overline{E} = \text{curl curl } (r\Pi_1) + k \text{ curl } (r\Pi_2)$$

where Π_1, and Π_2 are scalar potential functions and are given by equations (3) and (4) of Pridmore-Brown (1972). The field components are given by the following expressions

$$E_\theta = \frac{V_o}{r} (2\pi ka)^{\frac{1}{2}} \cos m\phi \exp[i(kr - \pi/4)] P_\theta$$

where

$$P_\theta = P_{1\theta} - \frac{im^2}{\sin\theta \sin\theta_o} P_{2\theta}$$

$$P_{1\theta} = -\frac{1}{2\pi i} \int_{C_\nu} \frac{\nu d\nu}{\nu^2 - \frac{1}{4}} A_{1\nu}'(\theta, \theta_o) i^{-\nu} J_\nu(ka)$$

$$P_{2\theta} = -\frac{1}{2\pi i} \int_{C_\nu} \frac{\nu d\nu}{\nu^2 - \frac{1}{4}} A_{2\nu}(\theta, \theta_o) i^{-\nu} J_\nu'(ka)$$

$$A_{1\nu}(\theta,\theta_o) = \frac{P^{-m}_{\nu-\frac{1}{2}}(\cos\theta)}{P^{-m}_{\nu-\frac{1}{2}}(\cos\theta_o)}$$

$$A_{2\nu}(\theta,\theta_o) = \frac{P^{-m}_{\nu-\frac{1}{2}}(\cos\theta)}{(\partial/\partial\theta)\ P^{-m}_{\nu-\frac{1}{2}}(\cos\theta)\Big|_{\theta_o}}$$

$$\mathfrak{J}_\nu(x) = \left(\frac{x}{ka}\right)^{\frac{1}{2}} J_\nu(x)$$

and

$$E_\phi = \frac{V_o}{r}\ \sqrt{2\pi ka}\ m\ \sin m\phi\ \exp[i(kr - \pi/4)]\ P_\phi$$

where

$$P_\phi = \frac{-1}{\sin\theta}\ P_{1\phi} + \frac{i}{\sin\theta_o}\ P_{2\phi}$$

$$P_{1\phi} = -\frac{1}{2\pi i}\int_{C_\nu} \frac{\nu d\nu}{\nu^2 - \frac{1}{4}}\ A_{1\nu}(\theta,\theta_o)\ i^{-\nu}\ J_\nu(ka)$$

$$P_{2\phi} = -\frac{1}{2\pi i}\int_{C_\nu} \frac{\nu d\nu}{\nu^2 - \frac{1}{4}}\ A_{2\nu}'(\theta,\theta_o)\ i^{-\nu}\ \mathfrak{J}_\nu'(ka)$$

The integrals are taken over a hairpin contour enclosing the positive real axis of $\nu > \frac{1}{2}$. (Primes denote derivatives with respect to the argument or with respect to the first argument in the case of two arguments. For clarification, we have also added the the subscript θ, ϕ to denote quantities corresponding to E_θ and E_ϕ, respectively.)

The integrands have poles along the positive, real ν-axis and the modal series is obtained by evaluating the residues at these poles. The approach used by Pridemore-Brown(1972) obtains a portion of the modal series by evaluating the residue at a number of poles, N. The remaining portions of the fields are now

represented by the displaced contour shown in Figure 25. By imposing the restriction $1 \ll N \ll ka$, it is assumed that the Legendre functions in the contour integrals may be represented by asymptotic expressions valid for large ν and that the Bessel functions in the residue series may be represented by asymptotic expressions valid for $ka \gg \nu$. The contour integrals are then evaluated and the limit taken as N approaches infinity with $ka \gg N$. This operation results in a non-vanishing value for the contour integrals that represent what are termed optical and transitional fields. The sum of the residue series yields the term that is designated as the tip diffraction coefficient,

A complete expression for the E_θ component of the radiation field in terms of the optical, transition, and diffraction fields may now be written from the results of Pridmore-Brown (1972, 1973). Thus,

$$\mathcal{E}_\theta = \cos m\phi \left\{ \left(\frac{-\cos\theta_o}{\sin\theta} \right)^{\frac{1}{2}} [\exp(ikR) + \Gamma \exp(ikR') H(\pi - \theta_o - \theta) + TF] \right.$$

$$\left. + \frac{\exp[ik(r+a)]}{(ka)^{\frac{1}{2}}} \sigma_m(\theta, \theta_o) \right\}$$

where

$$\mathcal{E}_\theta = E_\theta \frac{r}{V_o} \left[\frac{2\pi i \cot(\pi - \theta_o)}{ka} \right]^{\frac{1}{2}}$$

$$R = r - a\cos(\theta - \theta_o)$$

$$R' = r - a\cos(\theta + \theta_o)$$

$H(\alpha)$ is a step function, ($H(\alpha) = 1$ for $\alpha > 0$), $\theta \neq 0$.

TF is the transition field contribution

$$\Gamma = i(-1)^m$$

The first two terms in brackets represent the optical field contribution. The expressions for TF and σ_m are quite complicated. They are available in Pridmore-Brown (1972) and are not included here.

The expressions of Pridmore-Brown (1972, 1973) are being programmed and an anologous expression for the ϕ-component of

of the electric field has been derived and is also being programmed for numerical computation. The general form is similar to that for the θ-component but there is no optical contribution, and the transition fields and diffraction coefficients are different than for the θ-component. The form of E_ϕ is as follows

$$\mathcal{E}_\phi = m \sin m\phi \left\{ \left(\frac{-\cos\theta}{\sin\theta_o} \right)^{\frac{1}{2}} TF_\phi + \frac{\exp[ik(r+a)]}{(ka)^{\frac{1}{2}}} \sigma_{m\phi}(\theta, \theta_o) \right\}$$

$$\mathcal{E}_\phi = E_\phi \frac{r}{V_o} \left[\frac{2\pi i \cot(\pi - \theta_o)}{ka} \right]^{\frac{1}{2}}$$

It should be noted that as defined by Pridmore-Brown σ_m has a singularity at $\theta = \pi - \theta_o$. However, there is a compensating singularity in TF, so that the total field remains finite at that angle. A similar thing occurs for $\sigma_{m\phi}$. It appears that by combining the singular terms in the transition fields with the singularity in the tip diffraction coefficients new diffraction coefficients could be defined, that remain finite everywhere and that describe the diffraction due to the tip of the cone. The total tip-diffraction could then be obtained by summing over the σ_m and $\sigma_{m\phi}$ weighted by the corresponding strength of the m'th source coefficient. The remainder of the field could be obtained by the geometric theory of diffraction and the results combined to give the total field valid for large values of ka.

The combination of the complete modal series solution when ka is small and the geometric theory of diffraction with tip-diffraction coefficients when ka is large provide the capability for pattern calculation for slots at any distance from the cone tip.

5. Conclusion

The problems of pattern synthesis for arrays on conformal surfaces, and element pattern calculations for slots on conical conducting surfaces have been discussed and the results of pattern calculations have been summarized. The synthesis techniques and pattern calculation methods discussed provide some of the tools necessary for the design of arrays on such surfaces. Specifically, the synthesis techniques yield the required element excitations for a specified pattern, while the element pattern calculation techniques provide the ability to verify the correctness of the synthesis procedure. These capabilities, combined with the results of impedance calculation techniques make it possible to design and predict performance of arrays on surfaces that could hitherto only be estimated.

6. Acknowledgment

The work summarized in this paper represents contributions by a number of members of the Antenna Department. Major contributors were: P. C. Bargeliotes, A. F. Seaton and W. H. Kummer. Experimental support was provided by M. C. Behnke, D. R. Bostrom and B. J. Stevens. The encouragement of Mr. J. W. Willis is gratefully acknowledged. The work was supported by the Naval Air Systems Command.

REFERENCES

1. Bailin, L. L. and S. Silver, 1956, "Exterior Electromagnetic Boundary Value Problems for Spheres and Cones, "IRE Trans. on Antennas and Propagation, Vol. AP-4, January, 1956, pp. 5-16.

2. Bailin, L. L. and S. Silver, 1957, "Exterior Electromagnetic Boundary Value Problems for Spheres and Cones, "IRE Trans. on Antennas and Propagation, Vol. AP-4, January, 1956, pp. 5-16. corrections, IRE Trans, Vol. AP-5, July, 1957, p. 313.

3. Bargeliotes, P. C., W. H. Kummer, and A. T. Villeneuve, 1974 "Dynamic Impedance Matching In Conformal Arrays" Final Report on Contract N000 19-73-C-0127, Report No. 2265.30/184, Hughes Aircraft Co., January 1973 to January 1974.

4. Bargeliotes, P. C., 1974a, "Pattern Synthesis of Conformal Arrays" Quarterly Report on Contract N000 19-74-C-0127, Report No. 2265.30/297, Hughes Aircraft Co., January 1, 1974 to April 1, 1974.

5. Bargeliotes, P. C., 1974b, "Pattern Synthesis of Conformal Arrays" Quarterly Report on Contract N000 19-74-C-0127, Report No. 2265.30/326, Hughes Aircraft Co., April 1, 1974 to July 1, 1974.

6. IRIG Standard, "Coordinate System and Data Formats for Antenna Patterns", Document 111-65 revised Aug., 1965, Published May, 1966 by Secretariat, Range Commanders Council, White Sands Missile Range, New Mexico 88002.

7. Kummer, W. H., and A. T. Villeneuve, 1969, "Integrated Conformal Arrays", Quarterly Report on Contract N00019-69-0281, 3 June 1969 to 3 September 1969, Report No. 27-67.01/178, Hughes Aircraft Co.

8. Kummer, W. H., A. F. Seaton, and A. T. Villeneuve, (1973). "Conformal Antenna Arrays Study", Final Report on Contract N00019-72-C-0212, Report No. 2765, 31/421, Hughes Aircraft Company, January, 1972 to January, 1973.

9. Pridmore-Brown, D. C. and G. Stewart, 1972, "Radiation from Slot Antennas on Cones, "IEEE Trans. on Antennas and Propagation, Vol. AP-20, No. 1, January, 1972, pp. 30-39.

10. Pridmore-Brown, D. C., 1972, "Diffraction Coefficients for a Excited Cone" IEEE Trans. on Antennas and Propagation, Vol. AP-20, No. 1, January 1972, pp. 40-49.

11. Pridmore-Brown, D. C., 1973, "The Transition Field on the Surface of a Slot-Excited Conical Antenna", IEEE Trans. on Antennas and Propagation, Vol. AP-21, Number 6, Nov. 1973, pp 889-890.

12. Shmoys, J. and A. Hessel, 1974 "Radiation from Apertures on Conducting Conical Surfaces", in "Ray Analysis of Mutual Coupling In Conformal Arrays, Final Report for Phase I on Contract N00123-73-C-1481, Report No. POLY-EP-74-141, Polytechnic Institute of New York, April 1, 1973 to March 31, 1974.

Surface Ray Analysis of Conformal Arrays

A. Hessel, J. Shmoys, Z.W. Chang
Department of Electrical Engineering and Electrophysics
Polytechnic Institute of New York
Farmingdale, New York 11735

ABSTRACT

This paper will describe the progress for the period from July 1, 1972, to March 31, 1975, at the Polytechnic Institute of New York in application of surface ray methods to analysis of radiation patterns and mutual coupling in arrays of aperture elements on convex conducting surfaces, with particular emphasis on conical arrays. This effort has been partly in cooperation with NELC, and has been funded by NAVAIR.

I. Introduction

In order to put the material of this report in a proper prospective, it is desirable to first review the basic features of the surface ray methods and their state of the art, as reflected in the published literature.

The two basic ingredients required for the theoretical evaluation of the performance of a conformal array of aperture elements are the far field pattern and the surface magnetic field due to a tangential magnetic current element located arbitrarily on the unperforated convex conducting array surface. With this information, it is a simple matter to determine the elements of the mutual admittance matrix and also the isolated element patterns, which in turn yield array patterns, once the array aperture illumination is known. The latter is obtained by inversion of an admittance matrix, the diagonal terms of which are the sum of the element self admittance and the admittance "seen" from the aperture plane "looking" into the respective feed waveguides.

Analysis of conformal arrays is complicated by the fact that for surfaces other than circular cylinders, spheres and cones, Maxwell's equations do not separate, and consequently, exact solutions are not available. Even for these three separable geometries, when the radii of curvature become large compared to wavelength, a rigorous field representation in terms of modal series is slowly convergent, and their numerical evaluation require excessive computer time. These difficulties may be avoided, for not too small radii of curvature, i.e., for $ka \geq 10$, by recourse to the surface ray methods, based on Keller's Geometric Theory of diffraction (GTD)[1]. Surface ray solutions do not require separability of geometry, yield very simple formulae which largely reduce the computing time, and simultaneously provide an understanding of the far field pattern formation and of the physical mechanism operative in mutual coupling.

The basic reason for the relative simplicity of ray solutions as compared with the rigorous modal methods is that in contrast to the exact modal methods which deal equally with all the global field details on the entire surface, the approximate, asymptotic ray methods have an inherently local character.

GTD postulates, in accordance with Fermat's principle that propagation of high frequency E-M waves on a smooth convex conducting surface with a sufficiently large radius takes place along surface rays the trajectories of which are, in accordance with Fermat's principle, goedesics of the surface (See Fig. 1). Surface ray fields travel with near-free space velocity along their ray paths and while traveling, attenuate. The attenuation is a result of radiation, since at every point of its trajectory, (See Fig. 2) a surface ray sheds energy to far field, along the local ray direction.

The local character of surface-ray fields manifests itself in their independence from the neighboring ray fields (except at a caustic) and in addition, in that the field at an observation point can be determined from the local geometries at the source, at the observation point, and from the local properties of the surface along the ray. As a result, GTD can assign to each point along a surface ray a field amplitude, phase and polarization. Once these quantities are known at the launching point, they may be traced along the entire ray path.

For example, if a surface ray is launched by a magnetic current element $\underline{p}_m$ located at a point Q on a convex conducting surface and observed at Q (See Fig. 1), then the expression for the surface ray magnetic field at Q for the so-called hard polarization is given by

$$\underline{H}^h(Q) = C(\underline{p}_m \cdot \underline{b}')\underline{b}L^h(Q')L^h(Q)e^{-\int_{Q'}^{Q}\alpha^h(s)ds - j\int_{Q'}^{Q}\beta(s)ds}\delta(Q', Q) \tag{1}$$

For the hard polarization the current flow is along the ray direction. Formula (1) has a typical GTD format. It consists of a product of several factors. Some of them, like the launching coefficient $L^h(Q')$ or $L^h(Q)$ depend solely on the local environment at Q' or at Q and are weakly dependent on the transverse curvature to the ray direction. As a result they may be calculated once and for all from a rigorous solution of a canonical problem of a cylinder or a sphere The exponential factors on the other hand yield the propagation characteristics of the surface ray field. They furnish the overall attenuation and phase delay over the ray path from Q' to Q as an integrated effect of the local differential phase delays $\beta(s)$ and attenuations $\alpha(s)$. The $\alpha(s)$ and $\beta(s)$ depend to first order only on the local radius of curvature. $\rho_g(s)$ of the surface in the plane con-

taining the surface normal and the local ray direction. Thus $\alpha(s)$ and $\beta(s)$ are equal to their counterparts on a conducting circular cylinder with the radius $\rho_g(s)$ and with its trajectory plane normal to cylinder axis.

The factor $(\underline{p}_m \cdot \underline{b}')$ in Fig. (1) indicates that a hard polarization ray is not launched in the direction of $\underline{p}_m$ since b′ is the local ray-binormal at Q′ (Fig. (1). The second factor $\underline{b}$ indicates that for hard polarization the surface magnetic field is directed, at every point, along the local binormal. The third factor, the launching coefficient $L^h(Q')$ depends on $[k\rho_g(Q')]^{-1/3}$ at the source point and vanishes for planar geometry. The fourth factor $L^h(Q)$ has an identical form with $L^h(Q')$, but is evaluated at Q, i.e. is proportional to $[k\rho_g(Q)]^{-1/3}$.

The presence of the factor $L^h(Q)$ symmetrizes the expression (1) with respect to an interchange of Q′ and Q and is required because of reciprocity. Finally $\delta(Q', Q)$ is the ray divergence coefficient. It accounts for an algebraic amplitude decay with increasing s due to the usual ray spreading, when their trajectories are not parallel.

The analogous formula for soft polarization is

$$\underline{H}^s(Q) = -C(\underline{p}_m \cdot \underline{t}')\underline{t}\; L^s(Q')L^s(Q)e^{-\int_{Q'}^{Q}\alpha^s(s)ds}\, e^{-j\int_{Q'}^{Q}\beta^s(s)ds}\, \delta(Q', Q) \tag{2}$$

The surface ray is launched at Q′ in the direction $\underline{t}'$ with a coefficient $C(\underline{p}_m \cdot \underline{t}')L^s(Q')$. The local direction of the surface magnetic field for the soft polarization is along the ray. Each polarization has its own launching coefficients, the expressions for which may be found in [1]. The terminology hard and soft originated in acoustics. Hard boundary conditions are $\frac{\partial \Psi}{\partial n} = 0$, soft - $\Psi = 0$ on the surface.

It turns out that for a hard surface ray the electric far field has the direction of the surface normal at the point of contact (Fig. 2), at which the ray leaves the surface to the far field. For the soft polarization, the surface ray far field $\underline{E}$ is along the surface ray binormal at the point of contact. The factors $(\underline{p}_m \cdot \underline{b}')L^h(Q')$ and $(\underline{p}_m \cdot \underline{t}')L^s(Q')$ appear also in the far field expressions.

But things are not so simple, because for either polarization, and a given ray trajectory there is an infinite number of surface rays with increasing attenuation. These are analogous to higher order leaky modes. The lowest attenuation is associated with the dominant hard polarization ray having $\alpha^h \approx 3.8.(k\rho_g)^{-2/3}$ nepers/λ. The next higher is $\alpha^s. \approx 2.3_1^h$ followed by $\alpha_1{}^h. \approx 2.3\alpha_1{}^h$ followed by $\alpha_2{}^h \approx 3.25\alpha_1{}^h$ and so on.

Because of the large difference in attenuation, the higher order surface ray fields damp out faster than the dominant, so that sufficiently far from the source only one ray field will dominate the surface. This region is termed deep shadow (See Fig. 3). As the observation point on the surface approaches the source, an increasing number of higher order surface ray contributions must be taken into account and the surface ray series becomes poorly convergent. To overcome this difficulty, one employs the so-called transition functions which near the source provide an alternative rapidly convergent representation of the surface field and yield a smooth transition between a single ray field description in the deep shadow and the planar result near the source.

Different transition functions due to Fock are employed in the far field. In the far field we distinguish between the Lit and the Shadow regions (Fig. 4) separated by the Shadow Boundary. To provide a smooth transition between the fields in these regions one introduces a transition region, the angular width of which is of the order $\lceil k\rho_g \rceil^{-1/3}$ at the source. The transition region in turn is subdivided into a lit transition part and a shadow transition part. We then actually have four far field regions, and in each different field expressions which blend continuously across the respective zone boundaries: in the Geometric Optical region the fields are described in terms of real ray expressions; in the deep shadow a single surface ray field suffices, and in each transition region, a different transition function is used.

II. Contract Accomplishments

Phase 1.

a) In order to gain an understanding of how well the surface ray methods work in conformal array applications and get an idea of accuracies involved, we have obtained during the first stage of the program GTD element patterns in mutually coupled array environment of axial, parallel plate guide-fed slit arrays on circular cylindrical surfaces, and have compared the answers with the available modal results. The agreement was excellent. We have subsequantly extended the analysis to slit arrays on cylindrical surfaces of variable curvature, with application to parabolic cylindrical surfaces. These results have been published in [2] and [3].

b) During the second stage of Phase 1 we proceeded to the analysis of radial slot arrays on conical surfaces. In the far field formulation we have made an extensive use of the GTD treatment in [4]. A shortened and improved version of this report appeared in [5]. These very well written expositions of the state of the art of GTD contain certain deficiencies which were corrected by us for the special case of conical geometry.

The basic deficiency stems from the fact that the GTD formulae of [4] and [5], as the authors also point out, are valid for torsionless surfaces, such as spheres, for which the surface ray trajectories are plane curves. The authors do not elaborate on the consequences of this restriction. For example GTD formulae in [4] and [5] invariably predict simultaneous excitation of both hard and soft polarizations. Yet we know very well that an axial slot on a torsional surface such as a circular cylinder, or a radial slot on a cone excite only one (hard) polarization. Kouyoumjian has later obtained a heuristic correction factor to the soft launching coefficient [6], which suppresses the soft polarization when the radius of curvature in the plane containing the slot direction and the surface normal becomes infinite. But this correction factor is too heuristic, and needs to be proven for the general case.

Another deficiency of the published GTD formulae for a magnetic point current source is that the far field polarization on a cone does not blend with

the geometric-optical polarization across the g. o. -lit transition boundary. This was corrected in our computer programs.

We turn now to mutual coupling. Asymptotic expressions had to be developed for the surface magnetic field due to a short axial slot on a circular cylinder. In this development we have followed [7]. These expressions were subsequently generalized to a cone and applied to analysis of element patterns in mutually coupled conical array environment of open ended circumferentially polarized rectangular waveguides. This topic is covered in the companion paper by G. Vaughn of NELC.

Phase 2

In the second phase of the contract we have developed a computer program for the GTD radiation pattern due a circumferential short slot on a cone. We have also obtained, starting from a rigorous integral representation, the necessary transition function for the surface magnetic field H_ϕ due a circumferential short slot on a circular cylinder. The expressions were subsequently generalized in a GTD manner to a cone. In the deep shadow, the result checks with the rigorous asymptotic solution for a surface ray obtained directly in a conical geometry. [8]

Development of a computer program for mutual admittance calculation between two circumferential slots on a cone was started, and some initial results were obtained.

III. Numerical Results

Since a report summarizing Polytechnic Institute's effort in Phase 1 has been issued [9], we shall limit ourselves here only to the presentation of specific results obtained at P. I. N. Y. in Phase 2 plus some additional relevant results for far field patterns for radial slots on a cone. We shall first present examples of GTD far field patterns for a short radial slot on a cone along with a comparison with harmonic series data from ref. [10], then results for circumferential slot patterns, and subsequently some preliminary results for mutual coupling between circumferential slots on a conical surface. Fig. 5 shows the cone geometry and the spherical coordinate system. In all subsequent figures the cone half angle was chosen $\theta_o = 10^o$. The elevation angle ϑ is measured from the positive z axis. The center of slot is located at $\varphi = 0^o$. R is the distance of the element center from the tip.

Fig. 6 shows a conical cut for $\theta = 80^o$ (i. e. cut normal to cone surface) for a short radial slot located about 6.2λ from the tip. Solid lines are GTD results, points are experimental results from [10] for a $\lambda/2$ radial slot, crosses are harmonic series calculations from [10]. One observes an excellent agreement between GTD and harmonic series in both polarizations. This is remarkable, in view of the value of $k_a \approx 6.5$. The agreement is expected to be better for radial slots than for circumferential ones because for the former the tip is weakly excited. The ripple near 180^o is caused by the interference between a clockwise and a counterclockwise traveling surface ray. This feature is schematically shown in Fig. 7.

In Fig. 8 we see the elevation pattern of a radial slot for $\varphi = 40^o$ and $\varphi = 140^o$ or by symmetry $\varphi = 220^o$. Again the agreement between GTD and harmonic series results is quite good. The null near 10^o is found in the geometric optical region and therefore is not due to an interference, but to the fact that the g. o. ray in this particular direction is θ polarized.

Fig. 9 shows a conical cut $\theta = 80^o$ for a short circumferential slot in both polarizations. Again agreement is good for E_φ and less for E_θ in the $\varphi = 180^o$ region. The discrepancy, however, may be also due to an insufficient number of terms in the harmonic series. This is not an uncommon problem with harmonic series on a cylinder, near 180^o.

Fig. 10 is a comparison between a GTD and harmonic series results for a $\lambda/2$ circumferential slot for a conical cut $\theta = 80^{\circ}$. The tip effect is small in this cut and there is a very good agreement except in $E\theta$ again near $\varphi = 150^{\circ}$.

The differences between GTD and harmonic series patterns show up best, as expected, in the elevation patterns (Fig. 11). Here we have an E_{θ} elevation cut through the center of the circumferential slot. On the lit side we notice a good agreement except near the tip and near the cone surfaces. One may estimate the level of the tip scattering from the difference between harmonic series result on the axis and GTD in the axial direction. The total level difference is about 2db above the geometrical optical contribution. Consequently, for kR = 39 the tip scattering level near the axis should be about -12 db below the geometrical optical contribution. Proceeding into the shadow region, one observes in the harmonic series a ripple. This ripple is a result of an interference between the surface ray field and the tip scattering. The ripple is absent in the GTD version, in which tip scattering is not accounted for. The null in the GTD pattern at about $\theta = 105^{\circ}$ appears because the particular surface ray that contributes to far field at $\varphi = 180^{\circ}$ $\theta = 105^{\circ}$ is launched in the direction of the long dimension of the slot, so that $(\underline{p}_m \cdot \underline{b}')$ is zero.

Fig. 12 presents an elevation cut for $\varphi = 90^{\circ}$ and both polarizations. The agreement for (E_{φ}) is very good. For E_{θ} in the axial region the harmonic series result shows presence of cross polarized tip scattering which is missing in GTD. The level of tip scattering is about 9.5db below the g.o. level on the axis.

IV. Mutual Coupling

Let us now turn to mutual coupling. The GTD results of [5] are inadequate for three reasons:

a) Because a conical surface has torsion and torsionless GTD formulae do not handle properly the soft polarization.

b) Because formulation in [5] does not permit a sufficiently close approach to the source, such proximity is required for calculation of mutuals between near neighbors, and

c) Because the soft polarization contribution (soft transition function) blows up along the $\varphi = 0$ cone generator.

To amend the situation we have started from a rigorous integral representation for the surface magnetic field due to a circumferential short slot on a circular cylinder and have obtained a transition function that on one hand permits a close approach to the source where it reduces to a planar result and on the other hand properly blends with the deep shadow formulation.
The expressions are finite on the $\varphi = 0$ generator, but are not entirely correct in the generator region because the Airy Function approximation of Hankel functions is no longer valid in this region. This solution has subsequently been generalized in a GTD fashion to a conical surface.

Fig. 13 shows some initial numerical results for the H-plane mutual admittance on a cone between two circumferential $\lambda/2$ slots of width 0.05λ. The slots are located at a constant distance $kR = 50$ from the tip. The magnitude of Y_{12} is plotted in db relative to the self admittance of a planar $\lambda/2$ slot. The minimum distance d between the slot centers is 0.6λ and further spacings that have been computed are in increments of 0.1λ. It is seen that for $kR = 50$ the decay of Y_{12} over 180° is about 57db.

The phase plotted is the difference of the phase of Y_{12} over 180° minus the phase kD, where D is the length along the geodesic between the slot centers.

Fig. 14 shows the magnitude and phase of H plane Y_{12} for various distances of circumferential slots from the tip. It is seen that with increasing distance kR which results in an increase of radii of curvature, the Y_{12} curves approach the planar ones.

The formulae on which the above numerical results are based may be found in [11].

V. Conclusion

We have come a long way since the beginning of the contract but there is yet a lot to be done, e. g..

a) determination of launching coefficients for the soft polarization on convex conducting surfaces with two unequal radii of curvature.

b) determination of fields near the cylinder axis or the cone generators.

c) the cone tip diffraction coefficient for a short circumferential slot excitation.

d) development of a computer program for a convex surface of revolution given in terms of a set of discrete points, both for radiation patterns and mutuals.

One can safely assert that Surface Ray Methods constitute an extremely useful computer time saving and versatile tool for analysis of conformal array performance.

References

1. J. B. Keller: "Geometrical Theory of Diffraction", Journal of the Optical Society of America, Vol. 52, pp. 116-130, 1962.

2. J. Shapira, L. B. Felsen and A. Hessel: "Ray Analysis of Conformal Antenna Arrays" IEEE Transactions on Antennas and Propagation, Vol. AP-22, pp. 49-63, January, 1974.

3. J. Shapira, L. B. Felsen and A. Hessel: "Surface Ray Analysis of Mutually Coupled Arrays on Variable Curvature Cylindrical Surfaces" Proceedings IEEE, Vol. 62, pp. 1482-1492, November, 1974.

4. P. H. Pathak and R. G. Kouyoumjian: "The Radiation of Apertures on Curved Surfaces" NASA Report 3001-2, December, 1972.

5. P. H. Pathak and R. G. Kouyoumjian: "An Analysis of the Radiation From Apertures in Curved Surfaces by the Geometric Theory of Diffraction" Proceedings IEEE, Vol. 62, pp. 1438-1461, November, 1947.

6. Y. Whang and R. G. Kouyoumjian: Private Communication.

7. G. Hasserjian: "Currents Induced on a Circular Cylinder by Slots", Document No. D2-11370, Boeing Aircraft Company, Seattle, Washington, 1961.

8. K. K. Chan, A. Hessel, J. Shmoys and L. B. Felsen: "Creeping Waves on a Perfectly Conducting Cone", to be presented at the June 1975 URSI meeting at the University of Illinois, Urbana.

9. L. B. Felsen, A. Hessel, J. Shapira and J. Shmoys: "Ray Analysis of Mutual Coupling in Conformal Arrays", Polytechnic Institute of New York, Final Report for Phase I, 1 April 1973 - 31 March 1974, Contract N00123-73-C-1481, August, 1974. Prepared for Naval Regional Procurement Office, Long Beach, California.

10. "Pattern Synthesis of Conformal Arrays". Report 2265.30/297 HAC Ref. D-0741, Contract No. N00019-74-C-0127, 1 Jan. - 1 April 1974, 1 April - 1 July 1974.

11. A. Hessel, J. Shmoys, Z.W. Chang, "Surface Ray Analysis of Conformal Arrays", Polytechnic Institute of New York, Final Report for Phase 2, 1 April 1974 - 31 March 1975, Contract N00123-73-C-1481, May 1975. Prepared for Naval Regional Procurement Office, Long Beach, Calif.

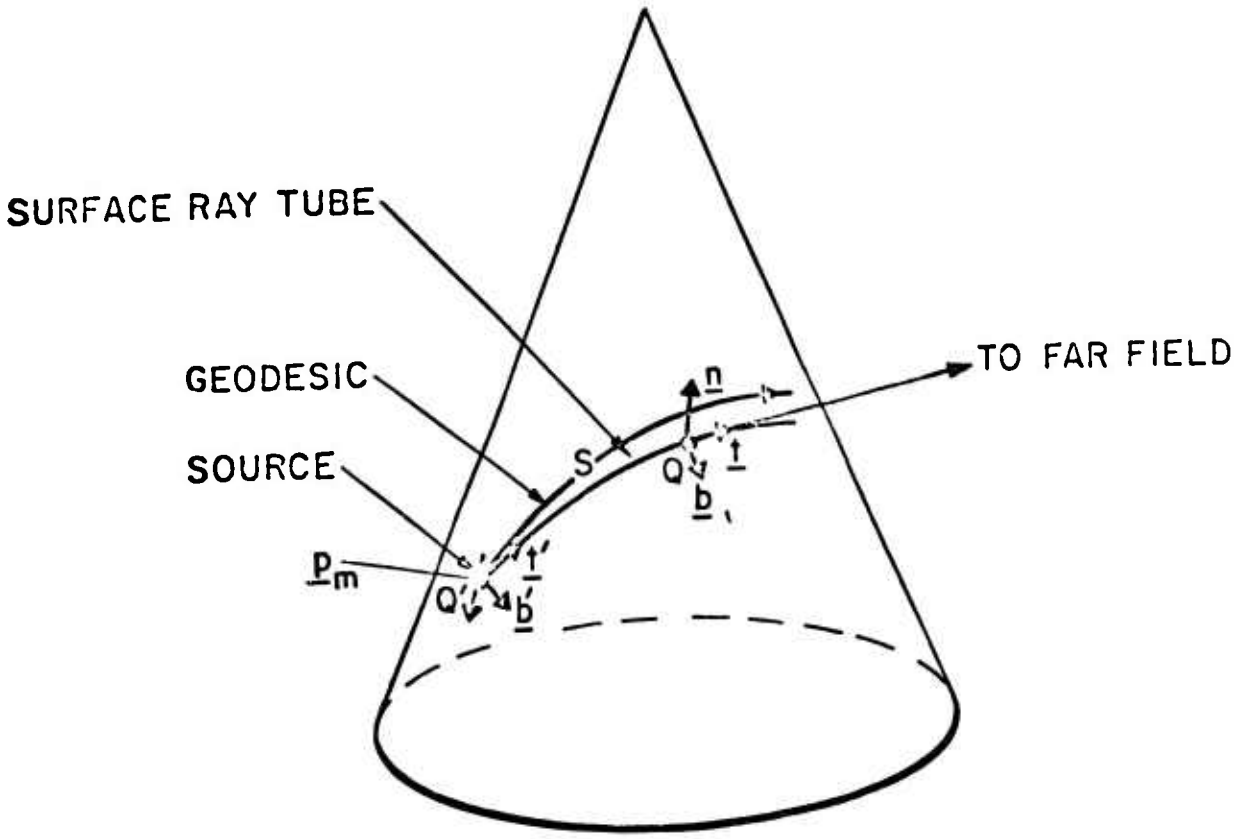

Fig. 1 Surface Rays on a Conducting Conical Surface

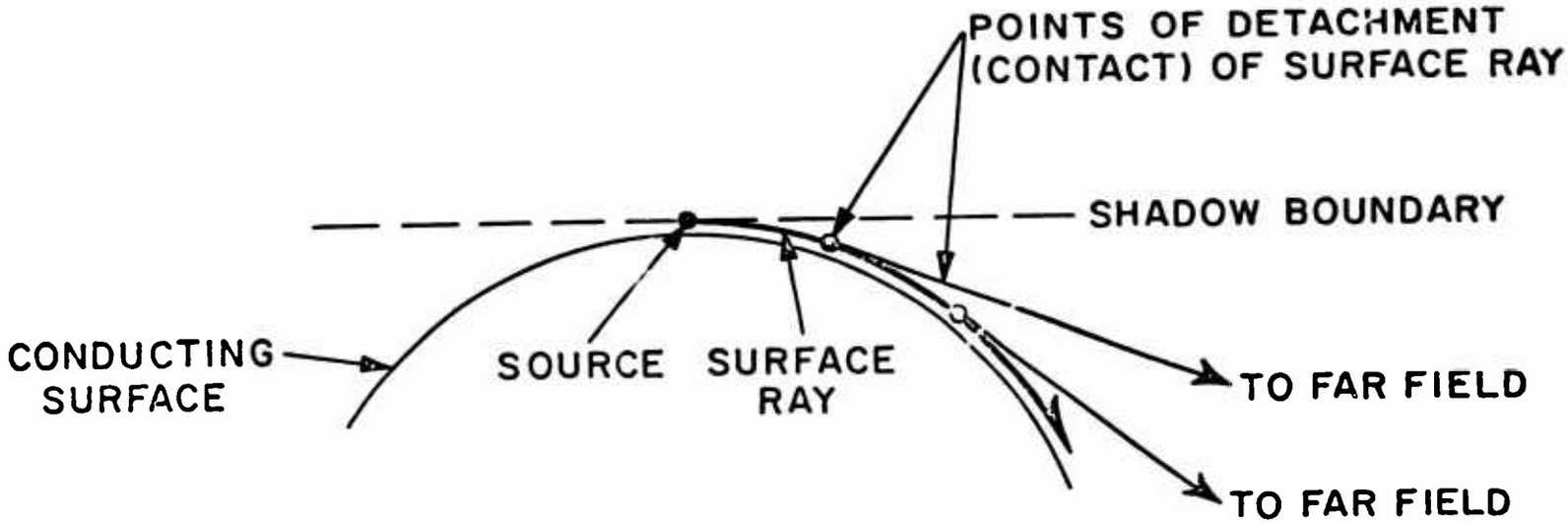

Fig. 2 Surface Ray and Its Points of Detachment

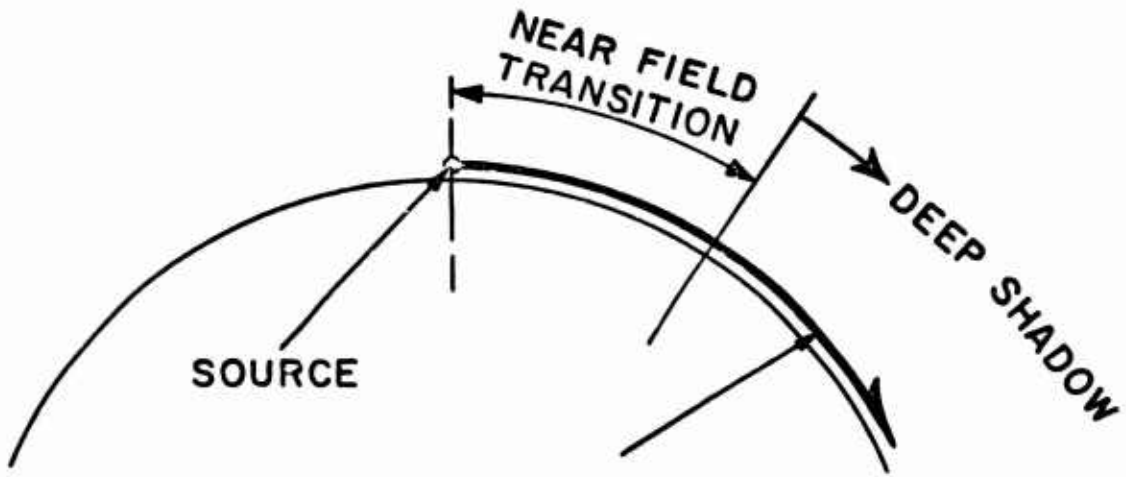

Fig. 3 Surface Field Regions for a Point Source

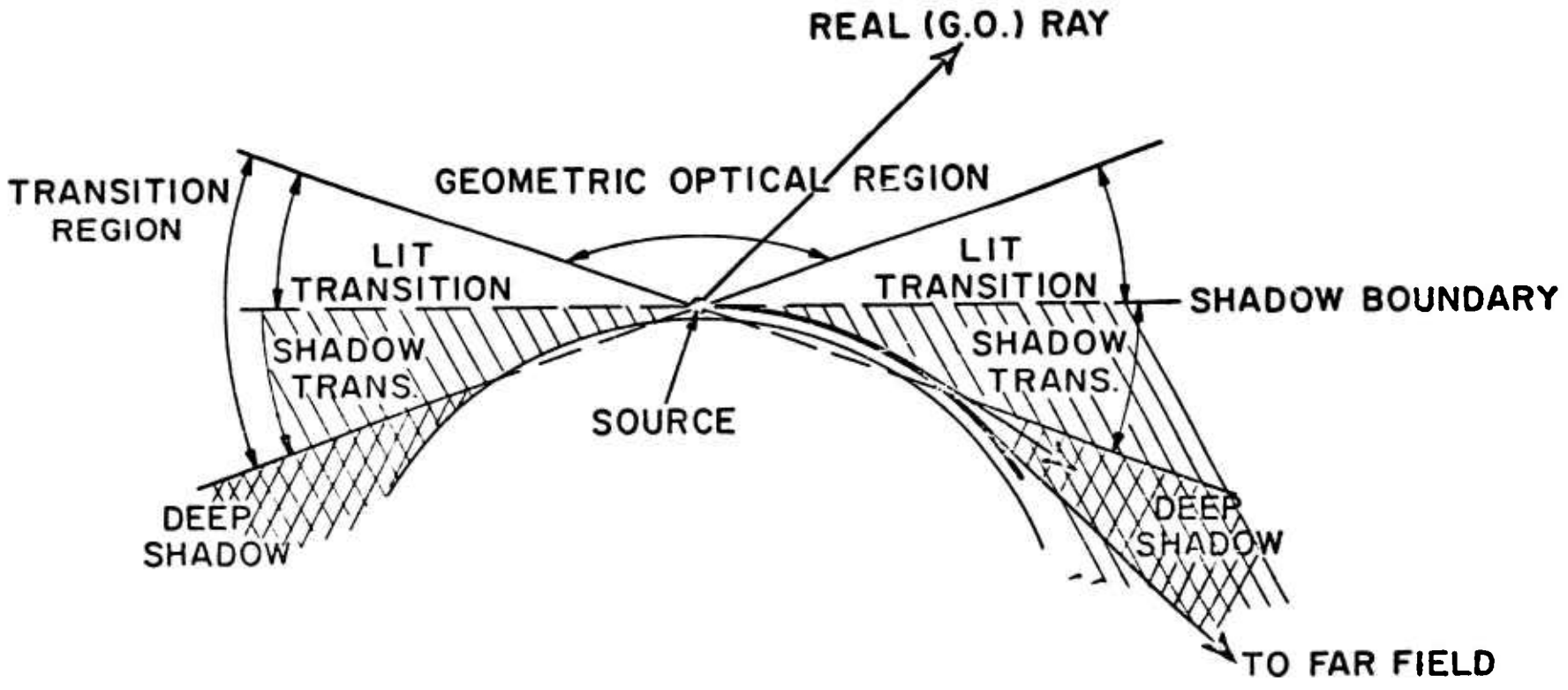

Fig. 4 Far Field GTD Regions for a Source

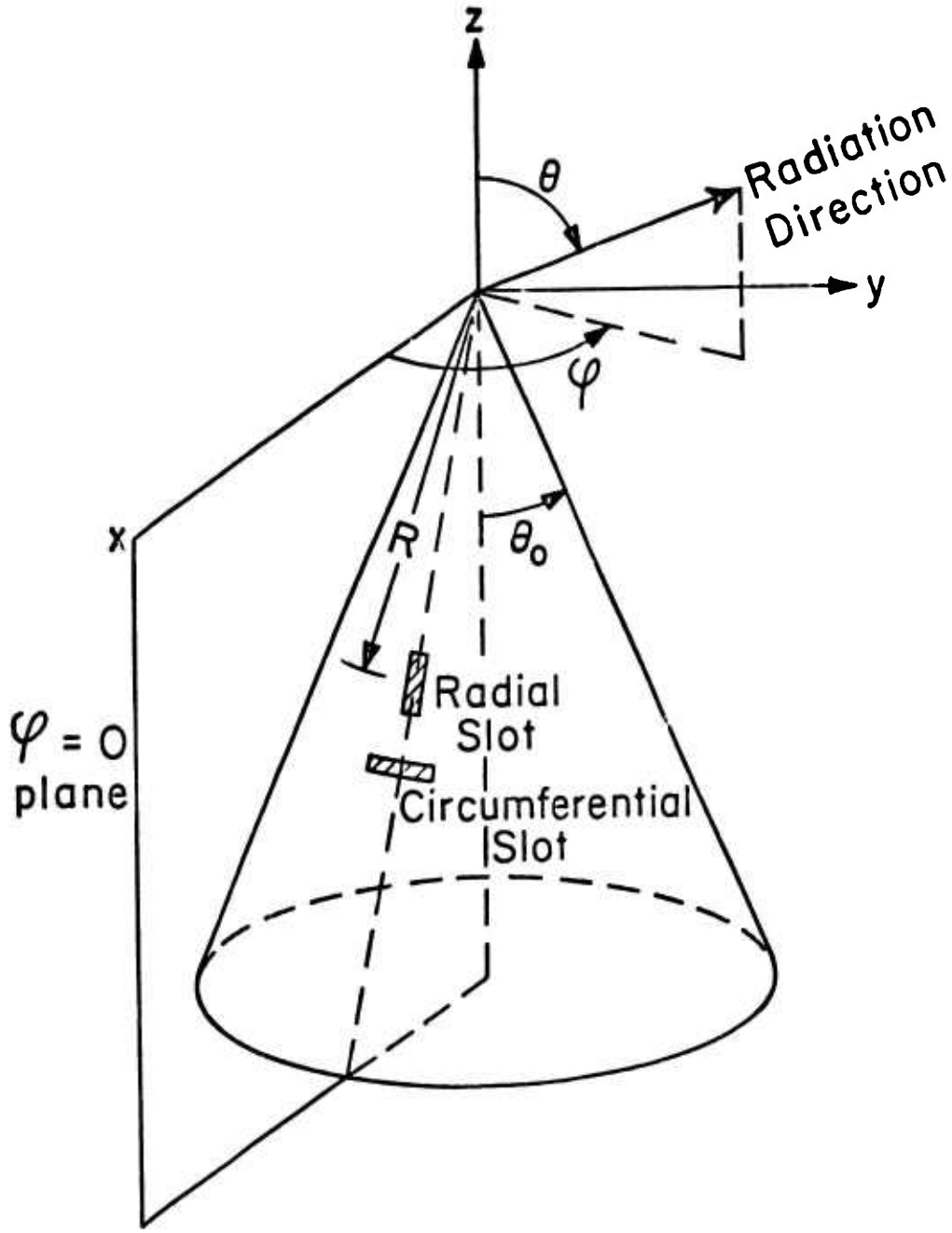

Fig. 5 Cone Geometry

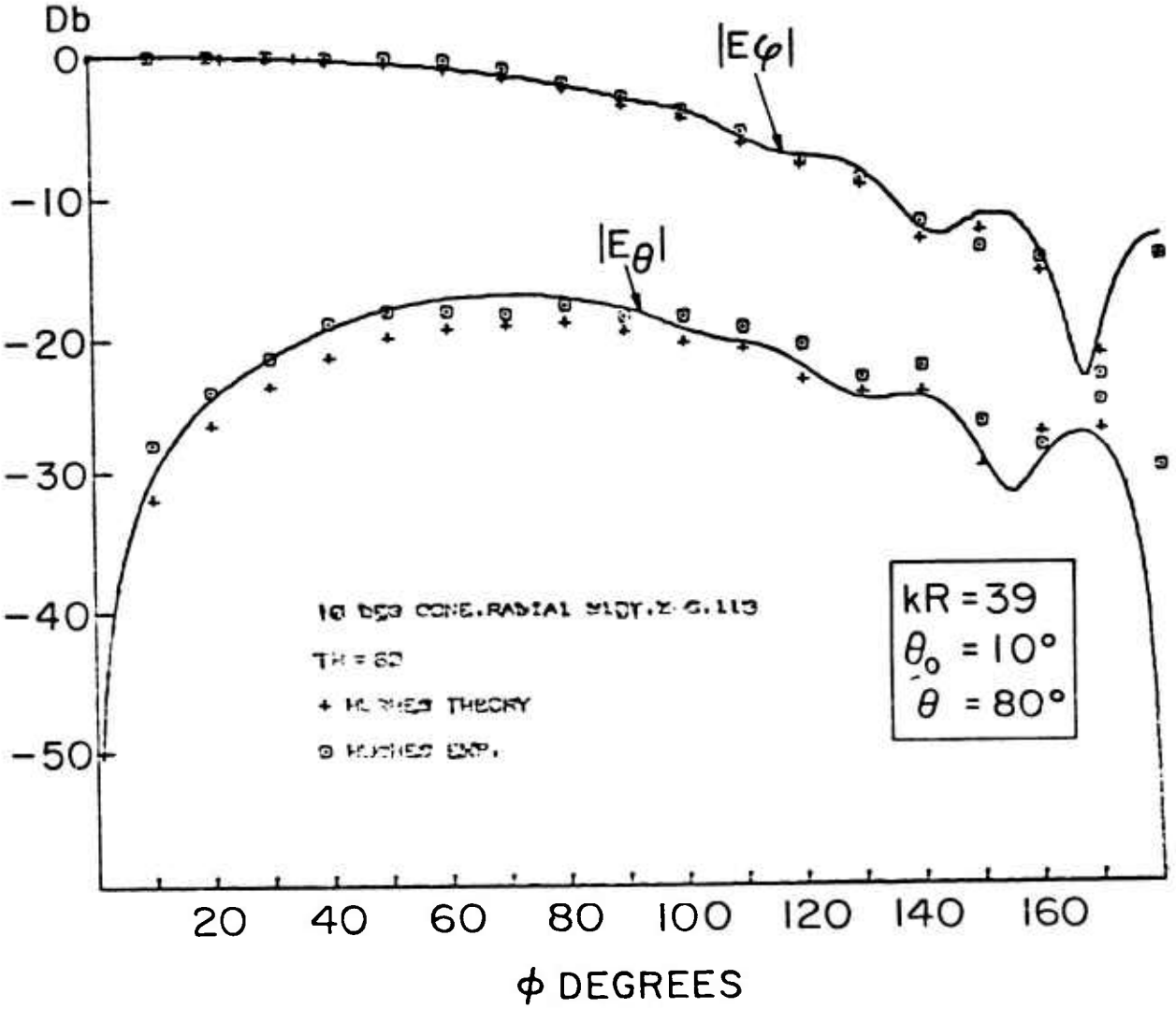

Fig. 6 Radiation Pattern of a Short Radial Slot on a Cone, $\theta = 80^{\circ}$ Conical Cut

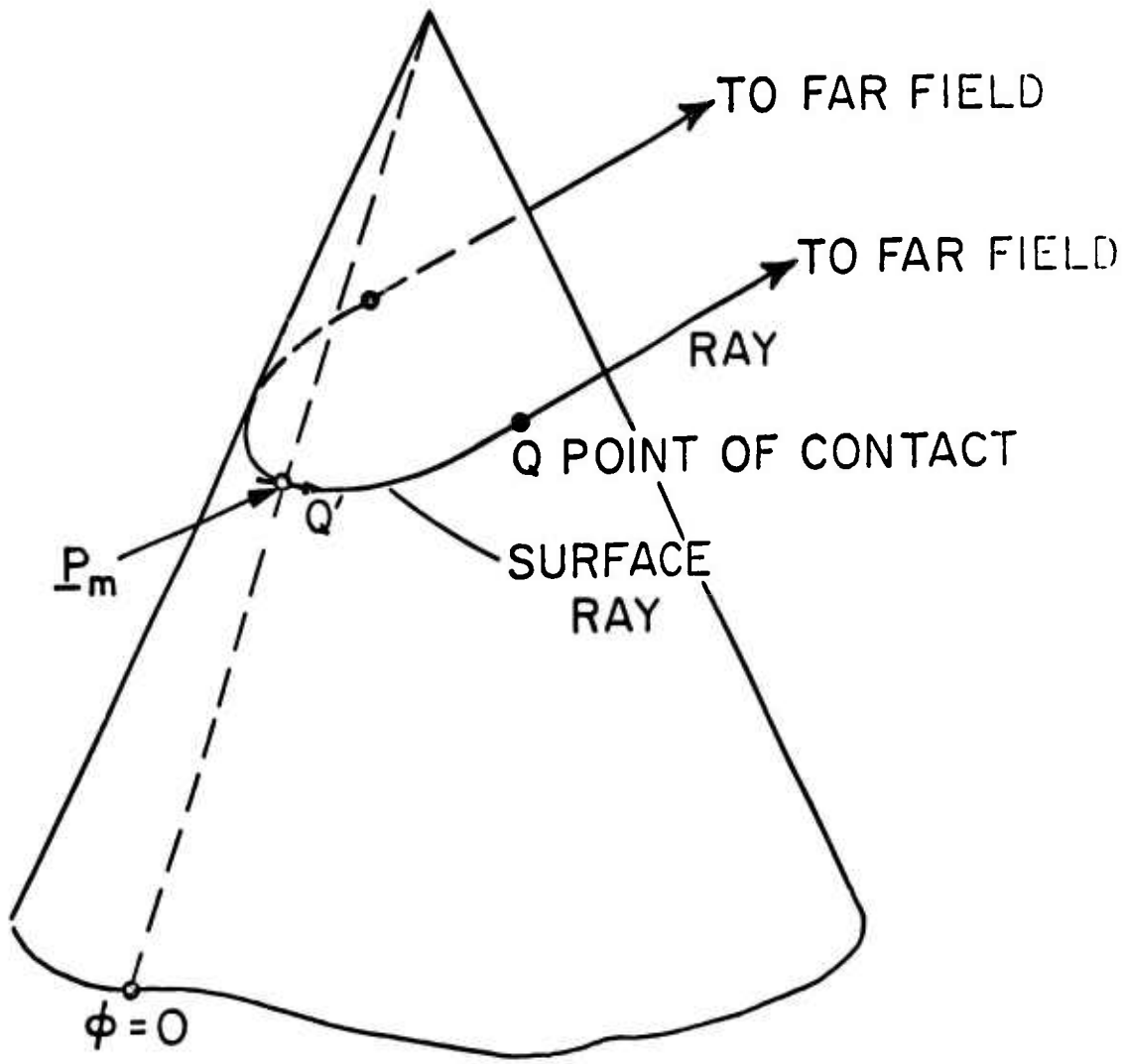

Fig. 7 Conical Geometry and Surface Ray Trajectories

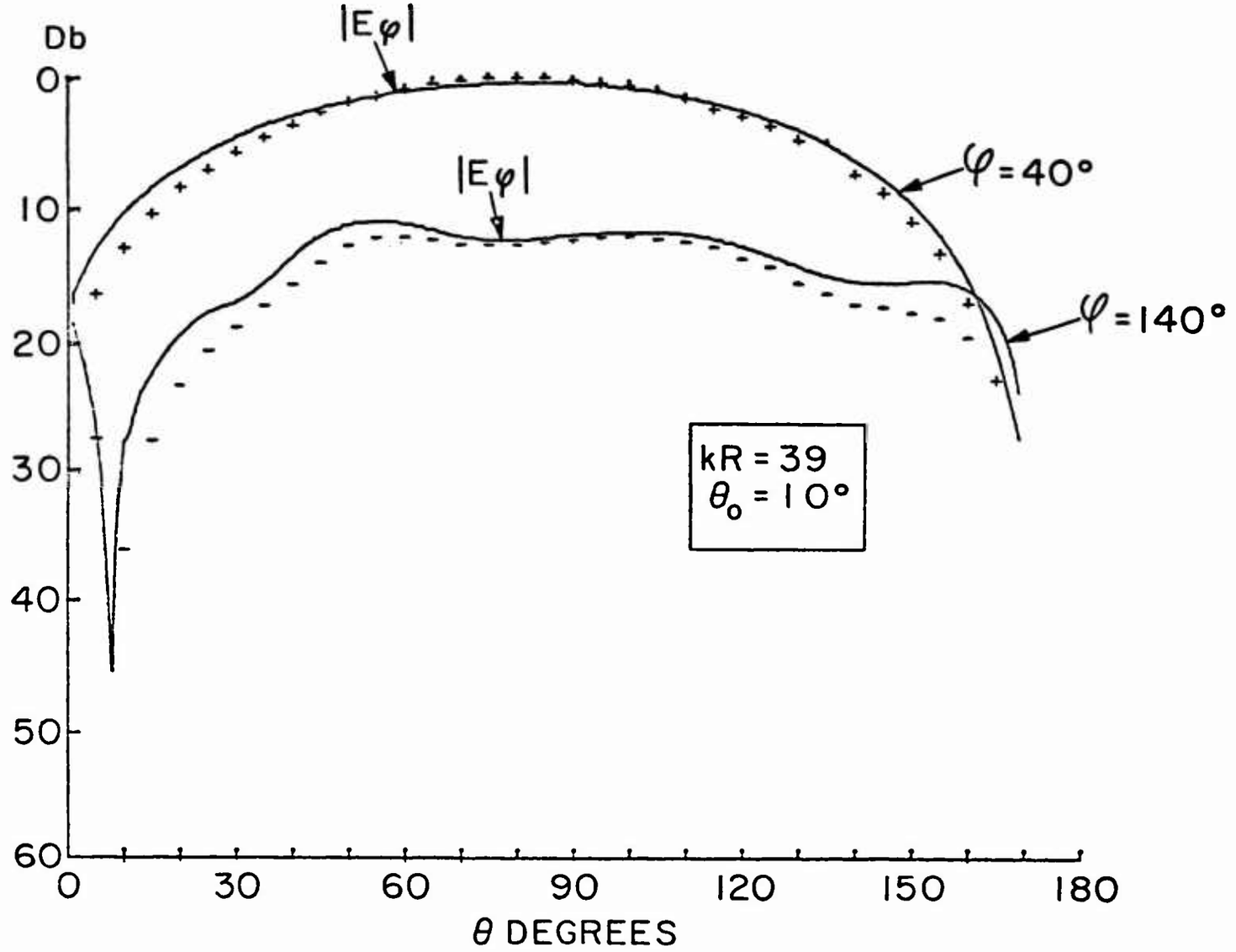

Fig. 8 Radiation Pattern of a Short Radial Slot on a Cone, Planar Cuts $\phi = 40^{\circ}$, $\phi = 140^{\circ}$

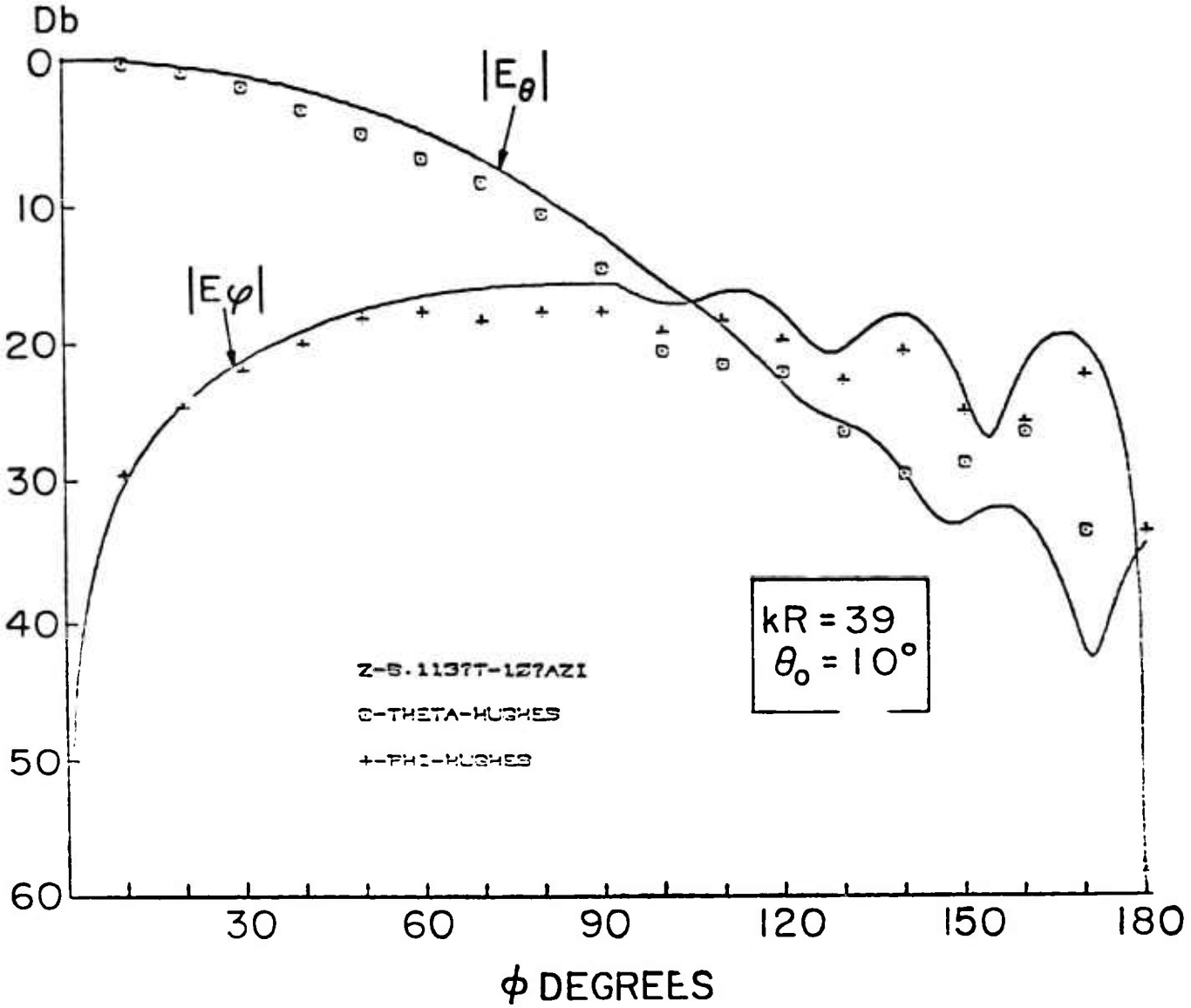

Fig. 9 Radiation Pattern of a Short Circumferential Slot on a Cone, $\theta = 80^\circ$ Conical Cut

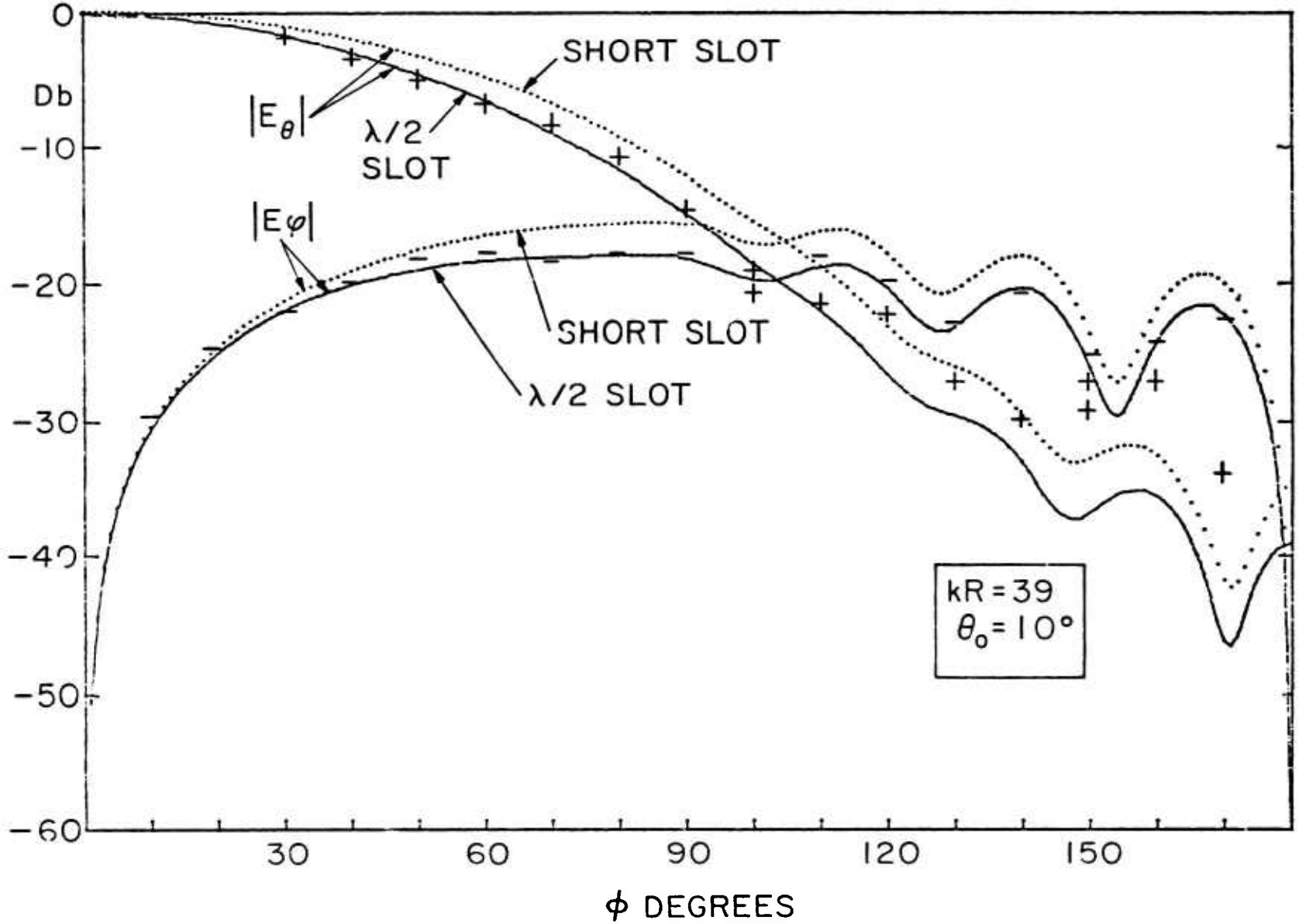

Fig. 10 Radiation Patterns of Circumferential Slots on a Cone, 80° Conical Cut

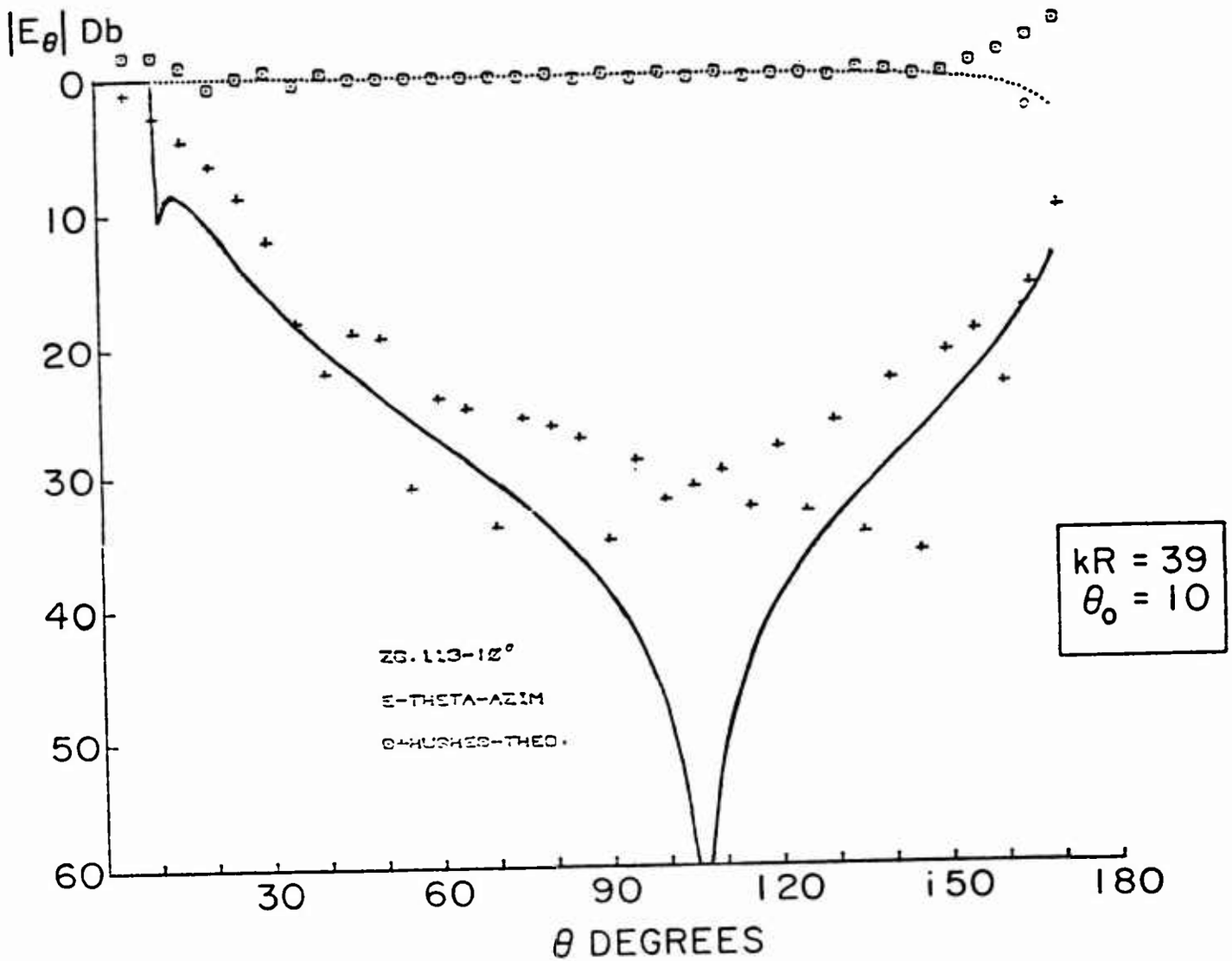

Fig. 11 E Pattern of a Short Circumferential Slot on a Cone, 0° and 180° Planar Cuts

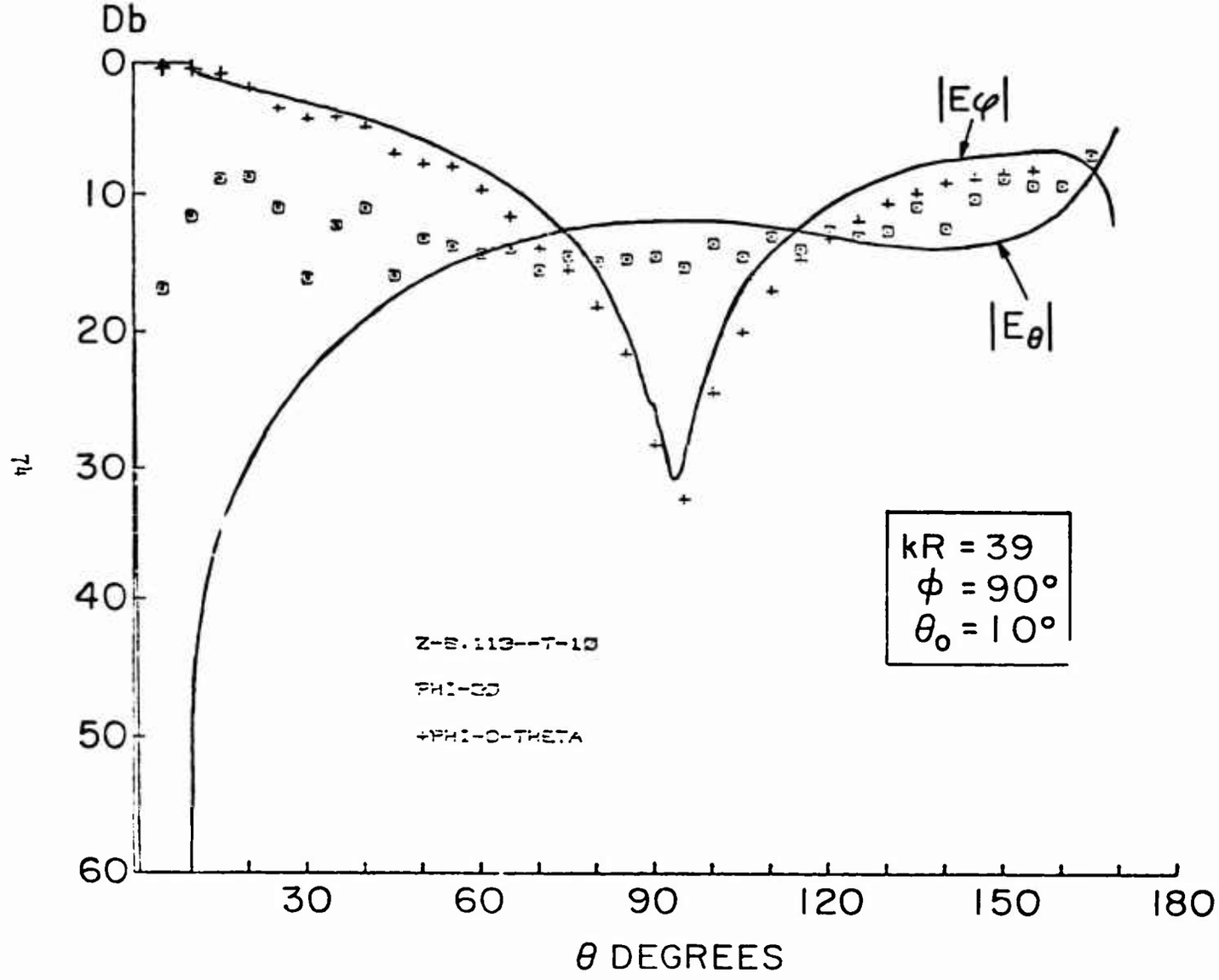

Fig. 12 Radiation Pattern of a Short Circumferential Slot on a Cone, $\phi = 90^{\circ}$ Planar Cut

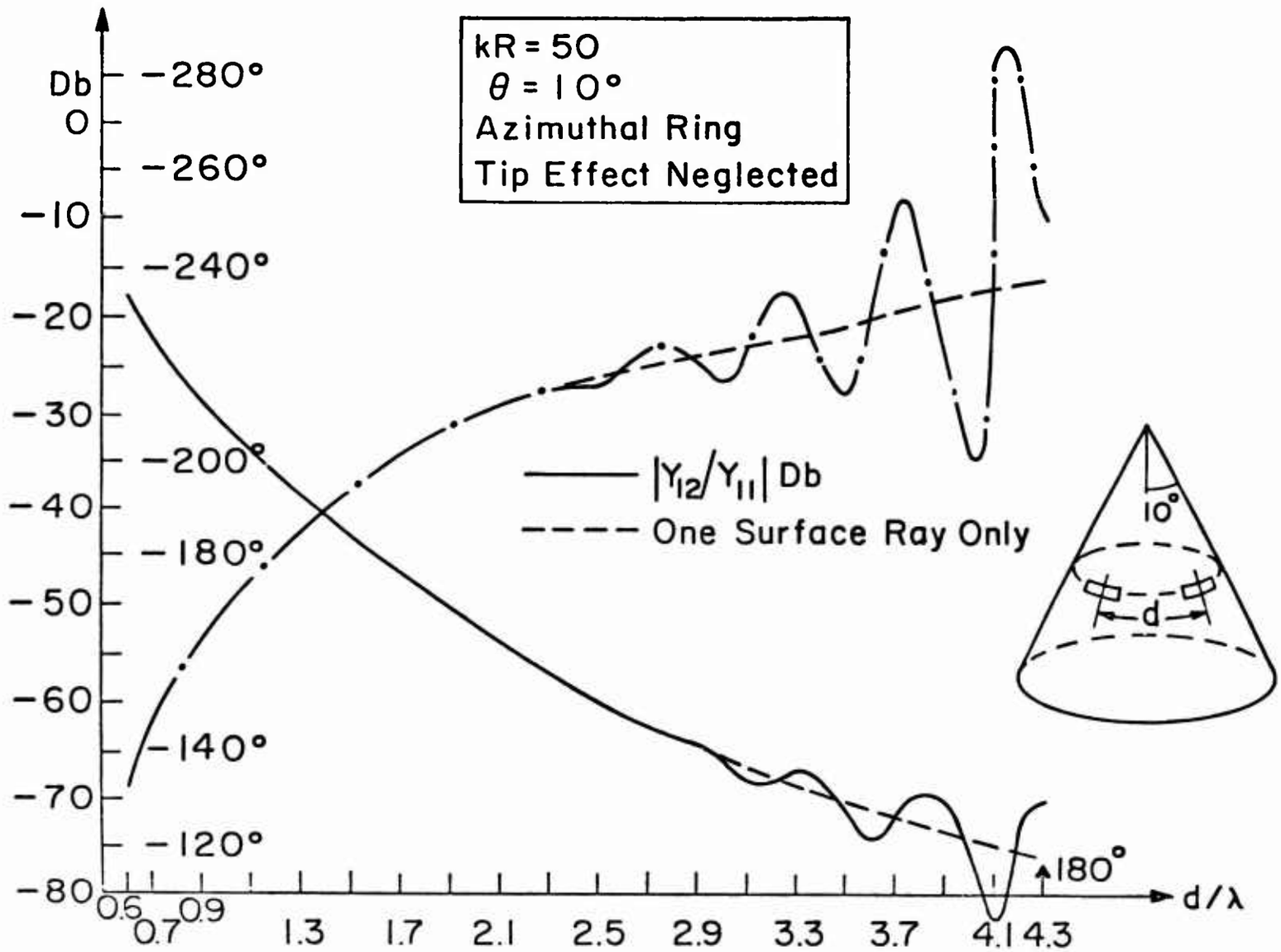

Fig. 13 Mutual Admittance between Circumferential Slots on a 10° Cone

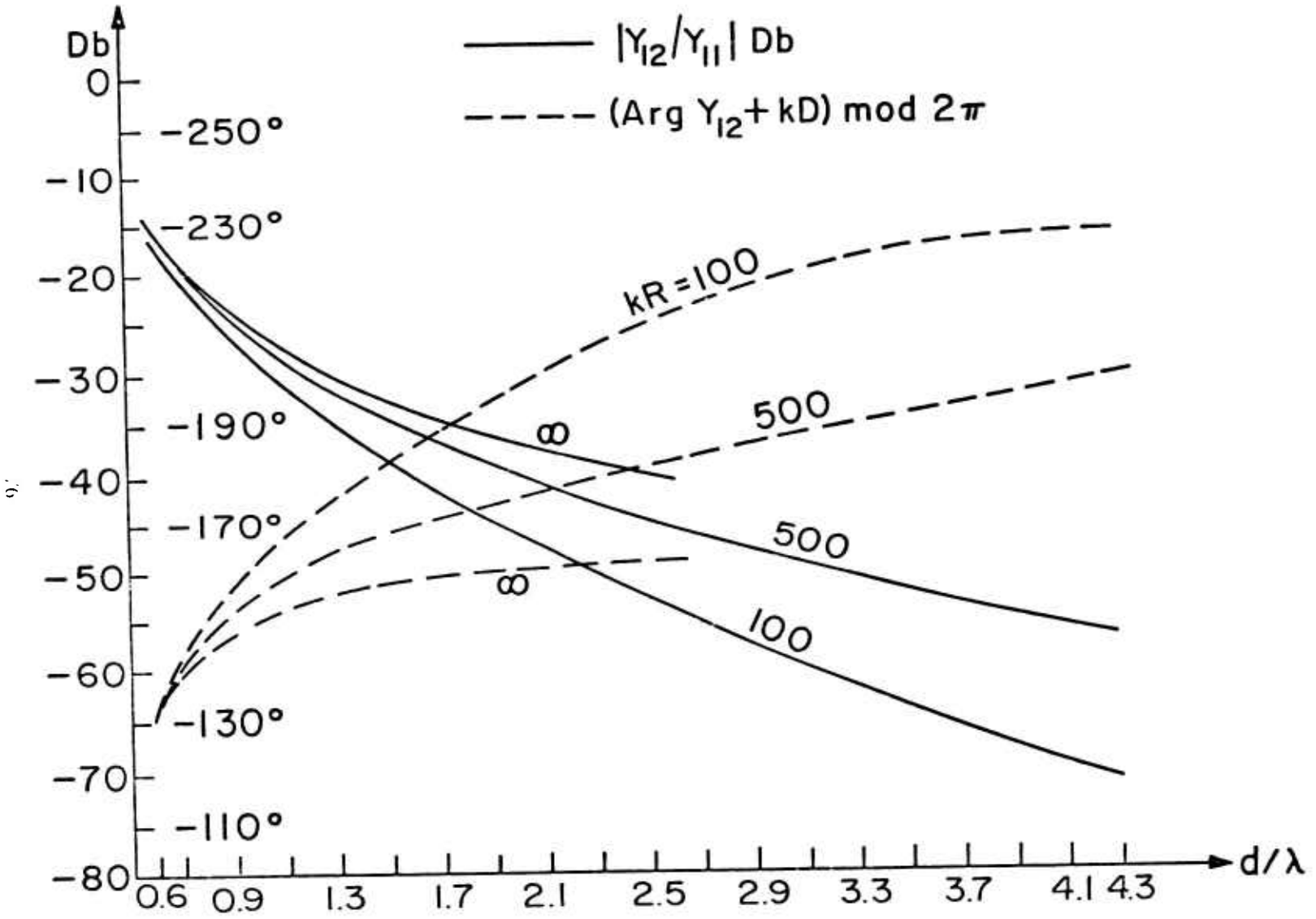

Fig. 14 Mutual Admittance between Circumferential Slots on a 10° Cone

3.1 Circumferential Slot

A narrow circumferential slot of width $2w << \lambda$ is considered as shown in Figure 15. The narrow slot has an azimuthal length $d = 2\phi_o a \sin\theta_o$ where $2\phi_o$ is the azimuthal angle subtended by the slot, θ_o is the cone exterior angle measured from the axis, a is the distance from the cone tip to the center of the slot and λ is the operating wavelength. The slot is assumed to be excited by a voltage V_o across its center and has a resulting field across it in the r direction given by

$$E_r(r', \phi') = \begin{cases} V_o \cos\left[\dfrac{\pi(\phi' - \phi_s)}{2\phi_o}\right] \delta(r' - a) & \left|\phi' - \phi_s\right| < \phi_o \\ 0 & \left|\phi' - \phi_s\right| > \phi_o \end{cases}$$

where $\delta(r' - a)$ is the Dirac delta function.

The following expressions are obtained for the electric field components:

$$E_\theta = \sum_{m=0}^{\infty} \frac{V_o e^{-j(kr - \pi/4)}}{r\pi(1 + \delta_{om})} \sqrt{2\pi ka}\, \frac{2ka\sin\theta_o \cos\left(\dfrac{m\pi}{2ka\sin\theta_o}\right)}{(ka\sin\theta_o)^2 - m^2} \cos m\phi$$

$$\left\{ P_{1\theta} + \frac{jm^2}{\sin\theta_o \sin\theta} P_{2\theta} \right\}$$

where $P_{1\theta} = \sum_{i=1}^{\infty} j^{\nu_i} \dfrac{\nu_i}{\nu_i^2 - 1/4} J_{\nu_i}(ka) \left.\dfrac{\dfrac{\partial}{\partial\theta} P_{\nu_i - 1/2}^{-m}(\cos\theta)}{\dfrac{\partial P_{\nu - 1/2}^{-m}(\cos\theta)}{\partial\nu}}\right|_{\substack{\theta = \theta_o \\ \nu = \nu_i}}$

$$\text{and } P_{2\theta} = \sum_{i=1}^{\infty} j^{\nu'_i} \frac{\nu'_i}{\nu'^2_i - 1/4} \left. \frac{P^{-m}_{\nu'_i - 1/2}(\cos\theta)}{\frac{\partial^2 P^{-m}_{\nu - 1/2}(\cos\theta)}{\partial\nu\,\partial\theta}} \right|_{\substack{\theta = \theta_o \\ \nu = \nu'_i}} \left[\frac{\left(\nu'_i + \frac{1}{2}\right) J_{\nu'_i}(ka)}{ka} - J_{\nu'_i + 1}(ka) \right]$$

$$E_{\phi} = \sum_{m=0}^{\infty} m \frac{V_o e^{-j(kr - \pi/4)}}{r\pi} \sqrt{2\pi ka} \cdot \frac{2ka \sin\theta_o \cos\left(\frac{m\pi}{2ka \sin\theta_o}\right)}{(ka \sin\theta_o)^2 - m^2} \sin m\phi$$

$$\cdot \left\{ \frac{-j}{\sin\theta} P_{1\phi} + \frac{1}{\sin\theta_o} P_{2\phi} \right\}$$

where

$$P_{1\phi} = \sum_{i=1}^{\infty} \frac{\nu_i}{\nu_i^2 - 1/4} j^{\nu_i} J_{\nu_i}(ka) \left. \frac{P^{-m}_{\nu_i - 1/2}(\cos\theta)}{\frac{\partial P^{-m}_{\nu - 1/2}(\cos\theta)}{\partial\nu}} \right|_{\substack{\theta = \theta_o \\ \nu = \nu_i}}$$

$$\text{and } P_{2\phi} = \sum_{i=1}^{\infty} \frac{\nu'_i}{\nu'^2_i - 1/4} j^{\nu'_i} \left. \frac{\frac{\partial}{\partial\theta} P^{-m}_{\nu'_i - 1/2}(\cos\theta)}{\frac{\partial^2 P^{-m}_{\nu - 1/2}(\cos\theta)}{\partial\nu\,\partial\theta}} \right|_{\substack{\theta = \theta_o \\ \nu = \nu'_i}} \cdot \left[\frac{(\nu'_i + 1/2) J_{\nu'_i}(ka)}{ka} - J_{\nu'_i + 1}(ka) \right]$$

FLUSH MOUNTED RADIATING ELEMENTS FOR CONFORMAL ARRAYS

Arthur R. Sindoris, Frank Reggia & Howard S. Jones, Jr.
Harry Diamond Laboratories
Adelphi, Maryland

ABSTRACT

A series of radiators for use in the 300-3000 MHz frequency range has been developed for flush-mounting applications. These radiators are essentially dielectric-loaded, cavity-backed slots whose exterior dimensions and form factors have been adjusted to allow flush-mounting of the radiators to the surfaces of projectiles and reentry vehicles. This paper describes the electrical properties, theory of operation and design techniques of several different types of radiators. The material properties of the dielectric substrate and the use of two types of slot radiators in a conformal array system for a reentry vehicle are also presented.

INTRODUCTION

A family of thin-wall, dielectric-loaded radiators have been designed to conform to projectile surfaces of arbitrary shape. Because their shapes can be molded and adjusted for flush-mounting to almost any surface contour, they have potential application in conformal phased arrays. Most of the work reported in this paper has been for the application of conformal antennas to small bodies such as RV's, RPV's, projectiles, and aircraft. One example using these conformal radiators is given for a four-element phased array in an RV application.

CONFORMAL RADIATIORS

The basic structure of the conformal radiators is a low-loss dielectric substrate material fabricated in the desired shape over which a thin copper wall is plated to form the radiating element. These compact thin-wall antennas are essentially dielectric-loaded cavity-backed slot radiators. The copper plating adheres strongly to the dielectric substrate to provide smooth, conducting surfaces for the cavity. The low-loss dielectric materials used for the antenna have a relative dielectric constant which depends on the particular application. Two commonly used materials include silicone fiberglass (G-7) having a dielectric constant (ε_r) of 4.2 and teflon fiberglass with $\varepsilon_r = 2.6$. Although an epoxy fiberglass material (G-10 or G-11) with an ε_r of 4.5 has a higher dielectric loss tangent, it too has been used successfully. The purpose of the dielectric-loading is to reduce the overall size of the antenna and to provide the desired shape and support for the cavity walls.

A variety of prototype conformal radiators is shown in Fig. 1. The cone-shaped antennas are designed for mounting on the nose of small projectile and the two-ring antennas are used on the outside surface of the projectile. Antenna (A) is composed of two microstrip radiators plated on the epoxy fiberglass cone shown at (B). The inner

surface of the cone is copperplated to form a small conformal ground plane. Antennas (C) and (D) are single-slot radiators cut into dielectric-loaded cavities which are formed by copperplating on the cone shaped dielectric substrate. An electric post is then used to couple the rf power into the cavity. For antenna (E), the radiating slot is formed between the inner conducting wall and the edge of the outer conducting wall. Antenna (F) is a dual purpose antenna comprised of one type (E) radiator and a two-slot version of the type (C) model. Antennas (G) and (H) have slot radiators excited by cylindrical cavities, (G) being a two-slot and (H) a single-slot version. Fig. 2 shows antenna (G) mounted conformal to the outside surface of a projectile, a typical application for this type of circumferential slot antenna. All the antennas shown in Fig. 1 produce dipolar radiation patterns with nulls along the axis of the projectile on which they are mounted. The frequency of operation for the above radiators is from 1 to 3 GHz with instantaneous bandwidths from 3% to 10%.

A family of parallel-plate radiators constructed in two different shapes (wedge and semicircular) for different applications is shown in Figs. 3 and 4. The wedge-shaped radiators (Fig. 3) are used in the nose of blunt, conical projectiles with the curved edge of the radiator conforming to the surface. The aperture of the radiator is the slot formed by the opening between the two conducting plate. The back edge of the radiator is short circuited and the excitation post is placed at a point near the shorting wall where the input impedance is 50 ohms. The antennas are generally characterized by small size ($< \lambda/8$), high efficiency (70%-90%), and they are inexpensive to fabricate. The radiation pattern of course, is a function of the shape and size of the projectile upon which the antenna is mounted.

The antenna shown in Fig. 5 is an example of an application for the semicircular parallel-plate radiator. The antenna is comprised of two orthogonally mounted radiators to give dual polarization capability. It can easily be mounted in the nose of a projectile to obtain a forward directed radiation pattern. By adjusting the curvature at the open end of the parallel-plate radiators, the antenna can be mounted on the surface of the projectile.

A simplified sketch of a four-element conformal phased array for a reentry vehicle application is shown in Fig. 6. The forward surface-mounted set of radiators is a circumferential ring antenna similar to that shown in Fig. 1G except that the cavity is mounted inside the vehicle and only the slots protrude the surface. The set of cavity-backed slot radiators mounted on the base of the projectile is also similar to that shown in Fig. 1G except that the cavity is designed to extend inward along the radius of the base, allowing the cavity to be flush-mounted.

The desired radiation pattern for the array of four conformal radiators has a maximum in the forward direction and a null out the back of the projectile. Because the operating wavelength is on the same order as the length of the vehicle, a strong rf coupling exists between the radiating slots and the vehicle. This allows for significant forward-directed radiation and makes it possible to obtain the desired pattern. By phasing the slots and adjusting the power distribution, the measured radiation pattern shown in Fig. 7 is obtained.

CONCLUSION

The design of many different conformal radiators for projectile applications and relatively small conformal phased arrays have been successfully demonstrated. These antennas are ideally suited for operation in the UHF and low microwave frequency range. The extension of the above radiator technology to large, conformal, electronically scanned phased arrays is the next step to be considered.

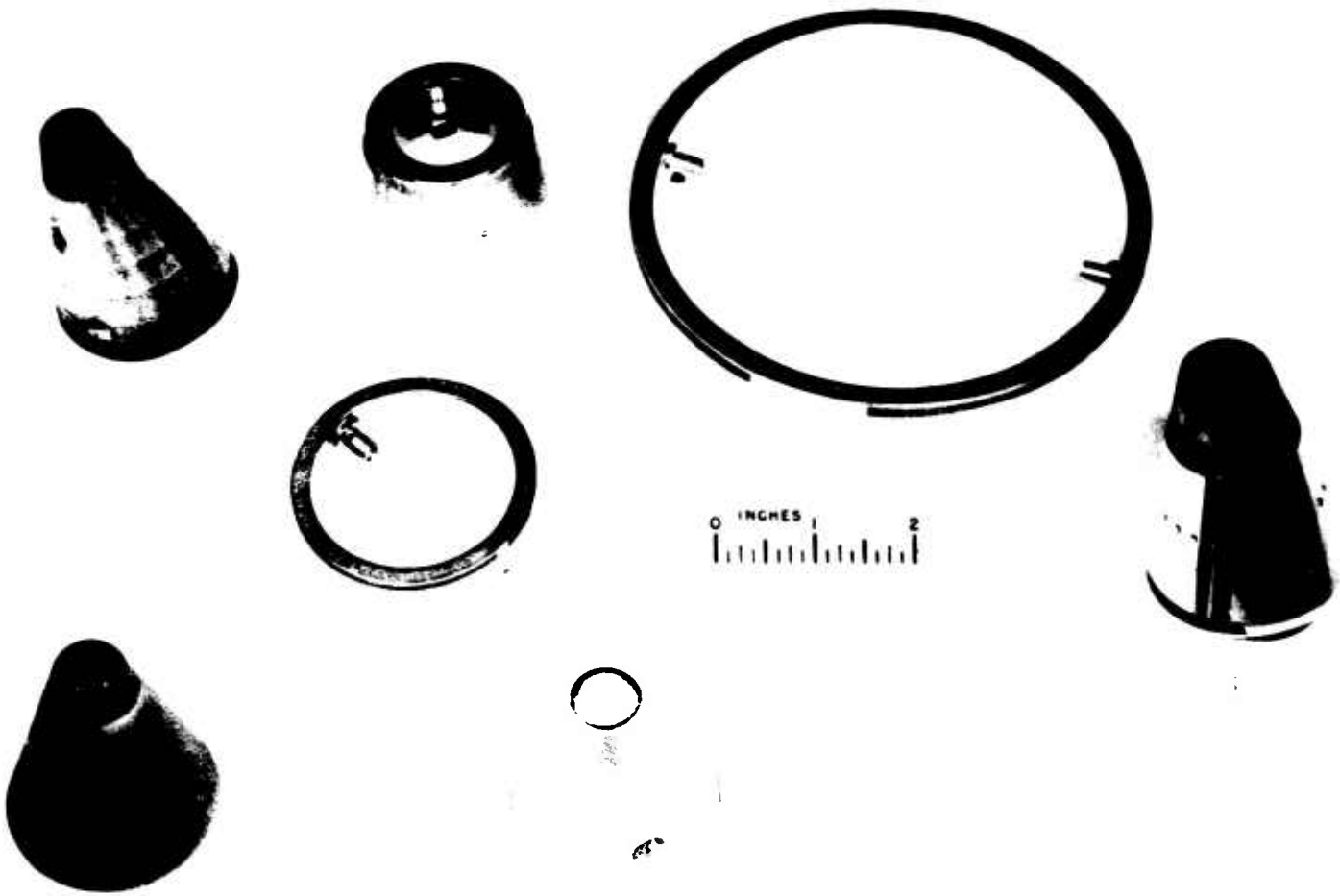

Figure 1 - Family of Conformal Radiators

Figure 2 - Circumferential Slot Radiator Mounted on a Projectile

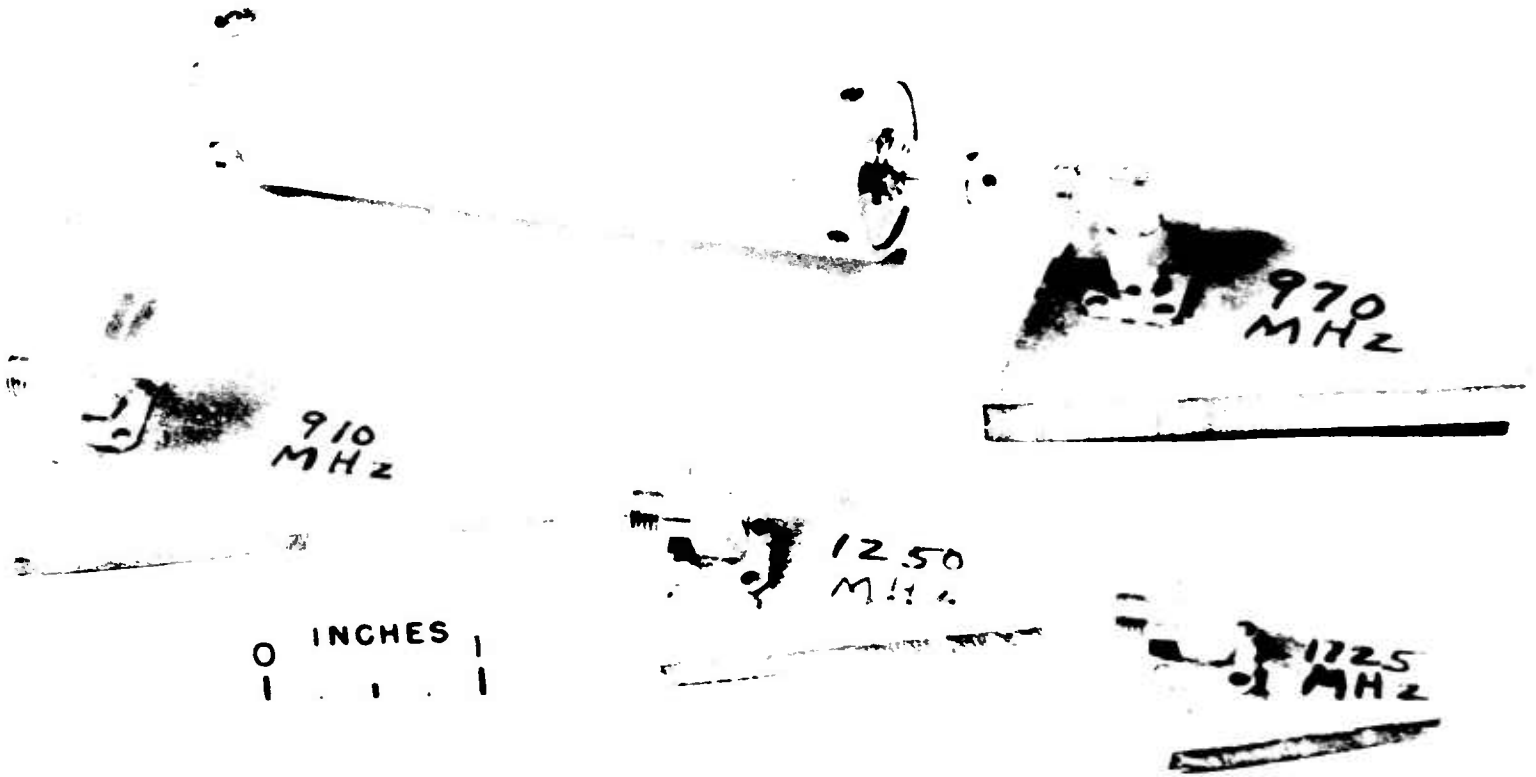

Figure 3 - Family of Wedge-Shaped Parallel Plate Radiators

Figure 4 - Family of Semicircular Parallel Plate Radiators

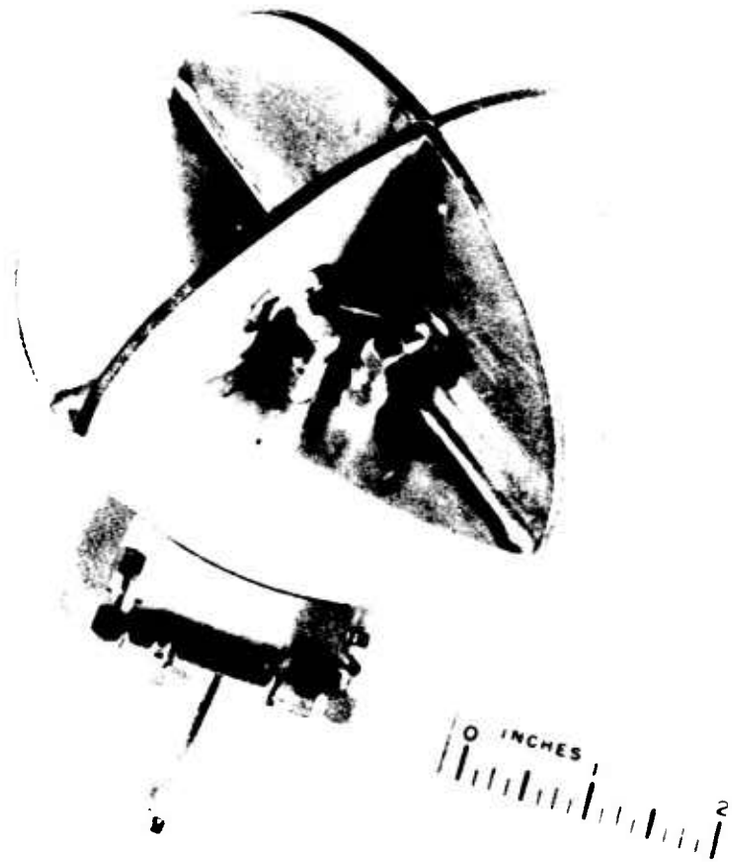

Figure 5 - Quadrature Parallel-Plate Antenna

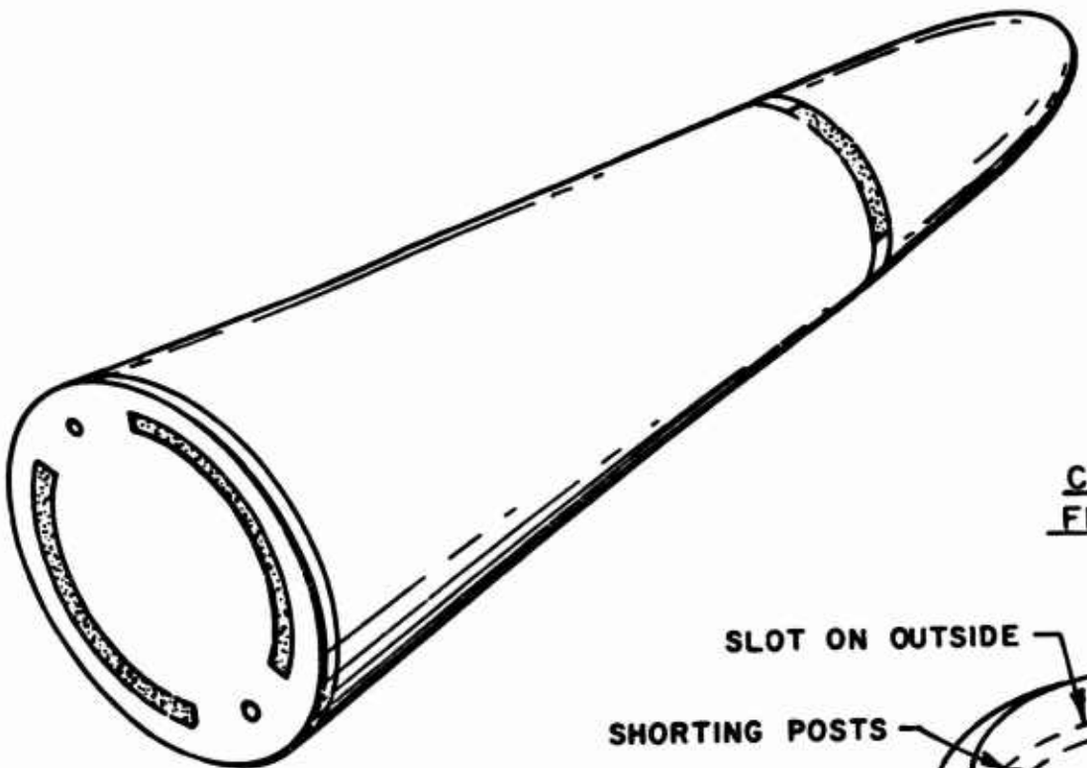

CROSS-SECTION OF
FIELD JOINT ANTENNA

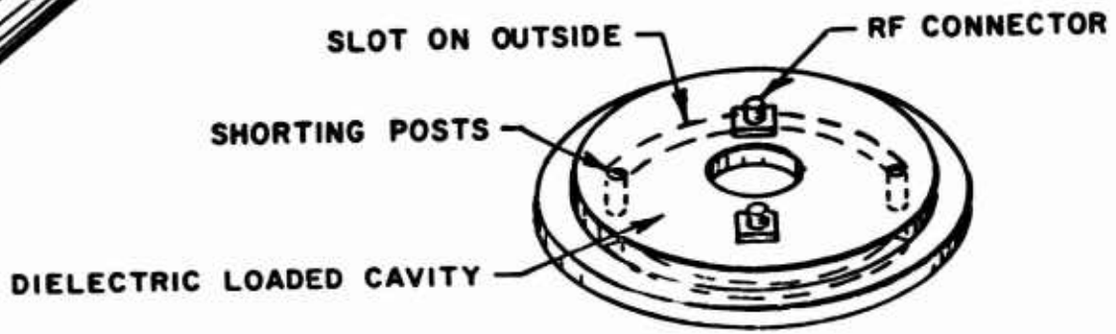

INSIDE SIDE OF BASE PLATE

Figure 6 - Conceptunal Drawing of a Four-Element Conformal Phased Array

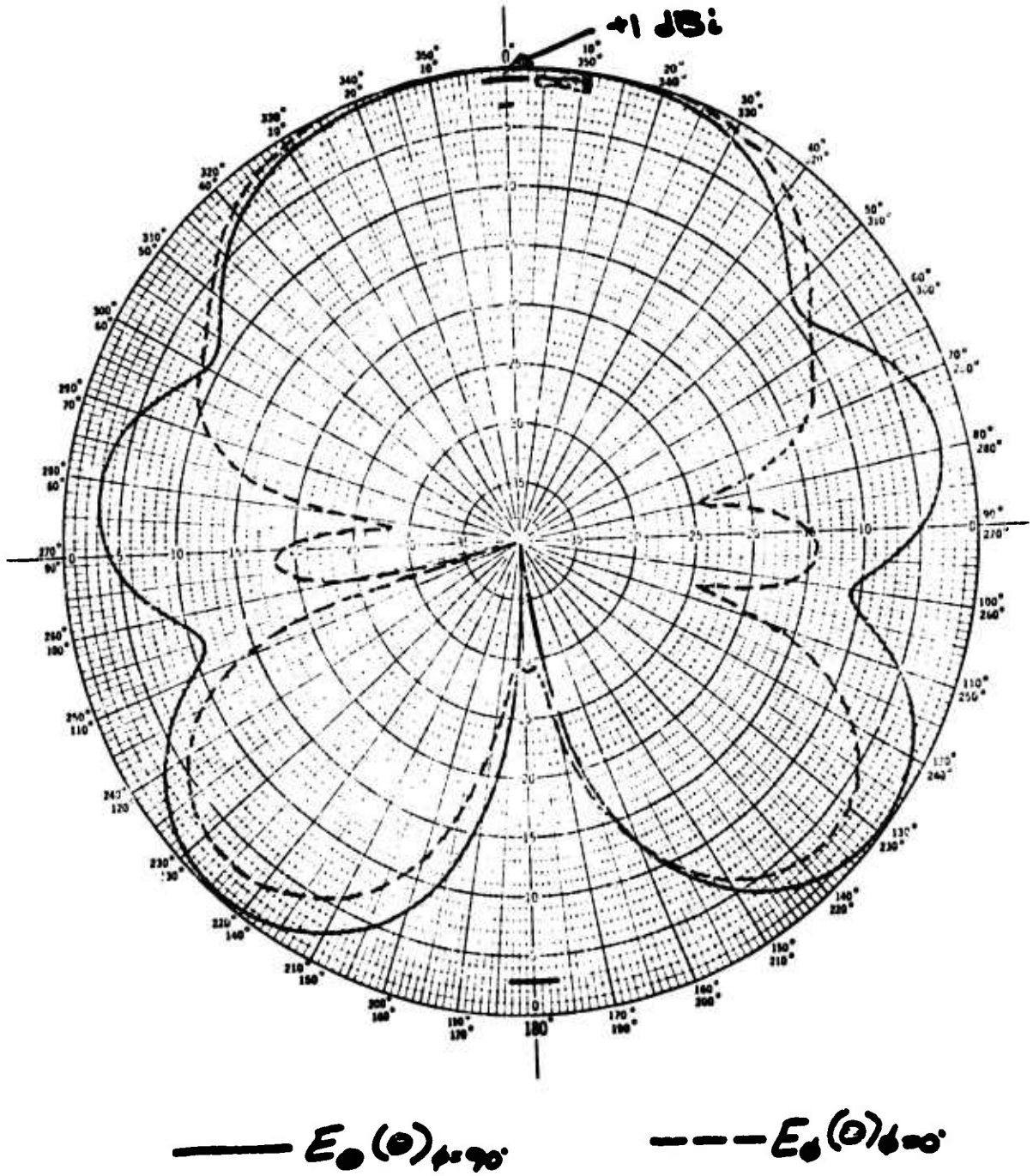

Figure 7 - Measured Radiation Pattern of Four Element Conformal Phased Array

ANALYSIS OF ARRAYS ON A CONDUCTING CONICAL SURFACE

G. V. Vaughn

(Naval Electronics Laboratory Center, San Diego, CA.)

I. BACKGROUND

In recent years, the realization of the advantages of conformal arrays have made such arrays a highly desirable configuration. Lately, advances in the Geometric Theory of Diffraction (GTD) have made the analysis of conformal arrays feasible. In this project, the problem of analyzing the properties of a conical array is undertaken.

The antenna under investigation is an array of open-ended RG (52)/U rectangular waveguides flush mounted in a conical conducting surface. The array and the dimensions of the cone are shown in figures 1 and 2. At the designed center frequency (9.0 GHz) the spacing of the center elements is 0.599 λ in azimuth and 0.760 λ radially.

II. APPROACHES

Using theoretical equations developed in conjunction with the Polytechnic Institute of New York, computer programs were created at NELC to:

a) Calculate the radially aligned magnetic Green's function on a conical conducting surface

b) Calculate the mutual admittance matrix for elements on the cone

c) Solve the matrix equation for excitation coefficients

d) Calculate array-element radiation patterns

e) Calculate array radiation patterns

A. Magnetic Green's Function on Cone

To achieve expressions for a radially directed magnetic dipole which are econo-

mically programmable, the space about the cone is divided into four regions: a) lit region, b) transistion-lit region, c) transistion-shadow region and d) shadow region. The expressions for the Green's function in each of those regions are given below.

In the lit region:

$$\underline{E} = \frac{jk}{2\pi R} e^{-jkR} [\hat{k} \times \hat{r}]$$

where $\hat{k}$ is a unit vector in the direction of the field point and $\hat{r}$ is the unit vector at the conical tip directed towards the source.

In the transistion-lit region:

$$\underline{E} = \frac{jk}{4\pi R} e^{-jkR} [\hat{k} \times \hat{r}] G(D)$$

where G(D) is the modified Fock function

$$G(D) = g(D) e^{j D^3/3}$$

and the argument of the Fock function is given by an integration over the geodesic path on the conical surface from the source point, Q', to the point of diffraction, Q.

$$D = \int_{Q'}^{Q} \frac{k^{1/3}\, ds}{2^{5/3} (\rho_g(s))^{2/3}}$$

and $\rho_g(S)$ is the principle radius of curvature as a function of distance from the source.

In the shadow-transistion region:

$$\underline{E} = \frac{jk}{4\pi R} e^{-jkR} \sin\gamma'\, g(D)\, e^{-jks + j\underline{k}\cdot\underline{S}}$$

where γ' is the angle between the geodesic ray and cone generator at the source, $\underline{S}$ is the vector from the source point to the point of diffraction, Q. The length of the geodesic path on the cone is S and g(D) is the Fock function.

For the cases under consideration in this project, the Green's function in the far field shadow region is the vectorial sum of the field of two rays diffracting from opposite sides of the cone:

$$\underline{E} = \frac{jk e^{-jkR}}{4\pi R} \sum_{m=1}^{2} \hat{\theta} P_m (\sin\gamma')_m [L(Q') D(Q)]_m e^{-(\alpha+j\beta)\ell_m - jks_m + j\underline{k}\cdot\underline{s}_m}$$

wher L(Q') is the launching coefficient at the source and D(Q) is the diffraction coefficient at the point of diffraction.

The expressions above were programmed and numerically integrated over the aperture of an open-ended waveguide flush-mounted on a cone. A single mode was assumed in the waveguide. The computed results are compared with measurements on two cones. The cone at NELC had a 20° half angle and the waveguides were flush-mounted at ka = 100. A second cone was built and patterns taken at Hughes, Culver City. The Hughes cone had a 10° half-angle and the waveguide mounted at ka = 20. The excellent agreement between calculation and measurement is shown in figures 3 and 4.

B. Mutual Admittance

The expression for the mutual admittance between two slots is given by an integral over slot two:

$$Y_{12} = \frac{1}{V_1 V_2} \iint_{S_2} \underline{E}^{(2)} \times \underline{H}^{(1)} \cdot \hat{N}\, dS_2$$

where:

$\underline{E}^{(2)}$ = electric field due to impressed voltage, V_1, across slot two.

$\underline{H}^{(1)}$ = magnetic field at slot two due to impressed voltage, V_2, across slot one.

$\hat{N}$ = outward directed unit normal at slot.

G. Hasserjian and A. Ishimaru derived expressions for the fields induced on a cylindrical surface by a short slot dipole. This analysis has been extended to apply to any surface with a slowly varying curvature. The component of tangential

magnetic current along a cone oenerator is given by:

$$H_r(Q) = \frac{-wekVdl}{2\pi} \frac{e^{-jks}}{ks} \frac{\sin\gamma' \sin\gamma}{\sqrt{f_g(Q')\, f_g(Q)}} \begin{cases} j\sqrt{\frac{ks}{2D}}\, g(D) & \text{near source} \\ \sqrt{\pi \frac{ks}{2}}\, e^{-j\pi/4} \sum_m \frac{e^{-jDt_m}}{t_m} & \text{far field} \end{cases}$$

where:

γ' = angle between cone generator and geodesic at source.

γ = angle between cone generator and geodesic at Q.

t_m = roots of Airy function.

$$f_g(Q) = \left(\tfrac{1}{2} k \rho_g(Q)\right)^{1/3}$$

The expressions above were used to calculate mutual admittance between slots on a conducting cone. The results were compared with results reported by Borgiotti in reference 3. These are shown in figure 5.

C. Scattering Matrix

The results of the previous section is a matrix whose elements are the mutual admittance between the various elements in the antenna array. To calculate the array-element pattern, the excitation coefficients are needed. The relation between the excitation coefficients when one element of the array is excited and the mutual admittance matrix is given by:

$$2Y_0 [00\cdots010\cdots00]^T = ([Y] + Y_0 [I])([V]$$

where Y_0 is the characteristic admittance of the feeding guide and [I] is the unit matrix and [V] is a vector of the excitation coefficients.

Thus, it is necessary to solve a large set of simultaneous equations with complex coefficients. For our array of 11 rows and 41 columns, the system of equations contains 451 equations and 451 unknowns. To reduce the amount of core required by the computer, the antenna array was assumed to have only 9 rows

and 33 columns. This assumption reduced the system of equations to 297 equations and 297 unknowns. It was found that the array-element patterns obtained using this assumption were in very good agreement with measurements. The resulting coupling coefficients along the center column and along the center row are plotted in figure 6.

D. Array-Element Radiation Patterns

By using the Green's function and the excitation coefficients from the previous section, the element pattern in the array environment can be calculated. The expression in the far-field is:

$$\underline{E}(\underline{R}) = \sum_{i=1}^{M\,N} V_i \int_{S_i} |\underline{e}(S_i)| \underline{E}\, e^{-jk\underline{r}_i \cdot \underline{R}}\, dS_i$$

where the integration is over the first element aperture and $\underline{e}(S_1)$ is the assumed model voltage in the aperture and $\underline{E}$ in the integrand is the Green's function of section A.

Computer programs were created to implement these expression. The results of these programs are compared with measurements in figure 7. The results show excellent agreement with experiment.

E. Array Patterns

To achieve a feeling for the types of patterns possible from a conical array of open-ended waveguides, the program for the Green's function was used with an assumed Taylor distribution with -30 dB sidelobes and $\bar{n} = 5$. Both sum and difference patterns were calculated. Elevation and azimuth patterns are shown in figures 8 and 9. From these pattern we see for the sum pattern the cross polarization is down a little more than 24 dB. For the difference pattern, a very nice null is obtained in the main polarization and the cross polarization is -22.3 dB in the null.

III. CONCLUSIONS

It has been shown that by using the results of GTD, it has been possible to analyze and accurately predict the behavior of array-element patterns on a conformal surface with varying curvature for the case of radially directed elements. Also, valuable information on the cross-polarization properties of conical arrays has been obtained. Effort should be expended to obtain similar information for arrays with elements arbitrarily oriented on the conformal surface.

REFERENCES

1. Shapira, Felsen and Hessel, "Surface Ray Analysis of Mutually Coupled Arrays on Variable Curvature Cylindrical Surfaces," Proc. IEEE, Nov 1974.

2. Pathak and Kouyoumjian, "An Analysis of the Radiation from Aperatures in Curved Surfaces by the Geometrical Theory of Diffraction," Proc IEEE, Nov 1974.

3. Borgiotti, "A Novel Expression for the Mutual Admittance of Planar Radiating Elements," IEEE Trans. Antennas Propagation, May 1968.

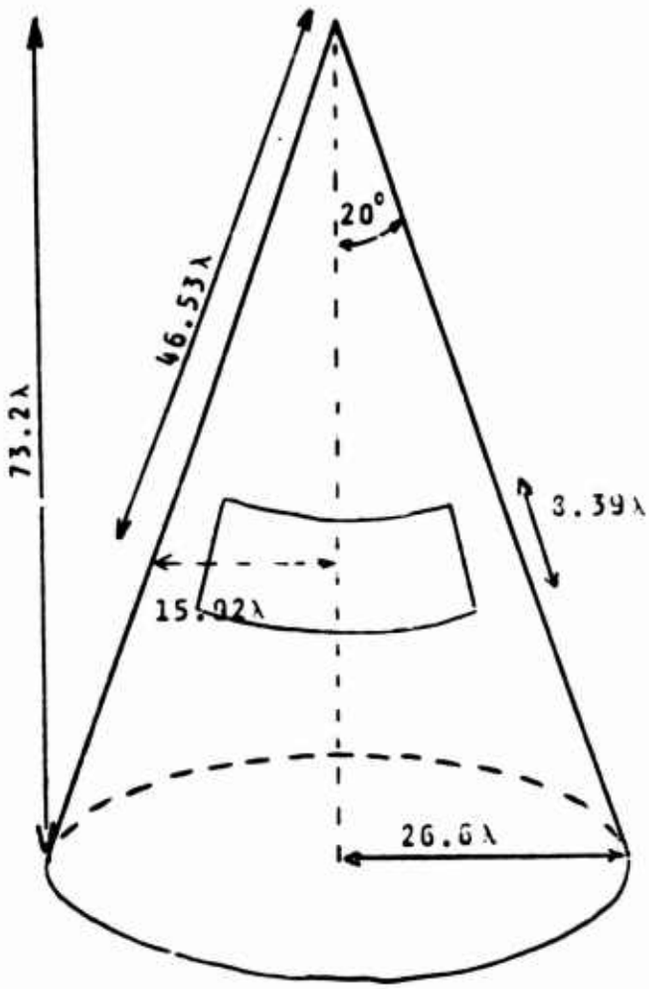

FIGURE 2 DIMENSION OF CONICAL ARRAY AT F=9.0GHz (λ=1.31 in.)

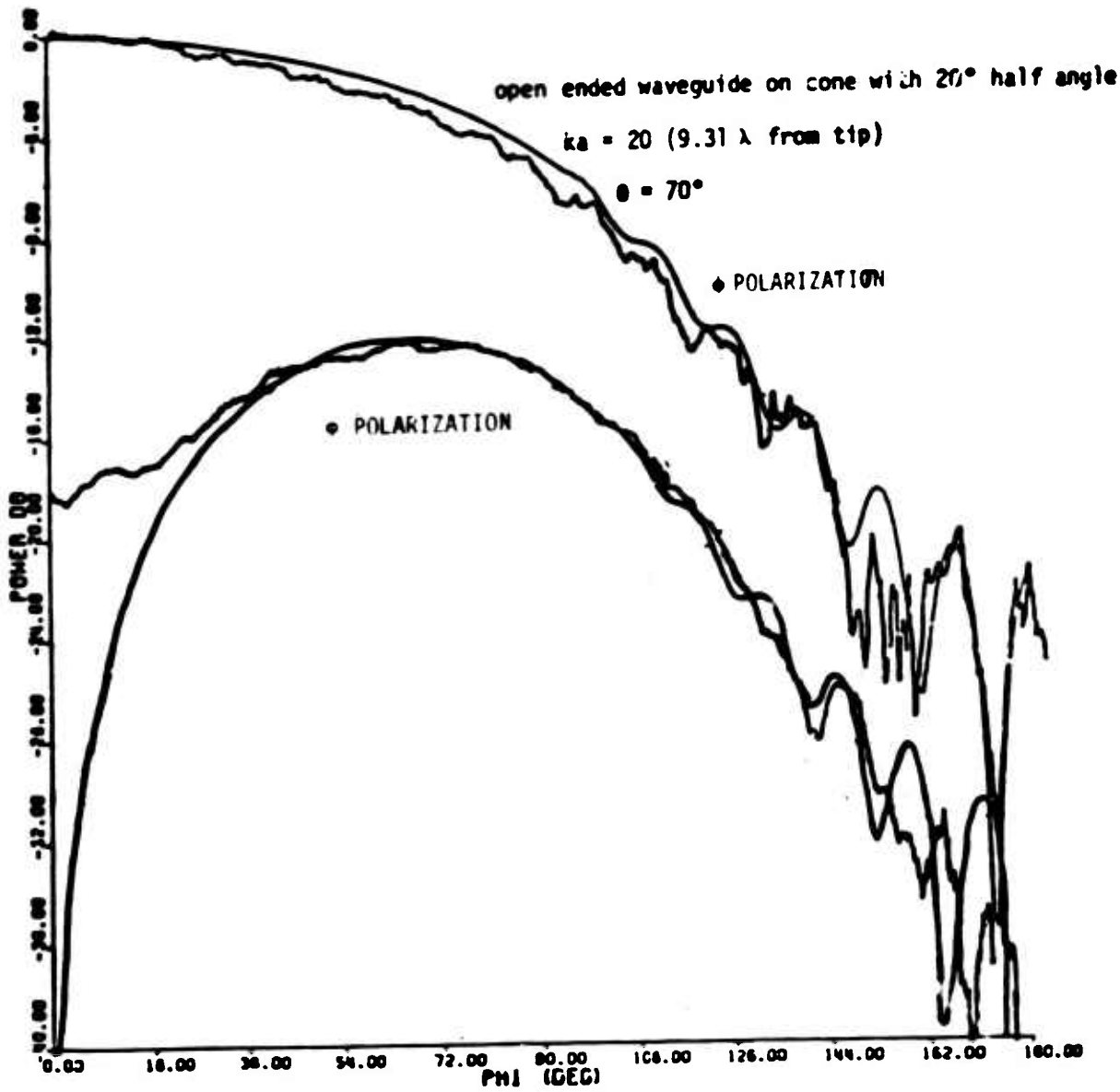

FIGURE 3 CALCULATED & MEASURED PATTERNS FROM AN OPENED-ENDED WAVEGUIDE ON A 20^{o} CONE AT ka=20 .

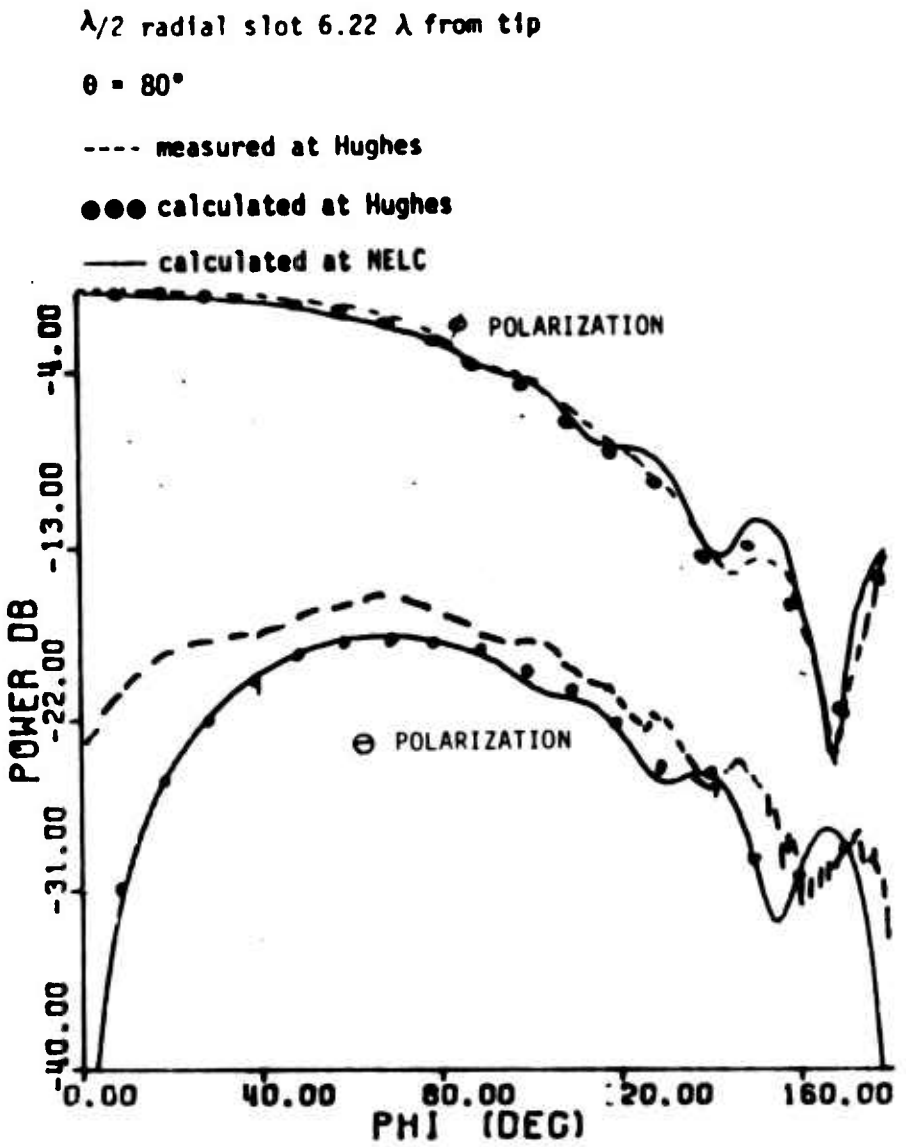

FIGURE 4 CALCULATED & MEASURED PATTERNS FROM A WAVEGUIDE ON A 10° CONE AT ka=6.77

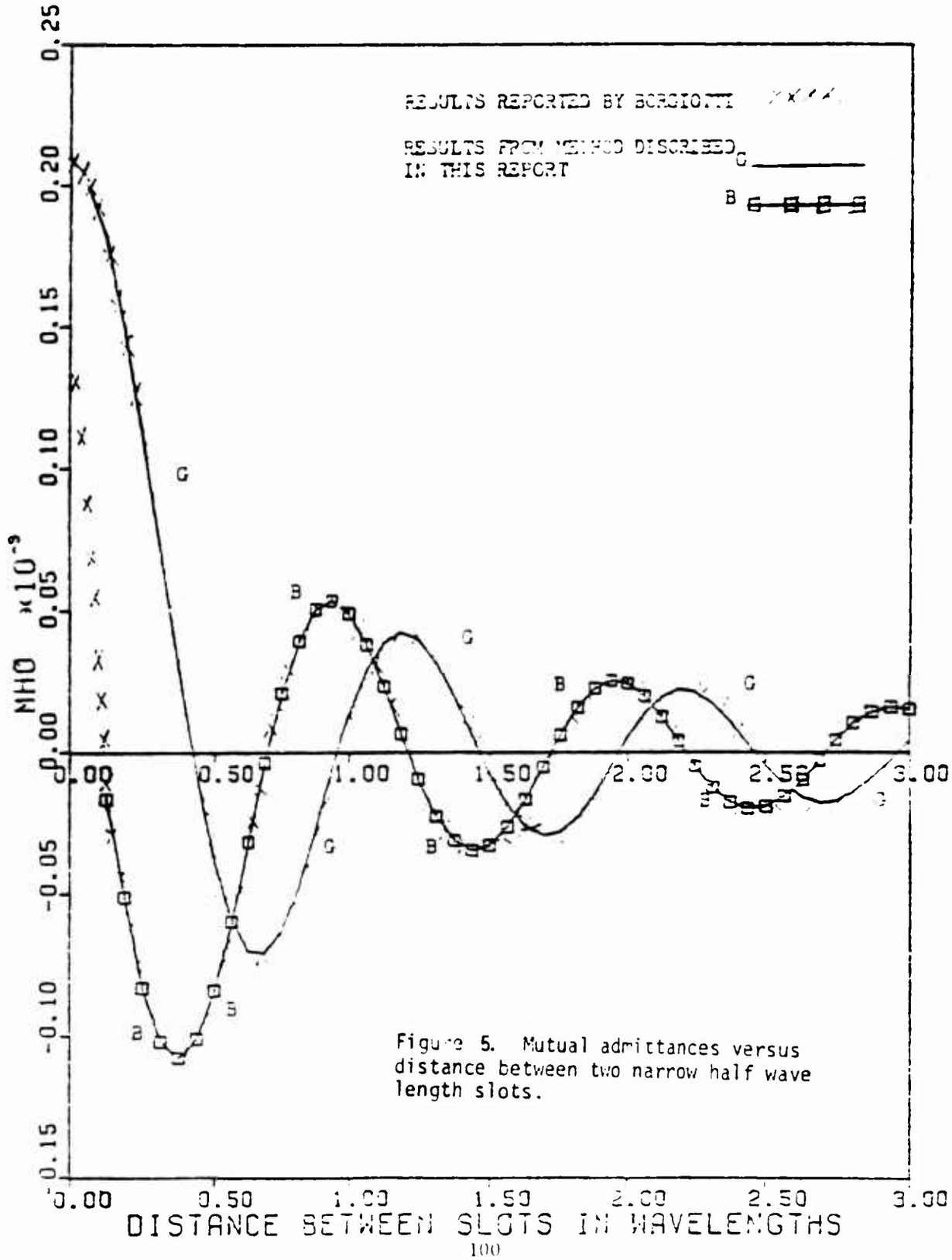

Figure 5. Mutual admittances versus distance between two narrow half wave length slots.

FIGURE 9 COUPLING ADJOINING TILE ELEMENTS IN TILE CENTER ROW AND TILE CENTER COLUMN IN THE CONFORMAL ARRAY WHEN THE CENTER ELEMENT IS FED

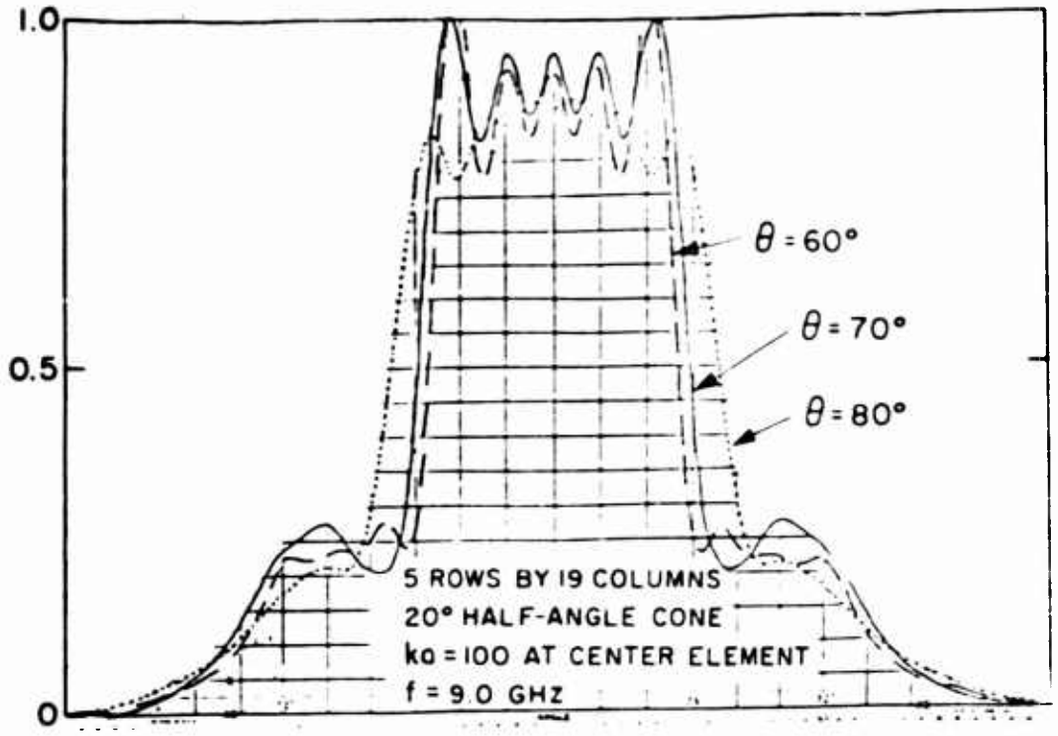

FIG. 7(a) CALCULATED AZIMUTHAL ELEMENT PATTERNS IN THE ARRAY ENVIROMENT IN LINEAR POWER

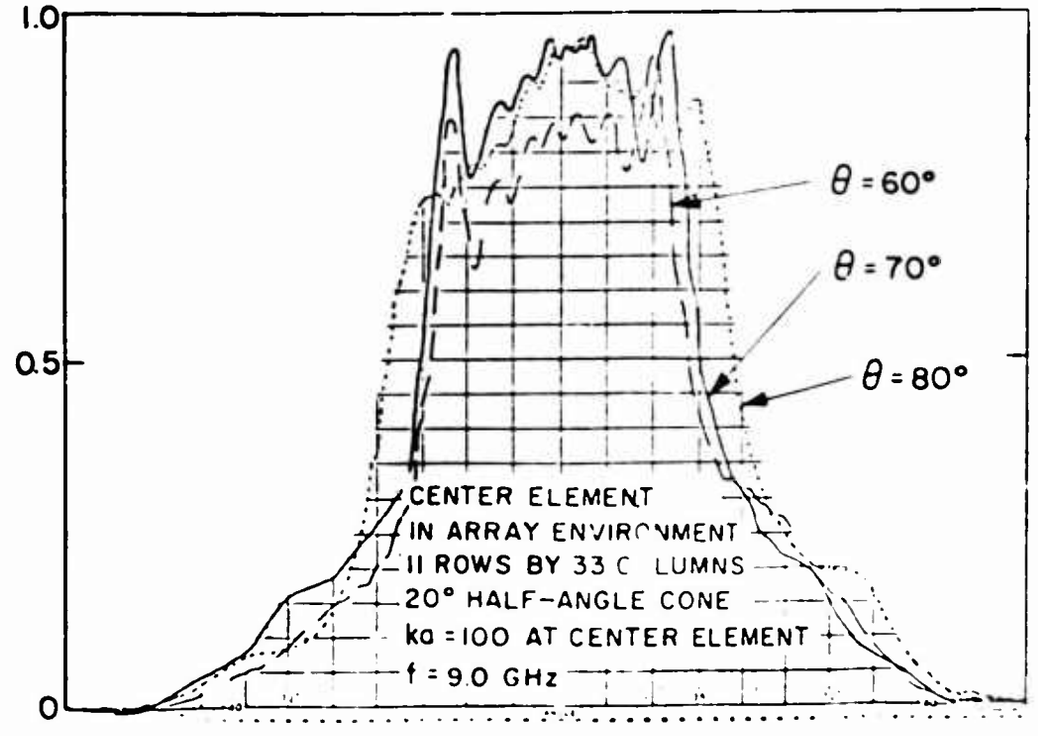

FIG. 7(b) MEASURED AZIMUTHAL ELEMENTS PATTERNS IN THE ARRAY ENVIROMENT IN LINEAR POWER

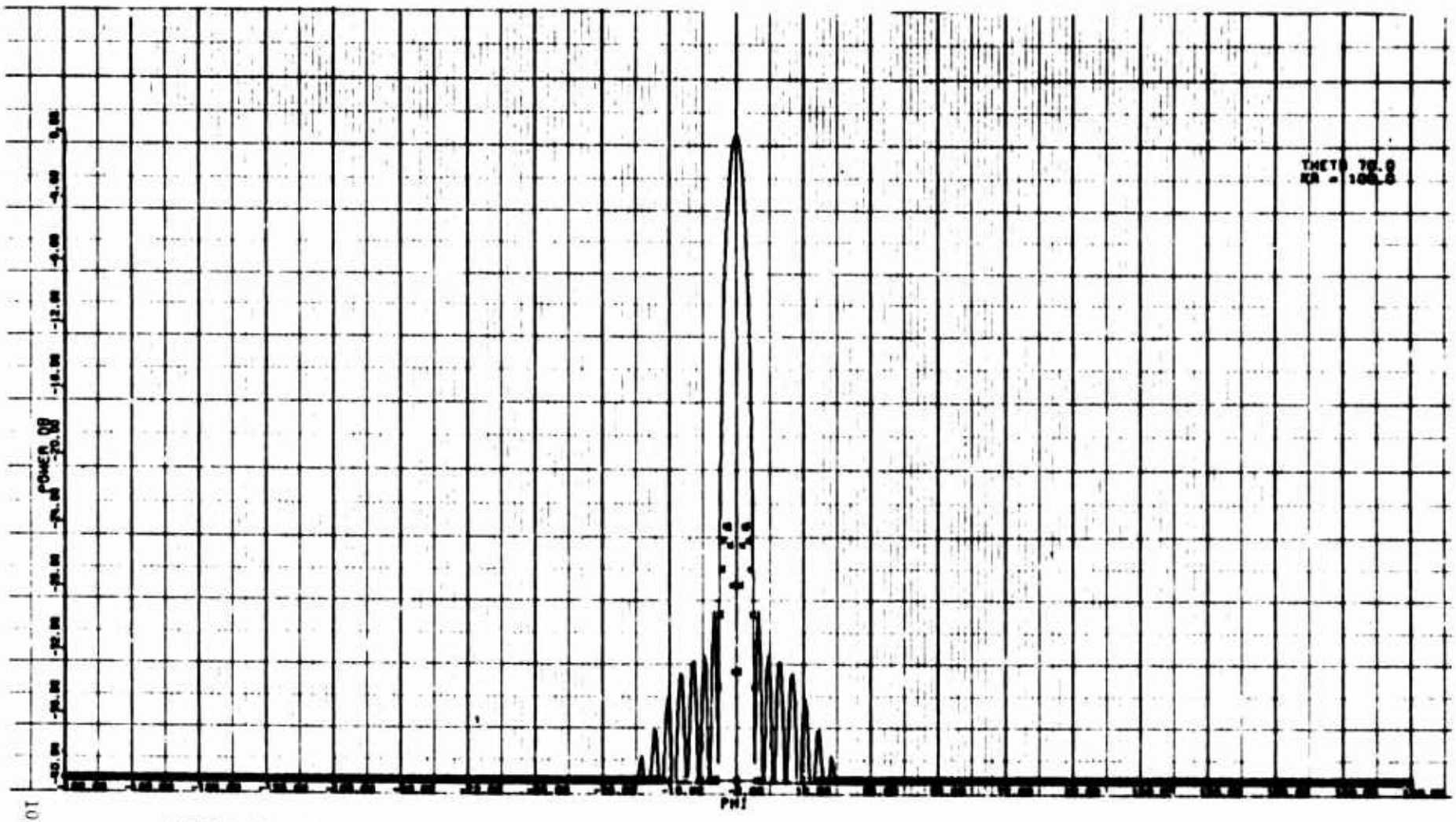

FIGURE 8a AZIMUTH SUM PATTERN FOR CONICAL ARRAY WITH TAYLOR DISTRIBUTION

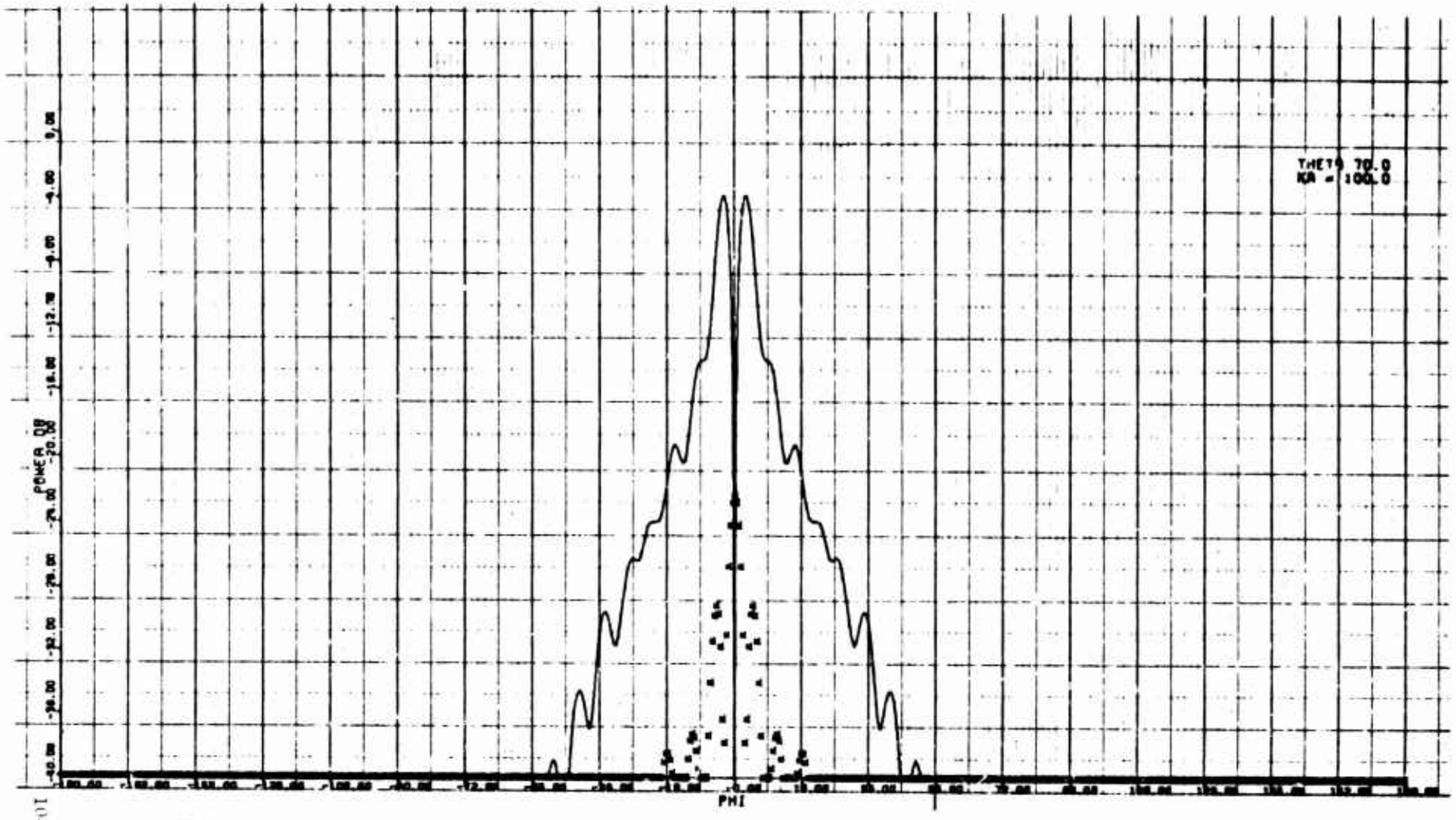

FIGURE 8: AZIMUTH DIFFERENCE PATTERN FOR CYLINDRICAL ARRAY WITH TAYLOR J STRIBUTION

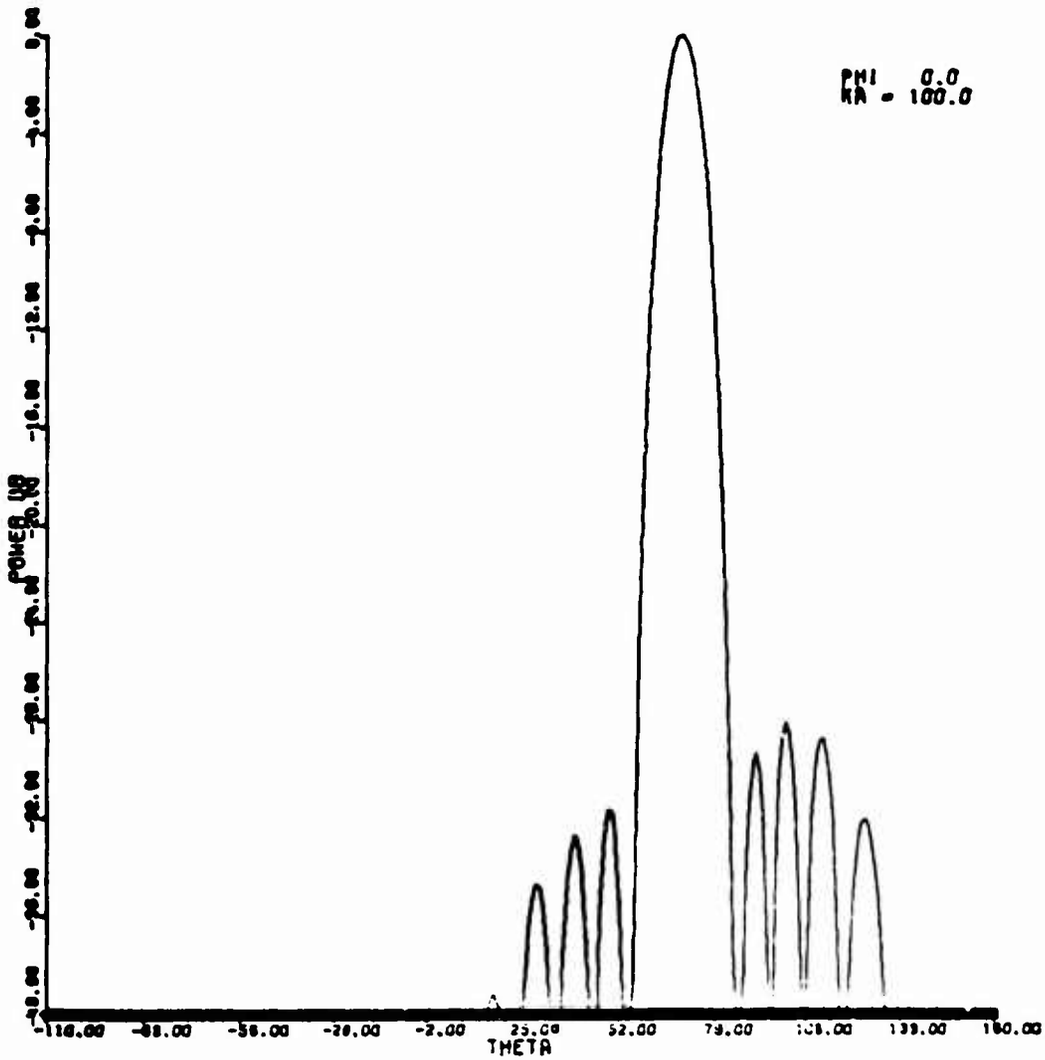

FIGURE 9a ELEVATION SUM PATTERN FOR CONICAL ARRAY WITH TAYLOR DISTRIBUTION

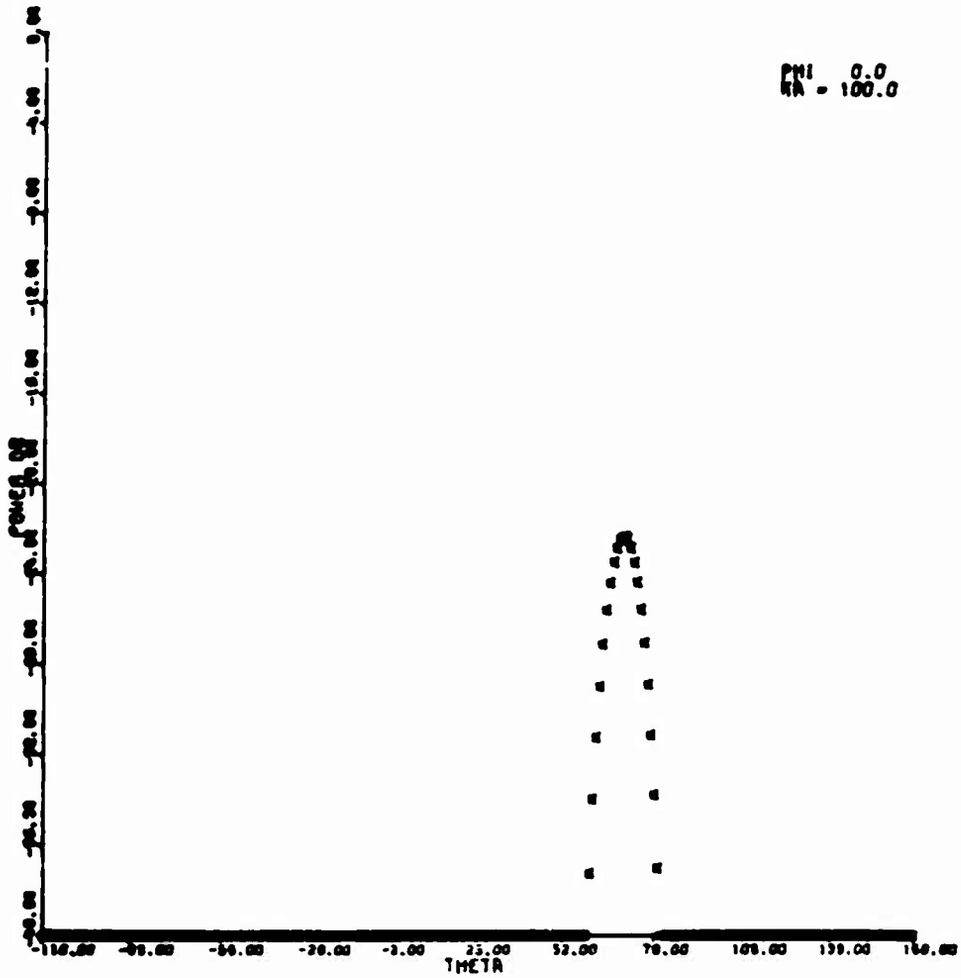

FIGURE 9b ELEVATION DIFFERENCE PATTERN FOR CONICAL ARRAY WITH TAYLOR DISTRIBUTION

CIRCULAR AND CYLINDRICAL ARRAYS

B. Sheleg, Naval Research Laboratory, Washington, D.C. 20375

Presented

CONFORMAL ANTENNA ARRAY WORKSHOP

15-16 April 1975

Naval Electronic Systems Command

TABLE OF CONTENTS

CIRCULAR AND CYLINDRICAL ARRAYS

B.Sheleg, Naval Research Laboratory, Washington, D.C. 20375

INTRODUCTION AND SUMMARY

This paper is based on two antenna programs, an electronically scanned L-band circular array and S-band cylindrical array, performed at the Naval Research Laboratory. The operation of a multimode circular array is reviewed and experimental results are shown. A discussion of special function Butler matrix antenna feed networks includes feed schemes for obtaining retrodirective performance, large array submatrix feed and the Butler matrix as a commutation switch. The cylindrical array has thirty-two radiating elements, each one a linear array of eight dipoles. This antenna uses a matrix of diode switches for scanning in azimuth and frequency scanning in elevation. The performance characteristics of this antenna are specified by the included measured radiation patterns.

THEORY OF OPERATION OF A MULTIMODE CIRCULAR ARRAY

The operation of a Butler matrix fed circular array is most easily described as the summation of the field field pattern modes that are generated by the excitation of individual inputs to the matrix feed. Paul Shelton [1],[2] first observed that if the radiators of a circular array are connected to the output ports of a Butler matrix, a focussed radiation pattern could be formed by establishing the proper current distribution on the input ports of the Butler matrix. He then showed that this beam could be scanned a full 360-degrees by changing only the phases of the input currents to the matrix feed.

The principles involved in scanning a multimode array are more clearly seen by considering a continuous distribution of current rather than an array. When the distribution is expressed as a Fourier series, in general infinite, each term represents a current mode uniform in amplitude but having a phase varying linearly with angle. The radiation pattern of each mode has the same form as the current mode itself, and these pattern modes are Fourier components of the radiation pattern of the original distribution. The expression of the radiation pattern as the sum of the modes of this form is then seen to be analogous to the summation of the contributions made to the pattern of a linear array by its elements, implying the operation of a multimode array can be explained by referring to an equivalent linear array.

In the plane of the array the radiation pattern of a continuous cylindrical sheet of vertical current elements is:

$$E(\varphi) = \sum_{n=-\infty}^{\infty} C_n e^{jn\varphi} \tag{1}$$

when C_n are complex constants given by:

$$C_n = 2\pi K j^n I_n J_n \left(\frac{2\pi\rho}{\lambda}\right) \tag{2}$$

Suppose now the current distribution is the sum of just a finite number of current modes with $-N \leq n \leq N$. The radiation pattern is given by:

$$E(\varphi) = \sum_{n=-N}^{N} C_n e^{jn\varphi} \tag{3}$$

and C_n, the relative phase and amplitude of each pattern mode, can be set by adjusting the relative phase and amplitude of the corresponding current mode. A linear array of 2N+1 elements with interelement spacing of a has a radiation pattern given by:

$$E(u) = \sum_{n=-N}^{N} A_n e^{jnu} \tag{4}$$

where $u = (2\pi a/\lambda)\sin\varphi$, φ is the angle off broadside, and A_n is the current on the n^{th} element. The similarity of Eqs.(3) and (4) suggests that the operation of a multimode circular array might be explained by referring to an equivalent linear array. One difference between these expressions is that, for a circular array the argument is φ, and for a linear array it is $(2\pi a/\lambda)\sin\varphi$. A second difference is that equally excited elements in a linear array make equal contributions to the radiation pattern--but not so for equally excited pattern modes because, in general, their elevation patterns are not identical. Although each pattern has precisely the same form as the current mode which is its source, it should be noted that their relative phases need not be the same (i.e. assume two current modes to be in phase at $\varphi = 0$, the corresponding pattern modes will not, in general, be in phase in this direction.) It may be seen from Eq.(2) which contains the factor j^n, that the N and N+1 modes differ in phase by $\pi/2$ radians at that angle for which the corresponding current modes are in phase. Another property peculiar to a circular configuration with isotropic radiators, is that there is always a value of the radius, ρ, to make the Bessel function zero and this results in some pattern modes making zero contribution in the plane of the ring. Fortunately however, this is not true

for practical antennas of interest such as a ring of dipoles placed $\lambda/4$ above a reflecting cylinder.

If now the current modes, I_n's in Eq.(2), are adjusted to give unity amplitude pattern modes and be in phase at $\varphi = 0$, the radiation pattern becomes:

$$E(\varphi) = \sum_{n=-N}^{N} e^{jn\varphi} \tag{5}$$

which may be summed to give the pattern characteristic of a uniform array

$$E(\varphi) = \frac{\sin\left[\frac{2N+1}{2}\,\varphi\right]}{\sin\left(\frac{\varphi}{2}\right)} \tag{6}$$

This expression suggests that this beam can be scanned by a linear variation of the phases of the mode excitations, just as the beam of a linear array is scanned by a linear variation of the element phases. If the phase difference between adjacent modes is φ_o radians, the resultant pattern is expressed as:

$$E(\varphi) = \frac{\sin\left[\frac{2N+1}{2}\left(\varphi-\varphi_o\right)\right]}{\sin\left(\frac{\varphi-\varphi_o}{2}\right)} \tag{7}$$

which is the original pattern scanned φ_o radians.

Although the foregoing analysis was based on a cylindrical sheet of infinitesimal current elements, the same reasoning applies to any circular array having similar pattern modes. The only difference in the analysis would be the relationship between the phases and amplitudes of the pattern modes and their respective current modes. As mentioned before, if a single ring of N elements is connected to the N output ports of a Butler matrix, it is possible to excite simultaneously and independently all the positive and negative modes n = 0, ±1, ±2, ..., $\pm(N-1)/2$, N/2. The analysis in terms of ideal modes is adequate for a qualitative description of its operation and does predict quite well the position and shape of the main beam, but not the structure of the sidelobes. A more accurate estimate requires that the actual current distribution on the array be determined and the pattern then calculated. For circular arrays fed by a Butler matrix, as many current modes can be established as there are elements but it may not be obvious how many of these modes have far field patterns that approximate the ideal pattern mode sufficiently well to be utilized. For example, the highest order mode for an N-element array is N/2 which has an element-to-element

phase progression of π radians. Hence, by symmetry this pattern mode must be scalloped with N nulls and N peaks. Obviously this is not a uniform amplitude mode and, in general, would be undesirable for beam forming. It should be evident that the radiation pattern of a circular array computed on the assumption that the modes are perfect is not the same as that computed from the actual current distribution and that some experimentation is usually required to determine the number of modes to be used and the adjustments to the intermode phase differences. Actually, instead of picking the mode excitation only to find that the corresponding aperture current distribution results in a poor radiation pattern, it would be preferable to first select an aperture current distribution having a desirable far field pattern and then find the mode excitation which will generate these antenna currents. Indeed, it has been shown that any prescribed output currents can be achieved with a zero-mode Butler matrix by properly exciting the matrix inputs.

CIRCULAR ARRAY EXPERIMENTAL PROGRAM

This study consisted of building an L-band (.900 GHz) Butler matrix fed circular array with 32 dipole radiators as shown in Fig.1. Each dipole was connected to an output port of the 32x32 Butler matrix by an equal line length. Figure 2 shows two phase shifters connected to each matrix input, a fixed phase shifter to phase align the pattern modes in the far field and a variable phase shifter to scan the focussed beam. Bringing the pattern modes into a phased condition at some φ requires that compensation be made for the intrinsic phase of each mode (Fig.3). In addition to the initial phase adjustment, the power divider, which determines the amplitude distribution across the current modes, must account for the gain difference of the modes as seen in Figures 3 and 4.

The measured pattern modes for this antenna (Fig.5) shows clearly that some judgment is needed to determine which pattern mode sufficiently approximate the calculated patterns to be used for beam forming. Much of the observed deviations are attributed to phase and amplitude errors in the matrix and, in general, not all current modes are used. A mode-by-mode buildup of a focussed beam is shown in Fig.6, with a modified cosine amplitude distribution on the modes. This beam can now be scanned by using the variable phase shifters at the inputs to the matrix to impose a linear phase shift on the current modes. If the beam is moved in periodic increments of $2\pi/N$ the beamshape would be expected to remain invariant because its position relative to the dipole radiators is unchanged. The effect on the pattern by scanning the beam in between positions is shown in Fig.7. Some change is observed in the sidelobe structure but the main beam remains virtually invariant. Figure 8 shows a full 360-degree scan for a pencil beam formed by a cosine squared amplitude distribution on the modes.

The Butler matrix feed network has been demonstrated to be very suitable for electronically scanned circular array application. The scanning scheme is simple and can be utilized for multiple beam operation. This matrix antenna feed has a built-in omnidirectional pattern capability (zero mode) and can be readily converted for monopulse performance. On the other hand, it is rare to find a large array fed by a Butler matrix feed system. This is primarily due to the following reasons. First, for a large number of radiating elements the Butler matrix becomes large and difficult to fabricate with practical tight tolerances on the phase and amplitudes of the output currents. Second, a large matrix is very expensive. The number of hybrids in a 2Nx2N Butler matrix is more than double the hybrids in an NxN Butler matrix. Third and last, a Butler matrix is connected to all the elements of a circular array which is normally undesirable since most of the elements are not looking in the direction of the beam and therefore make no contribution.

In spite of these criticisms, the Butler matrix feed network is highly desirable for some special function antenna systems. A description of a few of these applications follows.

SPECIAL FUNCTION BUTLER MATRIX FEED NETWORKS

(a) Retrodirective Antenna

Virtually the same circular array antenna described above may be used to provide automatically retrodirective performance [3]. This is accomplished by systematically connecting together pairs of input ports with equal length transmission lines as shown in Fig.9. The method of modal interconnection is analogous to the interconnection of elements in a linear Van Atta array [4]. If one wishes to change the pattern characteristic of the reradiated beam, active networks can be inserted into the lines connecting the mode terminals. This would offer the capability of performing frequency translation, modulation and amplitude adjusting on the incoming signal before reradiation.

(b) Submatrix Feed Systems

Ordinarily a multimode circular array or a multibeam linear array uses a single Butler matrix commensurate in size with the array (i.e. an NxN matrix for an N-element array). Seldom are all the available modes utilized, for circular arrays because of the scalloped patterns characteristic of the higher order modes, and for linear arrays because of the deterioration of the beams approaching endfire. The submatrix feed scheme [5] uses two or more interconnected small order Butler matrices to replace a single large order Butler matrix. A circular array feed system having two 16x16 Butler submatrices that replaces a standard single 32x32 Butler matrix feed network is shown in Fig.10.

Corresponding input ports (similar modes) of the two 16x16 matrices are connected to a common tee which goes to a beam forming and scanning variable phase shifter and then to an amplitude weighting board. Note that one of the submatrices has a fixed phase shift β at each modal input. These phase insertions are necessary to achieve the proper aperture phase distribution for each mode.

The submatrix feed network offers a substantial reduction in the complexity of the feed system resulting in a savings of system components and hardware. Also, this feed system can be used for arrays having M elements ($M \neq 2^n$) which normally cannot be fed by a single Butler matrix. The performance penalty paid for this simplified feed is an increase in beamwidth for circular arrays and a reduction of available beams for a multimode linear array, Fig.11.

One natural application for the submatrix feed is the 360° coverage antenna which uses four linear (or planar) arrays, each providing one quadrant coverage. The submatrix feed, in this case, need not impose any performance penalties. Another example is the circular array on a satellite where the desired beamwidth is determined by the angle subtending the earth and is broad enough such that it can be formed by a few modes.

(c) Butler Matrix As a Commutation Switch

It has been shown [6],[7] that for any set of input current, the Butler matrix has the unique property of obtaining a cyclic permutation of the output currents by phase shifts alone. This property suggests a circular array feed system combining a Butler matrix with a switch matrix. The Butler matrix excites a sector of the full circular aperture and the switch matrix commutes the excited sector around the array [8]. Consider the feed system shown in Fig.12, and 8x8 Butler matrix connects to one quadrant of a 32-element array through SP4T switches which select the excited sector. As the illuminated sector is moved about, the phase shifters must be adjusted to maintain the proper aperture current distribution. The prime virtue of this feed network is that only the elements contributing to the main beam are excited.

In Fig.13, another sector feed scheme [9] is shown with the Butler matrix replaced by a sector ordering switch matrix. This illustrates how the Butler matrix may be considered as a commutation switch.

CYLINDRICAL ARRAY

(a) Antenna Description

The purpose of this study was to demonstrate the use of the diode switch matrix for azimuth beam forming and scanning, and

frequency-scanned linear arrays for elevation control [10]. An S-band cylindrical array, Figure 14, was built with 256 elements for the experimental program.

Each of the 32 column elements is a linear array of 8 dipole radiators series fed by a serpentine line shown in Figure 15. Characteristically, this feed structure puts a linear phase progression across the radiators having a phase slope which is a function of frequency. This permits the beam to be frequency scanned in elevation.

A schematic of the azimuth switch matrix is shown in Figure 16. This matrix is fabricated in shielded stripline and uses 44 diode transfer switches. It is convenient to think of the matrix as consisting of two parts, the "permuting" matrix and the "pass around network." The function of the permuting matrix, in this case a network of 12 transfer switches having 8 inputs and 8 outputs, is to provide as outputs all the cyclic permutations of the input currents. These 8 output signals become the inputs to the "pass around network" whose 32 outputs connect to the 32 linear array radiators. Eight 4x4 switch modules make up the "pass around network" with each module having 4 output ports connected elements located quadratively in the array. This interlacing of the outputs preserves the order of the aperture current.

The most difficult problem in the design and fabrication of the switch matrix was that of maintaining uniform lengths for all paths for all switching states. At 3.2 GHz the measured electrical path length difference was less than ± 12 degrees. Each path contains 5 transfer switches in series and has a total measured insertion loss of about -3.5 dB. Tests showed a switching time of 0.5 microseconds and a peak power capability in excess of 1 kw.

Azimuth beamshaping is accomplished by a corporate structure with a 25 dB Tchebycheff amplitude taper across its in-phase outputs. Sum and difference patterns or monopulse lobing capability is obtained by splitting this feedboard and rejoining them together through a magic tee. Once the beam is formed in azimuth it can be scanned in elevation by changing the frequency. This scanning technique provides space coverage for a full 360° in azimuth and ± 40 degrees in elevation.

Unlike planar arrays, the elevation and azimuth scan are not independent for circular arrays. Each element of a circular array looking at an elevation angle θ_o sees a path difference which changes by the factor $\cos\theta_o$ meaning that for large arrays ($N > 32$) the azimuth phases must be adjusted for each elevation scan to retain the pattern shape. The minimum number of phase shifters needed to compensate for this error is one less than the

number of excited radiators and they should be located as close as possible to the radiators while stile able to be switched. In addition, these same phase shifters can be used to obtain "fine" azimuth scanning or scan positions located between the N step scans. In this study no correction was made for this EL/AZ scan dependence because the maximum phase error is tolerable for a 32-element circular array.

(b) Experimental Program

Figures 17 through 21 describe the radiation characteristics of this cylindrical array. These patterns are the result of exciting one quadrant of the array (8 linear elements) with a 25 dB Tchebycheff distribution in the vertical and horizontal planes. Sum and difference patterns are shown in Figs. 17 and 18 for elevation angles of 0 and +40 degrees respectively. A full set of elevation scan patterns are given in Figure 19; however, the relative gains are inaccurate because the transmitter was not leveled during this sequence of measurements. Figures 20 and 21 are full azimuth scans at 0 degrees and +25 degrees elevation. It should be noted that the apparent loss of gain for some beams in these full scan patterns is due to the fact that all the column radiators do not have exactly the same boresight frequency.

(c) Discussion

Three-dimensional scanning of a pencil beam was successfully demonstrated showing that the gain and shape of the focussed pattern remains relatively invariant in azimuth. The diode switch matrix proved to have sufficient bandwidth to accommodate frequency scanning in elevation but improvement of isolation and pathlength stability of the switches will be necessary if better patterns are to be obtained. The component count and low rf loss of this switch matrix makes it a suitable beamforming and scanning network for large arrays. By doubling the number of elements the number of switches in all paths is increased by one with its corresponding insertion loss; however, the total number of matrix components is somewhat less than double. Finally, the integrated shielded stripline linear arrays appears to offer a practical approach to low cost large arrays.

REFERENCES

[1] Chadwick,G.G., and J.C.Glass, "Investigation of a Multiple Beam Scanning Circular Array," Scientific Report 1 to Air Force Cambridge Research Laboratories, Contract AF19(628) 367, Dec.31, 1962.

[2] Sheleg, B., "A Matrix-Fed Array for Continuous Scanning," Proc.IEEE, Vol.56, pp.2016-2027, Nov.1968.

REFERENCES--cont'd.

[3] Coleman, H.P., "Circularly Symmetric Retrodirective Antenna System," IRE Trans.on Ant.& Prop.,Vol.AP-19, No.6, pp.784-785, Nov.1971.

[4] Sharp, E.D., and M.A.Diab, "Van Atta Reflector Array," IRE Trans.Ant.& Prop., Vol.AP-8, pp.436-438, July 1960.

[5] Sheleg, B., "Butler Submatrix Feed Systems for Antenna Arrays," IEEE Trans.,Vol.AP-21, No.2, pp.228-229, March 1973.

[6] Davies, D.E.N., "A Transformation Between the Phasing Techniques Required for Linear & Circular Aerial Arrays," Proc.Inst.Elec.Engrs.(London) 112 (#11): 2041-2045(1965).

[7] Brown, R.M., "The Uniqueness of the Butler Matrix as a Commutating Switch," IEEE Trans.AP, Vol.AP-19, pp.694-695 Sept.1971.

[8] Skahill, G., and W.D.White, "A New Technique for Feeding a Cylindrical Array," IEEE Trans.Vol.AP-23, No.2, pp.253-256, March 1975.

[9] Giainni, R.S., "An Electronically Scanned Cylindrical Array for IFF, Based on Switching & Phasing Techniques," Proc.of Conformal Array Antenna Conference, NELC, San Diego, CA, Jan.1970.

[10] Sheleg, B., and B.D.Wright, "A 3-D Electronically Scanned S-Band Cylindrical Array," Proc.of Conformal Array Antenna Conference, NELC, San Diego, CA, Jan.1970.

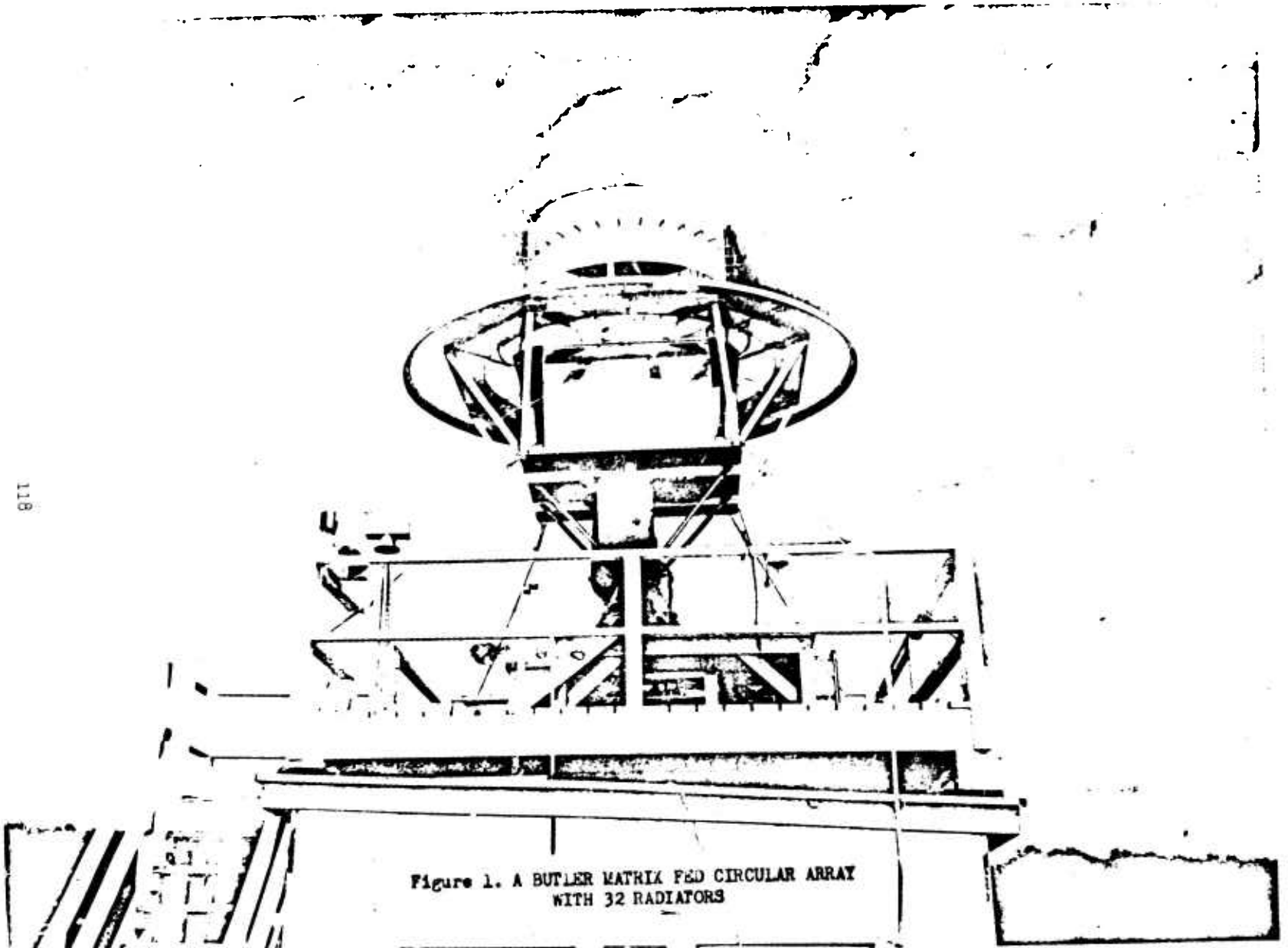

Figure 1. A BUTLER MATRIX FED CIRCULAR ARRAY WITH 32 RADIATORS

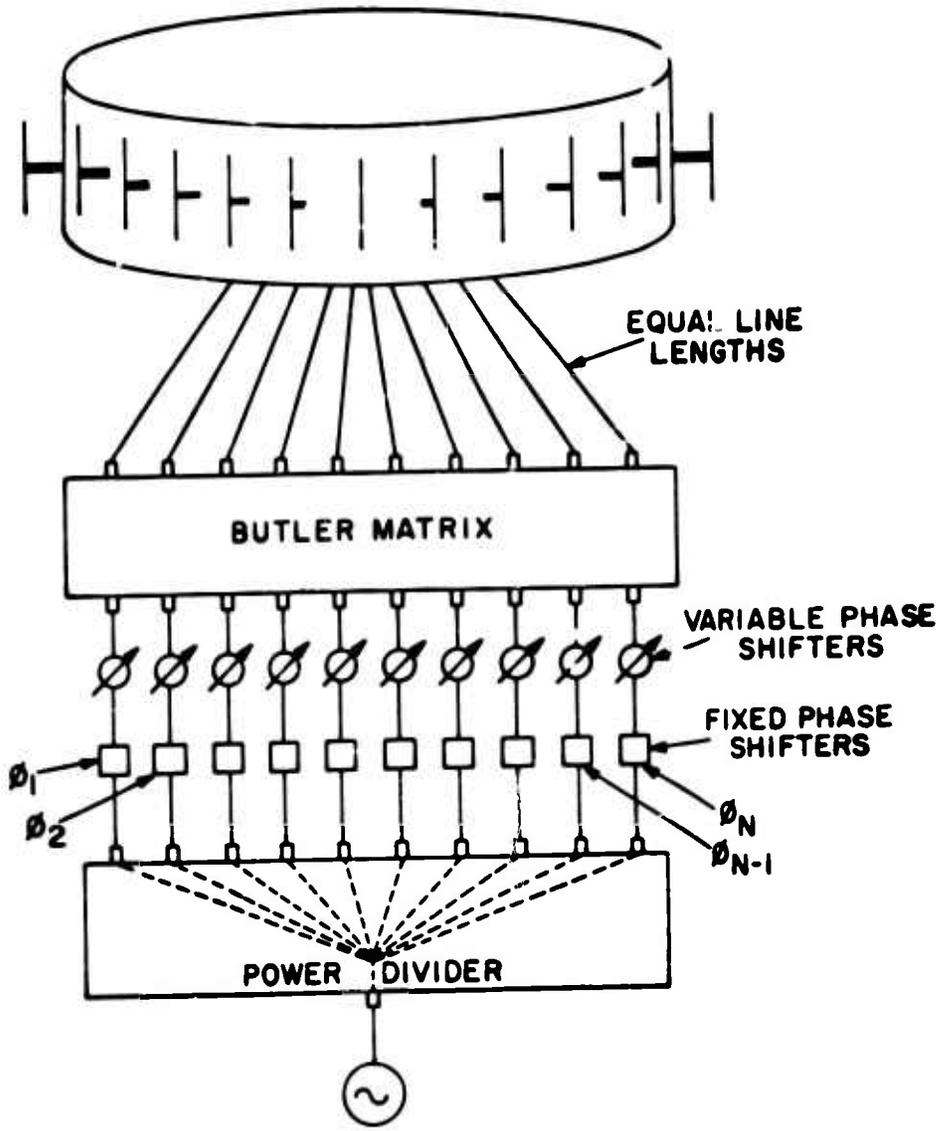

Figure 2. SCHEMATIC DIAGRAM OF AN ELECTRONICALLY SCANNED MULTIMODE ARRAY

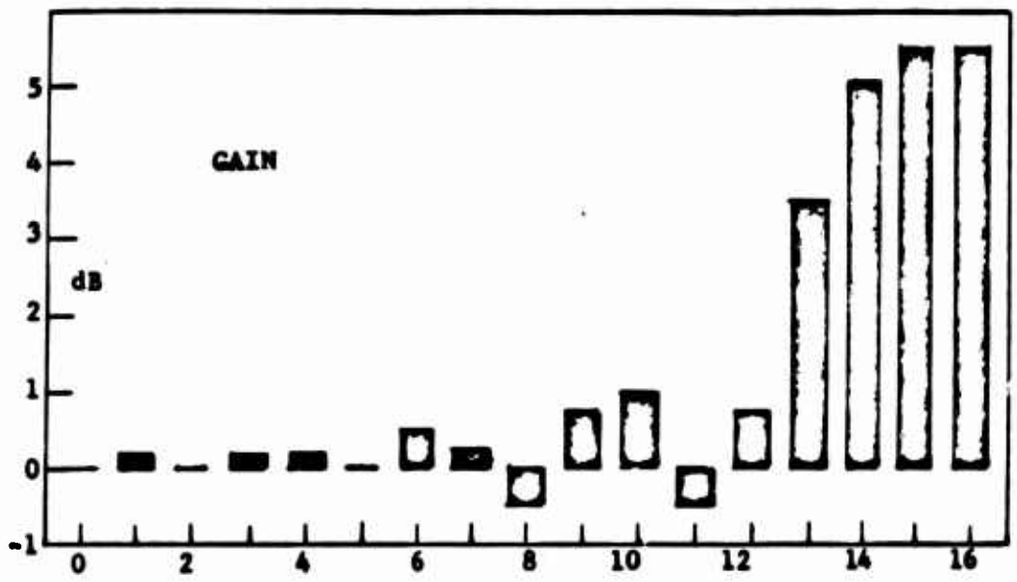

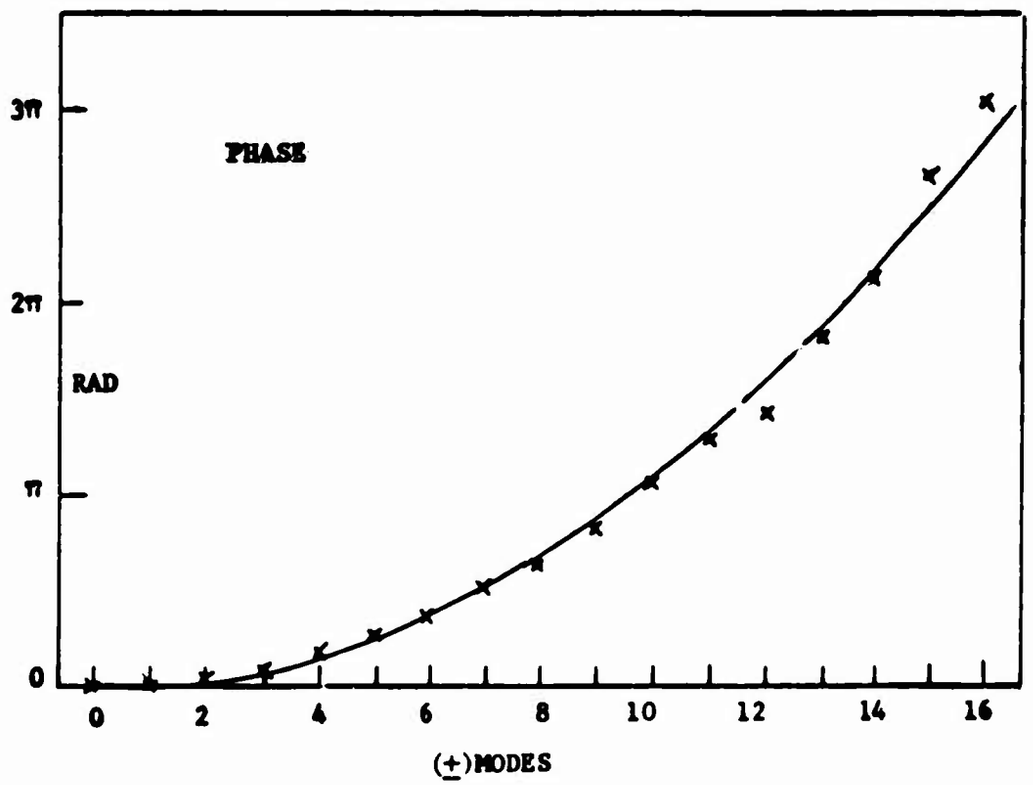

Figure 3. MEASURED PATTERN MODE CHARACTERISTICS FOR A 32×32 BUTLER MATRIX

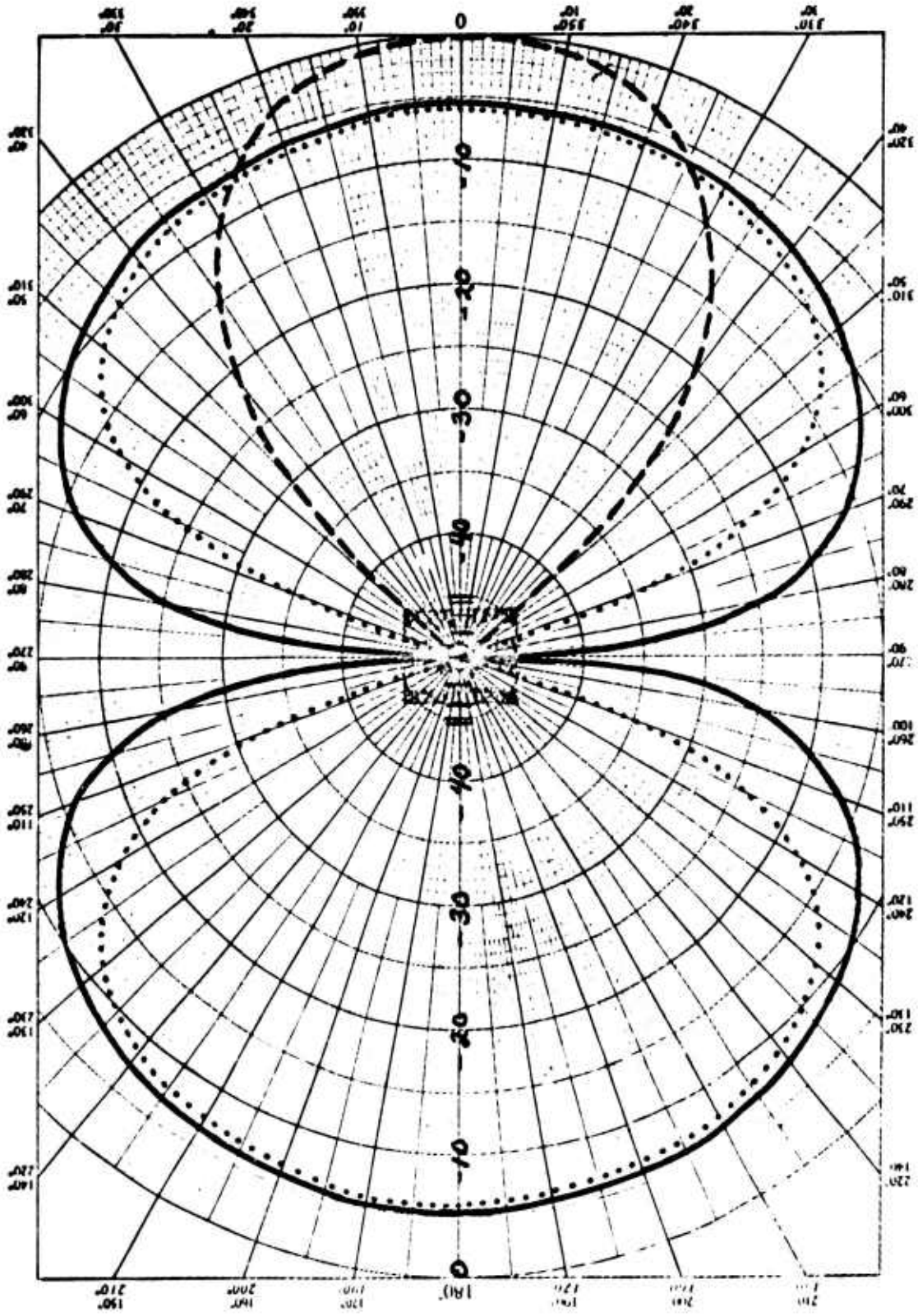

Figure 4. ELEVATION CUT OF THE ZERO, EIGHT AND SIXTEENTH PATTERN MODES

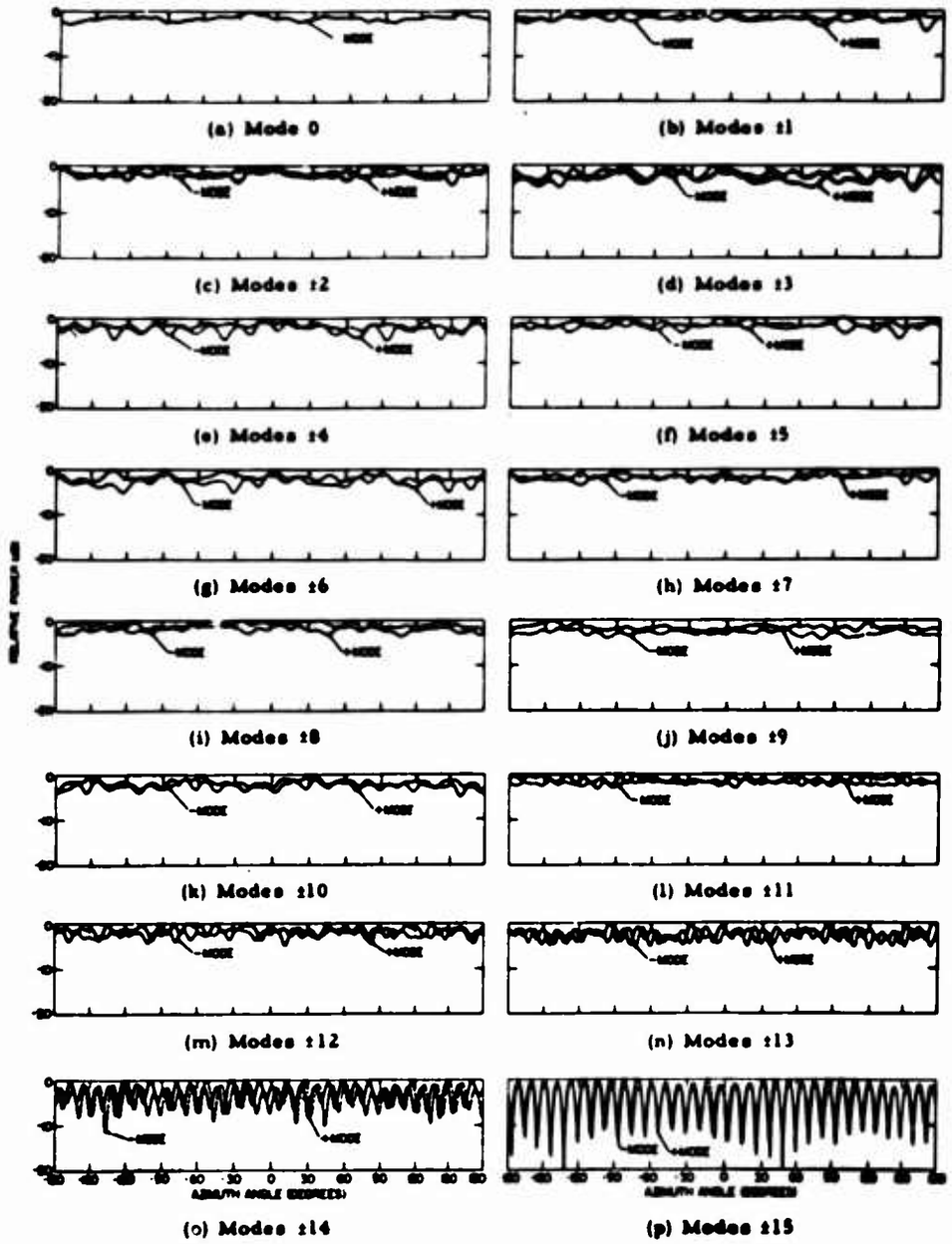

Figure 5. MEASURED PATTERN MODES FOR THE 32 DIPOLE CIRCULAR ARRAY

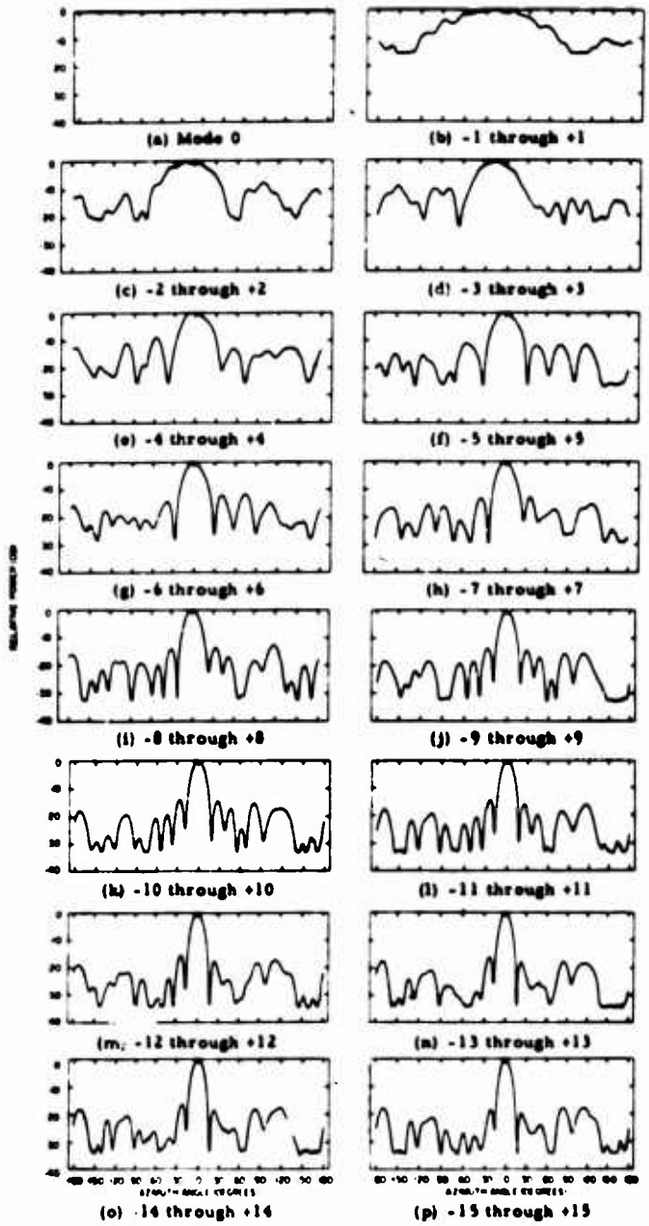

Figure 6. MEASURED MODE-BY-MODE BUILDUP OF THE BEAM WITH A TAPERED, STEPPED DISTRIBUTION ON THE MODES

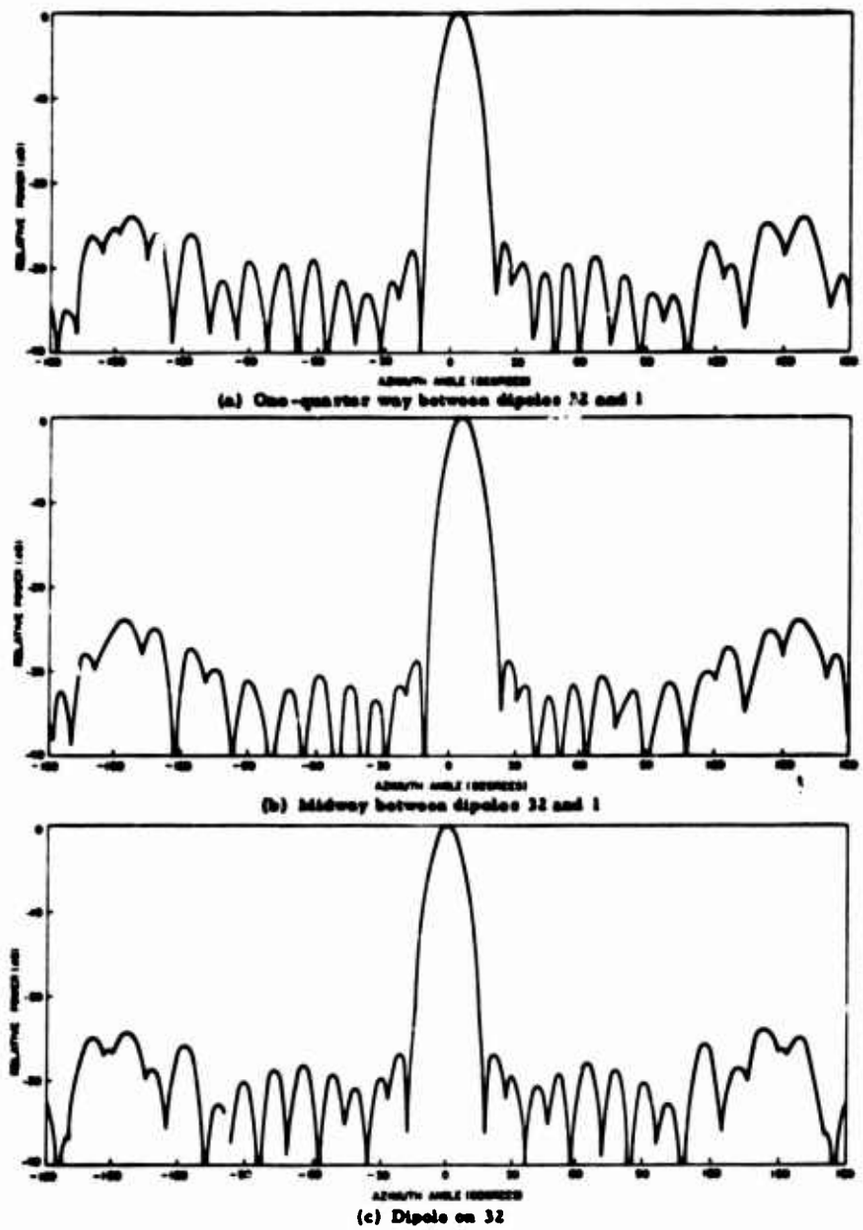

Figure 7. RADIATION PATTERNS FOR BEAM POSITION AT 0, 5.625 AND 11.25 DEGREES. AMPLITUDE TAPER ON MODES $B_k = \cos^2(\pi k/40)$ where $k = 0, \pm 1, \pm 2, \cdots, \pm 15$

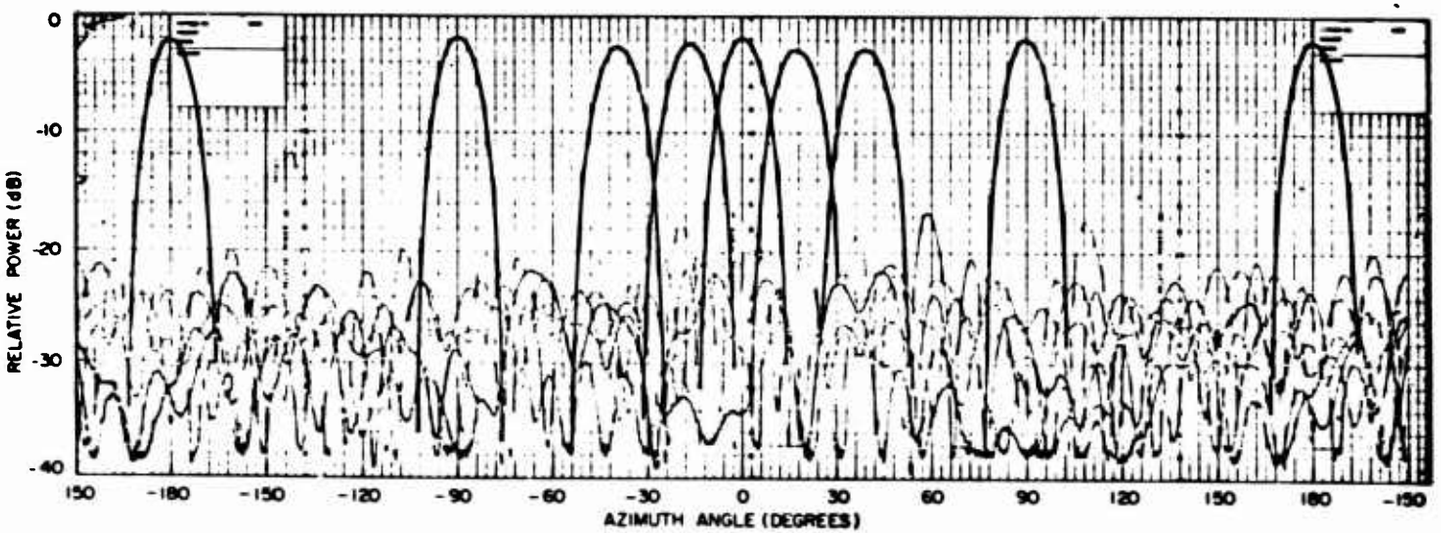

Figure 8. FULL 360 DEGREE AZIMUTH SCAN PATTERNS FOR 32 DIPOLE CIRCULAR ARRAY

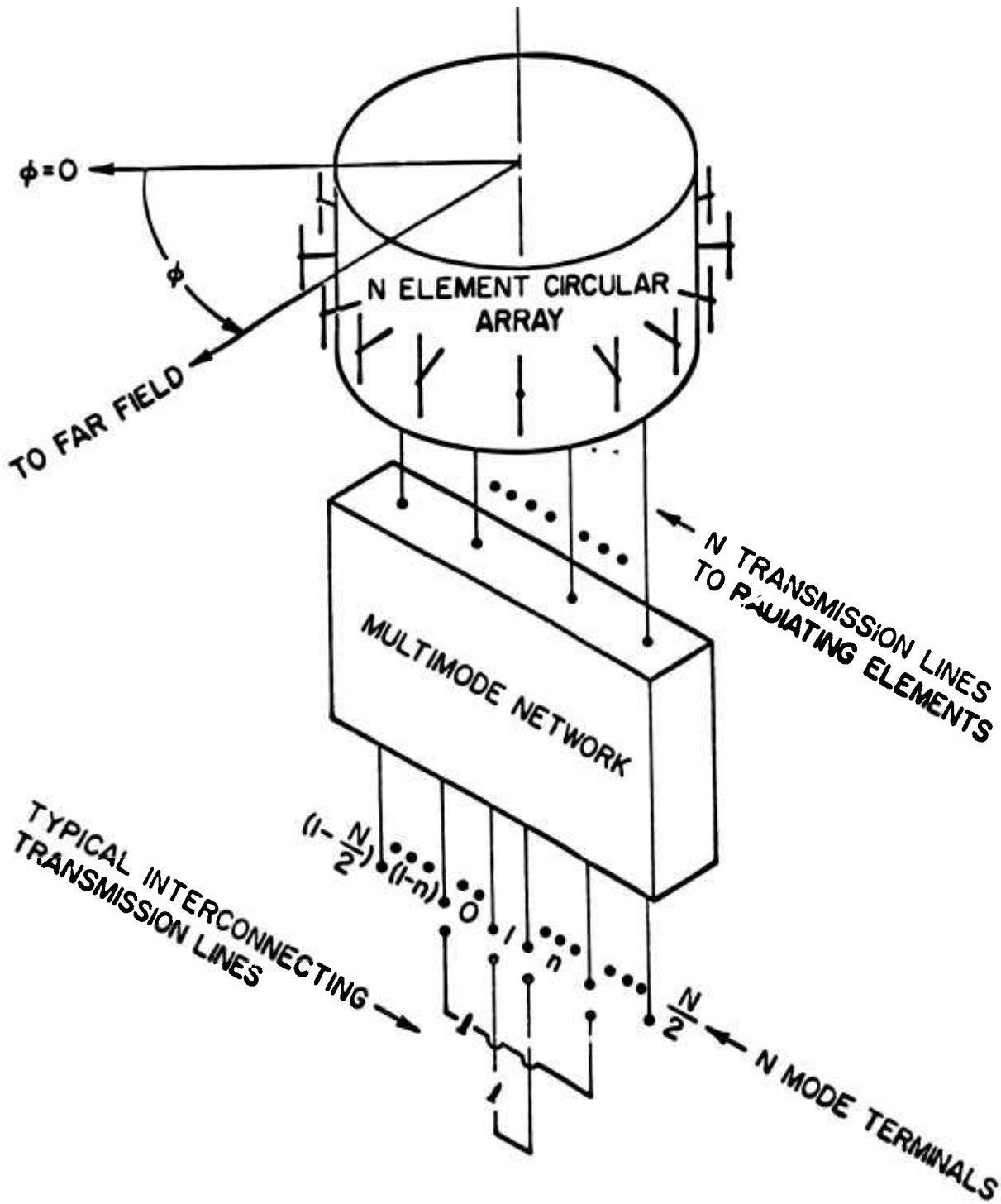

Figure 9. RETRODIRECTIVE ARRAY

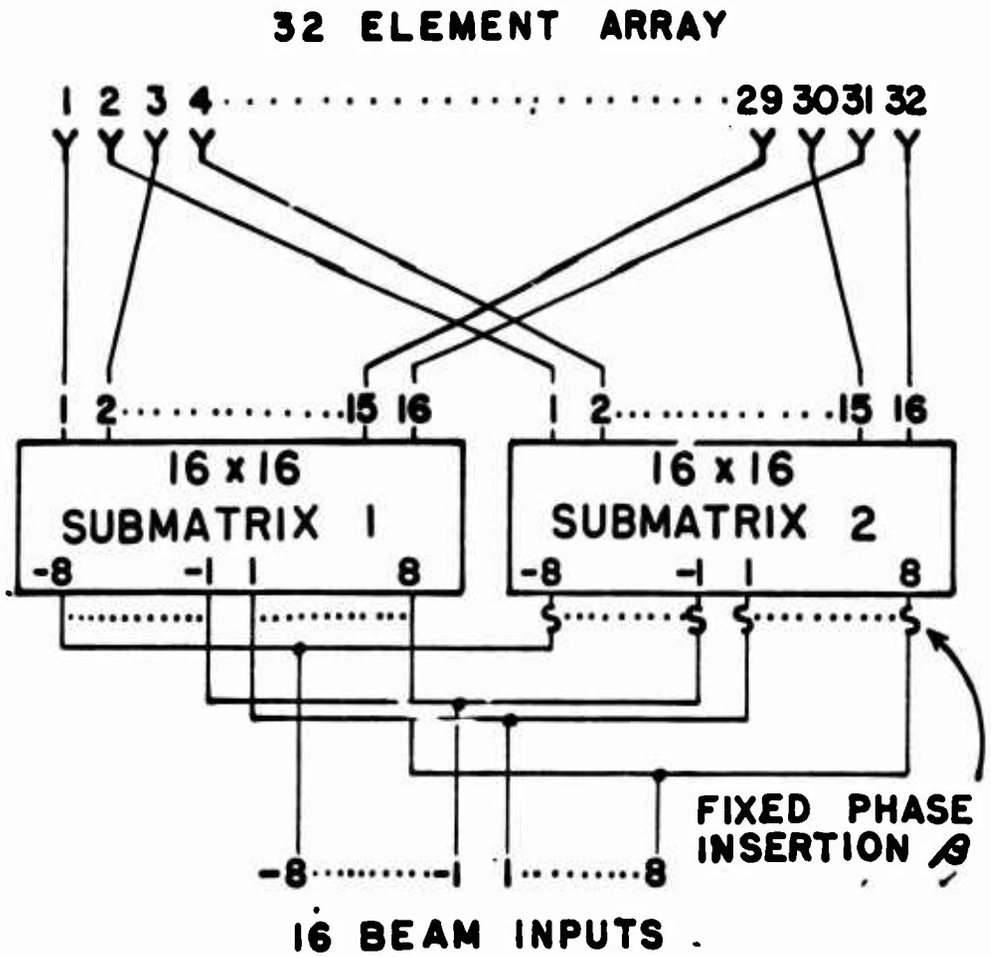

BUTLER MATRIX CIRCUIT COMPLEXITY

- 32 x 32 B.M.
  80 hybrids/matrix

- 2 (16 x 16 B.M.)
  32 hybrids/matrix
  64 hybrids total

- 4 (8 x 8 B.M.)
  12 hybrids/matrix
  48 hybrids total

Figure 10. SUBMATRIX FEED SYSTEM

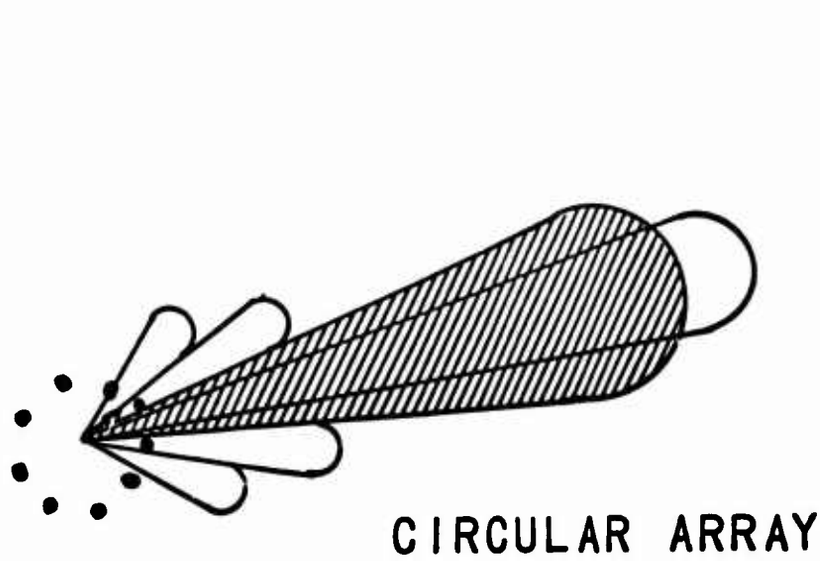

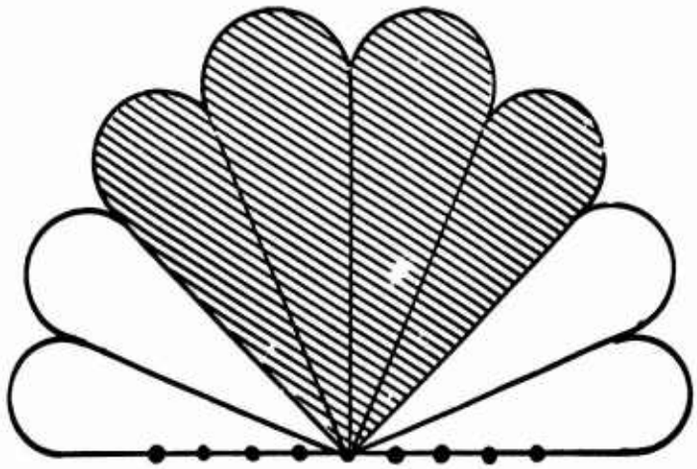

Figure 11. PERFORMANCE TRADE-OFF FOR SUBMATRIX FEED NETWORKS

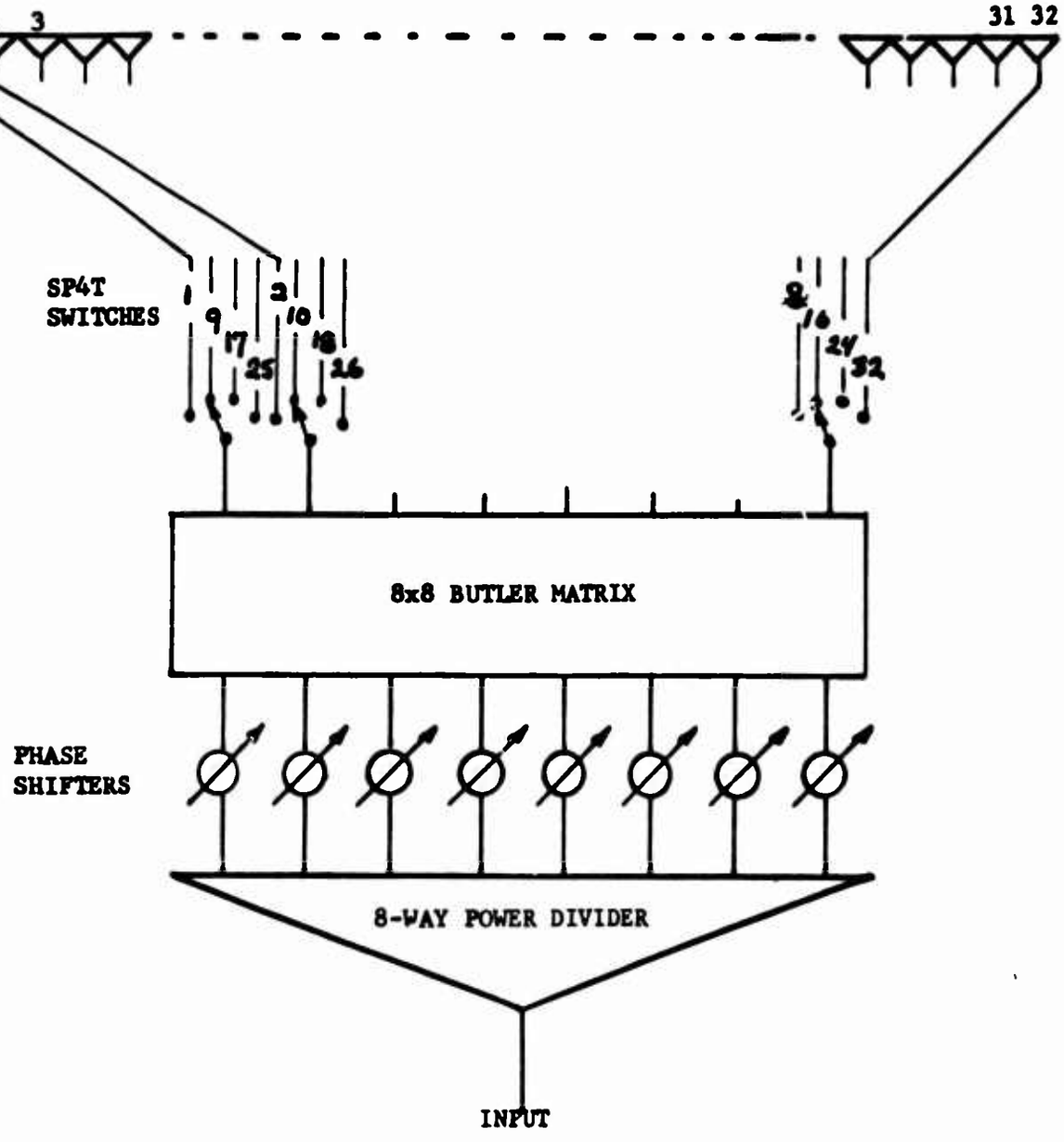

Figure 12. ALL 32 ELEMENT CIRCULAR ARRAY FEED

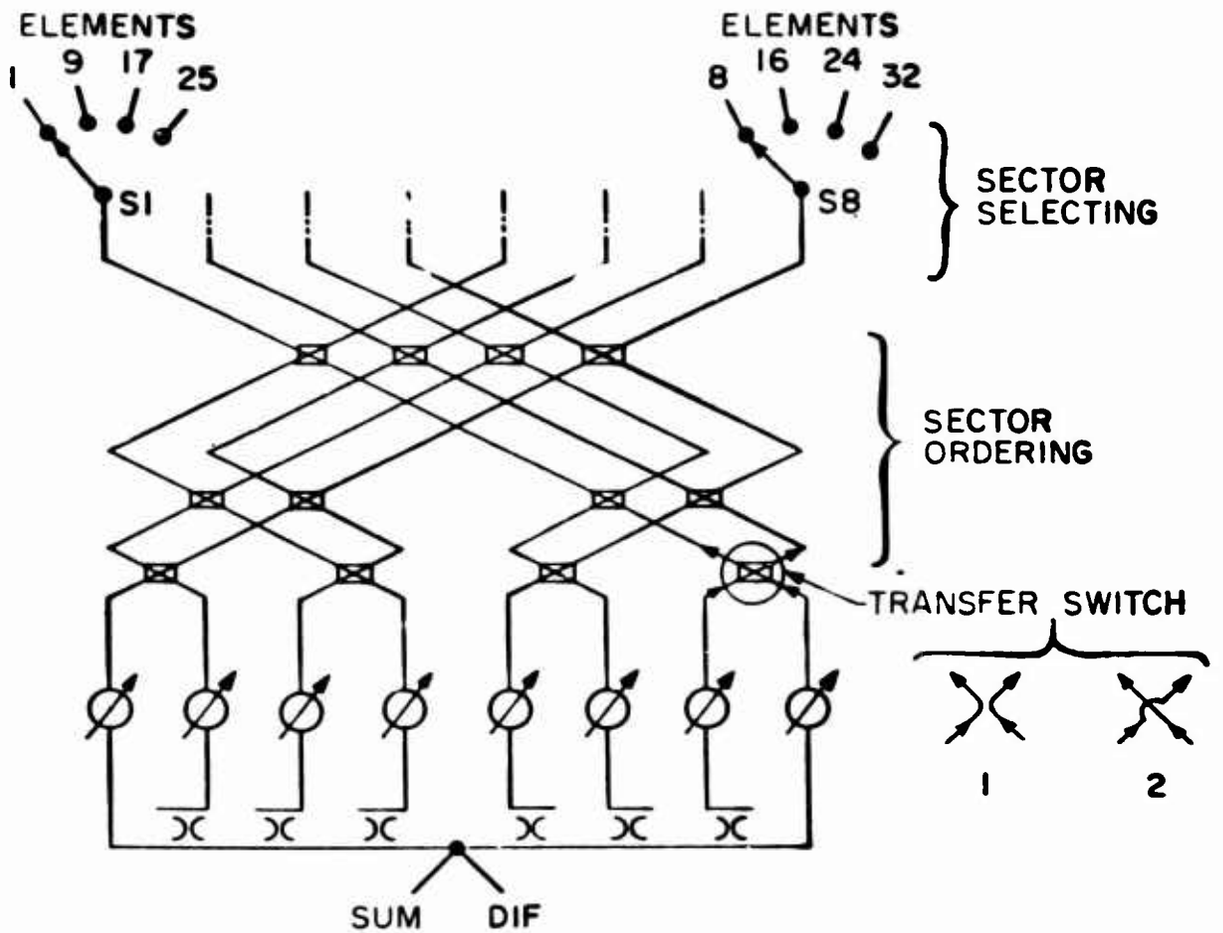

Schematic of network for 32 element array.

Figure 13. HAZELTINE 32 ELEMENT CIRCULAR ARRAY FEED

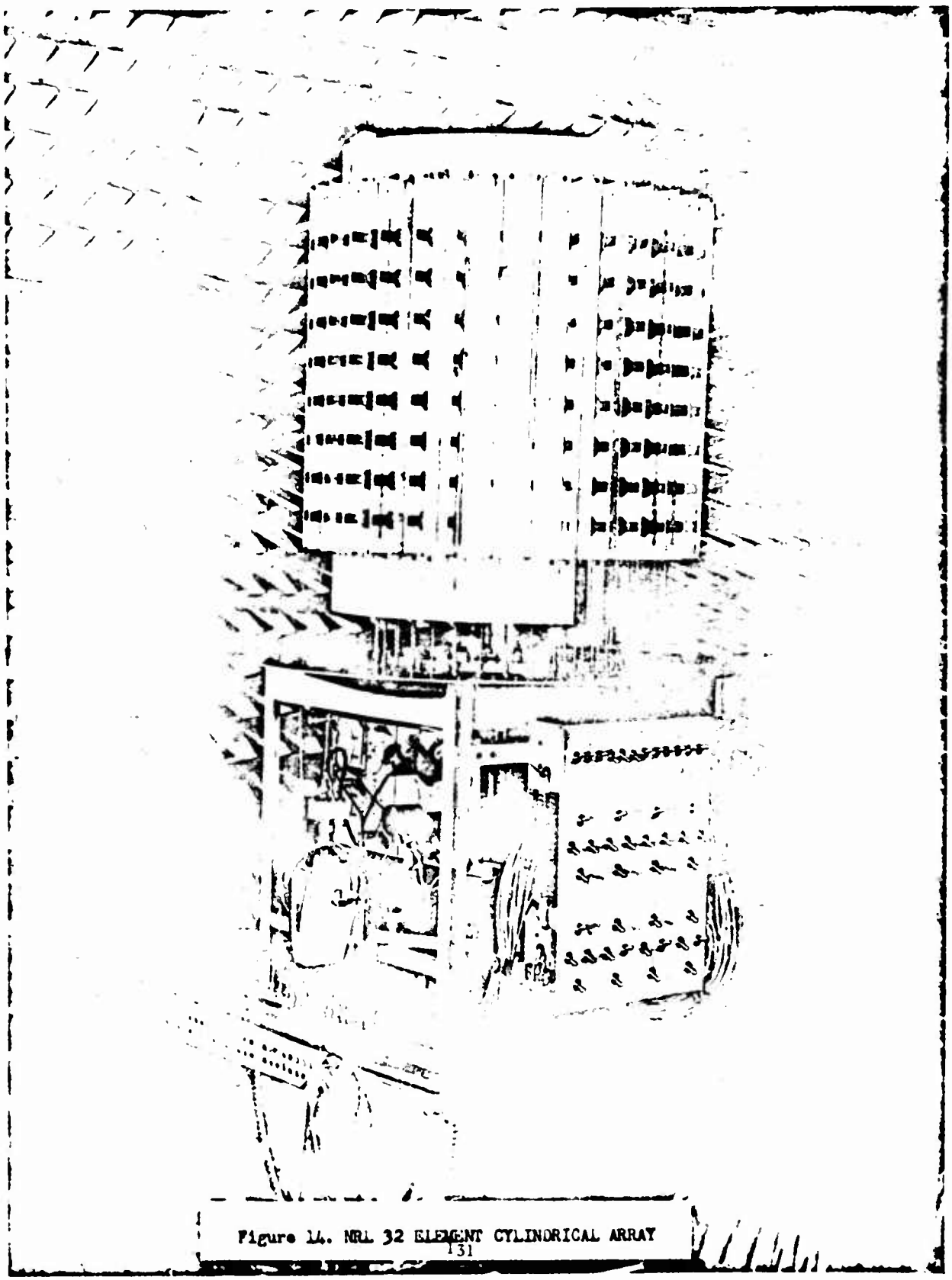

Figure 14. NRL 32 ELEMENT CYLINDRICAL ARRAY

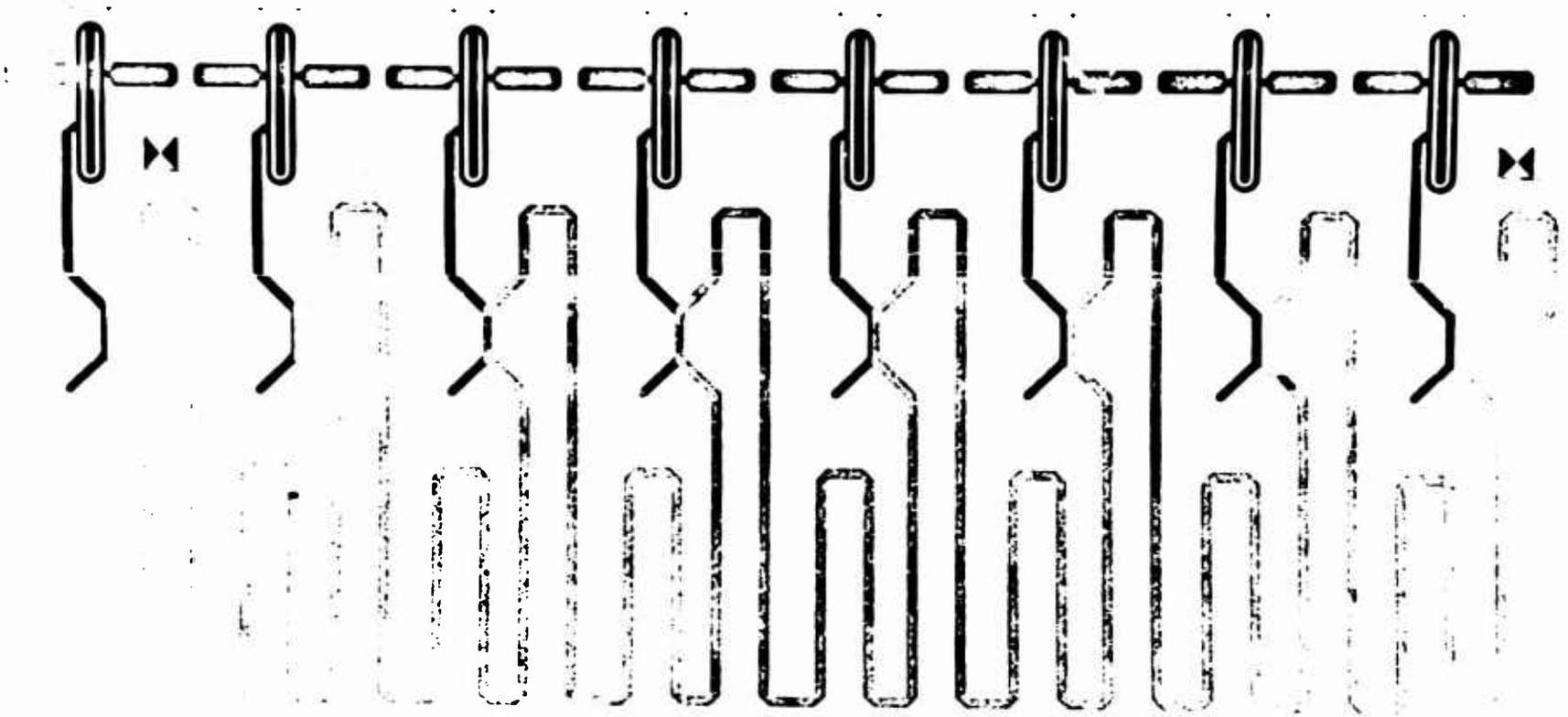

Figure 15. EIGHT DIPOLE LINEAR ARRAY RADIATING ELEMENT

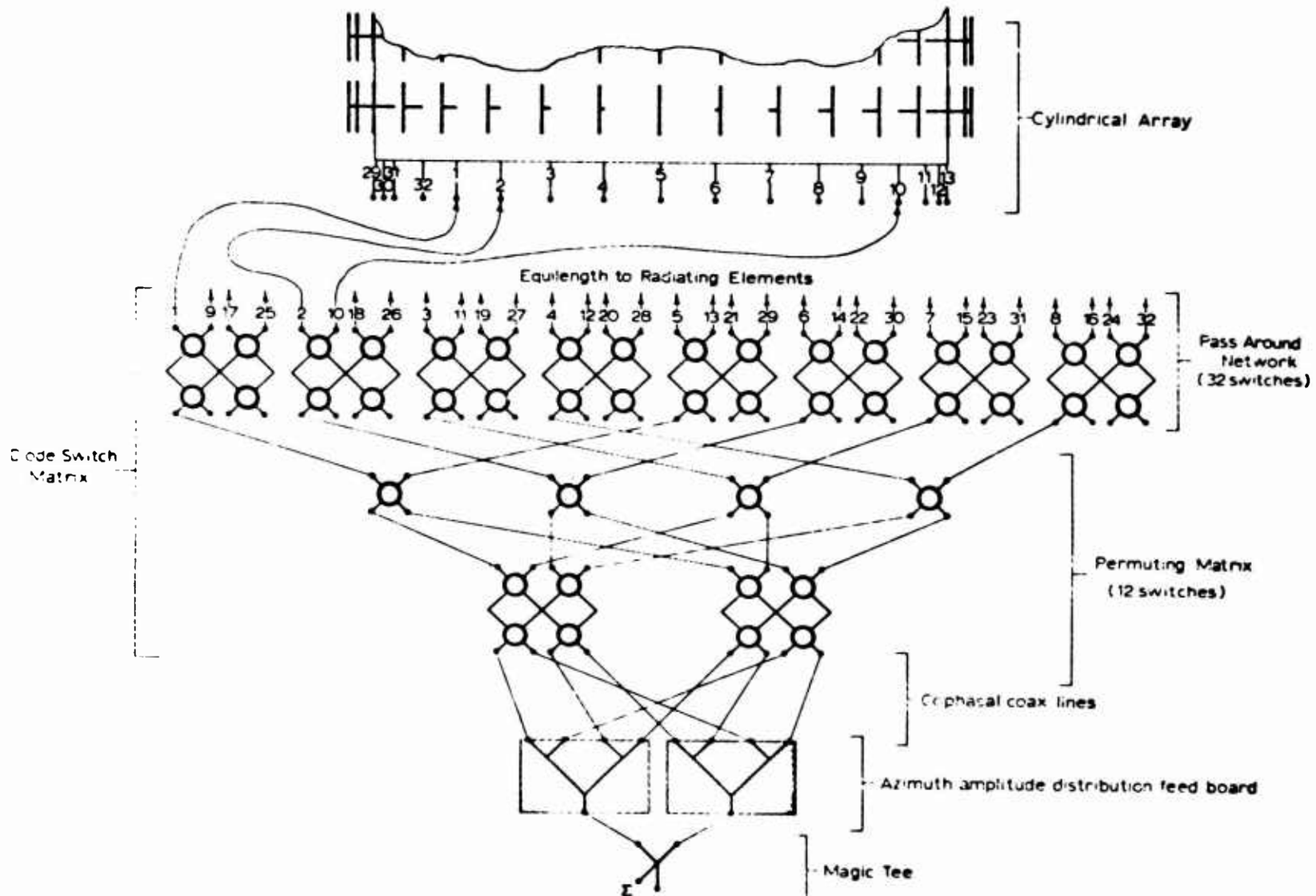

Figure 16. 32 ELEMENT CYLINDRICAL ARRAY FEED

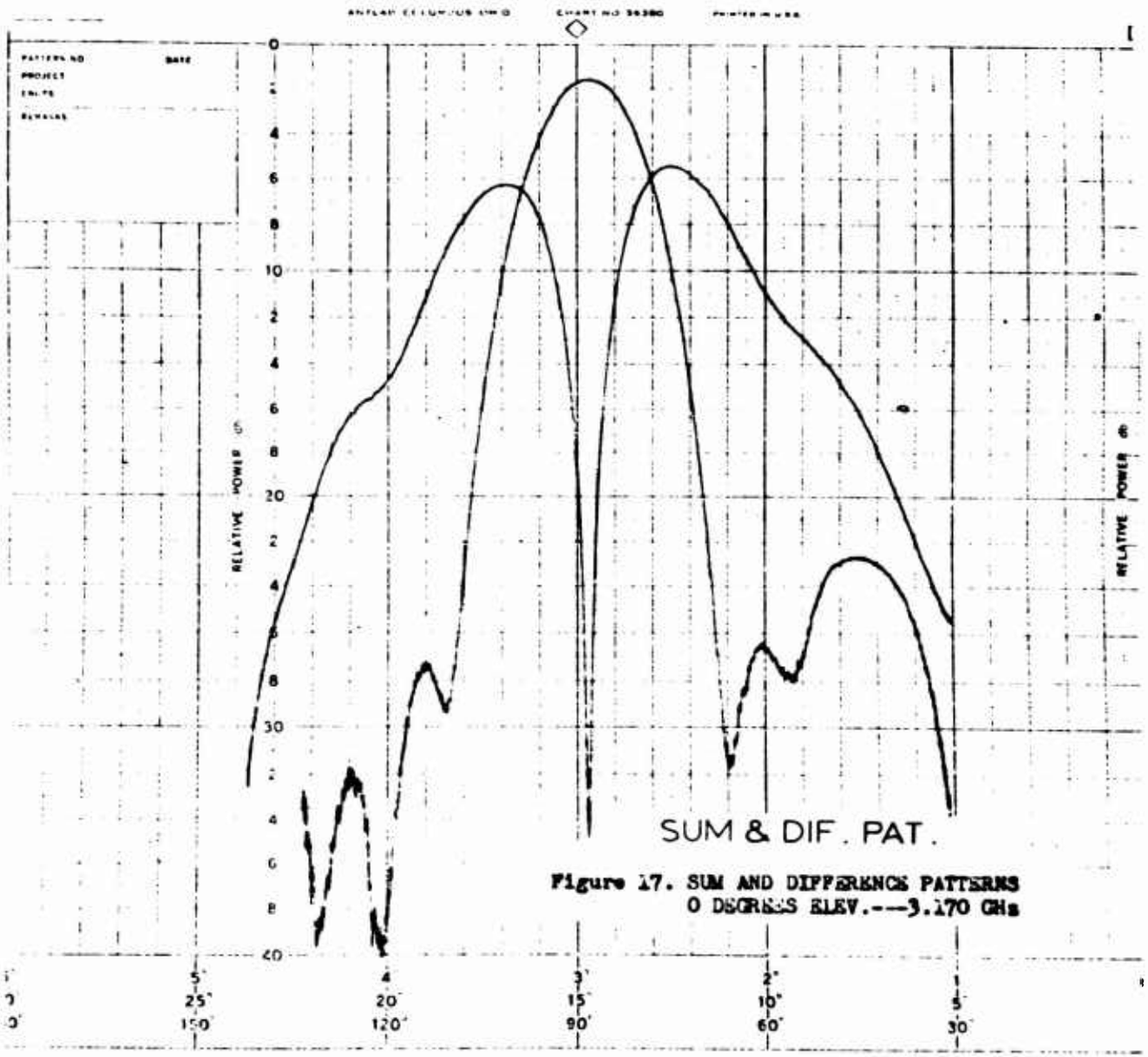

Figure 17. SUM AND DIFFERENCE PATTERNS
0 DEGREES ELEV.---3.170 GHz

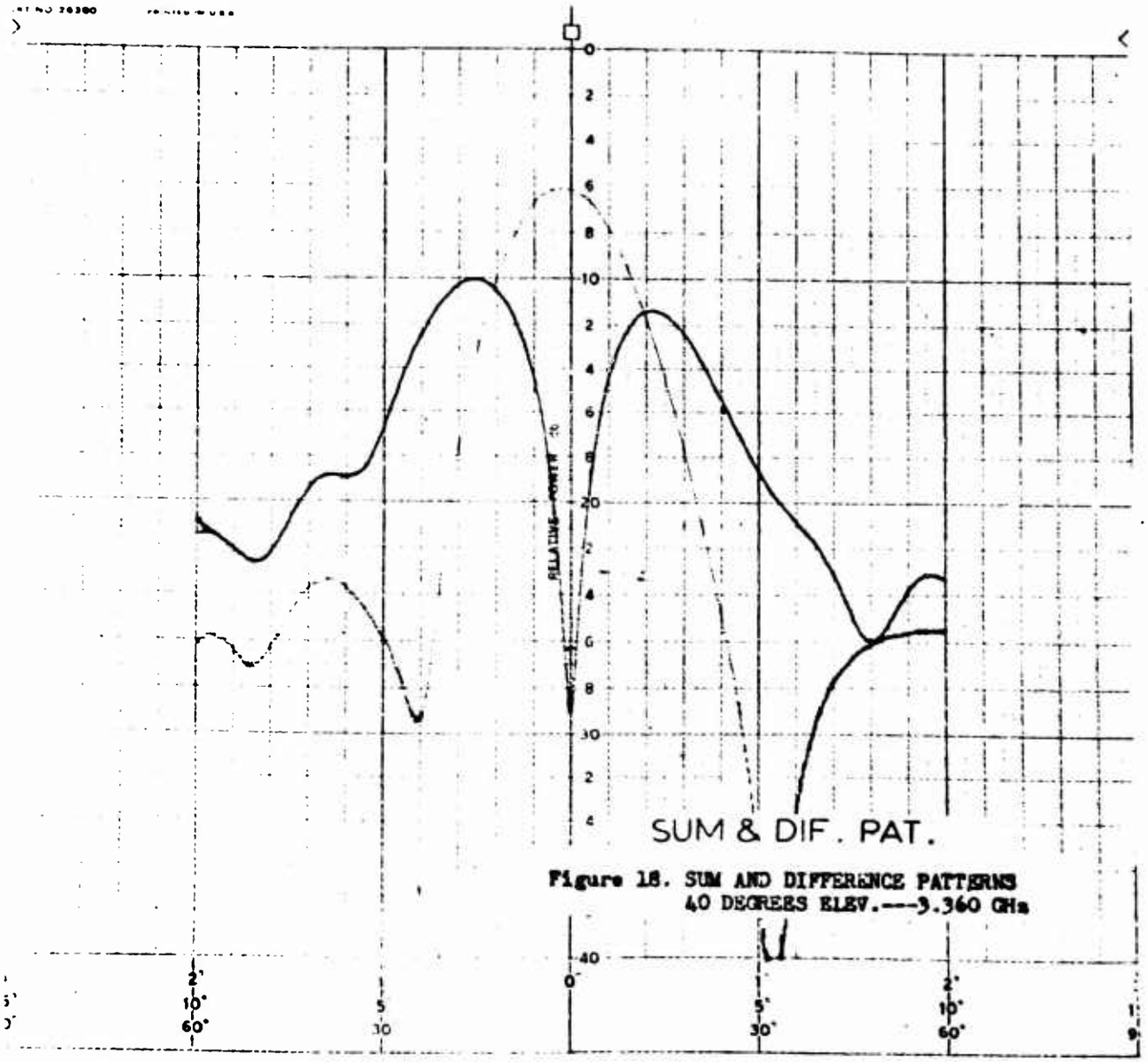

Figure 18. SUM AND DIFFERENCE PATTERNS
40 DEGREES ELEV.---3.360 GHz

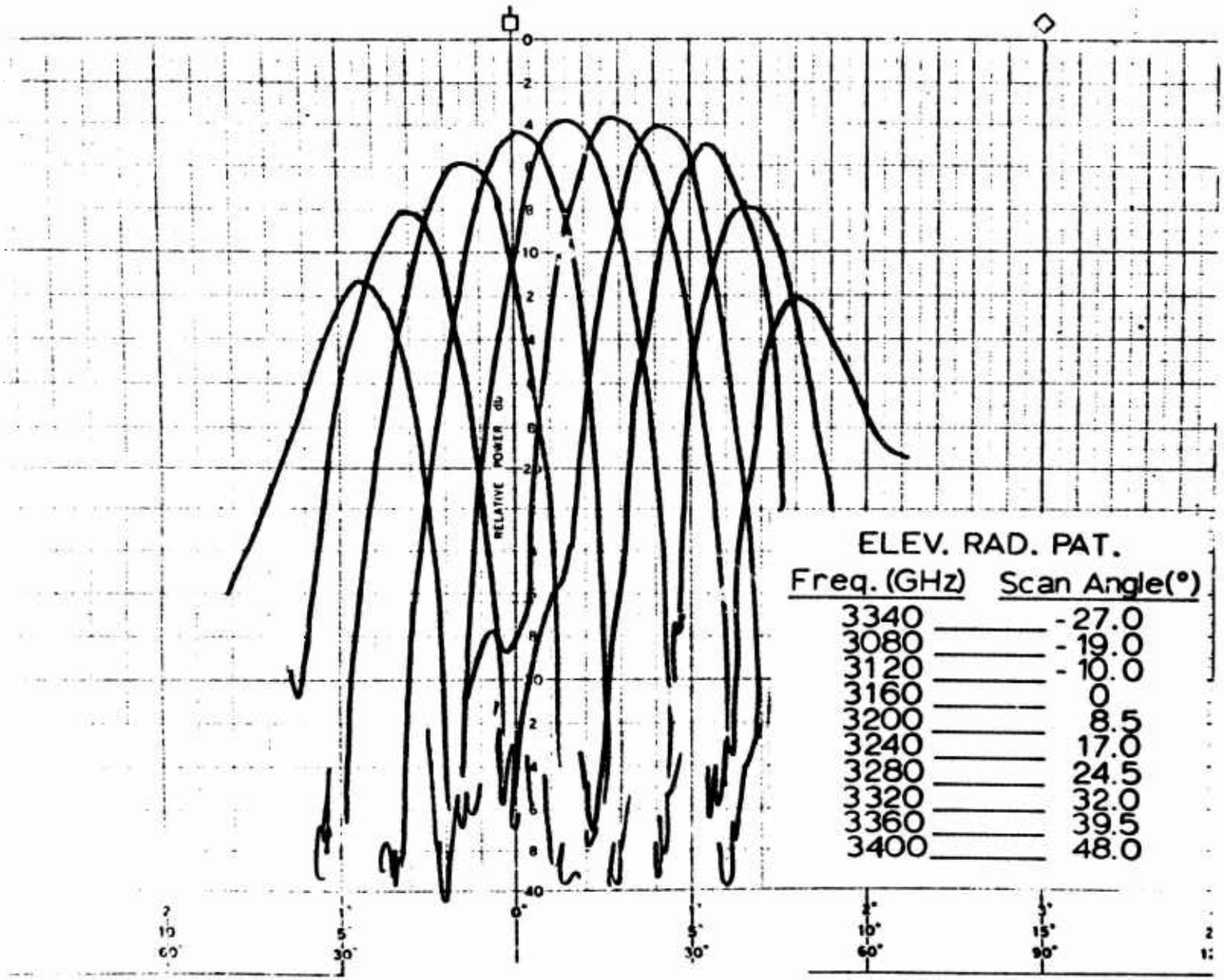

Figure 19. FULL ELEVATION SCAN

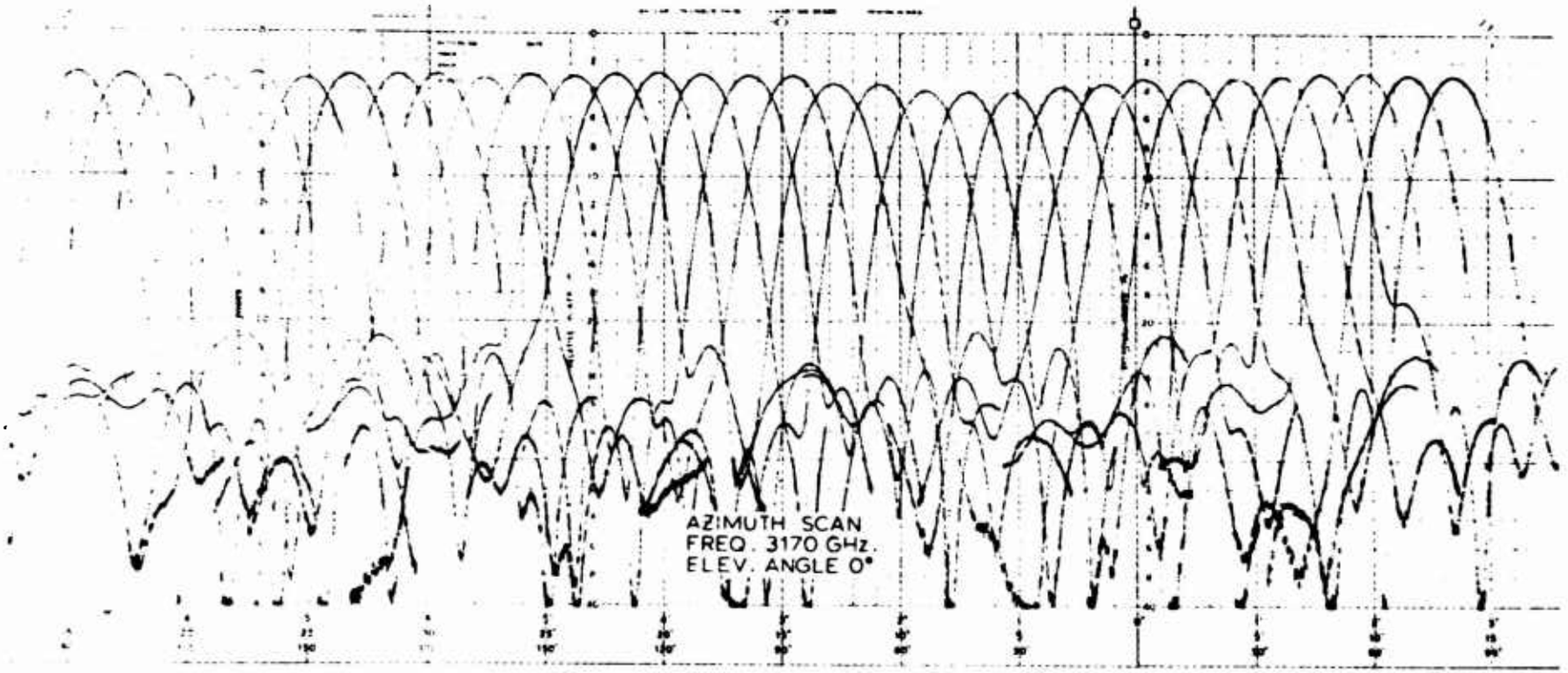

Figure 20. FULL 360 DEGREE AZIMUTH SCAN
0 DEGREES ELEVATION

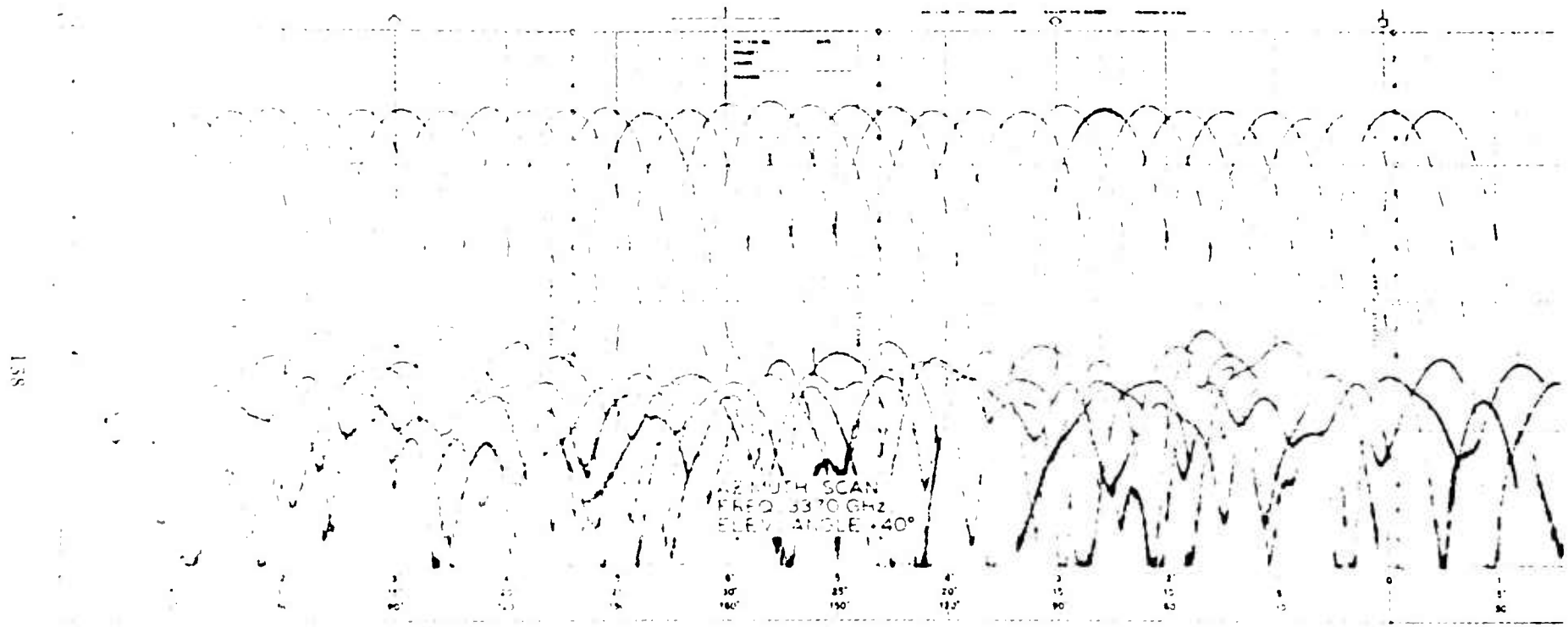

Figure 21. FULL 360 DEGREE AZIMUTH SCAN
40 DEGREES ELEVATION

STAR - A CONFORMAL ARRAY TECHNIQUE FOR AIRBORNE APPLICATION

John J. Stangel, Leon Schwartzman and
Pat A. Valentino

Sperry Gyroscope
Sperry Rand Corporation
Great Neck, New York

I INTRODUCTION

Scan Tailored Antenna/Radome (STAR) is an adaption of the Dome Antenna concept specifically for airborne applications. The Dome Antenna concept is a Sperry Rand patented[1] antenna design technique which uses conformal array technology to achieve hemispherical electronic scan coverage with a single planar phased array. The resultant antenna system will exhibit a variation of antenna gain with scan angle which is optimized for system requirements. When used in wide angle scanning applications, antennas incorporating this novel design technique generally afford substantial reductions in complexity and cost in comparison with alternate design approaches. These cost benefits, together with an inherent capability to present an aerodynamically conformal profile, makes STAR a likely cost effective candidate for a variety of future airborne antenna uses.

II CONCEPT

STAR employs a uniquely designed passive lens or dome to alter the scan characteristics of a planar phased array. The phased array thus modified is capable of generating beam patterns whose characteristics (e.g., gain, beamwidth, etc.) with scan angle conform optimally to a given operational requirement. That a single planar phased array can be modified by a passive lens to scan a full hemisphere is indicative of the flexibility of this concept. The lens efficiently transforms the scan characteristics of the planar "feed array" into the desired hemispheric coverage requirement with a minimal number of active components (i.e. phase shifters).

In general, a lens system can be hypothesized which alters the scan characteristics of a phased array. Such a system will employ a lens having generally a non-planar configuration positioned in the field of a conventional planar phased array antenna. A typical configuration illustrating this is shown in Figure 1. It consists of a planar feed array containing electronically variable phase shifters and a separate lens structure, circular in cross-section, possessing fixed phase

characteristics. The feed array elements are phased such that when energy is transmitted through the lens it combines to produce a collimated beam at a specific scan angle ϕ_L. By changing the phasing of the feed array different collimated beams at different scan angles are generated. In all cases the lens imparts a phase delay to the incident electromagnetic energy whose value depends on the portion of the lens upon which the energy is incident. By proper design, this causes the pattern characteristics of the collimated beams formed by the antenna to conform to the operational requirement.

The lens performs two major functions. First, it changes the direction of propagation of the energy from the feed array, acting as an r.f. analog to an optical prism. That is, the feed array radiates energy in a direction θ which is changed by the lens to a direction ϕ_L. Hence, the lens alters the feed array scan angle by a factor $K(\theta)$ where $K(\theta) = \phi_L/\theta$ and is termed the scan altering factor. Lenses for which the scan altering factor is generally greater than unity are called Wide Angle Scanning Array Lenses (WASCAL)[2] since the lens increases the wide angle scanning capability of the feed array. Antennas designed for hemispherical scan coverage are of this type. Conversely, lenses which are designed with scan altering factors which are generally less than unity are applicable to limited scan coverage. Second, the lens provides an effective antenna aperture in all scan directions. This is in contrast to a planar array where the effective antenna aperture is drastically reduced at wide scan angles.

The gain characteristics realized are dependent upon the lens phase gradient which is a function of $K(\theta)$. Examples of this are presented in Figure 2 where curves of the relative gain versus scan angle are plotted for various value of $K(\theta)$. The $K(\theta) = 1.0$ curve represents the relative gain and scan coverage of the feed array alone. For $K(\theta) > 1.0$ these curves illustrate that it is possible to greatly extend the scan range of the planar feed array with a corresponding gain loss near zenith. For $K(\theta) < 1.0$, the converse is illustrated. The gain of the antenna can be increased significantly over that of the feed array alone but with a corresponding reduction in scan coverage.

The action of the lens can now be better understood if it is thought of as a transformation device which transforms the gain envelope of the feed array into the corresponding gain curve. For a lossless system energy is conserved and from Stangel's theorem[3], it can be shown that the integral of the gain envelope over all space for any of the gain curves must be equal. This explains the tradeoff between gain and scan volume which is utilized in scan tailoring the lens design. An example of this is the scan tailored gain contour of Figure 2. Here $K(\theta)$ is varied with θ to shape or tailor the gain envelope to meet a specific requirement.

Figure 3 is a reproduction of far field radiation patterns computed for a typical wide angle scan design. The feed array is 40 wavelengths in diameter. The lens is spherical with a 28 wavelength radius. The system is designed for a constant scan altering factor, $K(\theta)$, of 1.5. Patterns for the zenith beam and beams scanned to 30, 60 and 90 degrees from zenith are overlayed in the figure and show a maximum sidelobe ratio of -29 dB.

Far field patterns for a typical limited scan configuration are reproduced in Figure 4. The feed array is 14 wavelengths in diameter. The lens is a spherical sector with a 50 wavelength radius and subtending an angle of 95 degrees at the origin. The system is designed for a constant scan altering factor of 0.25. Overlayed patterns for the zenith beam and for beams scanned 4, 7 and 10 degrees from zenith are plotted. A maximum sidelobe ratio of -21 dB is predicted.

III EXPERIMENTAL DEMONSTRATION

Conceived and initially studied as part of Sperry's internal research and development activities, the continuing development of the STAR technique for wide angle scanning applications has been partially supported by a number of government agencies including the U.S. Army Ballistic Missile Defense Advanced Technology Center (BMDATC), U.S. Army Missile Command (MICOM) and U.S. Air Force Rome Air Development Center (RADC).

Under BMDATC sponsorship, Sperry has recently completed the implementation and experimental evaluation of this technique in a three dimensional electronically scanned antenna at C-band[4]. Figure 5 is a schematic representation of the antenna system built to demonstrate and verify the Dome Antenna concept. The antenna consists of a passive constrained lens and an electronically scanned planar feed array.

The passive lens is hemispherical in shape and contains 3636 discrete element modules. Each dome module consists of a collector element, a radiator element and a fixed phase delay section and is fabricated with circular symmetry to achieve nominal polarization insensitivity. There are 18 different style modules, differing only in the insertion phase imparted by the fixed phase delay section to electromagnetic energy passing between collector and radiator elements. The refractive properties of the lens are determined by the arrangement of the module styles within the dome lattice. The modules are removable so that a multiplicity of dome phase gradient designs may be readily implemented and evaluated by simply rearranging the basic module styles. The collector and radiator element designs are dielectrically loaded open-ended circular waveguides and utilize evanescent mode matching structures to provide good impedance match for waves incident at angles up to 55 degrees.

The passive lens is irradiated by an 805 element planar phased array of conventional optically fed design. The feed array elements are open-ended rectangular waveguides. Electronic phase control is effected by three-bit ferrite phase shifters. The feed array is illuminated by a dual mode four horn feed/comparator capable of generating a sum and two monopulse difference beams. A monopulse processor provides a means of measuring the linearity of monopulse error slopes. The proper phase commands are generated at each phasor by a unique three-axis beam steering unit.

An extensive test program evaluating the performance of the antenna has been conducted. Measured data encompasses the following characteristics:

- antenna gain
- radiation patterns
- monopulse error slope linearity
- pointing accuracy
- polarization characteristics
- back lobe radiation
- signal bandwidth

Two gain/scan profiles (corresponding to two arrangements of the dome module styles) were evaluated. The variations of gain with scan angle from zenith for these profiles are shown in Figure 6. That one of these profiles exhibits scan coverage to 120 degrees from zenith (30 degrees below the equatorial plane) is a dramatic example of the unique capabilities of Dome Antenna designs. In Figure 7 the measured azimuth and elevation plane patterns for beams scanned 65 and 90 degrees from zenith are presented. These patterns further demonstrate the capability of the Dome Antenna to provide hemispherical (or greater) coverage with a single active planar phased array.

IV STAR CONFIGURATIONS

The demonstrated capability of providing optimized electronic scan coverage of a hemispherical (or greater) volume with an external antenna profile which conforms to aerodynamic requirements makes the STAR design technique especially suited for a range of airborne systems. Figure 8 depicts fuselage mounted configurations physically similar to that of the exploratory model. The scanning characteristics of these configurations can be readily designed to satisfy the requirements of early warning detection and surveillance systems. The top mounted fuselage configuration offers a lower center of gravity than alternate electronic scan antenna designs thus reducing aircraft stabilization problems normally associated with top mounted arrangements.

A more sophisticated arrangement is illustrated in Figure 9. Mounted in the nose of a modern high performance aircraft, this STAR configuration employs a streamlined lens for aerodynamic compatibility. Scan Tailoring will afford gain/scan variations which will facilitate optimization of avionics systems for a variety of missions.

Preliminary analysis of several nose-mounted STAR configurations indicate that good electronic scan coverage can be achieved to ± 140 degrees of broadside encompassing a total solid angle in excess of $3.5\ \pi$ stir-radians. Transverse ray diagrams for two such configurations for a constant K of 1.7 and a scan tailored design are reproduced in Figure 10. Patterns for the two dimensional design corresponding to the constant K configuration are shown in Figure 11. The feed array

illumination, a cosine on a pedestal with a 4 dB edge taper taper, is just sufficient to approximate an equivalent uniform illumination when projected through the lens for the broadside beam. The patterns show that beam shape and sidelobe levels are substantially preserved for beams scanned through 120 degrees from broadside.

V CONCLUSIONS

STAR embodies a new conformal antenna design technique for future avionics systems. Using the Dome Antenna concept, STAR employs a passive conformal lens to modify the scanning characteristics of a conventional planar array. The resultant antenna system is capable of electronically scanning more than a hemispherical volume with a gain/scan variations which is optimized for the specific system. This added capability, together with the aerodynamic compatability of the lens profile, makes this versatile design concept uniquely suited for airborne applications.

STAR configurations can be readily built using state-of-the-art components and fabrication methods. The concept has been experimentally verified via three dimensional electronically scanned model, and a system is presently being developed for a specific ground-based radar application.

By a novel marriage of current planar and conformal array technoligies, STAR provides a capability for electronically scanned systems which generally results in dramatic reductions in system cost and complexity.

REFERENCES

1. J.J. Stangel and P.A. Valentino, Phased Array Fed Lens, U.S. Patent No. 3755815.
2. L. Schwartzman, J.J. Stangel, and P.A. Valentino, "Wide Angle Scanning Array Lens (WASCAL)", 19th Annual Tri-Service Symposium, Colorado Springs, Colo., 1973.
3. J.J. Stangel, "A Basic Theorem Concerning the Electronic Scanning Capabilities of Antennas", 1974 URSI Spring Meeting, Atlanta, Georgia.
4. Final Report: Dome Antenna Phase III, Sperry Gyroscope, Great Neck, New York, Report No. SD-4261-0856, April 1975.

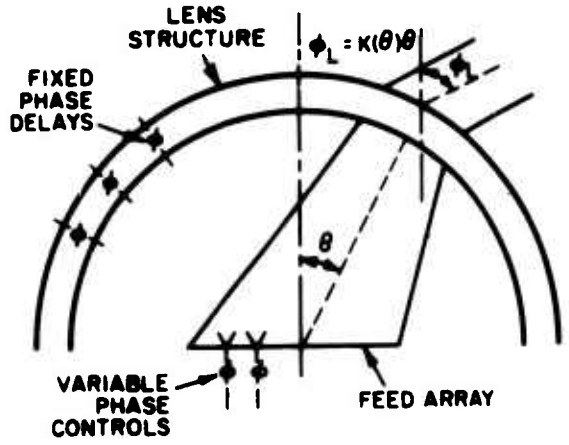

FIG. 1. DOME ANTENNA CONCEPT

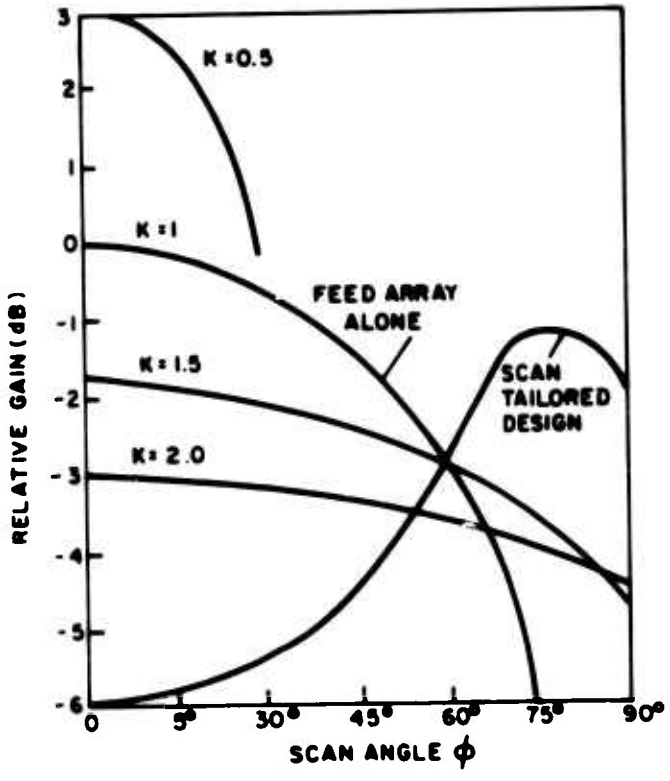

FIG. 2. TYPICAL GAIN/SCAN PROFILES

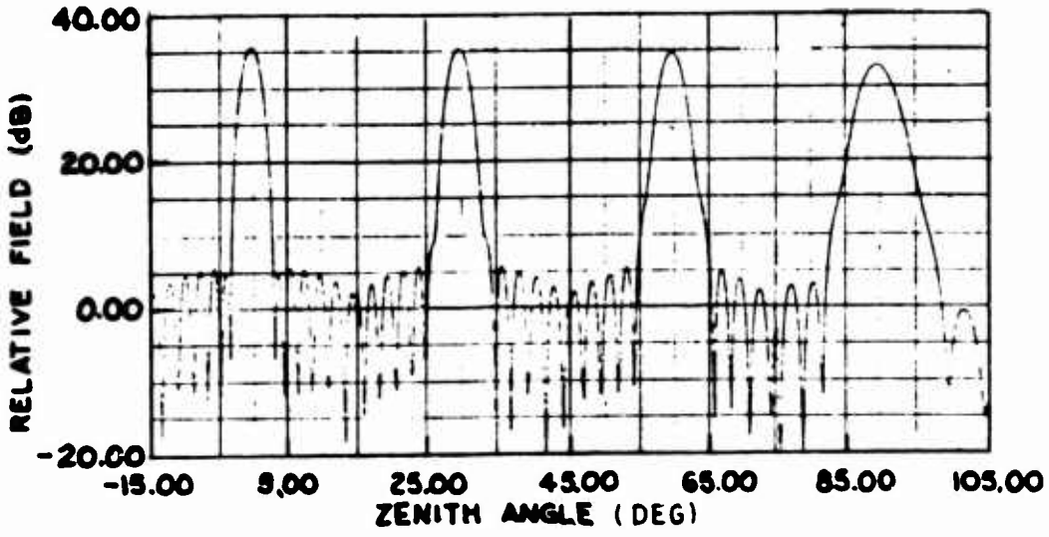

(K= 1.50)

FEED ARRAY DIAMETER = 40 λ

LENS RADIUS = 28 λ

FIG. 3. COMPUTED RADIATION PATTERNS FOR A TYPICAL WIDE ANGLE SCAN CONFIGURATION

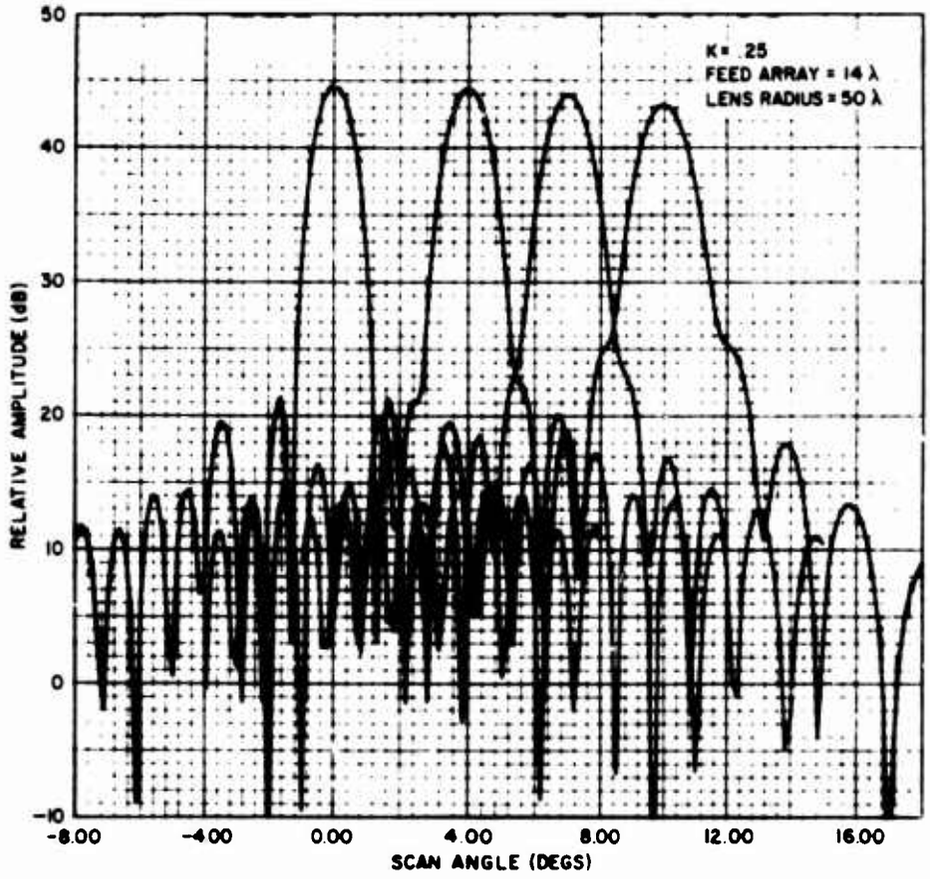

FIG. 4. COMPUTED RADIATION PATTERNS FOR A TYPICAL LIMITED SCAN CONFIGURATION

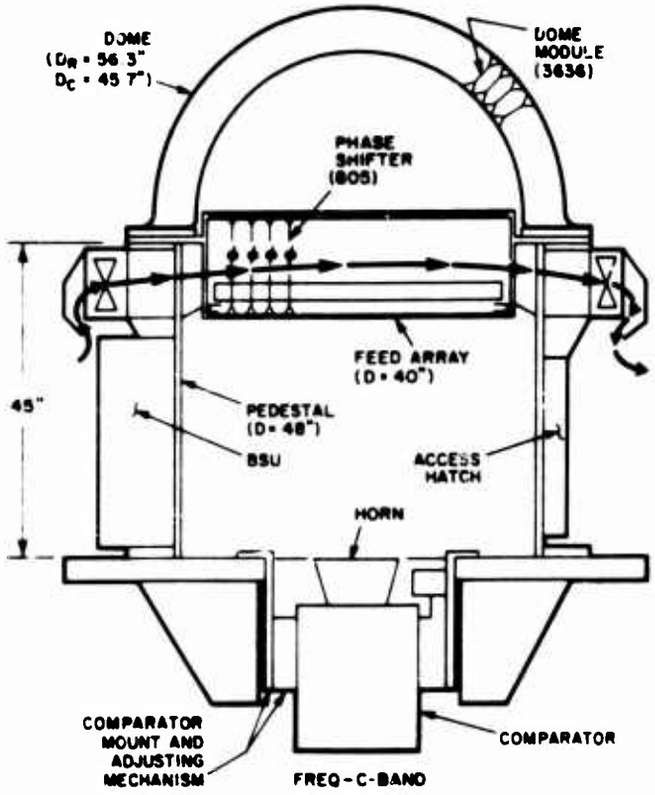

FIG. 5. DOME ANTENNA EXPLORATORY MODEL

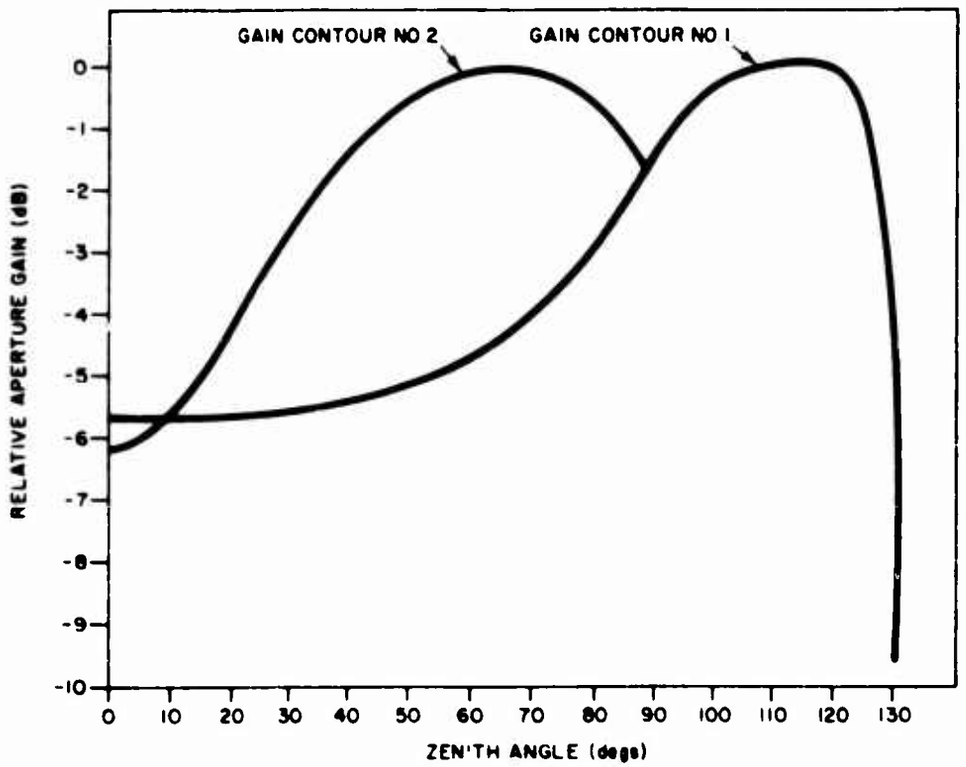

FIG. 6. EXPERIMENTAL GAIN/SCAN PROFILES

SCAN PLANE, $\phi = 0°$ f = 5.4 GHz

—— MEASURED LEVELS
—·— PREDICTED LEVELS

SCAN ANGLE, $\theta = 65°$

H-PLANE (AZIMUTH) E-PLANE (ELEVATION)

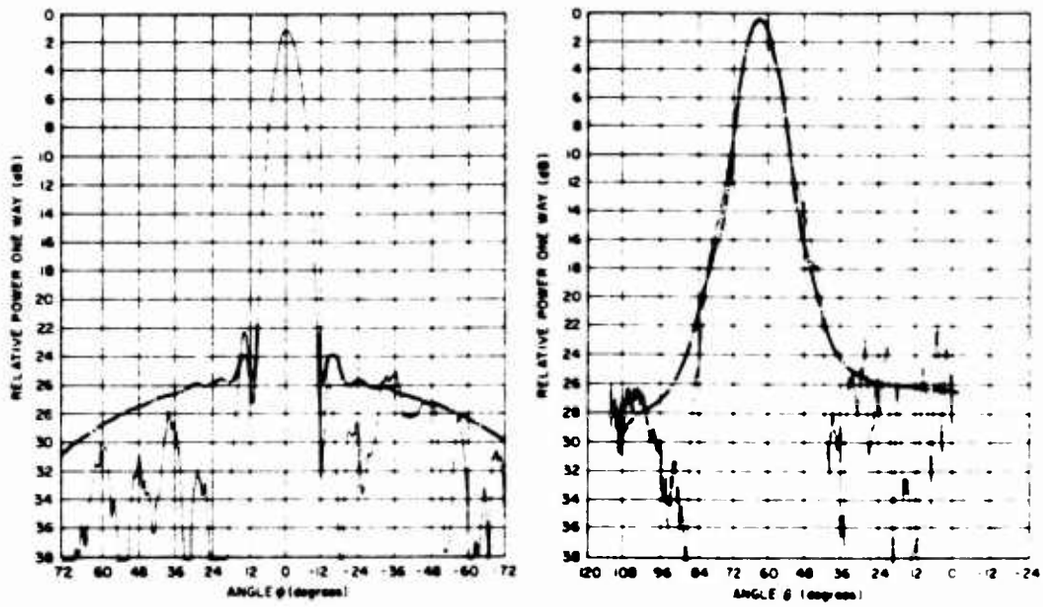

SCAN ANGLE, $\theta = 90°$

H-PLANE (AZIMUTH) E-PLANE (ELEVATION)

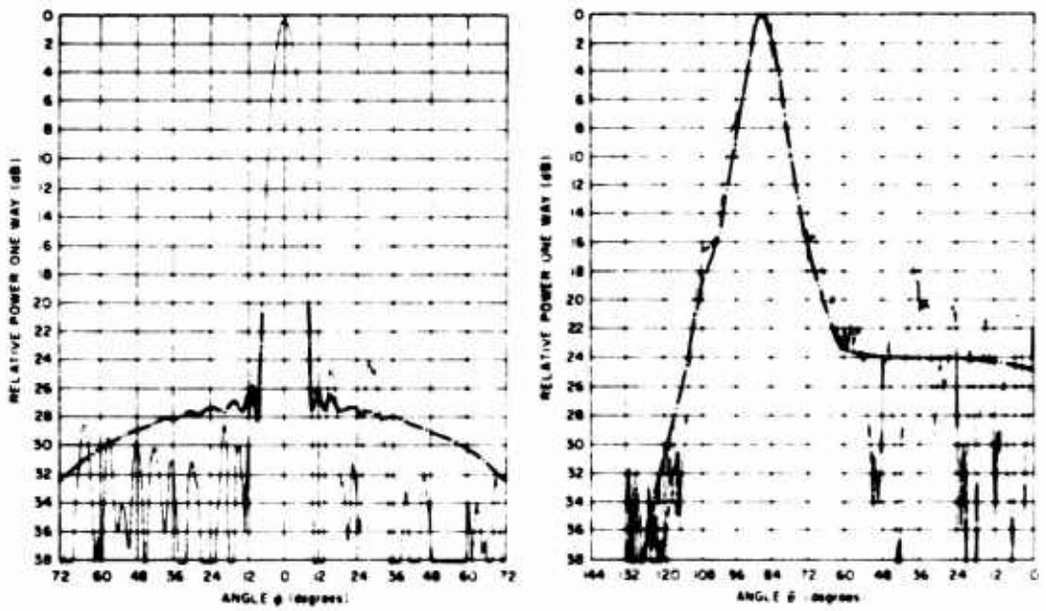

FIG. 7. MEASURED DOME ANTENNA PATTERNS GAIN CONTOUR NO. 1

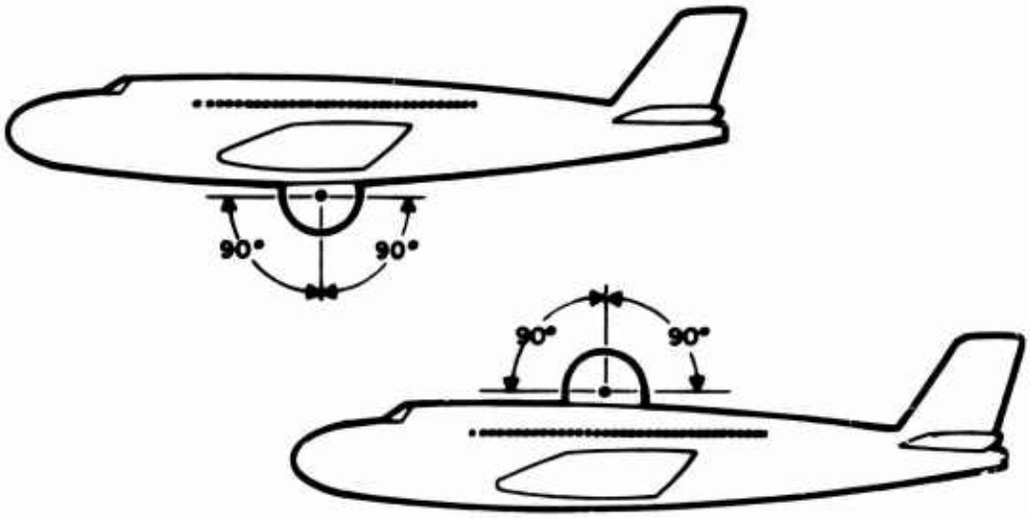

FIG. 8. FUSELAGE MOUNTED STAR CONFIGURATIONS FOR EARLY WARNING DETECTION AND SURVEILLANCE

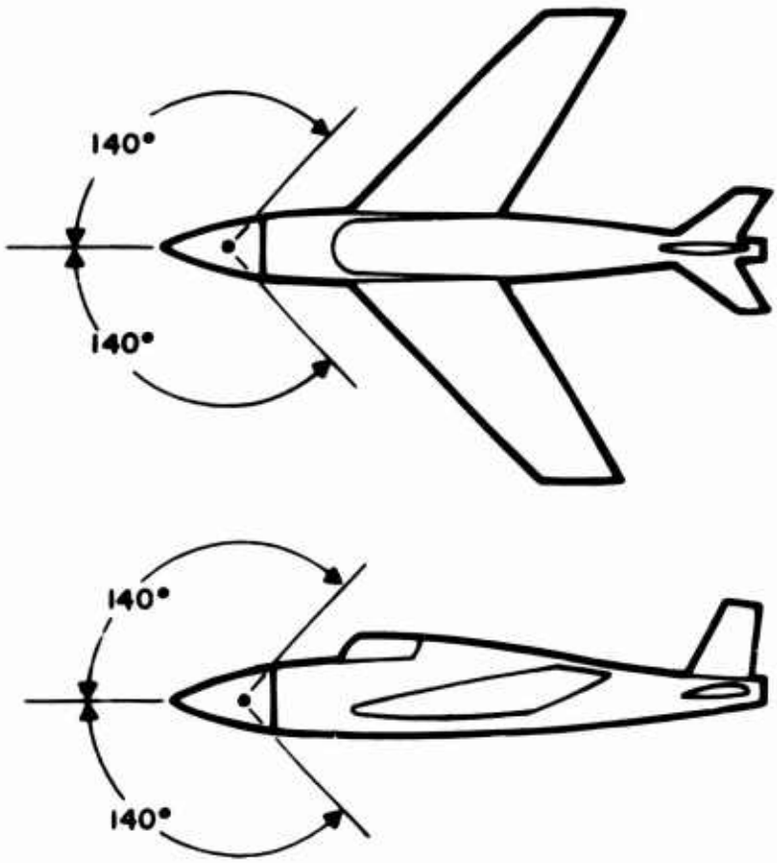

FIG. 9. MULTIPURPOSE NOSE MOUNTED STAR CONFIGURATIONS

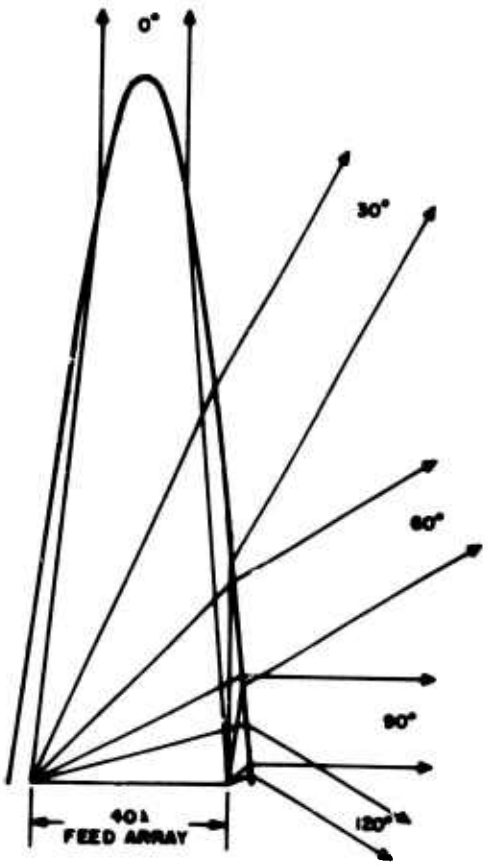

(a) K = 1.7 DESIGN

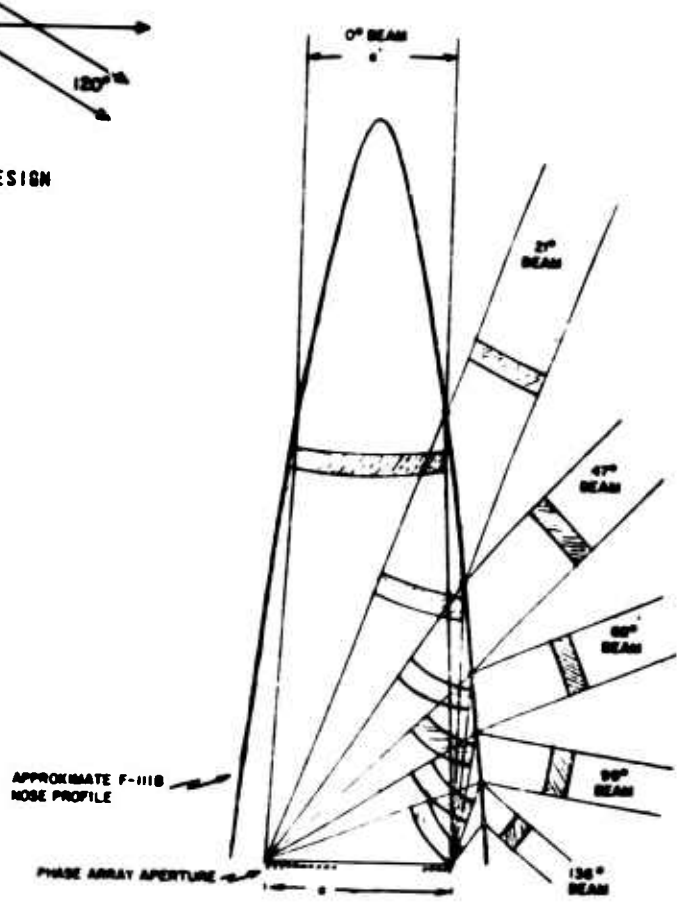

(b) SCAN TAILORED DESIGN

FIG. 10. RAY DIAGRAMS FOR TYPICAL NOSE MOUNTED STAR CONFIGURATIONS

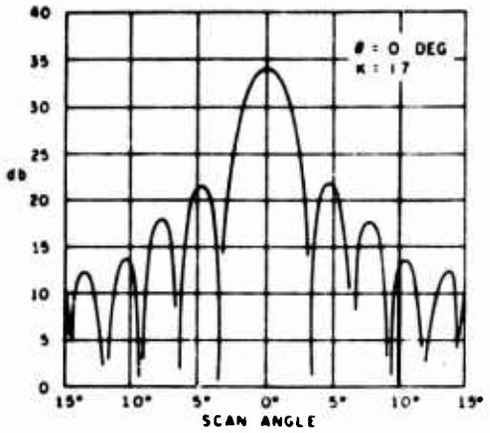

(a) θ = 0 DEG.

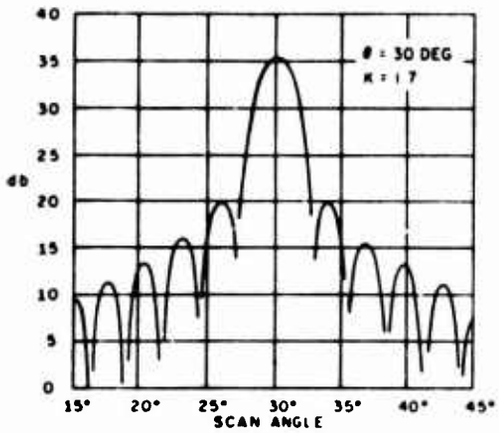

(b) θ = 30 DEG.

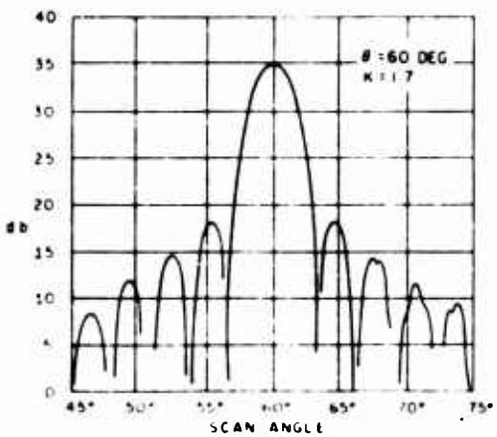

(c) θ = 60 DEG.

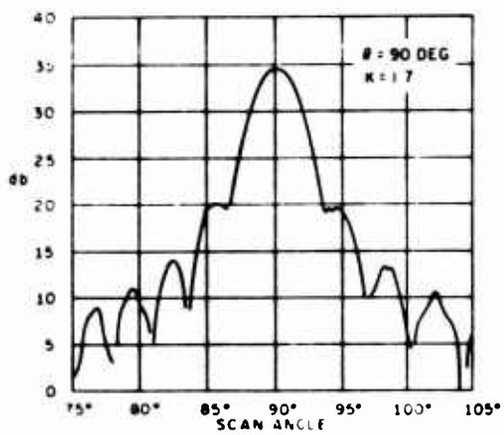

(d) θ = 90 DEG.

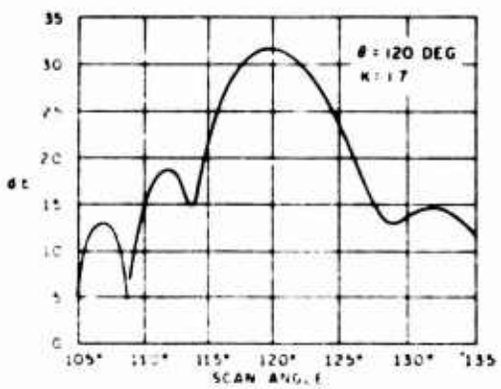

(e) θ = 120 DEG.

FIG. [illegible]. COMPUTED RADIATION PATTERNS FOR TYPICAL STAR CONFIGURATION

CONFORMAL ANTENNA ARRAY CONFIGURATIONS

REPORT

Troy E. Plunk
Missile Systems Division
Raytheon Company
Bedford, MA

ABSTRACT

Some practical aspects of conformal arrays are discussed through a review of several government conformalsponsored array programs completed at Raytheon company since 1960. Five programs considered are FAGT (Fixed Antenna Guidance Tracking: 1961-66 under Navy contract now-62-0154-d); PAATI (Phased Array Antenna Technology Investigation: 1971-73 under Army Contract DAHC-60-72-C-0070); SHF (Super High Frequency Array: 1968-70 under contract AF 33615-68-C-1592) Conformal Array Studies (1970-74 AFCRL F19-628-72-C-0202); and Extended Coverage Array (1973 contract F33615-72-C-1571). The discussion emphasizes componentary necessary to realize and implement conformal arrays in the feed network, phase shifter, radiator, and radome areas.

2.0 FAGT (Fixed Antenna Guidance Tracking)

This cylindrical X-band array seeker theoretical and experimental study, sponsored by Naval Air Systems Command was Raytheon's first major conformal array effort. The program consisted of a 5 year series of studies beginning in 1962 resulted in the design, fabrication and experimental evaluation of a complete conformal phased array seeker on a 14 inch diameter cylindrical missile shell. Supporting systems studies were performed relating antenna performance to miss distance.

The experimental array consisted of two phased array cylinders in tandum. Each cylinder consisted of an array of 64 linear waveguide radiators. Scan in a plane containing the cylinder axis was accomplished by a dielectric rod within each linear array. Scan and aperture amplitude circumferential to the cylinder were accomplished with a diode controlled waveguide ring feed.

The X-band experimental array, shown in Figure 2-1, consisted of two 12 inch long 14 inch diameter arrays whose outputs were monopulsed to obtain tracking information in a plane containing the missile axis. Scan was accomplished in the axial plane (i.e. a plane containing the missile axis and the beam peak) by rotating dielectric rods inside an array of co-axially oriented traveling wave waveguide arrays. A typical linear waveguide array with dielectric rod scanner is shown in Figure 2-2. Scan in the axial plane was accomplished by synchronously rotating all dielectric rods.

Each of the two cylindrical arrays of linear waveguide elements was fed through a diode controlled ring array as shown in Figure 2-3. For a given circumferential beam position, eight of the 32 diode switches were open and the remaining 24 were closed or shorted. Hence, the ring feed operated as a linear waveguide array feed which could be used to control the sector of linear arrays which radiated. This provided course beam position control around the missile. Fine circumferential beam steering and focusing of the otherwise curved radiated wavefront was provided by a reciprocal ferrite phase shifter at the input to each linear radiator as shown in Figure 2-4.

Experimental results from the experimental array of Figure 2-1 are shown in Figures 2-5 through 2-10. Figure 2-5 and 2-6 show typical patterns for axially and circumferentially scanned beams from the forward cylindrical array. Figures 2-7 and 2-8 show circumferential plane, (i.e. conical surfaces) monopulse patterns when the forward and rear cylindrical

arrays are amplitude differenced. Figure 2-9 shows a measured difference pattern in the axial plane resulting from a phase monopulse subtraction of the forward and rear array halves.

Figure 2-10 shows scan plane patterns from a linear radiator. Zero degrees corresponds to the forward missile axis. As indicated a useful gain level was achievable at end fire although the beam peak did not correspond to end fire. Gain versus scan was good to 60 degrees from end fire.

The FAGT program was initiated in 1962 prior to more recent advances in radiator, phase shifter, feed network and radome technology. The significance of the FAGT program is obviously not in the area of component technology except that perhaps it illustrates the significance and necessity of more recent component technology at Raytheon and elsewhere in relation to practical weights, volumes and control techniques. The significance of the FAGT program was that it 1) demonstrated that high near end fire gain from a cylindrical phased array was realizable & 2) it demonstrated that monopulse tracking was possible from a conformal missile seeker covering the region forward of the missile. A less obvious but perhaps quite significant component technique employed in the FAGT array is the "slotted metal radome". The technique of many small dielectric windows instead of one large radome may be a better approach to severe surface temperature and ablation problems. The metal thickness housing the slots could be metalic loaded heat shield material.

3. <u>SHF (Super High Frequency) Airborne Satellite Communication Antenna</u>

This two year experimental development program, sponsored by the Avionics Laboratory, WPAFB, addressed the question of a moderately curved phased array with a T/R module per

radiator. Several X-band T/R modules were designed, fabricated and evaluated. Other hardware developed and tested included the wide band radiator and a conformal interwoven dual corporate feed. A conformal array was selected to minimize the number of radiators, nominalize gain loss versus scan and provide hemispheric coverage from one antenna. This work was performed under contract F33615-68-C-1592.

The SHF antenna design consisted of an 18 inch diameter circular aperture of 256 circularly polarized radiators. Figure 3-1 shows the array aperture. The radiating aperture was designed to be slightly cylindrical to improve gain at large circumferential scan angles. The design goal was to achieve $\pm$ 70 degree scan with - 4 db gain scan loss with degraded coverage to $\pm 90^{\circ}$.

Each radiator, shown in Figure 3-2, was designed to facilitate radiation (or reception) of either RH or LH circular polarization by feeding two crossed dipoles in the radiator cavity through a microstrip hybrid circuit. RH circular polarization was transmitted through each element from a solid state transmit module per element. The array of per element transmitters was fed through an all stripline transmit corporate feed. A ferrite phase shifter at the input to each transmit module provided transmit beam control for the CW transmitter.

An amplifier-mixer per element was provided on receive with an i.f. corporate feed. The mixer LO power was supplied through a second stripline waveguide corporate feed. A ferrite phase shifter in the LO line to each mixer provided beam control of the CW receive beam.

The functional details of the SHF array are of less interest here than the conformal array hardware. To keep lost aircraft volume to a minimum required a compact feed which was packaged nearly conformal to the aperture surface. Figure 3-3 and 3-4 show the two independent stripline-waveguide corporate feeds integrated in an experimental array feed. The stripline-waveguide

feed loss was about 1.0 db. The two feeds would occupy a space only 1.5 inches in depth behind the array. Larger arrays could be fed in the same depth behind the aperture.

Performance of the array was theoretically predicted and design goals achieved based upon measured data from the major components in the array. Components which were designed, fabricated and evaluated included the dual frequency microwave feed, ferrite phase shifters, T/R modules and radiating elements. Each phase shifter was 0.1 x 0.33 inches in crossection, and less than one inch in length. Figure 3-5 shows an unplated ferrite phase shifter without transitions.

4. CATHI (Conformal Array Antenna Technology Investigation)

This two year theoretical study, sponsored by ABMDA was completed at Raytheon MSD in 1969 - 1972. The program objective was to configure and design a conformal phased array on a conical missile shape which, (with an on board transmitter and receiver/processor) would result in very small miss distances in severe environments. The study concluded that conformal seekers are a necessity in certain high performance missile configurations. This work was performed under Contract DAHC-60-72-C-0070.

Exact models of array element mutual coupling were developed for the conical arrays and used in gain predictions. A technique was designed to eliminate the seeker related polarization problems in conical and cylindrical arrays. Another conclusion of the study was that two distinct arrays (one for near end fire coverage exclusively) resulted in fewer phased array elements.

The complete seeker antenna was configured including radome, radiators, diode microstrip phase shifters and

conformal corporate feed. The antenna volume was a thin shell having an estimated displacement weight of 10 - 20 lbs.

For extremely high velocity vehicles such as RV or hyper velocity missiles, surface temperatures may exceed 2500°F to 5000°F, lateral g-loads and aerodynamic pressure may exceed 100 g's and operation in a severe ablative environment may be required. A conventional antenna - nose radome approach would be structurally unsound, unable to withstand the extreme forward tip temperatures and ablation and may utilize 20 - 30 percent of the vehicle volume. Such g-loads necessitate phased arrays instead of gimballed approaches. The only possible radar seeker antenna approach for such applications is a conformal phased array.

The baseline phased array antenna considered in CATHI was one which would cover the space forward of a conical vehicle having a half cone angle of 5 degrees. The baseline vehicle shape is shown in Figure 4-1. A baseline frequency of X-band was chosen with the objective of achieving a nominal 5° half power beamwidth over the scan space of ±60° from the forward missile axis.

An exact theoretical analysis of an array of circumferential rings of circumferential slots on a conducting cone was developed for an array of finite axial extent and to include cone tip diffraction. For fixed element matching structures and absorptive corporate feeds, this array model was used to compute gain and patterns versus axial plane scan. Two distinct arrays are required for optimum half space gain coverage with the fewest elements. Figure 4-1 shows the X-band apertures required to achieve the desired beamwidths. The forward array was used to cover ±10 degrees about the forward missile axis and the larger array (i.e. "broadside array") was used to cover the remaining space to ±60 degrees.

Bandwidth of the forward array was limited by strong interelement mutual coupling and cone tip diffaction in the $\pm 10^{o}$ forward beam space. A typical imbeded end fire region element pattern from one ring of slots on a cone about 45 wavelengths from the cone tip is shown in Figure 4-2. Axial plane element patterns from rings of slots in the broadside array were closely approximated by conical array results.

Results indicated that tip defraction was significant in the $\pm$10 degree forward sector. To maximize the blind side gain (i.e. gain at angles below the forward vehicle axis from an array on top of the vehicle), the array to tip distance is critical and must be properly selected. Tip ablation is not extremely critical since the differential path length between the tip diffracted and direct rays is slowly varying versus tip ablation. This may be obvious from Figure 4-4.

To achieve blind side gain to 10 degrees, a necessity if diagonal array sectors are to provide monopulse information in the forward region, requires a conducting conical surface forward of the end fire array. Figure 4-3 shows how this might be accomplished. If such a conducting surface is not provided, the tip diffracted multi-path signal will be modulated by ablation and variable coupling to a dielectric ablator causing significant boresight error slopes.

Monopulse information in the forward coverage region is obtained by independently feeding and processing signals from quarter sectors of the circumferential array. Monopulse information from the broadside array in Figure 4-1 is obtained by exciting one quarter of the circumference for a given beam position. Signal processing may be accomplsihed similar to that implied earlier for the FAGT array. Axial scan and fine control in the circumferential plane may be provided by a diode phase shifter per radiator.

The feed network for the forward (or rear) sectors in the broadside array must be able to switch the active aperture around the missile, provide the required illumination taper, provide the necessary monopulse processing and provide compensation for the non zero cross polarized difference null. One conformal circumferential feed candidate is a modified butler matrix with an output per each row of radiators with each of these outputs fed through a phase shifter and conventional corporate feed. Another circumferential feed is the optical feed shown in Figure 4-4 consisting of an inner ring of horns feeding a larger number of horns in an outer ring attached to a cylindrical array of linear radiators.

Construction of the broadside array is envisioned as shown in Figure 4-6. The 14 inch diameter 20 inch long array has about 22 50 slot radiators which are dielectrically loaded and extend through a metalic (or conducting) ablator. A thin thermal insulator protects the array phase shifters and feed network. Each slot is fed through a 3-bit diode microstrip phase shifter similar to that shown in Figure 4-7. The feed consists of three layers of conformal stripline-waveguide feed circuitry. For an all stripline feed construction in an array 14 by 20 inches as shown in Figure 4-6, the antenna weight less the displaced heat ablator is estimated at 10 - 15 lbs.

LIST OF FIGURES

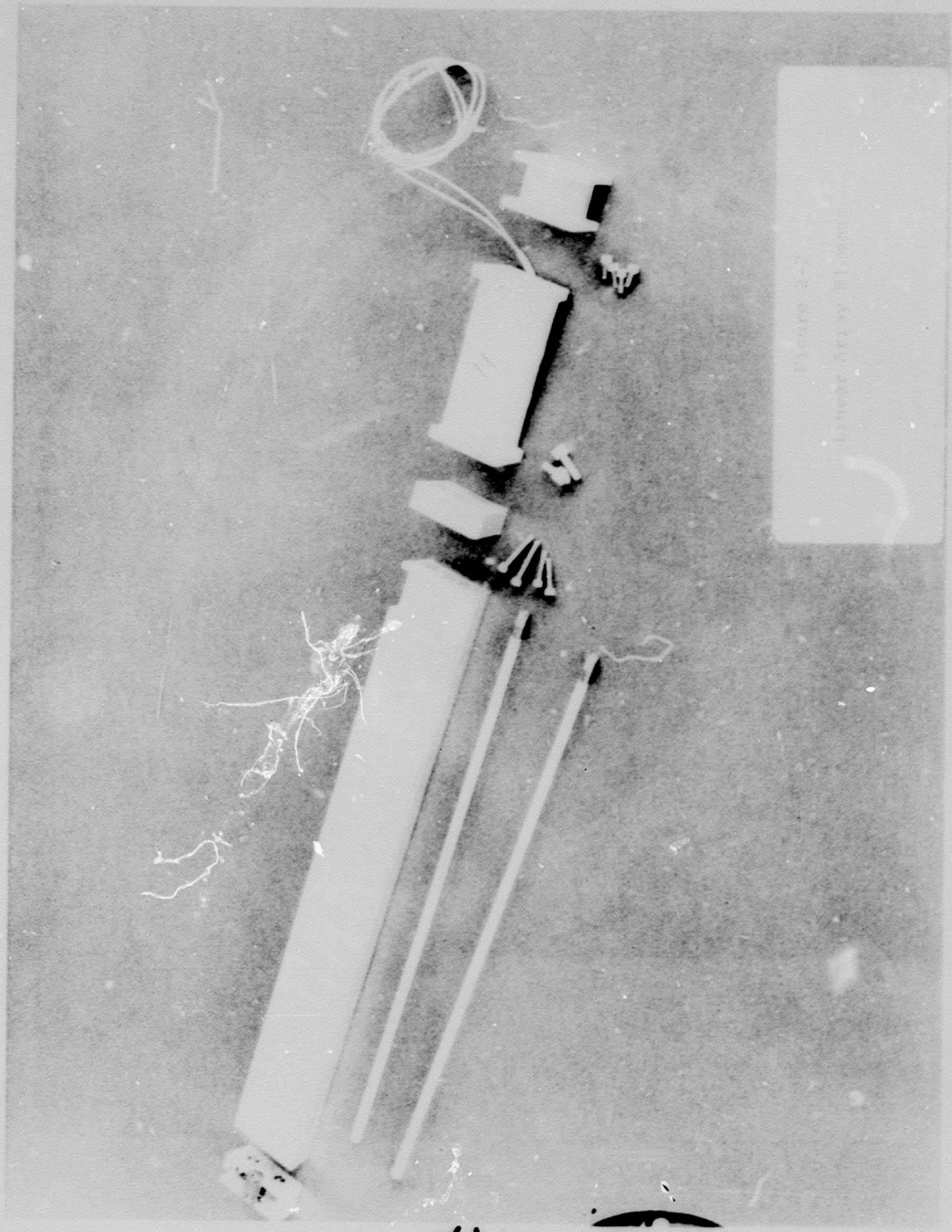

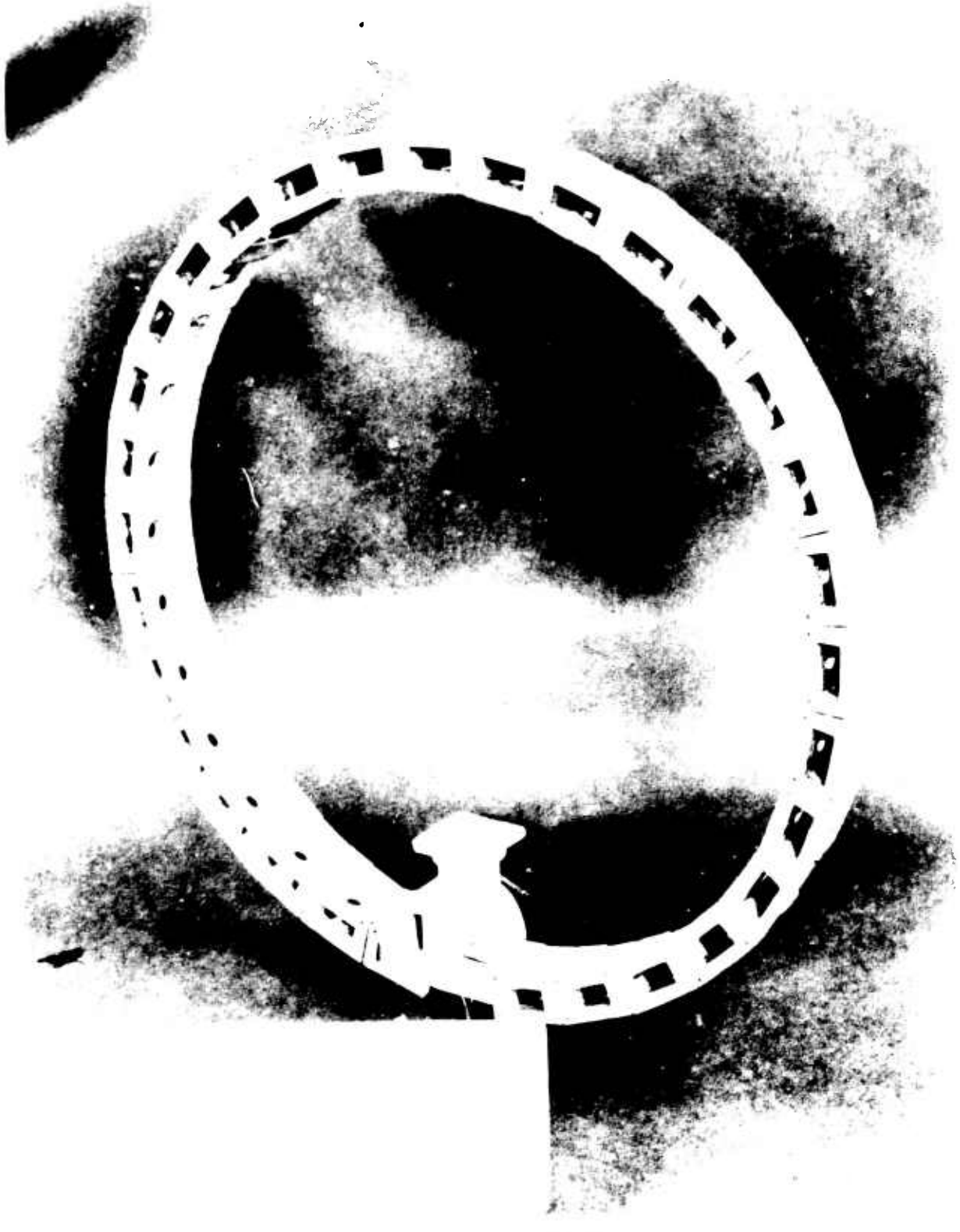

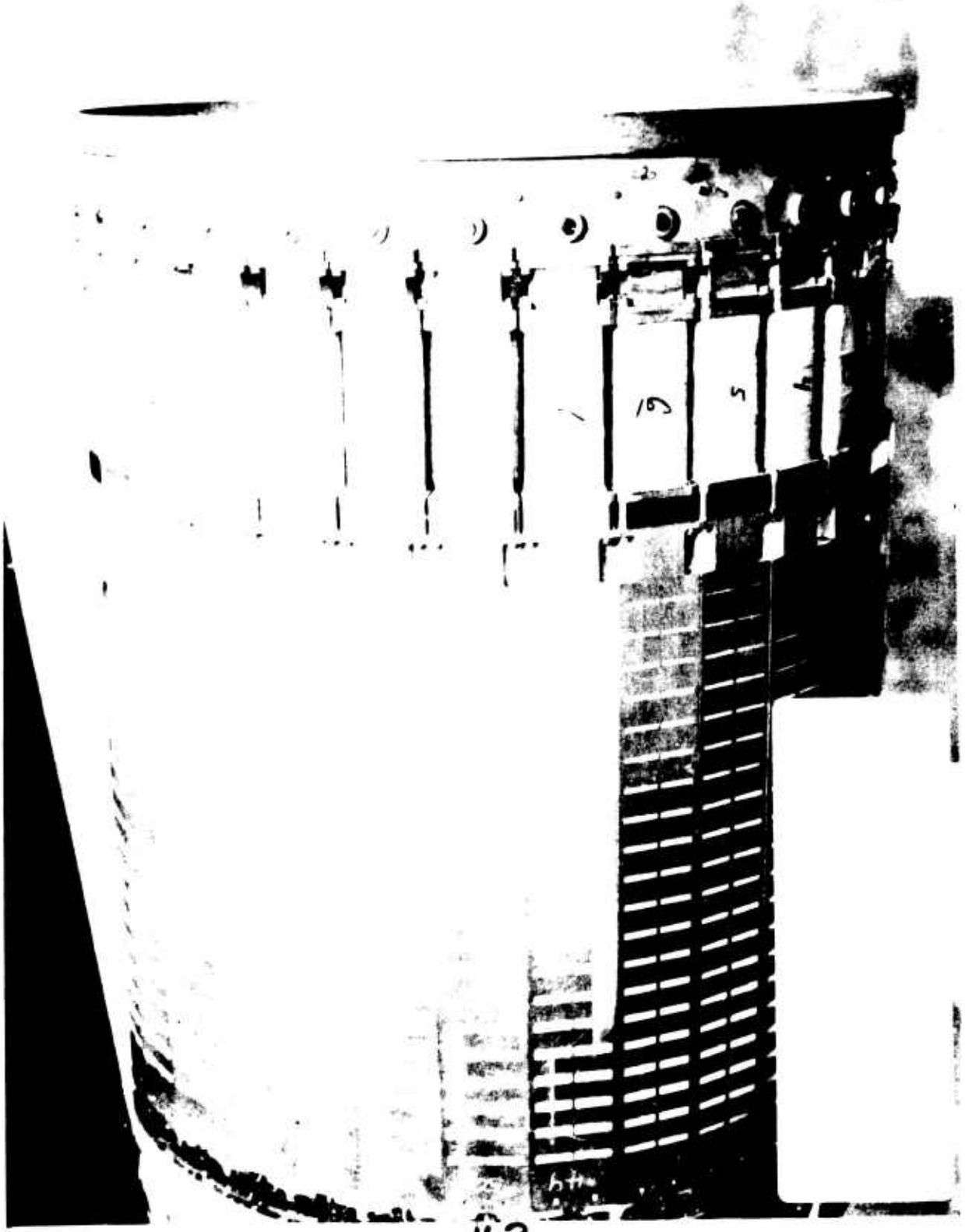

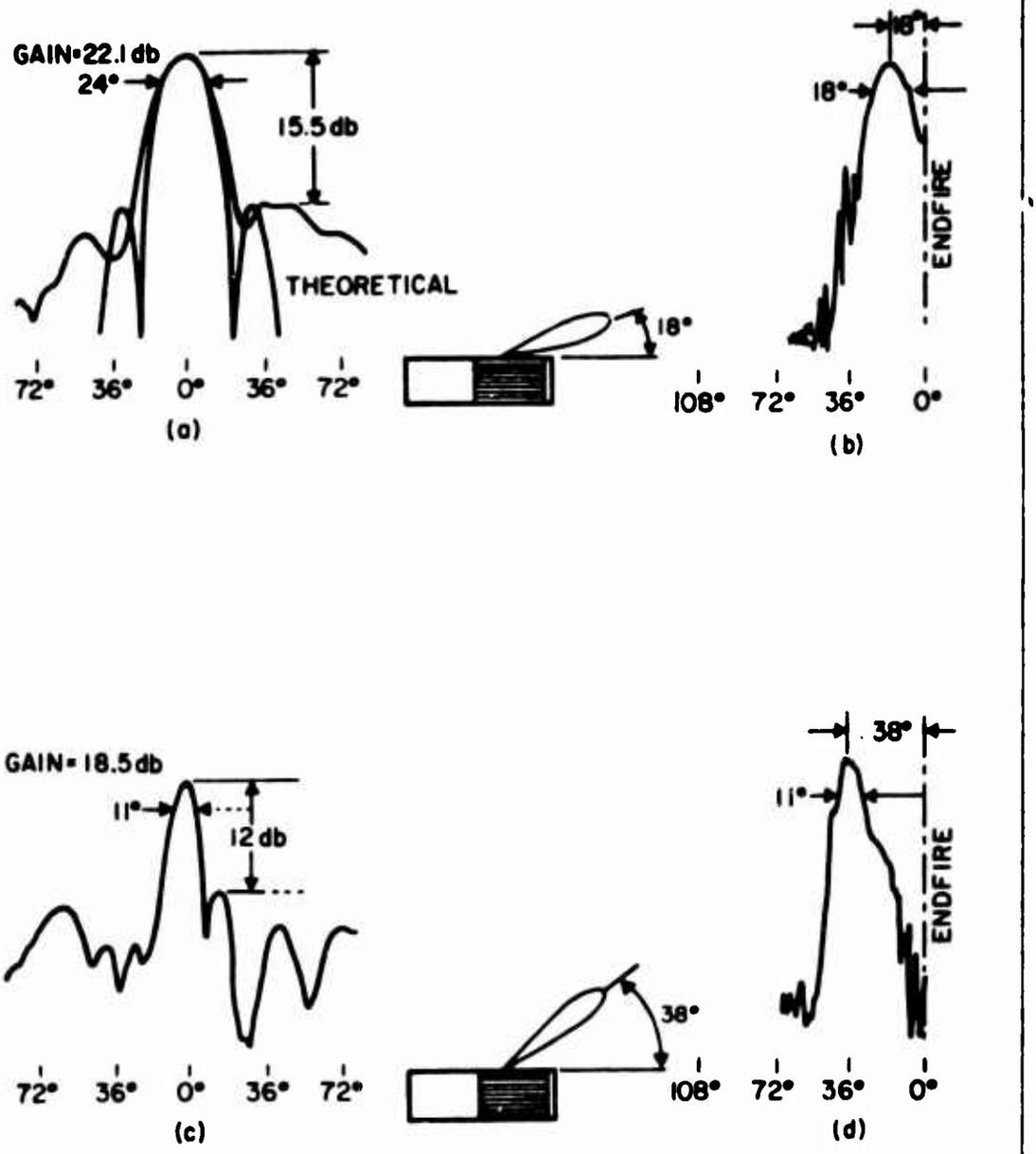

Fig 2-5
Axial Scan of
Forward Cylinder

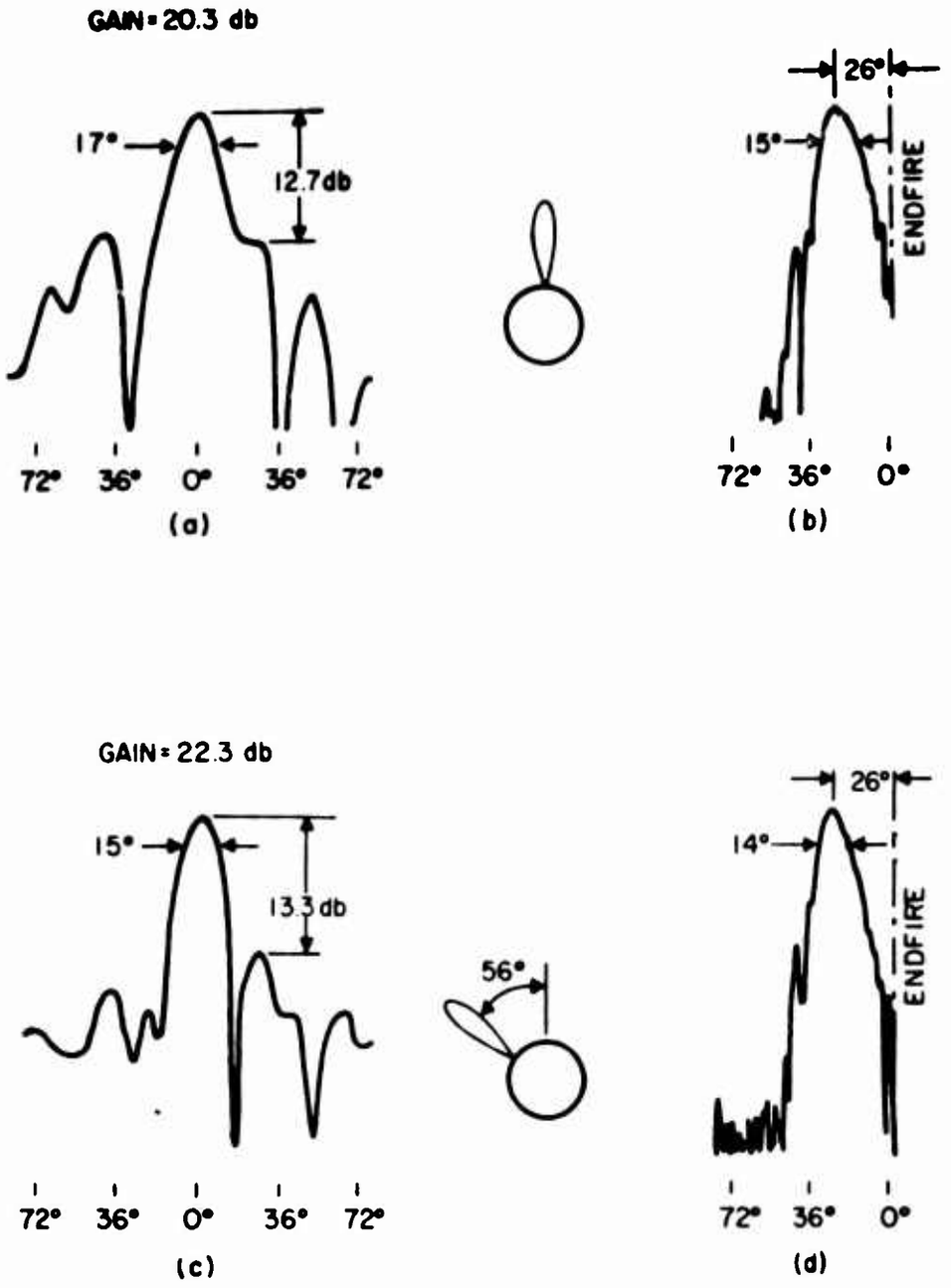

Fig 3-3
Circumferential
Scanning

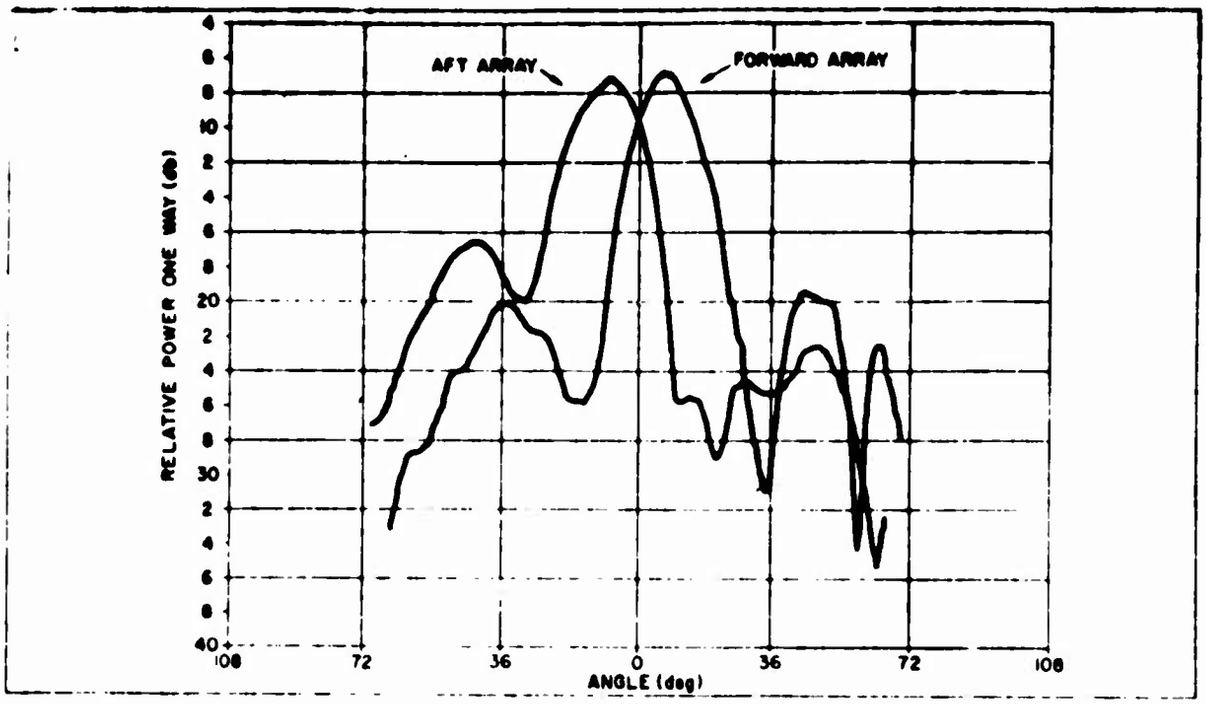

Fig. 2-7 Circumferential Plane Patterns, Forward and Aft Aperture Overlay for 8-Degree Beam Squint at θ = 30 Degrees

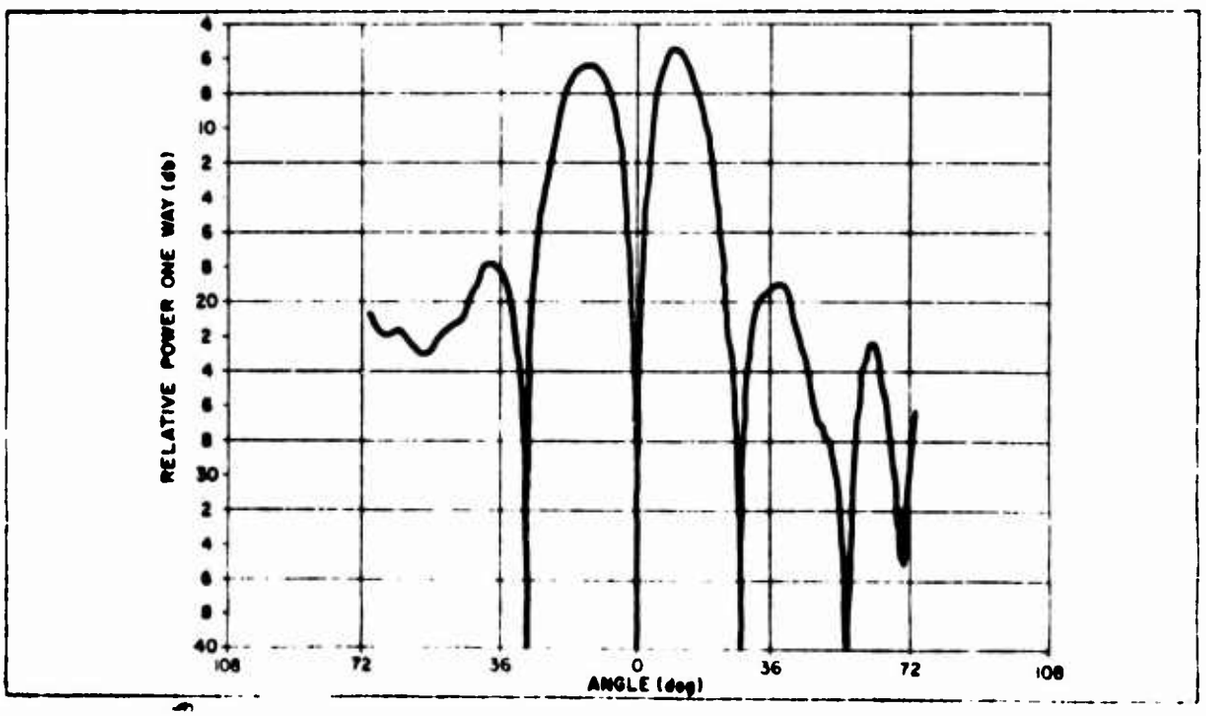

Fig 2-8- Amplitude Monopulse Difference Pattern, Circumferential Plane, for 8-Degree Beam Squint at θ = 30 Degrees

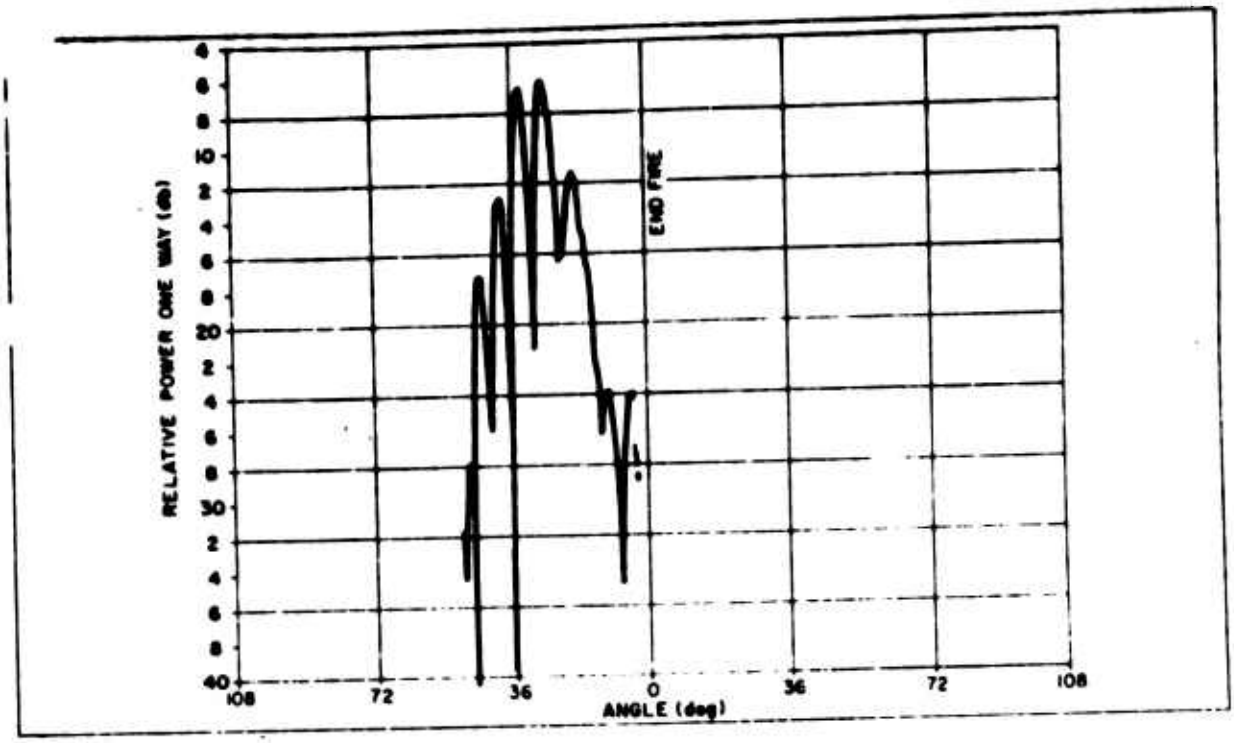

Fig. 2-9 - **Phase Monopulse Difference Pattern, Elevation Plane, at θ = 30 Degrees**

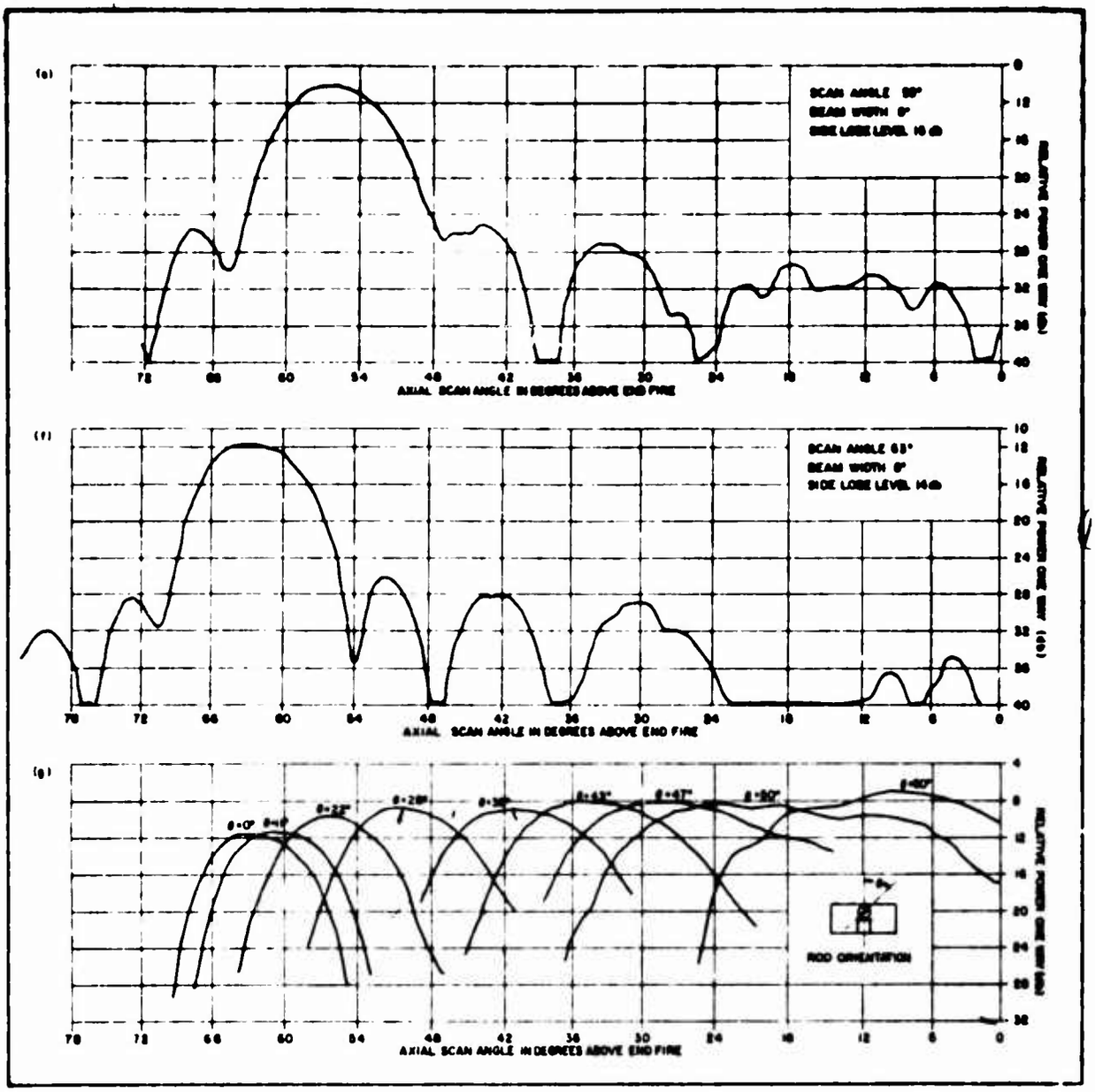

NOTES FOR g ONLY
AXIAL PLANE ANTENNA PATTERNS, FREQUENCY = 10,125 Mc
20 ELEMENT BRANCH GUIDE ARRAY, $d = 0.810$ ($D = .438\lambda$)
0.030 THICK ECCOCERAM ROD SCANNER, K = 34
MAIN GUIDE, 0.622 X 0.311 RIDGED

Fig 2-10
Axial Plane Pattern
from Linear Array
Element

NOTES FOR a, b, c, d, e, f:
AXIAL PATTERN, FREQUENCY = 10,125 Mc
20 ELEMENT BRANCH GUIDE ARRAY, $d = 0.810$ ($D = .438\lambda$)
0.030 THICK ECCOCERAM ROD SCANNER, K = 34
MAIN GUIDE, 0.622 X 0.311 RIDGED

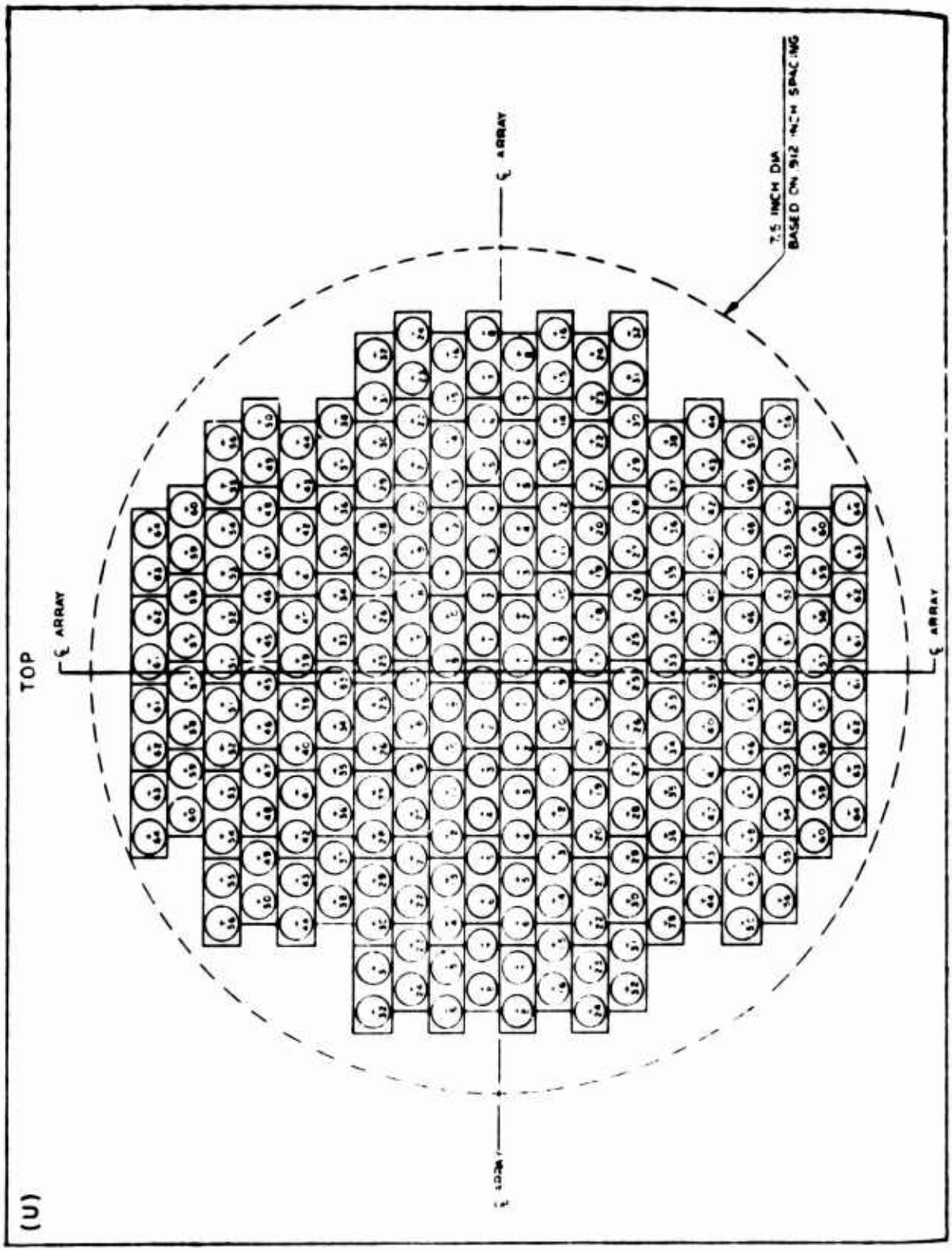

Fig 3-1 - Arrangement of RF Modules for 256 Element Array for SHF

RAYTHEON

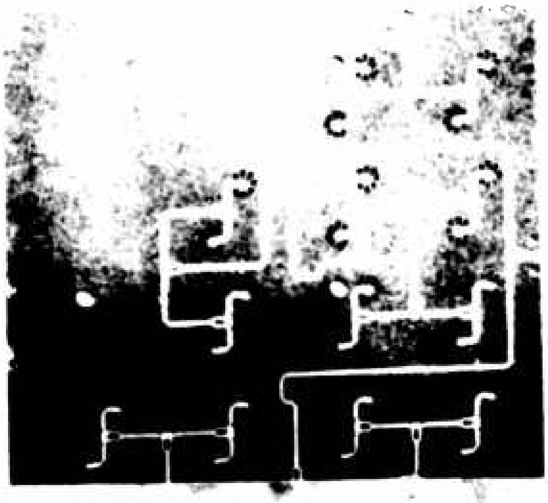

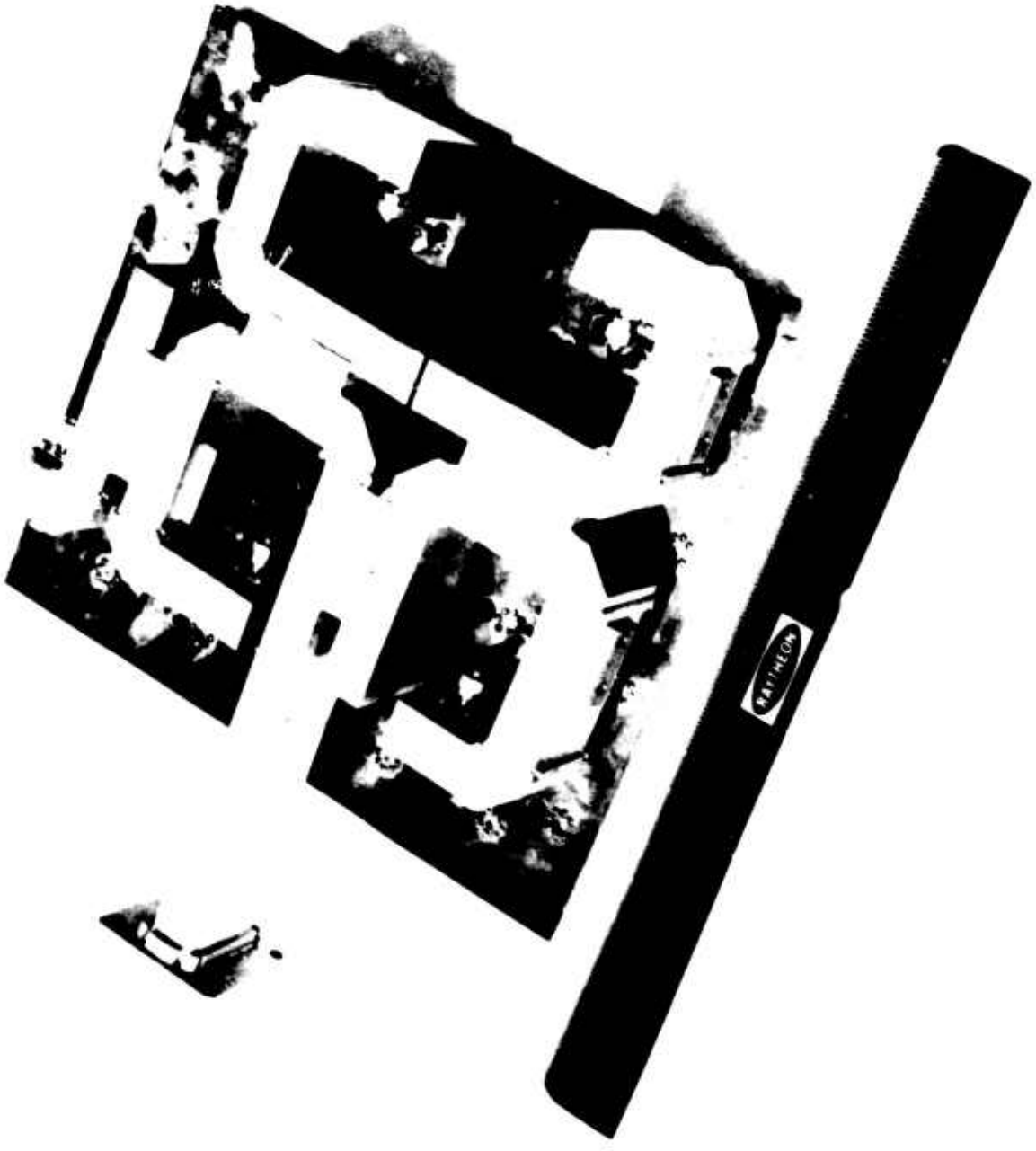
RAYTHEON

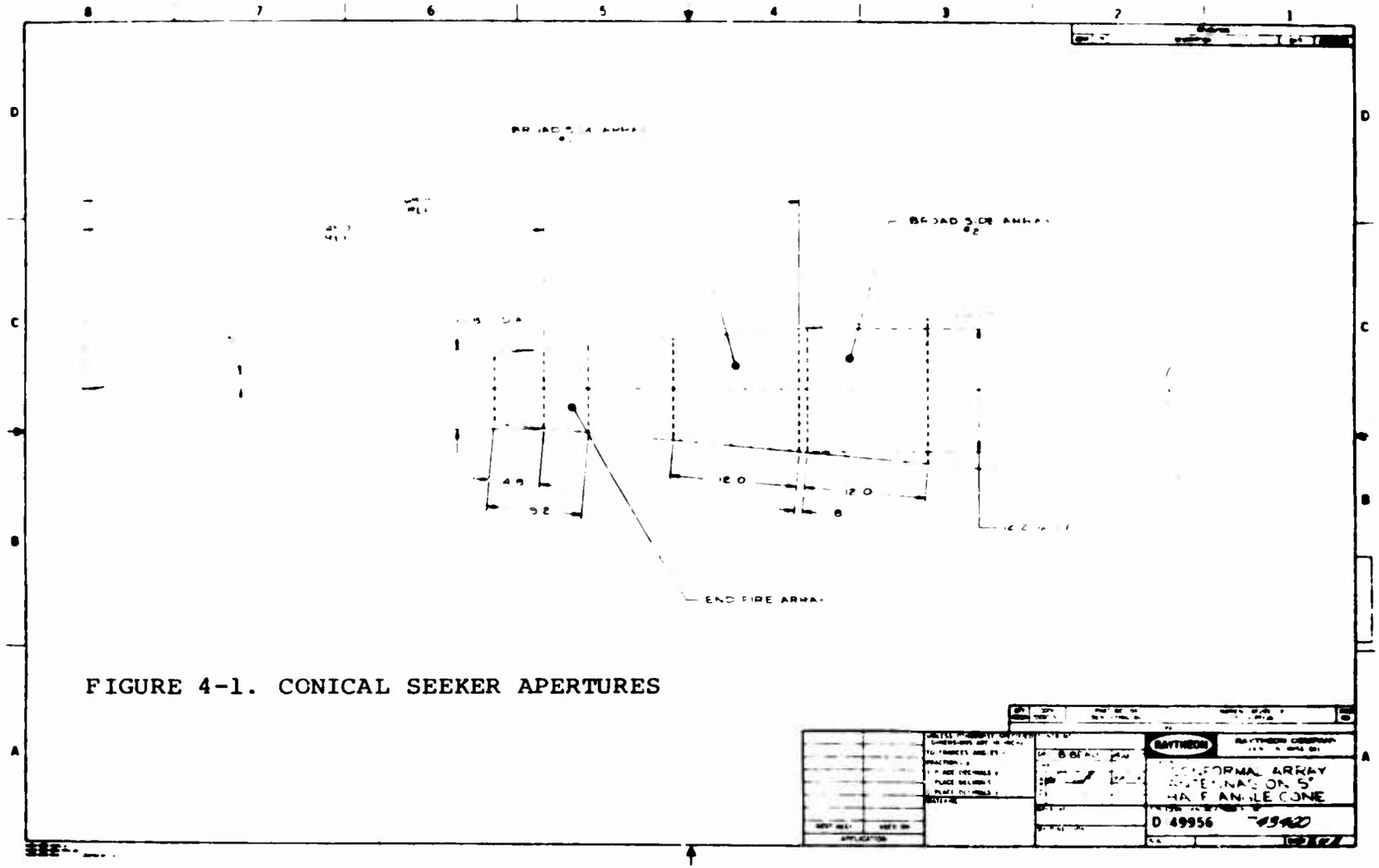

FIGURE 4-1. CONICAL SEEKER APERTURES

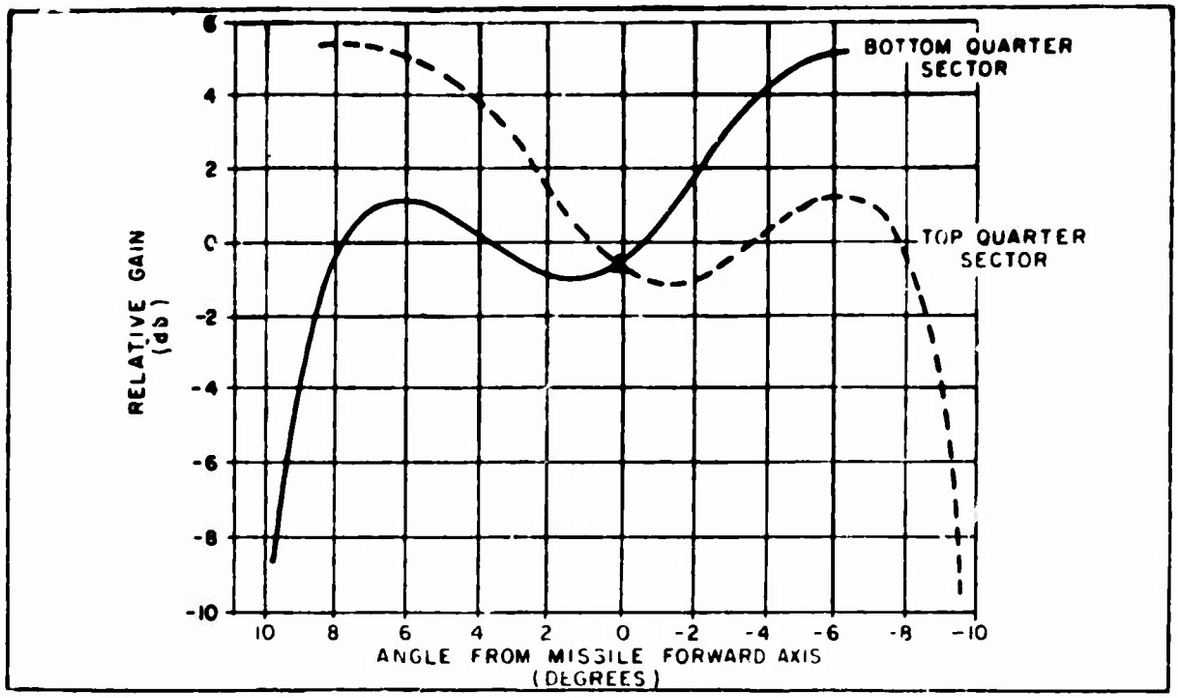

Figure4-2 - Quarter Sector Array Gains

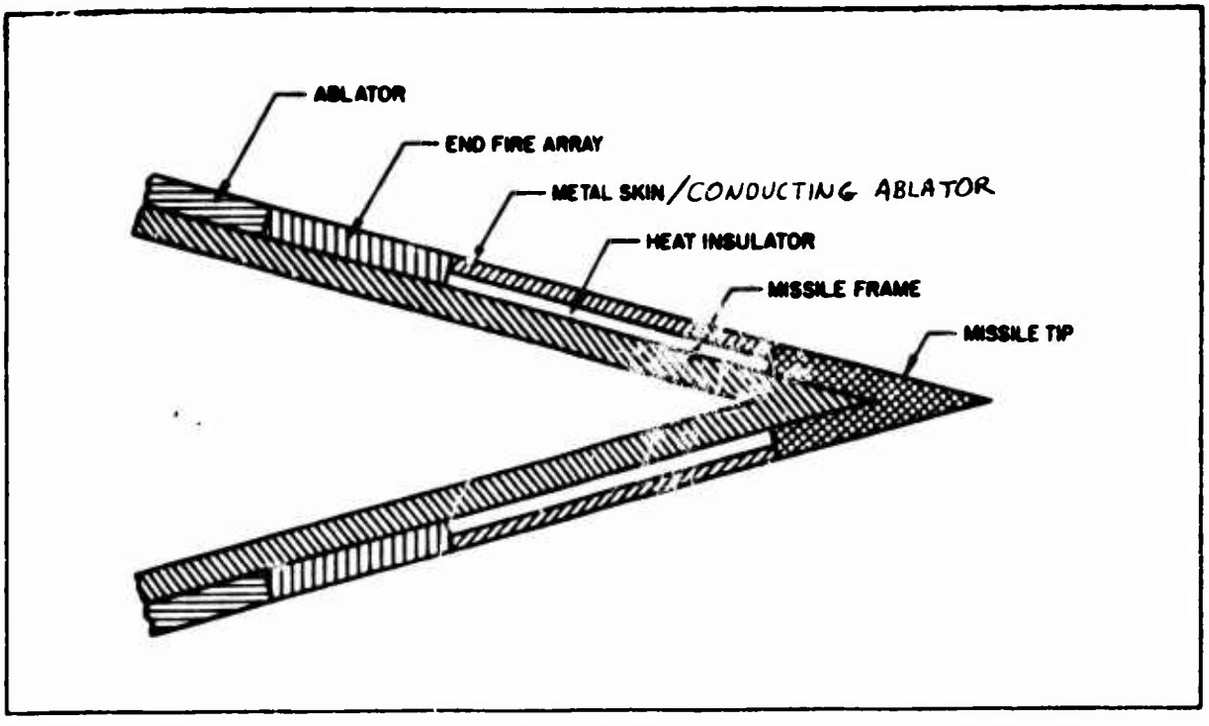

Figure 4-3 - Forward Missile Surface Configuration

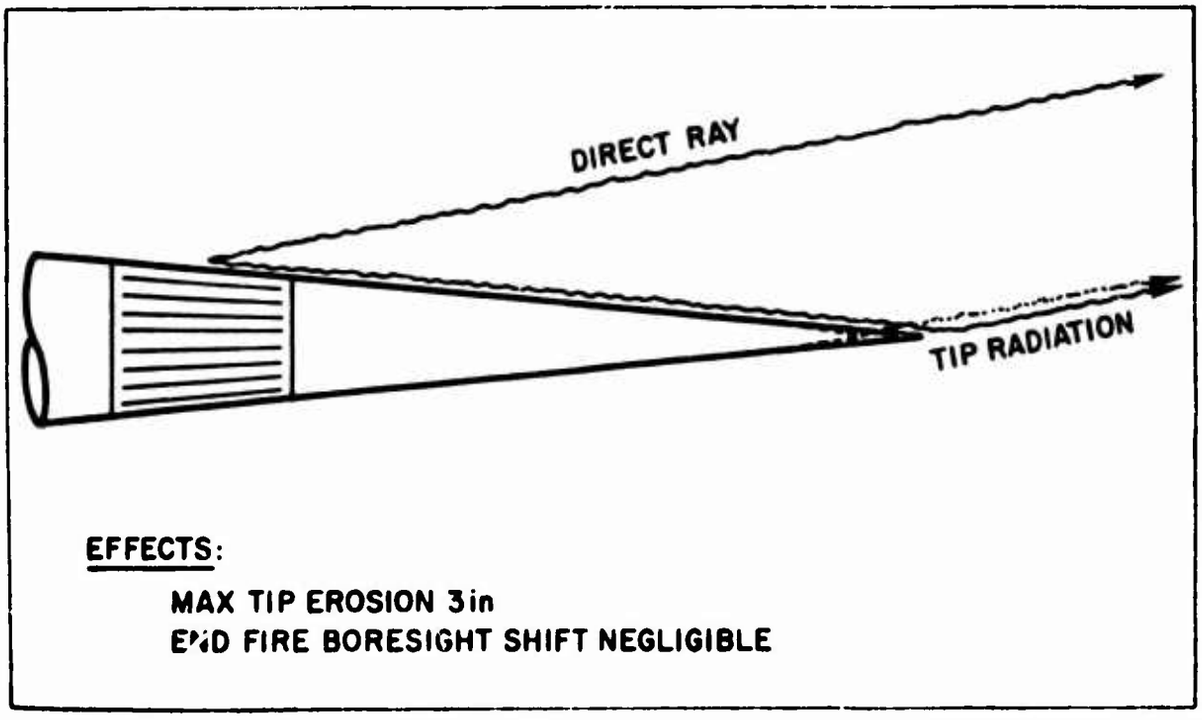

Figure 4-4 - Tip Erosion Geometry

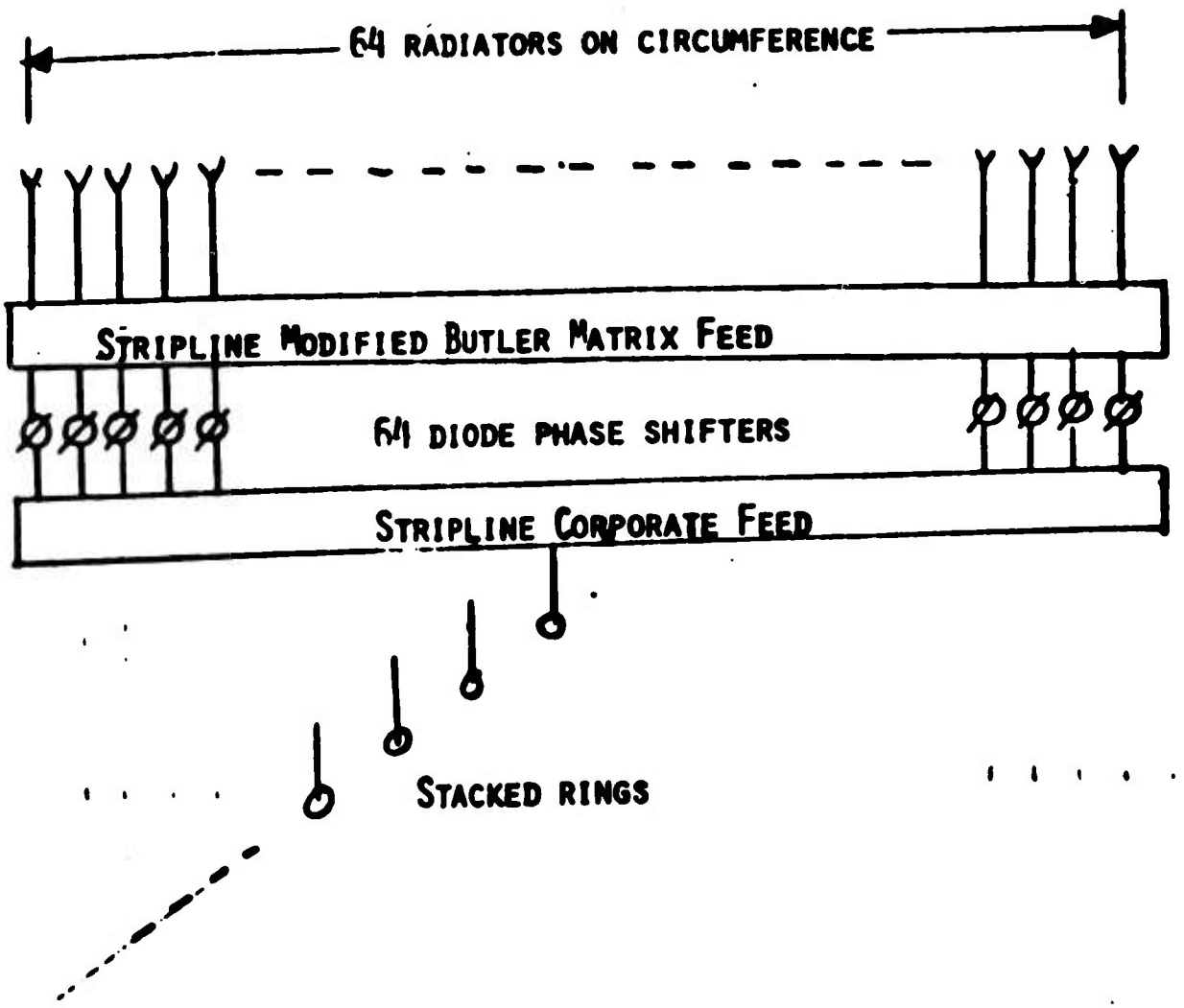

FIGURE 4-5. CIRCUMFERENTIAL FEED

CATHI ARRAY

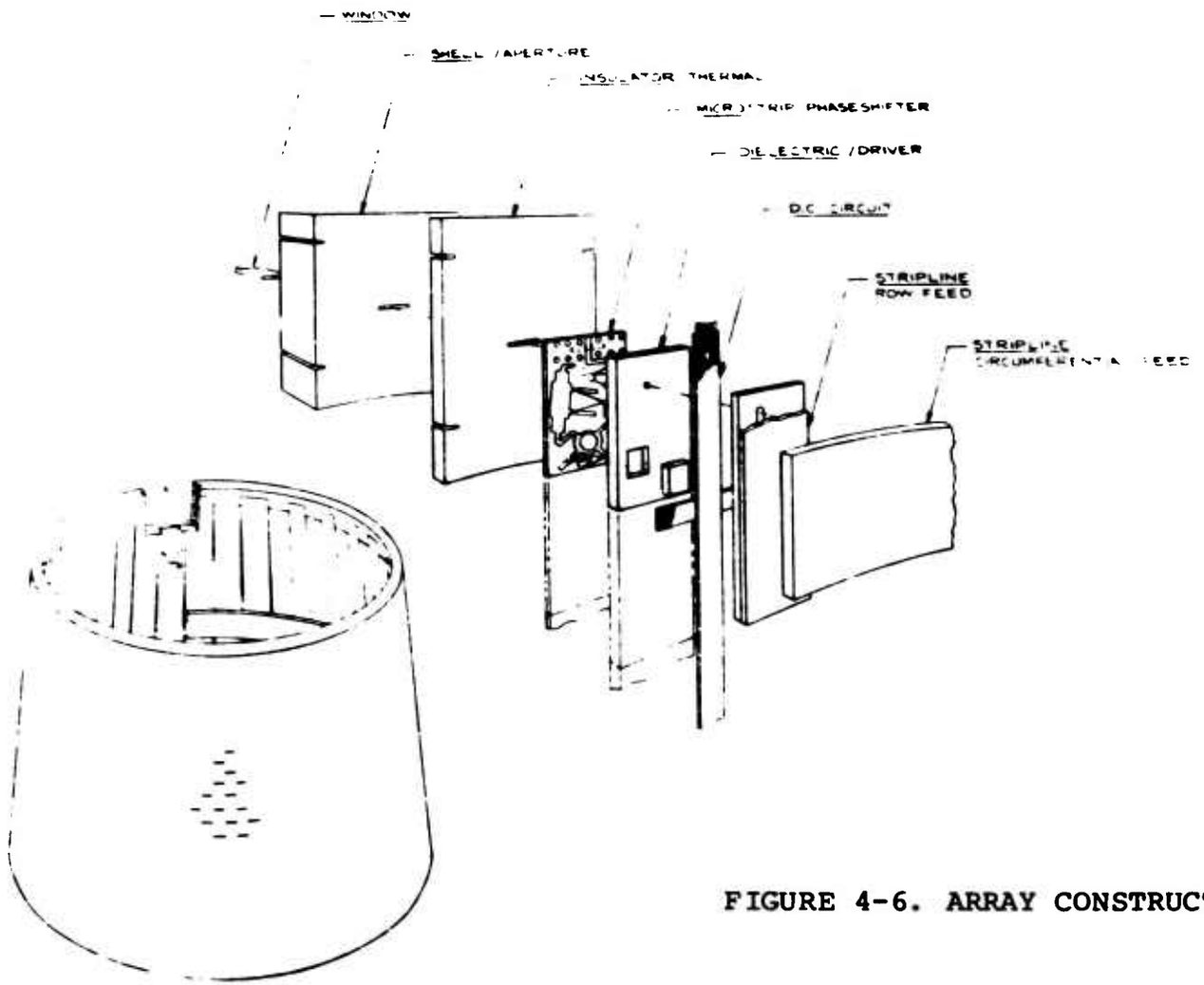

FIGURE 4-6. ARRAY CONSTRUCTION

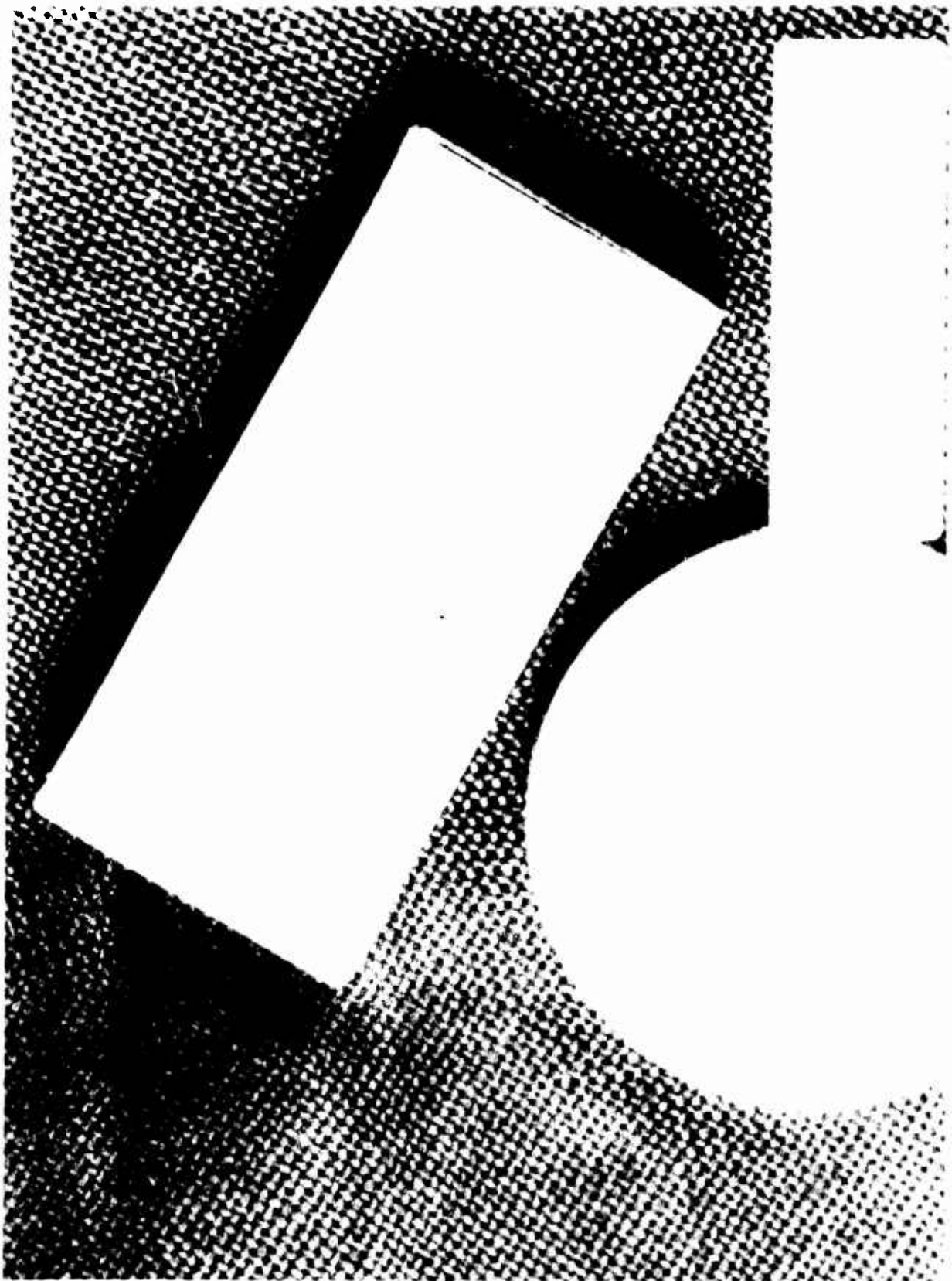

SOME ISSUES IN THE APPLICATION OF CYLINDRICAL ARRAYS TO SURVEILLANCE RADARS*

J-C. Sureau
M. I. T. Lincoln Laboratory
Lexington, Massachusetts 02173

Among the current trends in ground-based surveillance radars two of the more significant ones are the desire for sharp reductions in operation and maintenance costs and the requirement for instantaneous netting to a central data gathering facility. Since the former implies the virtual elimination of dedicated site personnel, the hardware must be such that a simple routine scheduled maintenance will guarantee continuous availability of the system. Also, the radar processing must provide some form of automatic target detection. If efficient remoting and utilization of the data from several sensors is to be successfully accomplished, the quality of this data must be improved over what is currently available from existing systems; specifically, improved clutter rejection and a reduction in the number of false targets reported must be achieved.

Cylindrical arrays have been forecast for some time to be able to play an important role in such future radar systems because they are in several ways uniquely matched to the requirements stated above. When taken collectively, their characteristic features are unmatched by any other system.

1. Electronic scanning eliminates all moving parts and brings about the kind of reliability suitable for periodic maintenance.

2. The beam can be step-scanned through discrete positions, hence it can be held stationary during an MTI processing interval. This eliminates the antenna rotation contribution to the clutter frequency spread, and MTI performance is then limited principally only by the clutter's own internal motion and the processing can be greatly simplified.

3. Scanning techniques exist for stepping the beam in increments equal to the inter-element spacing and with complete pointing agility. These generally result in the minimum number of active components for the desired level of scanning flexibility.

4. Their rotational symmetry in structure and performance means that the system need not be overdesigned to compensate for deficiencies in certain directions; i.e., there are no "off-axis" losses as in planar arrays.

---

* This work was sponsored by the Department of the Air Force.

5. An elevation fan beam can be scanned through 360° without the "coning" or beam skewing effect typical of aperture phase scanned arrays.

Further basis for the optimism in the future role of cylindrical arrays lies in some of the results obtained with experimental systems implemented by Lincoln Laboratory, in particular a UHF array which was used for ground surveillance and air surveillance (with different processors). The array, a semi-circle as shown in Figure 1, was made up of 110 columns of 4 dipoles each; 64 columns spanning a 120° arc were excited resulting in a fan beam 15° wide in elevation and 2.7° in azimuth. Scanning was accomplished by a complete "pass around" transfer switch. The system successfully exploited the unique signal processing possibilities offered by the step-scan feature. In the air surveillance mode for example, two groups of 16 pulses each were processed separately for each beam position. Rejection of stationary clutter was accomplished by removing the DC from the complex video and noncoherently integrating the remainder. Separate thresholding of each group was used, and a target was declared when detection occurred in each group. The basis for the success of this simple signal processing is provided in Figure 2 which shows the result of a discrete spectral analysis of the return from 64 pulses: ground clutter indeed appears as a DC component only; in this case, 55 dB above the system noise.

Given all the above attributes, why then is the future of cylindrical arrays as applied to ground-based surveillance radars still somewhat clouded?

Probably the simplest cylindrical array configuration is one in which the elevation pattern is fixed and the beam is scanned in steps equal to the inter-element spacing. For many of the applications of interest, the azimuth beamwidth is typically less than 2° and the elevation pattern is shaped according to some desired range/altitude coverage diagram with a 3-dB beamwidth of several degrees. This has for its direct competitor the conventional spoiled paraboloidal reflector with focal point feed. In recent years, numerous ways have been found to feed and scan such an array. Each technique has its own unique merits, but they all seem to focus on minimizing the number of active elements. While these are certainly valuable and necessary efforts, the dominant obstacle to the commitment to cylindrical arrays does not lie in the cost of the feed but in the cost of the remainder of the antenna; that is, the passive array aperture and associated support structure. This is further aggravated by the limited flexibility of this basic system.

Typically, the passive aperture accounts for 70% or more of the RF portion of the array including the ground plane screen, the dipoles and the elevation power dividers. This breakdown is consistent with cost analyses and experiences of several manufacturers and is corroborated by the Laboratory's own experience with the UHF array. Figure 3 shows a detailed breakdown of the actual

component's purchase costs for the semi-circular array shown in Figure 1. This particular configuration tended to be dominated by feed costs because only half the cylindrical array was built and because the vertical aperture was smaller than desired in an operational system. If one extrapolates to a complete circle and 16 elements in a column (4° elevation beam), the distribution shown in Figure 4 obtains. Clearly in this case, most of the cost is indeed in the array aperture. If the array cost is to be significantly reduced, this calls for different (or novel) fabrication techniques. To further emphasize the need for a different approach, a mechanically scanned system where the antenna is implemented as a spoiled reflector is several times less expensive (by a factor of 2 or 3) than the comparable cylindrical array fabricated by conventional techniques.

Reference was made earlier to the lack of flexibility of this basic system. As configured, there is a limitation on the elevation coverage caused by azimuth defocussing as a function of elevation angle. This problem gets worse as the azimuth beamwidth narrows. For a 2° beam, the useful maximum angle is around 20°. This can be alleviated by expanding the system to provide elevation coverage by a few independent squinted beams (so called "multiple-level" focussing) but at a tremendous cost in comparison to the additional coverage volume provided. Similarly, any attempt at providing other than a fixed elevation pattern results in steep cost increments. Even a simple in-the-field adjustment of beam tilt angle, if desired, becomes practically impossible.

The principal technological challenge for the cylindrical array, therefore, appears to have little to do with its conformal feature. It is simply the ability to implement an array of column elements (the distributional shape is immaterial) for a fraction of the cost incurred with conventional techniques.

Perhaps the immediate future of cylindrical arrays lies less in long or medium range radars requiring large apertures than it does in short range systems: when small apertures are used the absolute antenna cost is low enough that it becomes less of a factor in comparison to the clutter rejection benefits to be realized by the step-scan feature. This has already been corroborated by the success of a prototype ground perimeter surveillance system demonstrated in Vietnam. This possibility is currently being pursued for air traffic control applications.

Figure 1 - Demonstration UHF Array

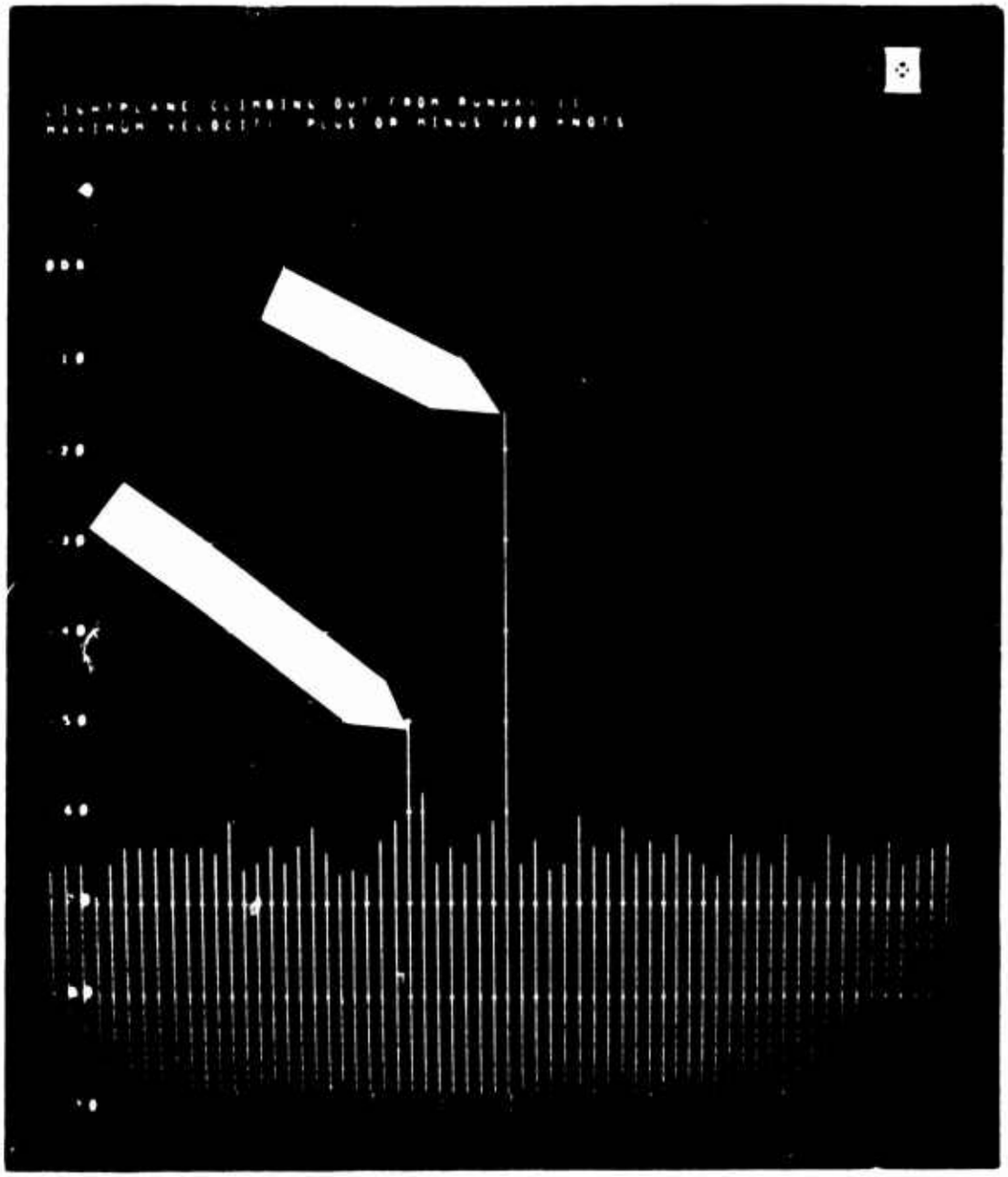

Figure 2 - Doppler spectrum of Ground Clutter and Aircraft Observed by UHF Array Radar

18-4-17021

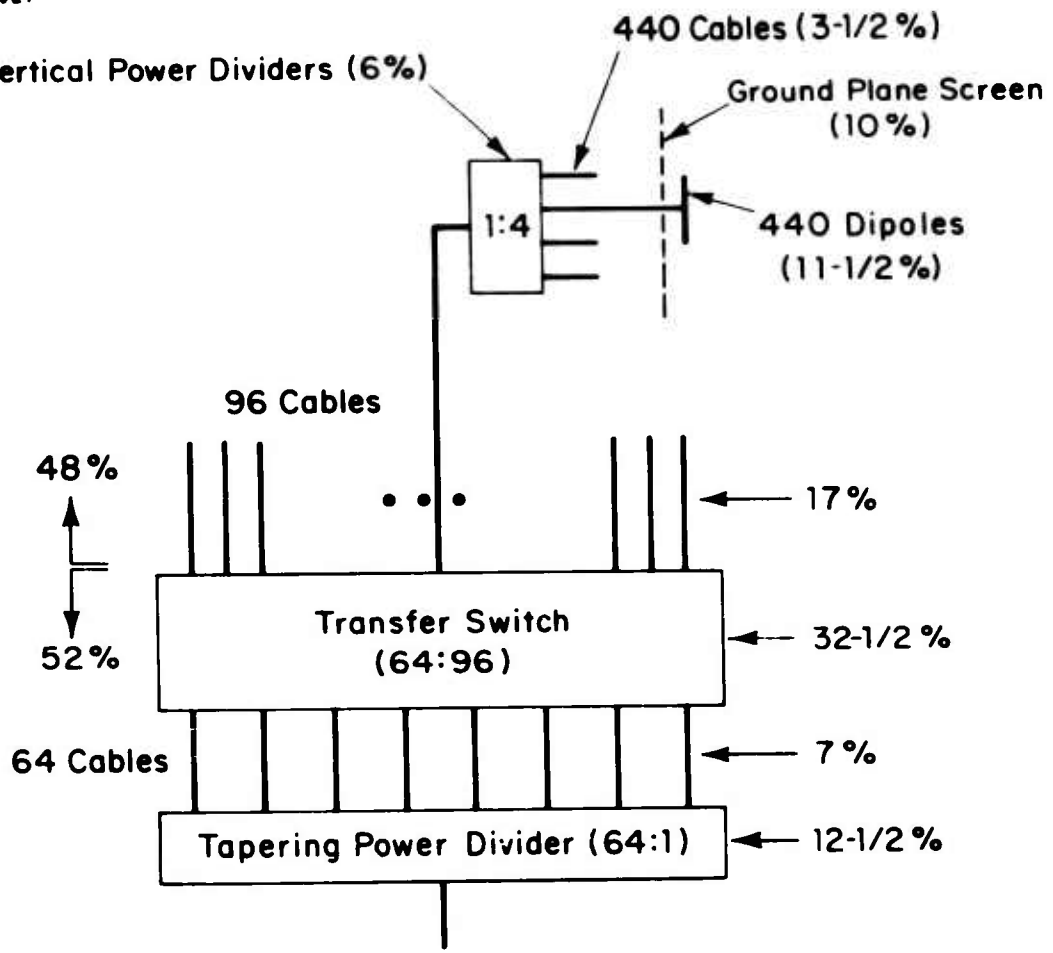

Total System Distribution: Antenna RF 56 %
Structure 44 %

COMPONENTS COST DISTRIBUTION FOR "LRDR" ARRAY

Figure 3

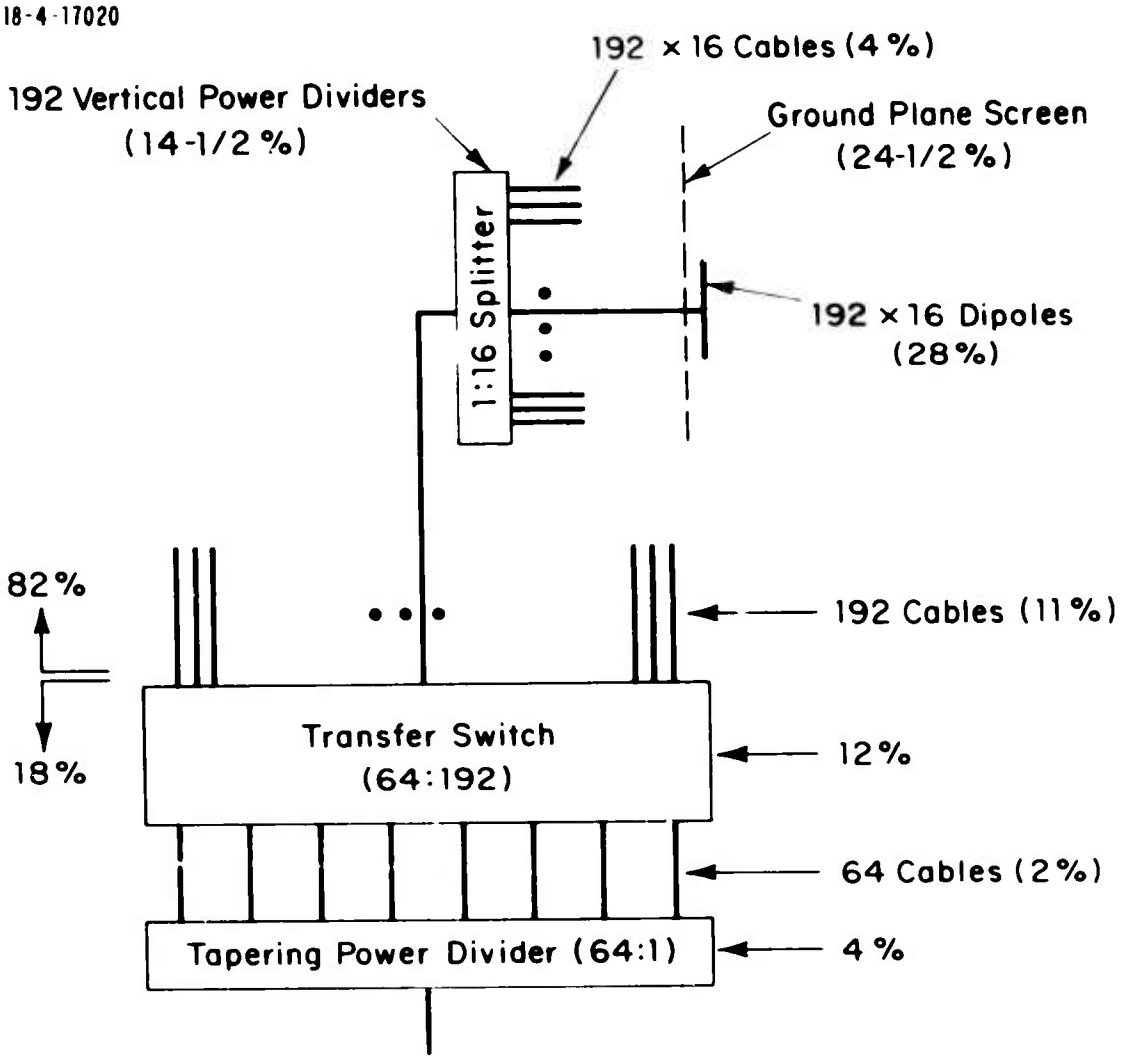

COMPONENTS COST DISTRIBUTION FOR FULL UHF ARRAY

Figure 4

SUMMARY OF WORKSHOP PANEL DISCUSSION

Moderator - Dr. R.C. Hansen, Consultant

Panel Members

Professor Alexander Hessel, Polytechnic Institute of N.Y.
Dr. W.H. Kummer, Hughes Aircraft Co.
Mr. B. Sheleg, Naval Research Laboratory
Dr. J-C. Sureau, Lincoln Laboratory
Mr. J.J. Stangel, Sperry

Following the formal presentations at the Workshop, a panel discussion was held. Comments of the panel members are summarized below:

Most of the conformal array work has been on cylindrical arrays, and most of the conformal arrays have used phaser scan in only one plane (azimuth). In this the conformal array is following the planar array, where most implementations also use phaser scan in one coordinate. Common to all arrays is the cost problem, and this is aggravated by a lack of standardized (low cost) components such as phasers, variable power splitters, feeds, etc.

Dividing the conformal array into exterior and interior areas for convenience, there have been major advances in the last several years on the exterior problem, i.e. how to analyze and design a distribution of slots over conducting conformal surfaces such as cylinders, spheres, and cones. This has been due to the two-pronged attack of GTD and harmonic series analyses. There are problems remaining, such as identifying the tip scatter terms for a conical array, but the exterior design problem can now be consolidated.

The interior area is less far advanced. Included here are the element feed structure, phase and amplitude control, element matching. The only components available are those originally developed for planar arrays. Combinations of optical and electronic scan capabilities such as the Dome array appear promising.

An area that transcends the exterior-interior division and needs more work is the optimization of the system and conformal array together. For example, should explicit sum and difference receive beams be formed at all, and how can integrated circuit transmitter and receiver modules or sub-modules best be used in a conformal array? Present cost estimates are both high and inaccurate, due to a sparcity of prototype conformal arrays. More prototyping and again, some standardized components should help reduce costs and make more realistic costing possible.